Synthesis and Characterisation of Water Soluble Polymer Drag Reducing Agents

DAVID PHILIP COLE

Synthesis and Characterisation of Water Soluble Polymer Drag Reducing Agents

A thesis submitted for the degree of

Doctor of Philosophy

by

David Philip Cole

Department of Chemistry

Durham University

England

Abstract

Dilute solutions of high molecular weight (HMW) polymers can reduce friction experienced by a fluid in turbulent pipe flow, greatly decreasing energy required for transfer of the solution. These polymers are known as drag reducing agents (DRA). Polyacrylamide (PAM), synthesised using free-radical inverse-emulsion polymerisation, is most commonly used in commercial aqueous applications. Restrictions on the acrylamide monomer have recently been imposed due to its carcinogenicity, furthermore, the use of inverse-emulsions, containing oil and surfactant, has a negative impact on the environment. The susceptibility of HMW polymers to mechanical degradation in turbulent flow quickly decreases their drag reducing efficiency (DRE), a major problem for current systems.

The aim of this project was to produce an effective water soluble polymer DRA with the following properties; 1) acrylamide free; 2) environmentally friendly; 3) oil/surfactant free; 4) mechanically stable; 5) economically viable. It was proposed that by the synthesis of HMW, acrylamide free, star polymers using Cu(0)-mediated polymerisation, effective water soluble drag reducing polymers with enhanced mechanical stability could be produced. An aqueous polymerisation method at ambient temperature would greatly reduce the environmental impact of the process.

In Chapter 1, a general background of the drag reduction phenomenon, potential mechanisms of action and key properties for effective drag reducing polymers is given. This chapter also introduces branched polymers and controlled radical polymerisation methods; in particular, Cu(0)-mediated techniques.

Chapter 2 focusses on the synthesis of water-soluble, poly(ethylene glycol) (PEG) containing macro-initiators (**I4-S**, **I4-T** and **I2-S**) for use in Cu(0)-mediated polymerisation reactions. By coupling a branching unit containing two potential initiation sites to each end of a PEG chain, multi-functional initiators for the synthesis of star polymers were produced and fully characterised using ^{1}H and ^{13}C NMR spectroscopy as well as MALDI-ToF mass spectrometry.

In Chapter 3, the polymerisation of *tert*-butyl acrylate (*t*BA) is conducted in DMSO utilising a several initiators; 4,4'-oxybis(3,3-bis(2-bromopropionate)butane (**4AE**), **I4-S**, **I4-T** and **I2-S**, and a simple catalyst system (Cu(0)/TREN). The reactions proceeded as a self-generating bi-phasic system due to the insolubility of P*t*BA in the solvent. A model initiator, methyl 2-bromopropionate (MBP), was also used to investigate the polymerisation of *t*BA further by

introducing several changes in reaction conditions. The initiators were used to prepare polymer samples for drag reduction testing.

Chapter 4 describes the aqueous Cu(0)-mediated polymerisation of sodium acrylate (NaA) using the **I4-S** and **I4-T** macro-initiators. Kinetics study of the reaction using **I4-T** demonstrated the polymerisation proceeded via a free-radical mechanism. Although complete control over the reaction was not observed, a branched polymer was synthesised by the incorporation of the multi-functional macro-initiator in to the final product and HMW samples were generated for drag reduction testing.

The drag reducing properties of the P*t*BA and PNaA samples are tested in Chapter 5 using a pipe flow test rig. The P*t*BA samples were first hydrolysed using trifluoroacetic acid (TFA) to provide water soluble poly(acrylic acid) (PAA). For comparison, several commercially available HMW PAM (**Praestol**, **PAM-6M**), poly(ethylene oxide) (**PEO-8M**) and PAA (**PAA-1M**) samples were also measured. The results demonstrated that the branched PAA/PNaA samples were effective as DRAs. Furthermore, by cycling the polymer solution through the test rig the mechanical stability of the polymer samples was investigated. An increased resistance to mechanical degradation was observed for the star polymers when compared to linear analogues.

In Chapter 6 general conclusions and future perspectives for the work are discussed.

Acknowledgements

First of all I would like to thank my supervisor Dr Ezat Khosravi whose advice and support over the last few years have helped me to develop both as a chemist and as a person. I would like to thank Ashland Inc. and my industrial supervisor Dr Osama Musa for the opportunity to undertake this research. Furthermore, particular thanks go to Tony Whittaker for his kind help during my visits to Ashland Bradford for sample testing, and to Nigel Crabtree to aqueous SEC analysis. I would like to thank the Durham University NMR and MS services and Prof. Lian Hutchings for his assistance regarding SEC. Thanks to Douglas Carswell for the all the help throughout my time in Durham, but mostly for the education in whisky.

I cannot thank enough the members of the Khosravi group for making it such a pleasure to come to work everyday; Dr Iain Johnson for his patience and advice, Dr Ahmed Eissa, Peter King, Shenghui Hou, Kieran Timothy Atter, Russell Balster, Cat Blackwell, Andrew Longstaff and Rose Simnett. I would also like to thank Becky Edwards, Paul Brooks, Serena Agostini, Chris James, Alex Hudson and Dr David Johnson as well as all the other members of CG156 past and present.

I owe a lot to my partner Tatiana for her endless patience and her relentless positivity throughout the time of writing this thesis. Finally for the support of my parents, sister and family I will be forever grateful. Without their support I would not have reached this point today.

Memorandum

The work reported in this thesis was carried out in the Department of Chemistry, Durham University, between October 2010 and December 2013. This work has not been submitted for any other degree in Durham and is the original work of the author except where acknowledged by means of appropriate reference.

Signed:_____ Date:_____

Financial Support

I gratefully acknowledge Ashland Inc. for their funding of this research.

Contents

List of Abbreviations

%DR$_{MAX}$ = Maximum %DR

[M]:[I] [L] = ratio of monomer : initiator : ligand

4AE = 4,4'-oxybis(3,3-bis(2-bromopropionate)butane

4AE-A/B = P*t*BA samples synthesised using **4AE** initiator and tested for drag reducing properties

AA/PAA = Acrylic acid/Poly(acrylic acid)

AGET ATRP = Activators generated by electron transfer ATRP

AIBN =α,α'-Azisobutyronitrile

ARGET ATRP = Activators regenerated by electron transfer ATRP

ATRA = Atom transfer radical addition

ATRP = Atom transfer radical polymerisation

Bis-MPA = Dimethylolpropionic acid

BU-S = 2,2-Bis(methyl 2-bromopropionate) propionic acid

BU-T = 2,2-Bis(methyl 2-bromoisobutyrate) propionic acid

CAN = Ceric ammonium nitrate

$CDCl_3$ = Deuterated chloroform

CMC = Carboxymethyl cellulose

COSY = Correlation spectroscopy

CRP = Controlled radical polymerisation

Đ = Polymer molecular weight dispersity, = M_w/M_n

D_2O = Deuterium oxide

DCC = Dicyclohexylcarbodiimide

DCM = Dichloromethane

DCTB = Trans-2-[3-tert-butylphenyl)-2-methyl-2-propenylidene)malonitrile

DEPT = Distortionless enhancement by polarisation transfer

DLS = Dynamic light scattering

DMAP = 4-dimethylamino pyridine

DMSO = Dimethylsulfoxide

dn/dc = differential index of refraction

DR = Drag reduction

DRA = Drag reducing agent

DRE = Drag reducing efficiency

DRI = Differential refractive index

DT = Degenerative transfer

E_c = Critical strain rate

EG/PEG = Ethylene glycol/Poly(ethylene glycol)

EO/PEO = Ethylene oxide/Poly(ethylene oxide)

ESI = Electrospray ionisation

ET = Electron transfer

F =Friction factor

FT-IR = Fourier transform infra-red spectroscopy

HMBC = Heteronuclear multiple-bond correlation spectroscopy

HMW = High molecular weight

HPAM = Partially hydrolysed Polyacrylamide

HSQC = Heteronuclear single-quantum correlation spectroscopy

I2-S = Poly(ethylene glycol) monomethyl ether mono(2,2-Bis(methyl 2-bromopropionate)propionate

I2-S-A = P*t*BA sample synthesised using **I2-S** macro-initiator and tested for drag reducing properties

I4-S = Poly(ethylene glycol)-di-2,2-Bis(methyl 2-bromopropionate) propionate

I4-S-A/D = P*t*BA samples synthesised using **I4-S** macro-initiator and tested for drag reducing properties

I4-T = Poly(ethylene glycol)-di-(2,2-Bis(methyl 2-bromoisobutyrate) propionate

I4-T-A/F= PNaA samples synthesised using **I4-T** macro-initiator and tested for drag reducing properties

ICAR ATRP = Initiators for continuous activator regeneration ATRP

ICP-OES = Inductively coupled plasma optical emission spectroscopy

I_{eff} = Initiator efficiency

ISET = Inner-sphere electron transfer

k_{act} = Rate constant for activation

K_{ATRP} = ATRP equilibrium constant = k_{act}/k_{deact}

k_{comp} = Rate constant of comproportionation

k_{deact}= Rate constant for deactivation

k_{disp} = Rate constant of disproportionation

k_p^{app} = Apparent rate constant of propagation

LAM = Less activated monomer

LS = Light scattering

MA/PMA = Methyl acrylate/Poly(methyl acrylate)

MALDI-ToF MS = Matrix assisted laser desorption/ionisation- time of flight mass spectrometry

MAM = More activated monomer

MBP = Methyl 2-bromopropionate

MBP-A = P*t*BA sample synthesised using MBP initiator and tested for drag reducing properties

Me_6-TREN = Tris[2-(dimethylamino)ethyl]amine

MEHQ = Methyl ether hydroquinone

$MgSO_4$ = Magnesium sulphate

M_n = Number average molecular weight

M_w = Weight average molecular weight

MW = Molecular weight

MWD = Molecular weight distribution

N = number of monomer units

NaA/PNaA = Sodium acrylate/Poly(sodium acrylate)

***n*BA/P*n*BA** = n-butyl acrylate/Poly(n-butyl acrylate)

NEt_3 = Triethylamine

NMP = Nitroxide mediated polymerisation

NMR = Nuclear magnetic resonance

OMe-PEG = Mono-methoxy poly(ethylene glycol)

OSET = Outer sphere electron transfer

PAM = Polyacrylamide

PEG-3350 = Poly(ethylene glycol) – MW = 3350 g mol^{-1}

ppm = parts per million

PRE = Persistent radical effect

RAFT = Reversible addition-fragmentation chain transfer

Re = Reynolds number

REACH = Registration, Evaluation, Authorisation and Restriction of Chemicals

R_g = Radius of gyration

RI = Refractive index

rpm =Revolutions per minute

RT = Room temperature

SA = Surface area

SARA ATRP = Supplemental activator and reducing agent ATRP

SEC = Size Exclusion Chromatography

SET-DTLRP = Single electron transfer-degenerative transfer living radical polymerisation

SET-LRP = Single electron transfer-living radical polymerisation

SR&NI ATRP = Simultaneous reverse and normal initiation ATRP

***t*BA/P*t*BA** = *tert*-butyl acrylate/Poly(*tert*-butyl acrylate)

TEMPO = 2,2,6,6-tetramethyl-1-piperidinyloxy

TFA = Trifluoroacetic acid

TQD = Tandem quadrupole

TREN = Tris(2-aminoethyl)amine

UHMW = Ultra-high molecular weight

VCl/PVCl = Vinyl chloride/Poly(vinyl chloride)

V_h = Hydrodynamic volume

XG = Xantham Gum

Chapter 1

General Introduction

1.1. Background

Oil Fields in remote locations require vast pipelines to transport oil between well and refinery. Friction experienced by oil flowing past the pipe walls leads to a pressure drop between two points on the pipe, necessitating regular pump stations to maintain the required rate of flow.[1] The ability of ppm quantities of high molecular weight (HMW) polymer additive to greatly reduce friction experienced by a turbulent fluid was first observed by Toms in 1948.[2] Such polymers were termed 'Drag (or Friction) Reducing Agents' (DRAs) and the potential of the 'Toms phenomenon' was quickly established, particularly in the oil and gas industry. The capacity to reduce friction up to 80 % reduces the energy required to pump liquid at a certain rate, or increases rate for a given energy input. As a result the field has been a focus of attention both academically and industrially for over 60 years. Despite this activity, the combination of two poorly understood fields (turbulent flow and polymer dynamics in dilute solutions) has led to an incomplete understanding of the underlying mechanism by which a small quantity of polymer can have a large effect on gross turbulent flow. In addition to oil-soluble polymers for oil transport, there are a range of applications for water-soluble DRAs both oil field (fracking, acid stimulation, secondary oil recovery)[1] and non-oil field (field irrigation, slurry transport).[3]

1.2. Introduction to fluid mechanics

To study drag reduction in detail it is important to consider some key basics of fluid mechanics. Starting from the most basic principle, a fluid is defined as 'a material which continuously deforms when a shear, or tangential, stress is applied'.[4] This includes liquids and gases and excludes solids which deform under stress only until the material's elastic limit is reached. Stress is the force applied to a material over a given area and shear stresses arise in fluids due the application of a force tangential to the area upon which it is acting, such as those experienced as a fluid passes a pipe wall. These are transferred through the fluid via interactions between individual fluid particles, known as viscous flow. To visualise the effect of shear stress, consider a fluid contained between two infinite sheets (Fig. 1). A fluid at rest experiences no shear stress (Fig. 1a). As force is applied to the upper plate, this plate is dragged across the fluid at constant velocity. The no-slip rule dictates that, due to friction, the relative velocity of fluid adjacent to a surface must equal the surface movement; therefore, the fluid deforms (Fig. 1b-c). This also applies to the stationary, lower surface and so shear stress is passed through the fluid and a velocity gradient is established with the highest velocity at the upper surface and zero velocity at the lower.

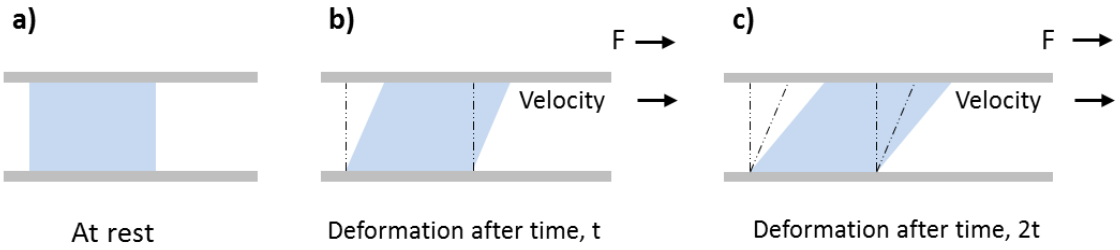

Figure 1: Fluid contained between two infinite plates; **a)** At rest; **b)** Deformation at time, t, after constant force (F) moves the upper plate at a constant velocity; **c)** Deformation at time, 2t.

The viscosity of a fluid dictates its resistance to deformation. The rate at which the fluid deforms is known as the shear rate (or strain) and at low shear rates the flow of a viscous fluid divides into ordered layers which move smoothly past each other (laminar flow). The relationship between shear stress and shear rate is important when classifying the behaviour of fluids. Fluids which show a linear relationship between shear stress and shear rate, for example water, are known as Newtonian (Fig. 2) and those with a non-linear relationship are non-Newtonian (e.g. custard).[4] Depending on the effect of shear rate on non-Newtonian fluids, these can be further sub-divided as pseudoplastic (viscosity decreases with increased shear stress) or dilatant (viscosity increases with increased shear stress).

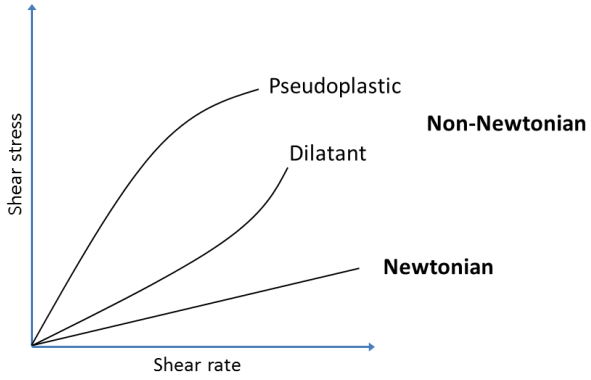

Figure 2: Relationship between shear stress and shear rate for Newtonian and non-Newtonian fluids.

1.2.1. Pipe flow

The principles of Figure 1 can be extrapolated to a variety of flow systems. This work aims to develop DRAs for transport of liquids through pipes. Flow through a pipe is classified as an internal flow as it is completely bound by a solid surface. Pipe flow is usually studied some distance from the pipe entrance when flow is 'fully developed'; Figure 3 describes how this situation is reached. Upon entering the pipe, the no-slip condition dictates velocity is zero at the pipe wall. A boundary layer is established passing wall stress through the liquid due to its viscosity (Fig. 3b). Further from the pipe entrance, stress is experienced at a greater distance

from the wall. When the boundary layer reaches the centre of the pipe, flow is fully developed and the velocity profile remains constant for a straight and horizontal pipe of constant diameter (Fig. 3c).[4]

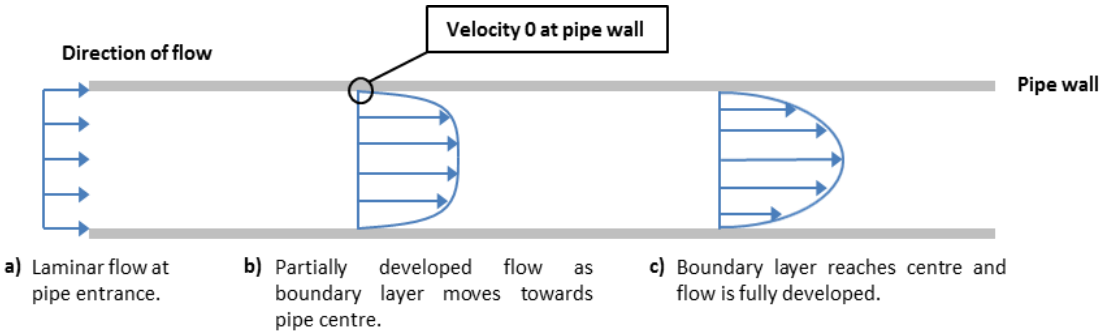

Figure 3: Development of flow near the entrance of a pipe.

1.2.2. Turbulent flow

As shear rate increases, laminar flow becomes less stable and a disturbance can cause a transition to disordered turbulent flow. Whereas laminar flow can be described by a mean velocity, turbulent systems require the addition of three randomly fluctuating velocity components.[4, 5] Analysis of turbulent flow is, therefore, highly complicated and the field must rely on a combination of experimental data and semi-empirical theories.

The transition between laminar and turbulent phases results when the inertial forces caused by shear stress outweigh the viscous forces counteracting them, described by the Reynolds number (*Re*). The specific *Re* of a system is subject to the exact parameters of each system and for pipe flow it is described by Equation 1. *Re* is dependent on fluid velocity (V), pipe diameter (*D*) and the fluid density (ρ) and viscosity (μ). Generally the transition occurs when $Re \approx 2300$ and so for most practical applications flow is turbulent.[4]

$$Re = \frac{\rho V D}{\mu} \qquad \textbf{(Equation 1)}$$

Random velocity fluctuations in turbulent flow mean it is no longer relevant to describe the system in terms of only wall shear stress as for laminar flow. Momentum is dispersed randomly between fluid layers and, therefore, an additional 'Reynolds stress' acts on the fluid. These Reynolds stresses maintain turbulence in a system despite viscous dissipation from the fluid. Total energy lost due to friction is referred to as head loss and to calculate this, an experimentally determined friction factor (a measure of friction experienced by the fluid) is used.[5] Friction in turbulent flow derives almost entirely from Reynolds stresses which rapidly

dissipate energy from the mean flow direction and increase conversion of kinetic energy to thermal energy at the pipe wall. As a result of this, a much higher friction factor and head loss is observed for turbulent flow when compared with laminar flow.

1.2.2.1. Turbulent flow structure

The structure of turbulence is important in order to appreciate differences between normal and drag reduced flow. Figure 4 shows the division of turbulent flow to an inner and outer region separated by an overlap. The inner region (or viscous sub-layer) occurs very close to the wall ($y/D << 1$, where y is distance from wall). Here there is a large influence of viscous wall stress (Fig. 5) and the sub-layer is characterised by near laminar flow. There is a rapid variation from viscous stress of the wall to Reynolds stresses which dominate turbulent flow. The outer region (or Reynolds plug, Fig. 4) is entirely turbulent and viscous stress is negligible (Fig. 5).[5]

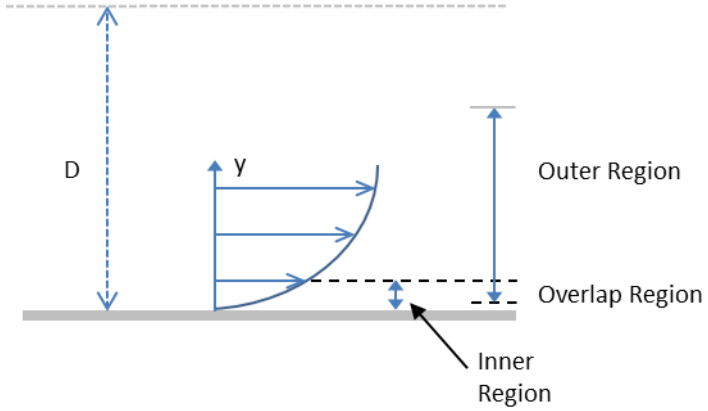

Figure 4: Schematic diagram describing the regions of turbulent flow. (*D* = pipe diameter, *y* = distance from wall)

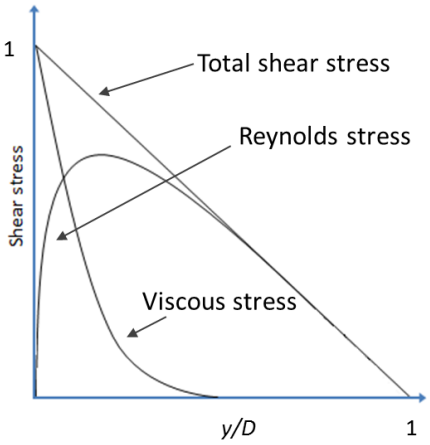

Figure 5: Relative contribution of viscous and Reynolds stresses to the overall stress of a system with increasing distance from pipe wall.

Whilst velocity in the inner region increases linearly with distance from the wall, the outer turbulent region is described by the log law of the wall (velocity ∝ log distance from wall). This is a rare general law in turbulence although it holds only for around 20 % of pipe diameter. In Figure 6, the fluid velocity (u) is plotted against distance from pipe wall. The inner laminar and outer log regions are separated by an overlap or buffer region ($5 < y < 30$) where there is a transition between the two velocity profiles. The buffer zone is an area of high activity, experiencing frequent turbulent bursts transferring energy to the centre of the pipe.

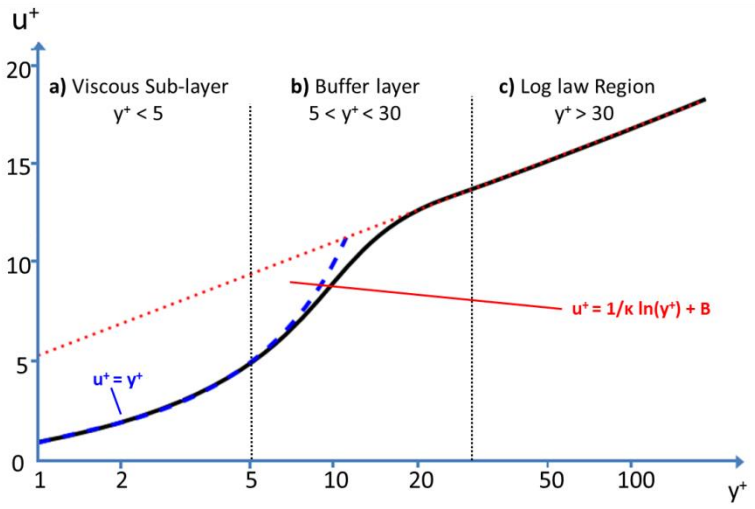

Figure 6: Variation of velocity (normalised u^+) with log distance from the wall (normalised y^+). Three distinct regions observed; **a)** Inner region (blue line); **b)** Buffer layer which transitions velocity to; **c)** log law region (red line, gradient 1/κ, shifted from 0 by B depending on viscous and buffer layers).

1.3. Polymer drag reduction

The graph in Figure 7 relates a measure of turbulence (Log($Re\sqrt{f}$)) with one of friction caused as a fluid moves past a pipe wall ($1/\sqrt{f}$). It describes how a drag reducing polymer solution differs from a Newtonian fluid, which is described by the Prandtl-Karman law (Fig. 7, black line). It also highlights two features of drag reduction; onset and maximum drag reduction (MDR) asymptote.[6, 7] A polymer solution of given concentration follows the Prandtl-Karman Law until a certain value of Re is reached. From this point the polymer curve departs from Prandtl-Karman law (Fig. 7, orange line) and drag reduction is observed, the onset of drag reduction. The slope then rises linearly (gradient concentration dependent) with Re until reaching an upper bound known as the MDR or Virk asymptote.[8] The MDR has been widely studied experimentally and is shown to be insensitive to the properties of the polymer, so universal for all systems.[9] If Re is maintained constant and instead the concentration is increased (Fig. 7, red line), the onset is seen at a critical concentration. Between the Prandtl-

Karman law, MDR asymptote and laminar region (Fig. 7, purple line) there must be a distinct turbulent regime which is a direct consequence of polymeric effects.[9]

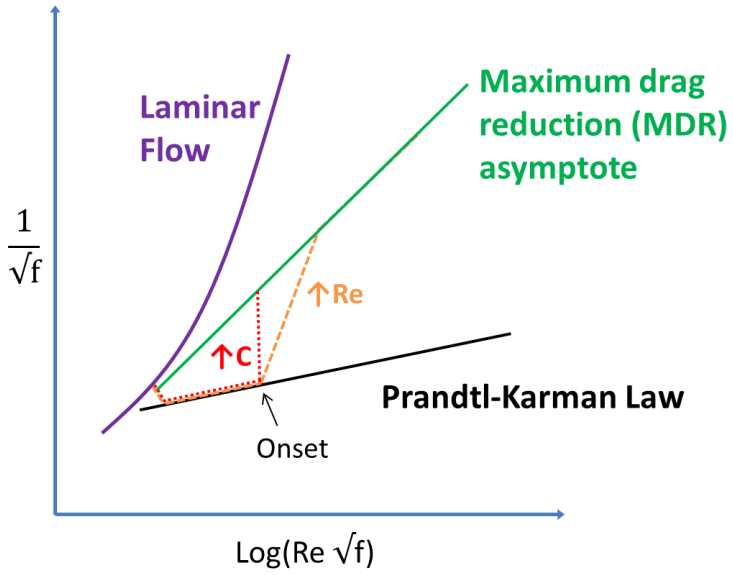

Figure 7: Relationship between friction and turbulence for Newtonian fluid (Prandtl-Karman law, black) and polymer drag reducing solution (orange/red). Laminar region shown by purple line.[7]

1.3.1. Effect of drag reducing polymer on turbulence statistics

Studying flow statistics, for example velocity fluctuations and Reynolds stresses, can provide further information on the drag reducing turbulent regime. This has been conducted using both numerical and experimental analysis.[10, 11] When compared with Newtonian turbulent flow, stream-wise (direction of flow) velocity fluctuations are increased whilst those normal (perpendicular to wall) and span-wise (across pipe) are decreased for a dilute polymer solution. For Reynolds stress an even more interesting result is observed. Whilst in Newtonian turbulent flow Reynolds stresses are entirely dominant, in the drag reducing regime they are hugely diminished. In particular the reduction is seen in the 'pressure-strain' term of Reynolds stress which is responsible for transferring stream-wise energy to the wall normal direction. Whether Reynolds stresses disappear entirely or are reduced to near zero is a matter of debate.[11] Reynolds stresses are vital in Newtonian flow to maintain turbulence in the face of viscous dissipation. If they are reduced to near zero, turbulent energy should in theory be dissipated and the flow should re-laminarise. The diagram in Figure 7 shows that this is not the case, as the frictional profile of drag reducing flow is bound between the lower Prandtl-Karman law and the upper MDR asymptote. At the MDR the friction is much less than for Newtonian turbulent flow, however, it is still much high than for laminar flow. There must, therefore, be stress from another source which maintains turbulence in flow and generates this distinct

turbulent flow regime described in Figure 7. The only alteration to the system is the addition of polymer and so in the drag reducing regime Reynolds stresses are replaced by polymer stresses which now distribute energy through the system. Whilst it is not currently possible to measure polymer stresses, they can be estimated by comparing the difference between total stress of the system and the effects of wall shear and Reynolds stress. Indeed, at MDR it has been found that polymer stress makes up around 40% of the total stresses in a system.[11] This demonstrates that the addition of a tiny amount of polymer can influence the overall statistics of turbulence and the huge decreases in drag/friction can be rationalised.

Drag reducing polymers increase a fluids mean velocity and so the change in velocity profile relative to a Newtonian fluid is also important (Fig. 8). In the buffer region of turbulent flow (Fig. 6) there is a transition between a linear and log velocity profile where velocity increases at a greater rate than the following log region.[9] It has been shown that the polymer action is most prominent in this buffer region.[12] In particular, polymers disrupt a critical part of the turbulence cycle by reducing vortices dissipating energy at the wall and decreasing the number of turbulent bursts to the core.[11, 12] Drag reducing polymers, therefore, act to widen the buffer region (Fig. 8) meaning the average velocity in turbulent pipe centre is shifted to a higher value. At low polymer concentration the log region then proceeds at a parallel gradient to the original log law (Fig. 8, red line). At higher concentrations (Fig. 8, green line) MDR is reached and the gradient of the log region is also increased.[9] Drag reducing polymers have no effect on the viscous sub-layer closest to the wall.

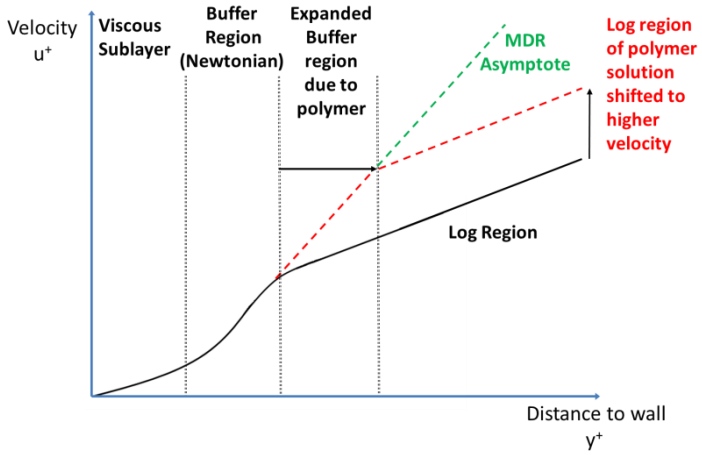

Figure 8: Demonstrating the increase in buffer region for a; Newtonian fluid (black), a dilute polymer solution (red) and a polymer solution at higher concentration (green).

1.3.2. Modelling of drag reduction

The exact mechanism by which polymers disrupt the turbulence cycle in the buffer region is unknown. Attempts to accurately model this can be divided into two themes. In the first, polymer effects are considered as an increased viscosity whilst the second considers polymer elastic effects most important. Though both theories go a long way to explain drag reduction processes and predicting both the onset and MDR, neither is currently able to give a complete description.

1.3.2.1. Viscous model

The viscous model was first suggested by Lumley in 1969,[13] more recent work by Den Toonder et al.[10] and L'vov et al.[14] has progressed the area. The principle is that, upon experiencing high shear rates in the turbulent buffer layer, polymer chains become fully extended and the relative viscosity of a polymer increases by up to 1 x 10^4 times.[13] Full polymer extension is only possible when the strain rates are very high and when strain is purely axisymmetric.[13] Full extension is not observed in a rotating strain field where polymers relax back to their equilibrium conformation before this can occur. It was argued by Lumley that both conditions are satisfied at the boundary of the buffer layer where strain rates are highest. When polymers extend and align with the flow, increased viscosity is seen perpendicular to the flow direction (Fig. 9).[10] This suppresses Reynolds stresses; the buffer thickens and the transfer of momentum towards the wall decreases. Using this model the onset of drag reduction can be explained as the point where enough polymer chains are fully extended and able to increase the relative viscosity. The MDR is more difficult to explain as, unlike viscosity, it is shown to be insensitive to polymer type and properties. The model cannot as yet satisfactorily explain MDR.

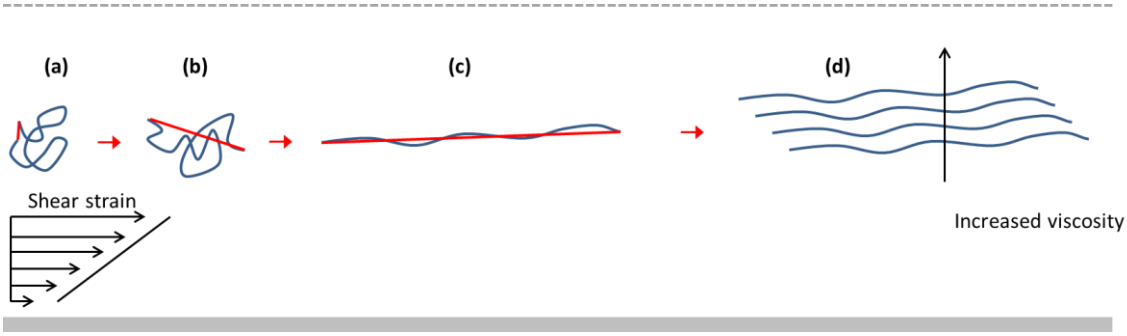

Figure 9: Viscous model; **a)** polymer experiences shear strain from flow in pipe; **b)** it is partially stretched; **c)** it becomes fully stretched if strain rate is large; **d)** polymers align with the flow - increase relative viscosity perpendicular to flow direction.

1.3.2.2. Elastic model

When developing the elastic model, De Gennes and Tabor contended that strain in turbulent flow is insufficient to fully extend polymers and that partially stretched polymers do not provide high enough viscosity to influence turbulence.[15] It was argued that polymers actually influence turbulent flow due to their ability to store elastic energy.

As in the viscous model (Section 1.3.2.1), stretching of polymer chains, which begins when inverse strain rate equals polymer relaxation time, is important. The elastic model states that as polymers stretch they store kinetic flow energy as elastic energy. If the elastic energy stored is equal to the kinetic energy of turbulence the polymer can influence turbulent flow (Fig. 10). However, for this to occur, stored energy must be on a scale higher than the Kolmogorov scale (point at which turbulent energy is dispersed by viscous forces). In effect, the Kolmogorov cascade (Fig. 11) is cut short and the buffer layer is thickened therefore decreasing drag.

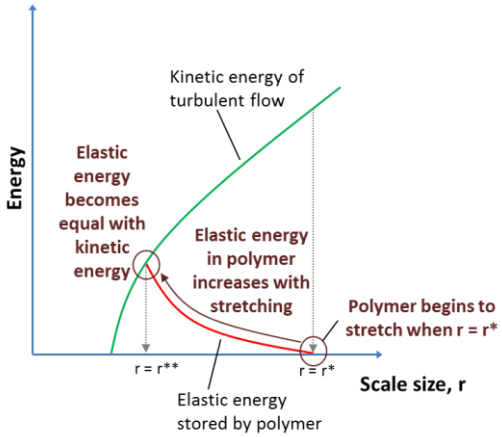

Figure 10: Increase in elastic energy stored as the polymer stretches (red line), and the decrease in kinetic energy as the turbulence moves down Kolmogorov cascade (green line).

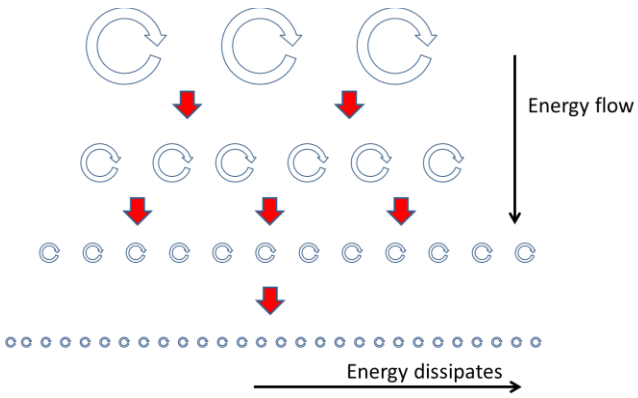

Figure 11: Kolmogorov energy cascade for turbulent energy. Energy flows from large eddies at the top continuously decreasing in size until reaching a scale where energy is dissipated by fluid viscosity.

Numerical modelling by Ptasinski et al. agreed that elastic energy in turbulent flow is stored by the polymer stretch and dissipated through polymer relaxation.[11] Further investigation by Sreenivisan and White concluded that both onset and MDR could be explained using the elastic model.[6] It was proposed that onset occurs when kinetic energy of turbulence and elastic energy stored by the polymer become equal. Moreover, MDR is the point at which even a very small amount of polymer stretching stores elastic energy on a comparable scale to kinetic energy.

1.3.2.3. Evidence for models

It should also be noted that although the two models are viewed separately, the elastic model could also be interpreted in viscous terms, as the point at which the Kolmogorov scale ends is the point at which the turbulent energy is dispersed by viscous fluid forces. Evidence for the elastic model comes from the observation that injection of polymer directly into the centre of the pipe causes immediate drag reduction.[16] Whilst this can be explained by the elastic model, immediate onset is not possible using the viscous model where polymers must move to the buffer layer and fully expand before onset can occur. On the other hand, studies by Virk using fully extended polymers do show immediate onset,[17] and Den Toonder argues that the drag reducing efficiency (DRE) of surfactants and fibres, which do not store elastic energy, is further evidence for the viscous model.[10] Den Toonder et al. used both experimental and numerical analysis to study the viscous and elastic model.[10] It was concluded that the viscous model provides the closest explanation of drag reduction and no elastic effect is seen. Though the elastic model used by Den Toonder was ineffective at explaining his experimental observations, it is important to note that it only takes into account elongational extension of polymers whilst neglecting an elastic modulus for shear.

1.3.3. Effect of molecular structure on polymer drag reduction

Although only a partial understanding of the mechanism of drag reduction has been demonstrated, it is still important to make correlations between experimental data and polymer properties. An early review by Lumley stated that for a polymer to be a successful DRA it must be linear, have a large number of monomer units (N) and be able to expand.[13] Although the consensus on key properties is still uncertain, more recent work has extended and refined this list. The study of polymer properties is complicated both by the difficulty of synthesising ultra-high molecular weight (UHMW) polymers in a controlled manner and mechanical degradation of polymer samples during testing, the effect of which is difficult to factor.

1.3.3.1. Polymer size

Whilst certain aspects of drag reduction (e.g. MDR asymptote) are insensitive to polymer type, the chemical structure is still very important in terms of polymer-solvent interactions as well as polymer-polymer intra- and intermolecular interactions. Despite often discussing 'UHMW polymers', it has been established that molecular weight (MW) is not the key factor in a polymer's efficiency. Instead, polymer size is considered most important, though it is unclear which definition of size correlates with DRE.[18] It may simply be the number of monomer units (N),[19] or a property of polymer size in solution. This could be represented by; end-to-end distance (average distance between chain ends), radius of gyration (R_g, root mean squared distance of polymer chain to its centre of mass) or hydrodynamic volume (V_h, volume occupied by the polymer in solution) (Fig. 12).[20]

McCormick et al. used an ionic polymer in solutions of varying ionic strength to determine the effect of V_h. They observed that for a polymer of constant MW the DRE increased with V_h.[20] When three polymers of similar MW were manipulated to give the same volume fraction by altering polymer concentration, a similar DRE was observed. This work also suggested a minimum MW boundary for drag reduction, something which was observed by Zakin and Hunston whilst studying hydrocarbon soluble polymers.[18] The effect of molecular weight distribution (MWD) was described and it was postulated that only a very small HMW portion of polymer contributes to drag reduction.[21]

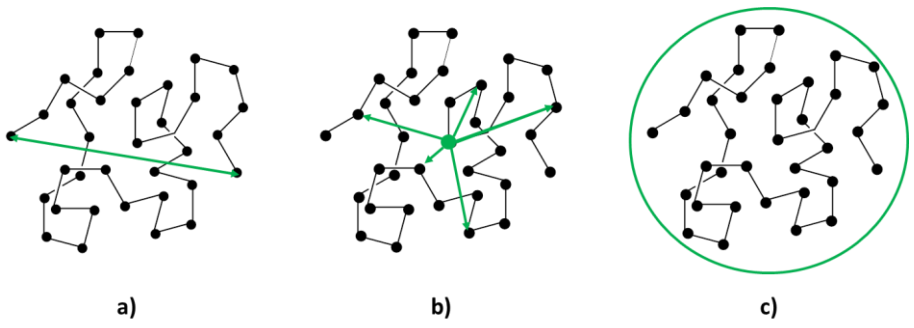

Figure 12: Parameters describing polymer size in solution; **a)** End-to-end distance; **b)** Radius of gyration (R_g); **c)** Hydrodynamic volume (V_h).

Due to this dependence on polymer size, associations between polymer chains may potentially contribute to drag reduction. The formation of polymer associations in such dilute (ppm) solutions seems unlikely, however it was proposed that such aggregations are encouraged by high shear flow.[22,23] To study this, McCormick et al. synthesised a range of polyacrylamide (PAM) co-polymers with varying hydrophobic percentage. In aqueous solution, increased

hydrophobicity promotes aggregation and enhanced DRE was observed as hydrophobic percentage was increased.[20, 24] The same group then co-polymerised acrylamide with various amounts of ionic co-monomer. Increasing ionic content allowed greater intramolecular interactions, inducing polymer chains to collapse and rapidly decreasing V_h. As expected, this reduced DRE, further supporting the importance of V_h. This work demonstrated that interactions between polymer chains only benefit DRE if they increase the volume of the polymer in solution.[20] These observations were supported by the correlation of DRE with the aggregation of HMW poly(ethylene oxide) (PEO) in solution, measured using dynamic light scattering (DLS). When $MgSO_4$ was added to disrupt the aggregations, DRE was greatly reduced.[25] The use of polymer aggregations could also have positive implications on mechanical stability of a polymer as secondary interactions between polymer chains can be broken and reformed without damaging the polymer backbone, *vide infra*.[26]

As polymer dimensions in solution are highly influenced by the interaction with solvent it is expected that polymers will be most effective in good solvents, where they are most expanded. This was confirmed using polystyrene, with toluene as a good and toluene/isooctane as a poor solvent.[27] Furthermore, the effect of polymer on the solvent may also be an important factor. Water is a fluid with a highly order structure. It was suggested by Hlavacek et al. that polymer domains can surround regions of solvent and dampen the formation of vortices.[28] Brostow et al. also proposed a model involving reduction of turbulence by the protection of solvent within polymer domains.[3, 29] Experimental studies by McCormick using urea, known to 'break' the structure of water, further supports the argument for the importance of water structure.[20]

1.3.3.2. Polymer structure and flexibility

It was originally proposed that polymers must be linear to be effective DRAs.[13, 30] This hypothesis correlates with observations described above, as branching is known to decrease the V_h of a polymer at a constant molecular weight. Despite this, both branched and graft polymers with HMW have since shown effective drag reducing properties.[31,32]

The equilibrium conformation of a polymer is dependent on its flexibility which derives from the chemical nature of the backbone and side-chains. Early studies supporting both the viscous and elastic model state chain expansion of flexible polymers is necessary for drag reduction.[13,15] As discussed, however, both non-extendable fibers and surfactants have been shown to cause drag reduction so this cannot always be the case.[33,34] Furthermore, it was observed that drag reduction of rod like polyelectrolytes (extended by the addition of salt) are

more effective at low flow rates than flexible analogues.[35] These conflicting observations may necessitate different models for different conditions. It is possible that flexible polymers are more effective at higher shear because they require these conditions to fully expand and increase V_h. This could suggest that the most important factor, irrespective of flexibility, is the ultimate size of the polymer once it has been expanded to its maximum dimensions.[36]

1.3.3.3. Mechanical degradation

A large polymer size is necessary for a polymer to effectively reduce drag, however, it is also widely known that HMW flexible synthetic polymer chains are highly susceptible to mechanical degradation.[37] A polymer chain breaks if the tensile stress on any one section of the chain is greater than the bond strength. For a C-C bond this value is 2.5-13.4 nN.[38] As polymers degrade their MW approximately halves as described by the mid-point chain scission theory.[39] Stress builds from chain end reaching a maximum in the centre and therefore breakage occurs at the mid-point. In turbulent flow, polymers experience very high strain and breakage can occur within seconds, rendering the polymer solution ineffective for drag reduction. Resistance to mechanical degradation is therefore as important as the DRE when testing suitability of polymer solutions.[32] The general relationship of increased degradation with polymer MW has been widely described.[40] Recently, both experimental and theoretical tools have been used to determine the exact effect of MW on degradation.[41, 42] Critical strain rate, E_c, is used to describe how easily a polymer chain is broken and the dependence of E_c on MW was shown to change under different flow conditions. In pure elongational flow the relationship is $E_c \propto M_w^{-2}$, in a mixed flow of elongational and shear strain the relationship is $E_c \propto M_w^{-1}$.[40] The exact flow conditions experienced in turbulent pipe flow are not obvious, however, at both extremes it is clear that chains rapidly become easier to degrade as their length increases. Other relationships have also been described. Kenis observed the relative stability of PAM over PEO due to the presence of side chains.[43] Zakin and Hunston proved the degradation of polystyrene chains was much greater in poor than good solvent.[27] Furthermore, faster degradation at lower concentration and a minimum MW threshold were also demonstrated.[44] When the polymer MW is constant, the rate of degradation increases with higher strain rate.

In addition to chain degradation, Hanratty considered loss of DRE due to the breakage of molecular associations.[42] Using partially hydrolysed polyacrylamide (HPAM), which is known to associate, large decreases in DRE were observed without a decrease in polymer MW (measured using size exclusion chromatography, SEC). When this work was repeated with a less associating polymer (PAM) similar results were found. However, in this case loss in DRE did

sometimes coincide with a drop in MW and it was concluded that both effects may be important. It may be expected that if the break-up of polymer associations was to occur there may be some recovery in DRE as molecular associations could reform.

1.3.4. Current polymer systems

A wide range of polymers systems, both natural and synthetic, are discussed within the patent literature, however, those studied in more depth are restricted to relatively few.

1.3.4.1. Natural

Polysaccharides are the most common biopolymers studied for drag reduction. The first polysaccharide discussed in the literature was carboxymethyl cellulose (CMC) whilst guar gum, a plant derived polysaccharide, has been most often used in oil field applications. Hydroxyethyl cellulose (HEC) and xantham gum (XG) have also been studied and used commercially (Fig. 13).[30]

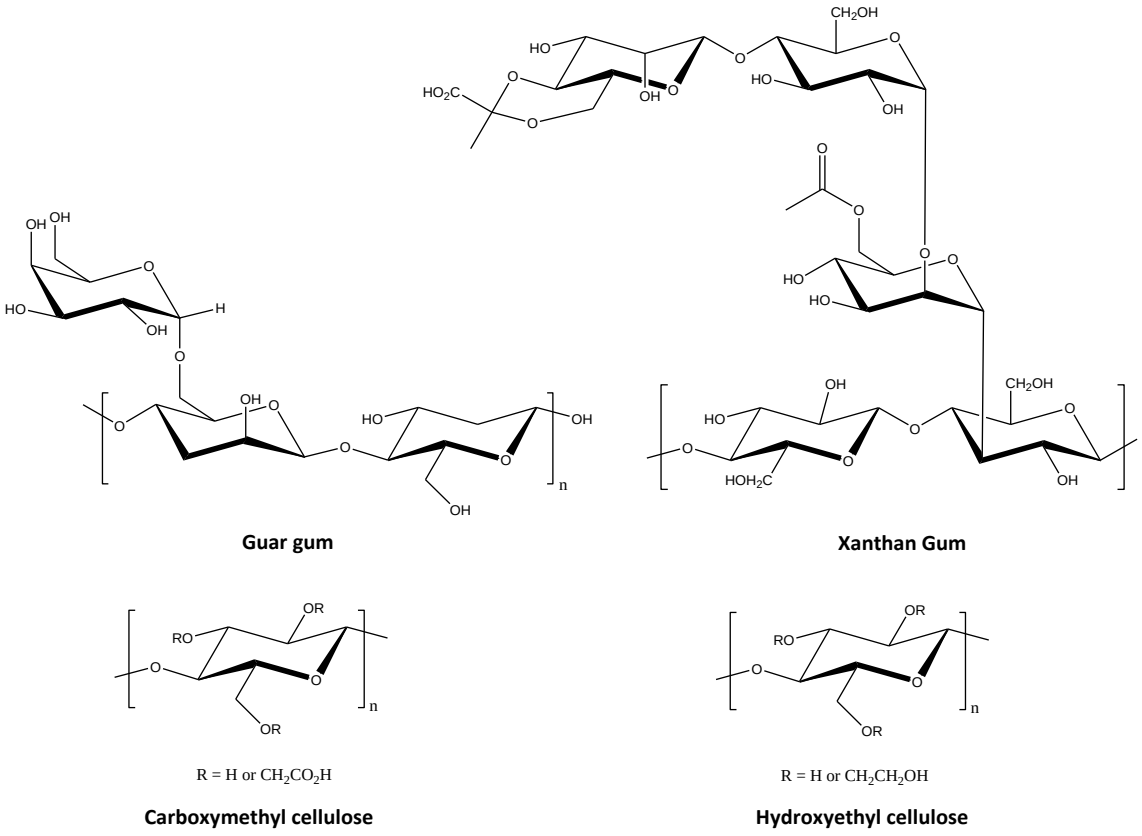

Figure 13: Natural polymers used as DRAs.

Of these natural polymers, XG demonstrates the best shear resistant properties, possibly due to its fully rigid back-bone when compared with semi-rigid CMC, HEC and guar gum. Furthermore, by forming a PAM-*co*-guar gum graft co-polymer, both shear and biodegradation

can be enhanced.[31, 45] Biopolymers have the benefit of a low environmental impact as they are easily broken down to non-toxic by-products. Unfortunately, high susceptibility to biodegradation has a negative impact on the DRE which limits their commercial use. DNA and proteins can also act as drag reducing polymers however their properties depend strongly on conformation and they are ineffective in their denatured, collapsed form.[46]

1.3.4.2. Synthetic

Synthetic polymers are the preferred materials for drag reduction. They can be easily synthesised to UHMWs and they show resistance to biodegradation. PEO is a flexible synthetic polymer which has been shown to demonstrate very high levels of DRE (Fig. 14). It has been widely studied and used commercially; however, it is extremely sensitive to mechanical degradation in turbulent flow. This susceptibility to degradation makes PEO unsuitable for many applications and generally it is restricted to single use applications, e.g. fire-fighting or snow making.

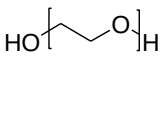

Poly(ethylene oxide)

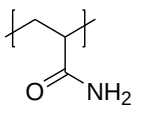

Polyacrylamide

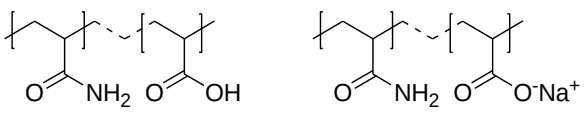

Hydrolysed Polyacrylamide

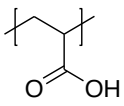

Poly(acrylic acid)

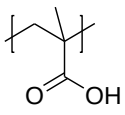

Poly(methacrylic acid)

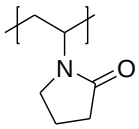

Poly(vinyl pyrrolidone)

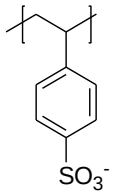

Sulfonated polystyrene

Figure 14: Common synthetic, water-soluble polymer DRAs.

Poly(acrylic acid) (PAA), poly(methacrylic acid) (PMAA), poly(vinyl pyrollidone) (PVP) and sulphonated polystyrene also show drag reducing properties (Fig. 14). The most common commercial DRA is PAM and its partially hydrolysed analogues (HPAM, Fig. 14). PAM shows high DRE, enhanced mechanical stability relative to PEO and greater biodegradation resistance when compared with polysaccharides.

1.3.4.3. Current polyacrylamide systems

PAM/HPAM, for use as a DRA, is synthesised using inverse-emulsion, free-radical polymerisation, a method which is used widely on an industrial scale due to its relative insensitivity to impurities and tolerance to a range of monomer functionalities. Though

effective and economical, the health and environmental impact of current drag reducing systems provides major concerns. The acrylamide monomer is carcinogenic and mutagenic and was classified a 'Substance of Very High Concern for Authorisation' under recent REACH (Registration, Evaluation, Authorisation and Restriction of Chemicals) legislation imposed in Europe. Though PAM is non-toxic to humans, its primary amine side-chains are protonated under certain conditions and the resulting cationic polymer is highly toxic to aqueous organisms. The insensitivity of PAM to biodegradation leads to accumulation at point of use, a particular concern for oil field applications where solutions may be pumped deep underground and risk entering the water board. Post-use degradation could provide a way to reduce the impact of accumulation. By the insertion an azo group into a PAM chain, Bismarck and Kot showed that a polymer, as well as being an effective DRA, could also be broken down with elevated temperatures after use.[47] For oilfield applications, polymer emulsions are used without purification and significant quantities of oil and surfactant are released into the environment. Commercial polymerisation of PAM often uses a light paraffin oil phase which is flammable and toxic in aqueous environments. Moreover, there is limited evidence that non-ionic surfactants disrupt the endocrine systems of aqueous organisms. Irrespective of whether this does occur, bioaccumulation of surfactants is undesirable. Their ultimate fate is difficult to determine due to their combined lipo/hydrophilic properties which give them different activity to other molecules of similar size. Moreover, thermal radical initiators require high polymerisation temperatures and reactions at lower temperature would greatly reduce energy consumption and environmental impact of the process.

1.4. Improving mechanical stability

1.4.1. Branched polymers

Reducing the degradation of polymer chains remains a very important issue. Little et al. observed that branched polymers can be effective DRAs whilst also reducing degradation by shear flow.[32] Branched polymers can take a variety of forms and therefore exhibit a distinct set of properties compared to their linear analogues. Dendrimers (Fig. 15) are perfectly branched structures.[48] Due to their high functionality and contracted globular structure, they display lower viscosity in solution and melt with potential applications as rheology modifiers.[49] They also show increased solubility and a lower glass transition temperatures.[48] However, synthesis of dendrimers is highly complicated, involving protection and deprotection steps for each monomer addition which limits their commercial use.

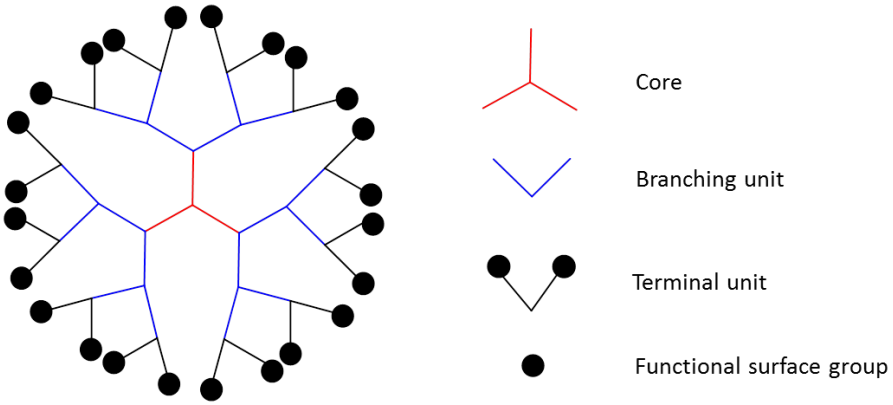

Figure 15: Schematic diagram demonstrating the structure of a dendritic polymer.

Hyperbranched polymers were developed to allow access to dendritic properties without such costly synthesis. Branching is not perfect and each monomer may introduce a branching, linear or terminal unit (Fig. 16). Exact rheological properties of hyperbranched materials depend on the degree of branching (0 = linear and 1 = perfect branching).

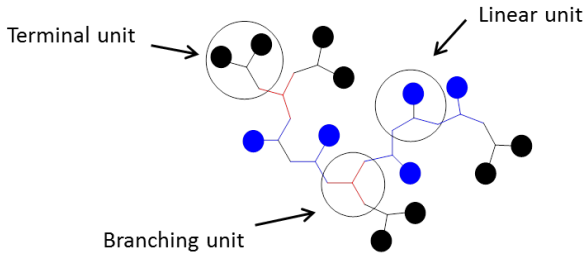

Figure 16: Schematic diagram demonstrating a hyperbranched polymer structure.

Star polymers are the most simple branched material and can be considered as a first generation dendrimer (Fig. 17).[50] The structure involves several linear macromolecular 'arms' attached to a single central core. The star is termed regular if every arm is the same polymer type or miktoarm if the polymer arms are different. Miktoarm can also refer to multiple polymer arms attached to a macromolecular core at one (Y-shaped) or both (H-shaped) chain ends (Fig. 17).[51] Despite lower levels of branching, stars share some properties with dendritic/hyperbranched materials.

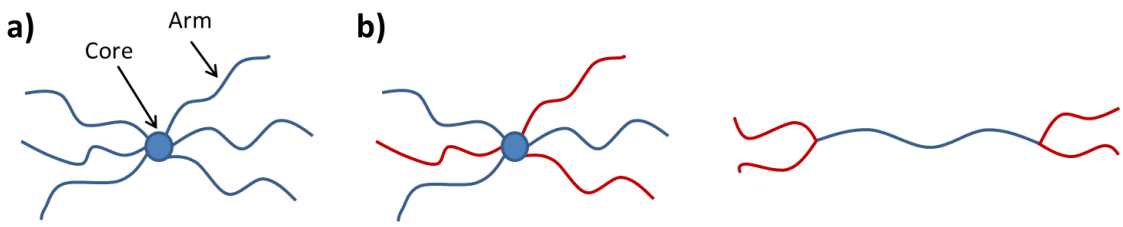

Figure 17: a) Regular star polymer; **b)** Miktoarm star polymer.

Little et al. synthesised a branched PAM DRA using ceric ion redox polymerisation and a core molecule containing multiple hydroxyl groups (Fig. 18).[32] A clear improvement in resistance to mechanical degradation was seen when compared with linear PAM and PEO. It was proposed that star polymers were able to distribute shear forces through all of the arms, decreasing the stress on each individual chain.[32] Furthermore, chain scission may occur through cleavage of individual arms with a much smaller impact on MW. The Ce(IV) redox technique was also used by Singh et al. to graft PAM to a variety of polysaccharides.[31, 45] When compared with un-grafted PAM chains these polymers demonstrated greater resistance to degradation in shear flow. Recent findings indicate that whilst a small number of HMW grafted chains do decrease shear degradation, this effect diminishes as grafting percentage increases and chain length decreases.[39] It was also suggested that a large percentage of grafted chains may increase the tensile stress experienced by the polymer backbone, therefore increasing degradation in some cases.

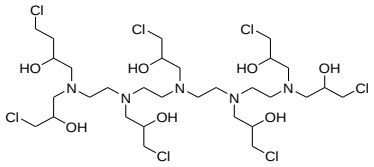

Figure 18: Core molecule used by Little et al.[32]

Agarwal et al. hypothesised that if star polymers contain a linear core, the branched arms would not break off individually.[38] Instead, tensile stress would build from the chain ends and mid-point scission would occur in the core, halving the polymer MW. To examine this, a poly(methyl methacrylate) (PMMA) star was synthesised with a fused core in order to distribute accumulated core stress through several bonds (Fig. 19). By preventing cleavage in the core, only degradation of individual arms could occur. Degradation of this fused core macromolecule was compared with that of a linear core macromolecule by applying an elongational force using a cross-slot rheometer; the resulting polymer MWD was measured using SEC.

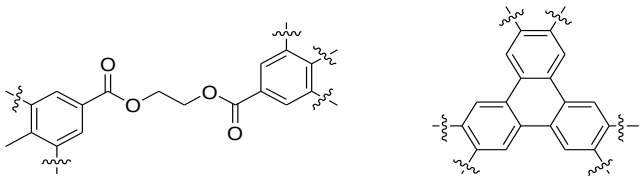

Figure 19: Linear and fused core molecules using by Agarwal.[38]

Unexpectedly, SEC analysis demonstrated consistent arm degradation for both the fused and linear core macromolecules, even at reduced strain rates. This may be explained by conformations adopted by star polymers in dilute solutions which may reduce stress in the core (Fig. 20). Furthermore, it was also proposed that the coil-stretch transition may occur individually for each arm resulting in reduced core stress.

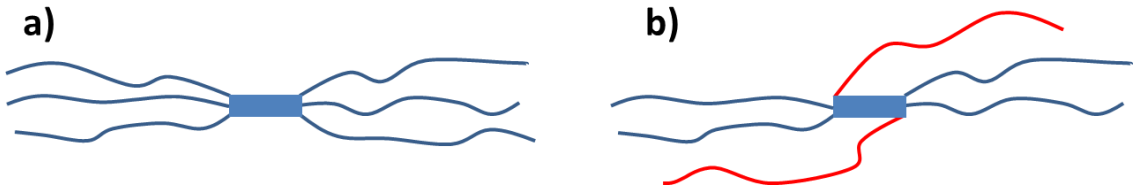

Figure 20: Possible conformations for star molecules under stress showing; **a)** High strain in core; **b)** Low strain in core.

1.4.2. Synthesis of star polymers

Star polymers are synthesised via one of two main methods: core-first (individual chains grown from sites on a multi-functional initiator) or arm-first (linking of several linear polymer arms to a central core). Whilst free-radical polymerisation of vinyl monomers provides around 50 % of all commercial polymers, the high concentration of radicals in the system prevents control over polymer MW or MWD. Furthermore, is it not possible to access block co-polymers or complex topologies such as combs or stars. Free-radical polymerisations are characterised by slow initiation and fast termination processes and radicals are produced continuously during the reaction, usually using radical initiators such as peroxide or azo compounds which are selected for their long half-lives. The chains propagate and terminate either through bimolecular combination or disproportionation reactions. When combined with chain transfer to monomer or solvent, control over polymer architecture becomes impossible.

Development of living anionic polymerisation by Szwarc et al. provided the first method to allow control over the polymerisation of vinyl monomers.[52] In contrast to radical polymerisation, this method involves fast initiation and no termination in the absence of oxygen and moisture. Propagation occurs at a much slower rate than free-radical polymerisation and continues until the monomer is entirely consumed. This allows the synthesis of HMW polymers with near perfect control. To consider a polymerisation 'controlled' it must fulfil the following criteria: 1) linear relationship between conversion and time; 2) predictable MW and linear increase with conversion; 3) narrow MWD; 4) 'Living' chain ends which can be reactivated to chain extend or form block co-polymers. Burchard first used living anionic polymerisation for the synthesis of star polymers using styrene and divinyl

benzene.[53] Whilst a very useful technique in polymer synthesis, and widely used commercially in the synthesis of rubbers, living anionic polymerisation requires extensive purification of reactants to remove impurities which may cause termination. Furthermore, it is limited to a small number of monomers due to intolerance to most monomer functionality.

1.5. Controlled radical polymerisation

The principles of fast initiation and slow propagation developed with living anionic techniques directly oppose those of free-radical polymerisation. Despite this obvious conflict, control over radical polymerisation is highly desirable to allow access to a larger range of polymer functionality. In order to maintain the living characteristics in radical polymerisation several controlled radical polymerisation (CRP) techniques have been developed.[54, 55]

The key to controlled radical polymerisation methods is to maintain a very low concentration of radicals in solution, greatly reducing termination. A low radical concentration is achieved via a dynamic equilibrium established between active and dormant chains. If the equilibrium favours the dormant species the radical concentration is low. Chains are reversibly deactivated so the dormant chain can be reactivated and propagate before deactivation back to the dormant state. Fast initiation is important in order to simultaneously initiate polymer chains which are rapidly trapped in the activation/deactivation process. This allows the slow propagation of each chain at approximately the same rate until the reaction is complete. Whilst in a truly living process the reaction concludes upon exhaustion of monomer, termination can never be completely avoided for a radical polymerisation.[55]

The reversible deactivation equilibrium is achieved through one of two mechanisms. One involves trapping the propagating chain in an activation-deactivation process with an equilibrium constant highly shifted towards the dormant species (Scheme 1). The other involves a degenerative transfer process in which the equilibrium reversibly moves a transfer agent between active centres, capping one chain whilst simultaneously releasing another to propagate (Scheme 2).[54]

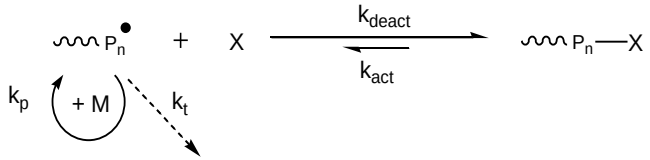

Scheme 1: Activation-deactivation process.

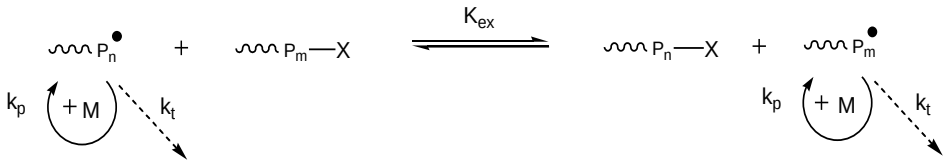

Scheme 2: Degenerative transfer process.

1.5.1. Nitroxide Mediated Polymerisation

The first truly controlled radical technique was a deactivation/activation process developed by Georges et al., in 1993, termed Nitroxide mediated polymerisation (NMP).[56] A nitroxide containing molecule, 2,2,6,6-tetramethyl-1-piperidinyloxy (TEMPO, Scheme 3), was used as a stable or persistent radical to reversibly trap propagating chains allowing the controlled polymerisation of styrene.[56] A monomer conversion of 90 % was achieved after 69 h and analysis of the resulting polystyrene demonstrated narrow polymer dispersity ($Đ$ < 1.3). This control was possible due to the strong bond formed between TEMPO and the radical chain end which allowed an equilibrium to be established favouring the dormant species. Control was aided by the persistent radical effect (PRE) which utilises the ability of the stable/persistent radical to deactivate the propagating chains without reacting with itself. Termination is inevitable early in the reaction due to a high proportion of radicals. The persistent radical does not terminate and the loss of some propagating chains leads to an accumulation of persistent radical relative to the chain ends.[54] This shifts the equilibrium further towards the dormant species and reduces the concentration of radicals in the solution. Termination becomes less frequent as the reaction proceeds, which increases control (Scheme 3). Unfortunately, the stability of the dormant species necessitates high temperatures (120 - 150 °C) and long reaction times (69 h) to reach high yields. Polymerisations with less active monomers such as acrylates were unsuccessful under these conditions.

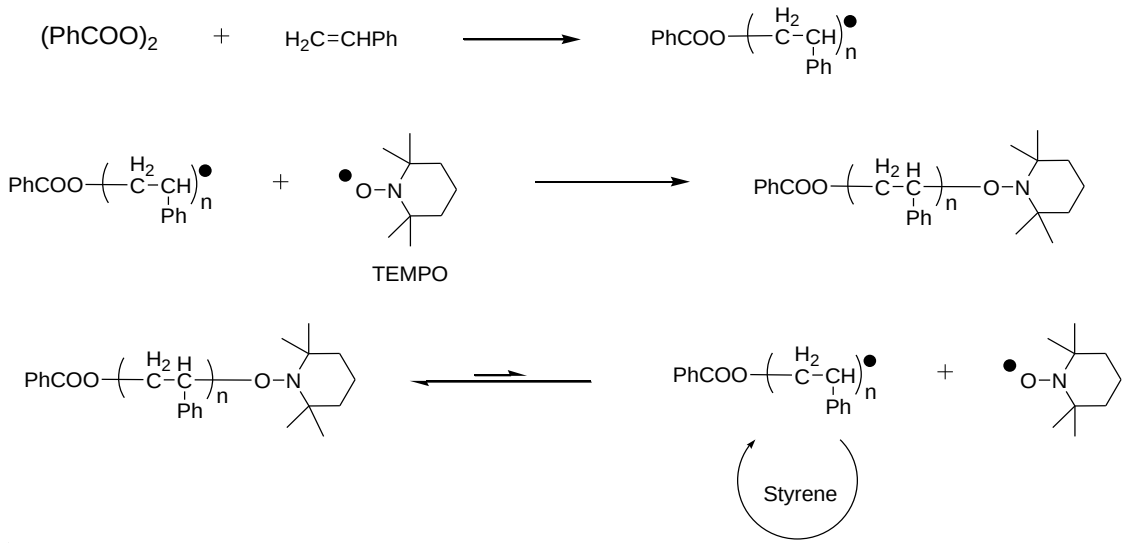

Scheme 3: Mechanism of nitroxide mediated polymerisation.

Attempts to increase the activity of NMP reactions have focussed on reducing the strength of the –C-O-N- link whilst maintaining control of the reaction. This was first achieved using bulky TEMPO derivatives however aliphatic nitroxides without a close resemblance to TEMPO have since proven to be most effective (Fig. 21).[57]

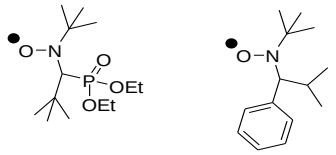

Figure 21: Modified nitroxide containing molecules for NMP.

Early examples of star polymer synthesis using CRP techniques were demonstrated by Hawker using the core-first method. [58] A tri-functional molecule (Fig. 22) was synthesised containing three nitroxide groups which could be initiated at high temperatures allowing polymerisation of styrene in a controlled manner. More recent examples include the synthesis of 3-armed Poly(acryloyloxyethyl 2-bromoisobutyrate)-*co*-poly(*n*-butyl acrylate) star to HMW (≈ 1 x 10^5 g mol^{-1}).[59]

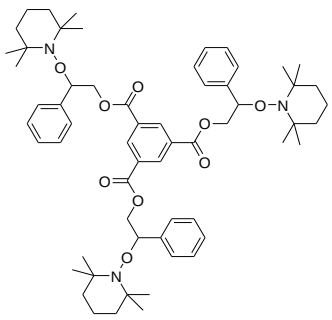

Figure 22: Tri-functional nitroxide containing molecule for synthesis of star polymer using NMP.

1.5.2. Atom Transfer Radical Polymerisation (ATRP)

Perhaps the most common reversible deactivation radical polymerisation (RDRP) technique is ATRP developed simultaneously in 1995 by Matyjaszewski and Sawamoto.[60,61] ATRP is an activation-deactivation process based on atom transfer radical addition (ATRA), a common C-C bond forming reaction in organic synthesis. ATRA involves the transfer of a halogen atom from an alkyl halide to a metal centre, oxidising the metal and generating an organic radical. The radical can be quickly deactivated by the reverse halogen transfer and reduction of the metal. When combined with an activated vinyl monomer, an alkyl halide can be used to initiate a polymer chain via inner sphere electron transfer (ISET). This chain can then propagate, terminate or be deactivated by halogen transfer from the higher oxidation state metal which acts as a persistent radical (Scheme 4).

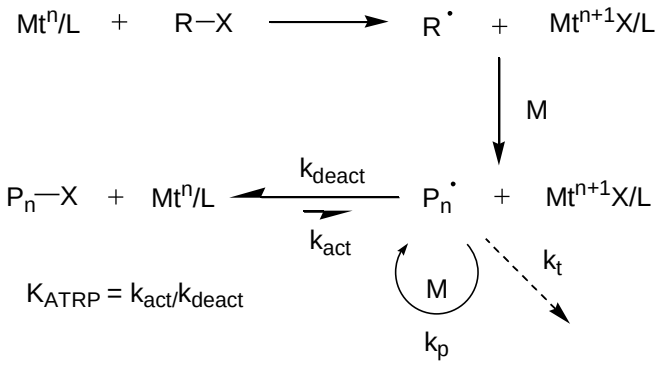

Scheme 4: Mechanism of ATRP.

To catalyse ATRP any transition metal salt which is able to expand its coordination sphere whilst reversibly altering its oxidation state by +/- 1 can be used. Catalysts based on; Fe, Ru, Ni and Pd all allow controlled polymerisation, however, the most efficient and commonly used is Cu. A multi-dentate nitrogen ligand which can stabilise Cu(I) and Cu(II) species is also necessary (Fig. 23). Counter-ions bound to the metal centre are almost exclusively halides (Cl, Br or I) and the initiator requires a C-Halogen bond, activated by its proximity to an α-carbonyl, phenyl or cyano functional group (Fig. 24). The activity of the initiator derives mainly from the C-Halogen bond dissociation energy as the halogen moves directly from initiator to metal via an atom transfer mechanism (rate of dissociation, I > Br > Cl).[62] The stability of the generated radical must also be considered, both in terms of halide substitution (rate of 3° > 2°) and adjacent stabilising groups.

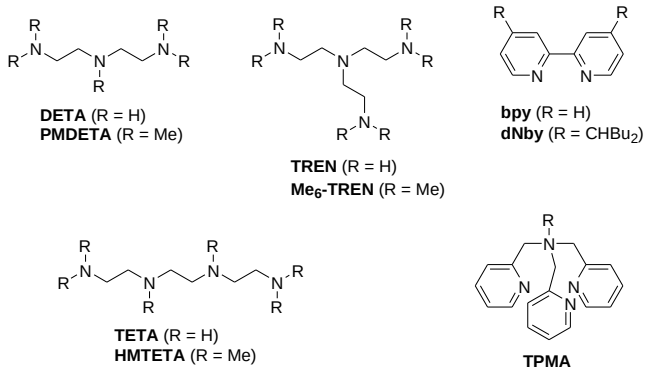

Figure 23: Common ligands used in ATRP and SET-LRP.

The most important factor for control over ATRP reactions is not the overall quantity of metal catalyst in the system, but the ratio between the activating (lower oxidation state) and deactivating (higher oxidation state) forms. By subtly altering the reaction components, for example using a ligand which preferentially stabilises Cu(I) or Cu(II), the rate constants for activation (k_{act}) and deactivation (k_{deact}) as well as the overall equilibrium constant (K_{ATRP} = k_{act}/k_{deact}) and propagation rate can be adjusted. Polar solvents promote dissociation of a halide ion from CuX_2/L which decreases the concentration of deactivator in solution. This decrease of k_{deact} increases the radical concentration and propagation rate. In a non-polar solvent more control is observed as K_{ATRP} more strongly favours the dormant species.[63,64]

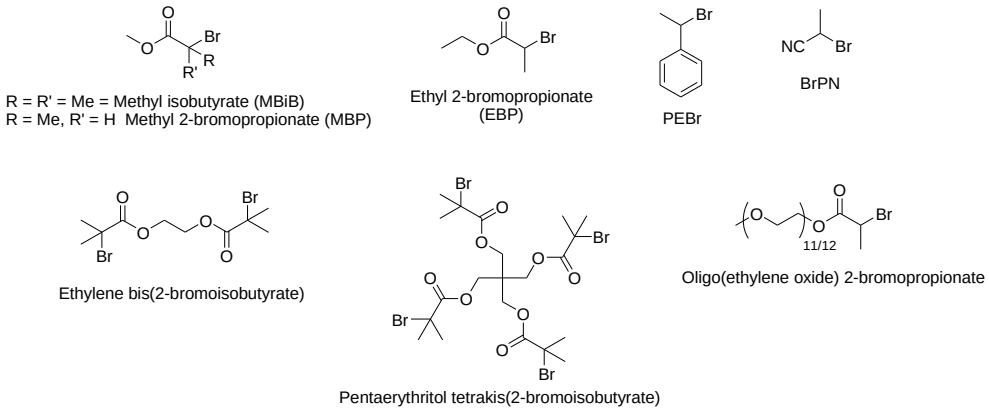

Figure 24: Common initiators used in ATRP and SET-LRP

The versatility of ATRP allows its application to a wide variety of monomers including; (meth)acrylates, styrenes, (meth)acrylamides and acrylonitrile. Unprotected acids and monomers which strongly coordinate to the metal catalyst (e.g. N-vinyl pyrrolidone) are unsuitable for this method. The commercial availability of ATRP components makes it potentially attractive as an industrial procedure. For this to become a realistic possibility the original method was improved, both in terms of catalyst handling and catalyst loading.

Due to their instability towards oxidation Cu(I) salts are difficult to handle, particularly on a large scale. Early modifications, known as Reverse and Simultaneous Reverse and Normal Initiation (SR&NI) ATRP, utilised more stable Cu(II) salts and generated Cu(I) in-situ using a radical initiator (Scheme 5).[65,66]

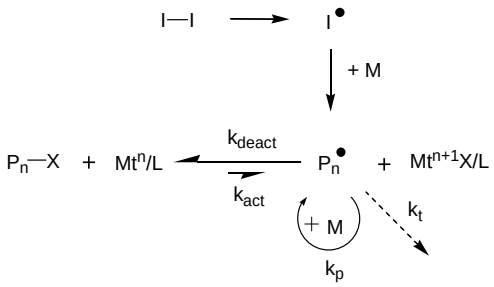

Scheme 5: Mechanism of SR&NI ATRP.

Loss of control due to parallel radical initiation led to the introduction of reducing agents to generate Cu(I) from Cu(II) in a process termed activators generated by electron transfer (AGET) ATRP. Reducing agents, which are themselves unable to initiate polymerisation such as Cu(0), $Sn(Et)_6$, ascorbic acid or triethylamine, were used in place of a radical initiator (Scheme 6).

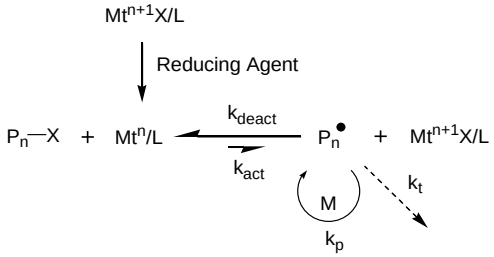

Scheme 6: Mechanism of AGET-ATRP.

In early ATRP reactions high copper loadings were necessary due to an effect similar to the PRE. As propagating radicals undergo termination, Cu(II) accumulates in the system shifting the equilibrium towards the dormant chains and reducing Cu(I) concentration. If the copper loading is low Cu(I) can be entirely consumed in this process leaving insufficient for re-activation and terminating the reaction at low conversion. High catalyst loadings are expensive and metal salts are difficult to recover and recycle from the reaction mixture. Cu is regarded as toxic and commercial products require extensive purification to remove traces. Fortunately, catalyst loading can be reduced as long as a high ratio of Cu(II) to Cu(I) is maintained whilst sufficient Cu(I) remains in the system for reactivation. By using an excess of radical initiator, initiators for continuous activator regeneration (ICAR) ATRP allows regeneration of Cu(I) through reduction Cu(II) during the reaction (Scheme 7).[67] In this method catalyst levels can be hugely reduced whilst maintaining Cu(I) activator in the system. Again, the radical initiator can

be replaced by a reducing agent to decrease side reactions; this is known as activators regenerated by electron transfer (ARGET) ATRP.[68] Further developments utilised Cu(0) (supplemental activator and reducing agent (SARA) ATRP), electric current (eATRP),[69] and light (photo-induced ATRP),[70] for the reduction of Cu(II) to Cu(I) (Scheme 7).

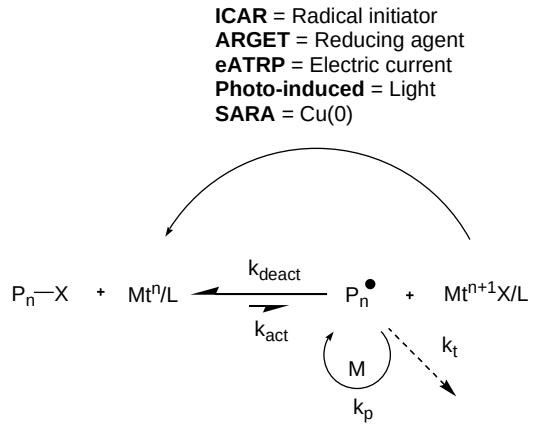

Scheme 7: Mechanism of ATRP by in-situ reduction of Cu(II).

ATRP has been widely used for the core-first synthesis of star polymers containing 3, 4, 6, 8 and even 16 arms.[71,72,73,74] Many multi-functional initiators are available commercially and access to complex architectures without the synthesis of complicated molecules makes ATRP a very useful technique. Unfortunately, some star-star coupling cannot be avoided due to the necessity to accumulate the Cu(II) persistent radical early in the reaction. In order to avoid extensive star-star coupling and possible gelation, reactions are usually restricted to low conversions and carried out in dilute solutions.[75] Star polymers have also been synthesised using the core-crosslinking method. First, by preparing the core through polymerisation of butyl acrylate in the presence of small amounts of divinylbenzene, the core then provides free-initiation sites which were used for polymerisation of the star arms.[76]

1.5.3. Cu(0)-mediated controlled radical polymerisation

Catalysis by zero-valent metals such at Cu(0) as opposed to Cu salts has many benefits which are highly desirable for industrial purposes. Cu(0) metals are cheap and abundant as well as being extremely easy to handle. The metal is easily recovered and recycled, and leaves a very low level of soluble copper species in solution (< 10 ppm). Furthermore, the development of continuous processes using Cu(0) catalyst is leading the way towards possible industrial applications for these methods.[77,78]

1.5.3.1. Supplemental Activator and Reducing Agent (SARA)-ATRP

While Cu(I) and Cu(II) salts are the predominant catalysts used in ATRP reactions, as early as 1997, the parallel addition of Cu(0) was shown to increase the rate of styrene polymerisation.[79] The process was further developed by adding the catalyst entirely in the zero-valent form. It was proposed that in these reactions Cu(0) was able to act as a supplementary activator alongside Cu(I) and a reducing agent to regenerate Cu(I) from Cu(II). The process was termed SARA-ATRP (Scheme 7) and is viewed as a variant of ARGET-ATRP. Despite several investigations claiming to prove the ATRP mechanism for Cu(0)-mediated polymerisation, there is still much debate in the literature. A second mechanism known as Single Electron Transfer-Living Radical Polymerisation (SET-LRP) was proposed by the group of Percec.[80,81,82] This contradicts the proposed mechanism for the ATRP process in several key areas.

1.5.3.2. Single Electron Transfer-Living Radical Polymerisation (SET-LRP)

Cu(0) catalysis was first utilised by Percec in 2002 whilst attempting the controlled polymerisation of vinyl chloride (VCl).[83] Due to the low reactivity of VCl, attempts to control the polymerisation had thus far proven unsuccessful as traditional ATRP catalysts (Cu(I)) were insufficiently active to reactivate dormant chains. When screening catalysts for polymerisation of VCl using sulfonyl halide initiators, Cu(0) demonstrated sufficient activity to reactivate dormant PVCl chains and allow controlled polymerisation.[80] Whilst it is well established that PVCl undergoes extensive chain transfer to monomer during polymerisation, very low levels of bimolecular termination are observed. Percec postulated that there would be insufficient Cu(II) accumulated by the PRE in order to control the polymerisation.[82] A distinct mechanism was proposed whereby alkyl halides are heterogeneously activated by Cu(0) in an outer-sphere electron transfer (OSET) process (Scheme 8). The initiation step proceeds via a radical anion intermediate before decomposing to an alkyl radical and a halide ion that associates with Cu(I) which is also generated. A key step of the reaction is the instantaneous disproportionation of Cu(I) which releases further Cu(0) activator and Cu(II) to deactivate the growing polymer chains. The “nascent” Cu(0) formed in the process is thought to be very active and contributes to the fast rate of SET-LRP reactions.

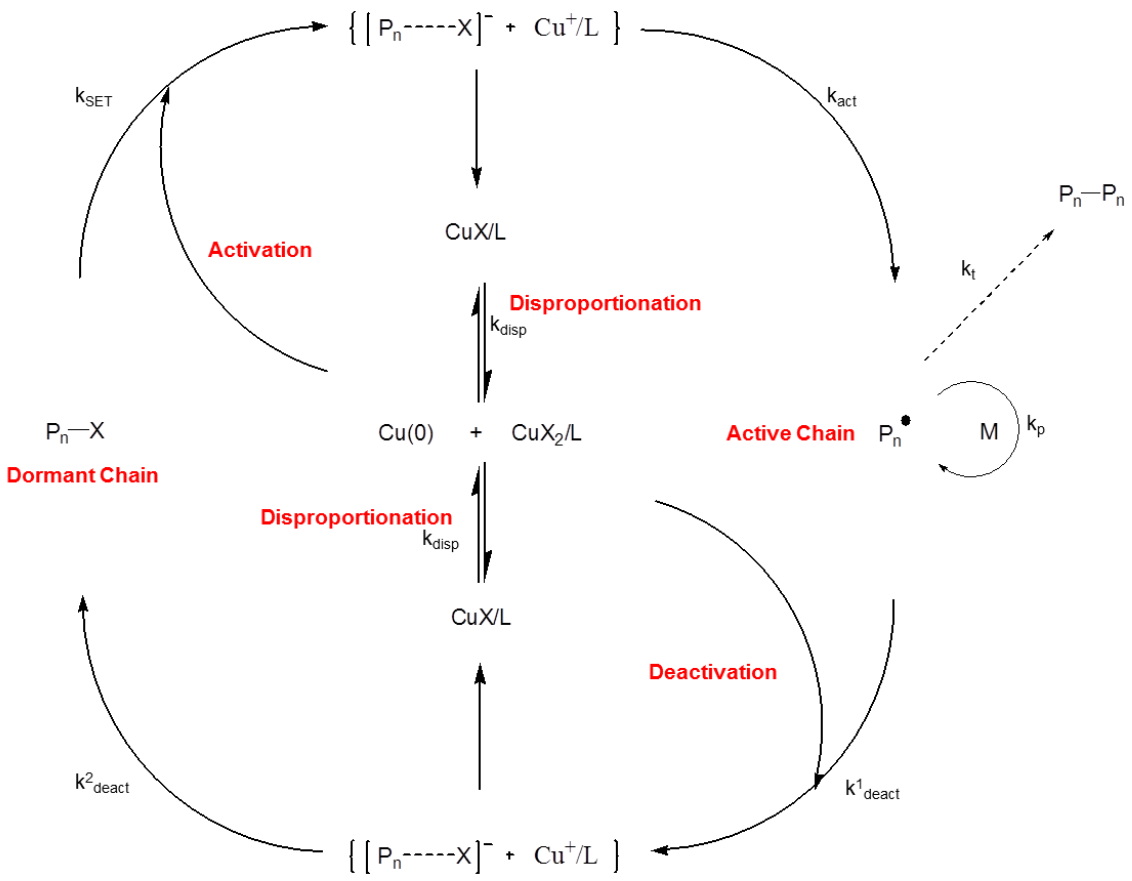

Scheme 8: Mechanism of SET-LRP.[82]

For early VCl polymerisations in H_2O/THF, the mechanism considered was based on competing SET and degenerative transfer processes (SET-DTLRP). By the modification of the reaction conditions this competition could be avoided giving a purely SET-LRP process.[81] When combined with more active monomers such as acrylates, the SET-LRP method provided extremely fast polymerisation rates at ambient temperatures whilst still allowing close control over polymer MW and *Đ*. Due to low levels of termination, HMW polymers were achieved using methyl acrylate (MA) and butyl acrylate (*n*BA) monomers.[81]

In SET-LRP reactions, components are chosen in order to maximise the OSET and disproportionation processes. Most important is the choice of solvent and ligand. The solvent must be polar, in order to promote disproportionation and favour OSET by the solvation and stabilisation of the halide anion. DMSO has proven the most successful for fast and controlled polymerisation reactions. DMSO has also been shown to stabilise nascent Cu(0) in the colloidal form, further increasing the rate. Water, alcohols and other polar solvents (protic and aprotic) are effective reaction solvents, though the suitability of alcohols decreases with increased hydrophobicity.[84] Ionic liquids, DMF, ethylene glycol and acetone have all been successfully employed in SET-LRP reactions.[85,86] Non-polar solvents which do not promote

disproportionation or stabilise nascent Cu(0), such as toluene or MeCN, are unsuitable for SET-LRP, however, they can be effective when combined with small amounts of polar additives such as phenol. This allows access to a wider range of non-polar monomers with limited solubility in polar media. The ligand plays a key role determining the relative stability of Cu(I) and Cu(II) complexes. The most effective ligands for SET-LRP are those which increase the stability of Cu(II) and so favour disproportionation. Most suitable are aliphatic ligands such as TREN or Me_6-TREN (Fig. 23) as these do not allow the tetrahedral/distorted tetrahedral conformation favoured by Cu(I). They instead prefer the trigonal bipyramidal Cu(II) structure.[87] Higher ligand concentrations can drive disproportionation and increase the rate of reaction through the formation of highly active nascent Cu(0).[88]

Activation of alkyl halides is via a heterogeneous, surface activated process and so a correlation is observed between Cu(0) surface area and reaction rate.[89] Whilst copper powder was used in early reactions, any Cu(0) source can be effective. Copper wire has been shown to allow a more controlled polymerisation due to its uniform surface area compared with powder which comprises a distribution of particle sizes.[81] Copper salts such as Cu_2Y (Y = Te, Se, S and O) can be used as catalysts as long as conditions favour disproportionation. Although Cu_2O is the least active of these salts it does show slow activation; this is important as it allows for some tolerance to oxygen during the SET-LRP process. Sensitivity to oxygen is a problem for all radical polymerisations, however, Cu(0) is able to scavenge oxygen to form Cu_2O. As this can act as an activator the polymerisation is still able to continue, though with an observed lag period.[90,91]

SET-LRP makes use of the same activated alkyl halides as for ATRP (Fig. 24), however, the activity is proposed to be less dependent on the bond dissociation energy.[92] This is in agreement with the OSET mechanism whereby the C-Halogen bond is broken via a halide anion in a step-wise manner. SET-LRP has been shown to be remarkably tolerant to impurities allowing the use of reaction components without extensive purification. Haddleton et al. demonstrated this with highly controlled polymerisations using a range of alcoholic drinks and even blood serum as solvent.[93,94] Importantly, the system has also been shown to be tolerant to radical inhibitors. When the rates of MA polymerisation were compared with and without mono-methyl ether hydroquinone (MEHQ) inhibitor, both reactions proceeded to high conversion with only a small rate decrease when the inhibitor was present.[95] Industrial applications of these techniques are much more likely if components can be used without the need for purification.

It has been shown that star polymers can be synthesised both to high conversions and MWs using core-first SET-LRP.[81] This is due to the low bimolecular termination levels and high livingness which can be achieved using this technique.[96] This was particularly demonstrated by the synthesis of a multi-block, 5-armed star co-polymer using a sugar based initiator.[97]

1.5.3.3. SARA-ATRP vs SET-LRP

The ATRP and SET-LRP models for Cu(0)-catalysed radical polymerisation conflict in several important areas. To maximise the potential of the technique, detailed knowledge of each mechanistic step is vital. Many studies have been dedicated to clarifying the following points:[98]

1. Whether Cu(0) acts as the major activator of alkyl halides or Cu(I) is the major activator and Cu(0) acts as a supplemental activator and reducing agent.
2. Whether disproportionation or comproportionation (reverse process reducing Cu(II) to Cu(I) using Cu(0)) dominates.
3. Whether alkyl halide activation occurs via ISET or OSET.

1.5.3.3.1. Cu(0) or Cu(I) as major activator

Fast activation is very important for controlled polymerisation as it allows the near simultaneous initiation and growth of all polymer chains.[54] Several recent publications by Matyjaszewski compare relative activity of Cu(I) and Cu(0) as activators of alkyl halides. In DMSO, k_{act} of CuBr/Me_6-TREN was shown to be extremely high both in pure solvent and in the presence of MA monomer (using methyl 2-bromopropioate (MBP) initiator and TEMPO as a radical trap).[99,100,101] Activation was calculated by following [$CuBr_2$] with UV-Vis spectroscopy and k_{act} = 3.2 x 10^2 mol^{-1} s^{-1} and 2.0 x 10^2 mol^{-1} s^{-1} was measured for solvent and solvent/monomer mix, respectively. Under aqueous conditions the rate of $CuBr_2$ production was so high that electrochemical techniques were necessary to monitor.[102] The rates of activation calculated using CuBr/Me_6-TREN, oligo(ethylene oxide) acrylate (OEOA) monomer and an oligo(ethylene oxide) 2-bromopropionate (OEOBP) initiator were much higher than those observed in DMSO; k_{act} = 6.6 x 10^4 mol^{-1} s^{-1} in pure solvent and k_{act} = 2.5 x 10^4 mol^{-1} s^{-1} using a monomer/solvent mix (OEOA (18 %)/ H_2O (84 %)).[102] This increase was expected due to the decreased stability of $CuBr_2$ in polar solvents which promotes the rate of propagation.

When activation by Cu(0) was measured, the rates of activation were much lower. In a pure DMSO model reaction, an average k_{act} = 1.8 x 10^{-4} cm s^{-1} was measured across a range of ligand concentrations (1 – 20 mmol). In the presence of MA the rate was even slower, k_{act} = 1.0 x 10^{-4}

cm s^{-1}.[101] These reactions did not use a radical trap but the conditions were selected to maximise termination and consume alkyl halide radicals. In aqueous conditions, much lower k_{act} was again seen for Cu(0) compared with Cu(I). Using Cu(0)/Me_6-TREN and an OEOBP initiator, k_{act} was measured as 4.0 x 10^{-6} cm s^{-1} in pure water and 1.0 x 10^{-5} cm s^{-1} with a OEOA/H_2O mix.[102] The activity of Cu(0) was also measured independently in a range of solvents by Harrisson and Nicolas using a TEMPO radical trap and ethyl-2-bromo-2-methylpropionate (EBiB) as initiator. Although the rates measured were high (k_{act}(DMSO) = 63 x 10^6 s^{-1}), an induction period was observed. This may be attributed to the time needed to accumulate nascent Cu(0) in the mixture but may also show that the reaction is activated by Cu(I) which is gradually generated in the system.[103]

These observations contradict Percec's view that Cu(0) must be very active in order to re-activate dormant PVCl chains where Cu(I) catalysts could not.[82] Percec used two experiments in which Cu(0) catalyst was removed during the reaction to prove activation was a surface mediated process. In the first the polymerisation mixture was decanted between two connected Schlenk tubes, one of which contained Cu(0) powder. The polymerisation proceeded when the solution was in contact with the catalyst, however, the reaction was reversibly interrupted when decanted into the second empty tube.[89] In the second experiment, Cu wire was used as a catalyst source. When it was lifted from the reaction mixture the polymerisation continued but at a much reduced rate. This was assumed to be a consequence of residual activation by nascent Cu(0) in the reaction mixture. When the solution was carefully decanted and nascent Cu(0) was eliminated, the reaction stopped entirely.[104] From this evidence Percec concluded that soluble Cu(I) was not important in the activation of R-X. Matyjaszewski argued, however, that the interruption is expected due to the low concentration of Cu(I) in solution which is then eliminated by the PRE without an external copper source.[98]

Percec also proposed that "nascent" Cu(0) formed through Cu(I) disproportionation is highly active and contributes to the high rates of the SET-LRP reaction. The activity of nascent Cu(0) was monitored by the addition of an alkyl halide to a pre-disproportionated mixture of CuBr/Me_6-TREN in DMSO.[105] Full disproportionation was observed through the formation of $CuBr_2$ (blue colour) and the collection of Cu(0) at the bottom of the flask. Within five minutes of adding the alkyl halide, nascent Cu(0) had disappeared from solution. Furthermore, when the process was repeated for solvents (e.g. MeOH) which cannot stabilise colloidal Cu(0), a

slower disappearance was observed. A slower rate is expected in these systems where Cu(0) forms larger agglomerations with a smaller surface area.[106] Haddleton et al. performed a pre-disproportion polymerisation reaction in order to prove activation by Cu(0).[107] After mixing CuBr/Me_6-TREN in water, immediate disproportionation was again observed by the blue-green colour of the solution and the appearance of Cu(0) in the flask.[107] Following addition of monomer and initiator, the polymerisation proceeded and the Cu(0) disappeared. Given that full disproportionation was observed before the reaction it was concluded that activation must only be from the nascent Cu(0). It was argued by Matyjaszewski that under conditions of full disproportionation only comproportionation can occur in the reaction mixture. This generates the necessary concentration of Cu(I) to activate the reaction and the mechanism must be by SARA-ATRP.[98]

1.5.3.3.2. Disproportionation or comproportionation

The role of Cu(0) in the SARA-ATRP mechanism is to supplement Cu(I) activation and to reduce Cu(II) to Cu(I) in a process known as comproportionation (Scheme 9). A key feature of the SET-LRP mechanism is an instantaneous and complete disproportionation. Therefore, a comparison of the extent and rate of the two processes should give an indication of the reaction mechanism.

$$2Cu(I)/L \underset{k_{comp}}{\overset{k_{disp}}{\rightleftharpoons}} Cu(0) + Cu(II)/L \qquad K_{disp} = k_{disp}/k_{comp}$$

Scheme 9: Disproportionation/comproportionation equilibrium.

Whilst the equilibrium constant of disproportionation in water is very large ($K_{disp} \approx 10^7\ M^{-1}$), in pure DMSO, a popular solvent for SET-LRP, it is slightly disfavoured. The addition of a suitable ligand, such as Me_6-TREN, reverses this and disproportionation becomes favoured. [106] Percec et al. demonstrated disproportionation of Cu(I) in a range of solvents by mixing CuBr/Me_6-TREN and following rate of $CuBr_2$ formation using UV-Vis spectroscopy.[106] Disproportionation reached equilibrium within an hour and nascent Cu(0) was observed at the bottom of the cuvette within 10 minutes.[106] For each solvent K_{disp} favoured the disproportionation reaction and the work was extended further by proving disproportionation in a range of monomers including acrylates and methacrylates.[108,106] These findings contradict similar studies by Matyjaszewski et al. when measuring disproportionation of CuBr/Me_6-TREN in DMSO.[109] Furthermore, comproportionation was also measured by the reduction of [$CuBr_2$] in MeCN, DMF and DMSO.[110,111] From these studies Matyjaszewski concluded that both comproportionation and disproportionation were slow when compared with the rate of

activation by Cu(I). Instantaneous disproportionation was not observed and equilibrium was only reached after around 2500 min in both model reactions. It was stated that, although disproportionation may be favoured thermodynamically due to the relative stability of Cu(II) over Cu(I), comproportionation will be favoured kinetically due to the low concentration of Cu(I) in the reaction mixture.[109] Moreover, disproportionation releases free ligand which should push the equilibrium even further towards the comproportionation reaction. When Nicolas et al. studied the rate constant of comproportionation (k_{comp}) in a range of solvents, it was concluded that comproportionation was dominant in Cu(0)-mediated polymerisations.[103] However, it was also noted that replacement of the PMDETA ligand used with Me_6-TREN was likely to decrease the effect of the comproportionation reaction.[103]

In addition to these model studies, Haddleton and Percec both monitored the change in [$CuBr_2$] during polymerisation reactions.[112,113] In each case, a constant increase in [$CuBr_2$] was observed and it was concluded that Cu(0) did not reduce $CuBr_2$ when the competing activation reaction was accessible.[112, 113] The steady increase in [$CuBr_2$] could alternatively be explained by the generation of $CuBr_2$ through the PRE. By monitoring [$CuBr_2$] during a polymerisation reaction demonstrating high-chain end retention (analysed as 99.8 % using MALDI-MS and NMR spectroscopy), Percec proved that a linear increase in [$CuBr_2$] was possible in the absence of termination reactions.[113] Finally, Percec observed that adding $CuBr_2$ at the beginning of a reaction had no effect on the rate of $CuBr_2$ production or the final [$CuBr_2$].[113] If the reaction was under the influence of the PRE a difference may be expected in these values.

Polar solvents, and the addition of water have been shown to increase the rate of Cu-mediated polymerisations. In the SARA-ATRP mechanism, this was interpreted as a shift of K_{ATRP} due to the decreased stability of the Cu(II) deactivator. This increases radical concentration and control over the reaction decreases. The SET-LRP mechanism, however, describes the rate increase in terms of a promotion of disproportionation which provides active Cu(0) in the solution.[82] A key difference with SET-LRP mechanism is that an increase in disproportionation should simultaneously increase the concentration of both activator and deactivator and control can be maintained over the polymerisation. Percec demonstrated that control could be retained over a reaction despite increasing the propagation rate through the addition of polar additives such as phenol.[81] This was considered evidence for the SET-LRP mechanism.

1.5.3.3.3. ISET or OSET

The mechanism of electron transfer (ET) during initiation or activation distinguishes the SET-LRP and ATRP processes. It is accepted, by the Taube classification, that ATRP proceeds via ISET first by halide bridging and then direct atom transfer of the halide to the oxidised metal centre in a concerted process.[114] SET-LRP is believed to occur via an OSET mechanism with no bridging ligand and a much weaker interaction between the donor and acceptor. Electron transfer occurs via a radical-anion intermediate in a stepwise process (Scheme 10).[82, 115] The proposed OSET mechanism has caused much debate centring on the validity of radical-anion formation and the relative rates of the ISET and OSET processes.

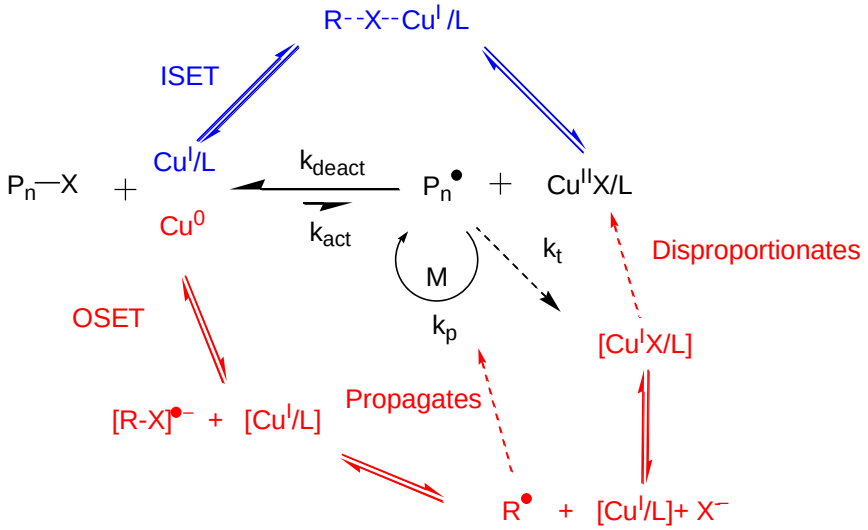

Scheme 10: Comparison of ISET (blue) and OSET (red) mechanisms in Cu-mediated polymerisations.

Radical-anions are already known for aromatic compounds. One example is the naphthalene radical-anion used to initiate living anionic polymerisations.[52] It is argued by Percec that their formation is also possible for activated alkyl halides initiators due to the presence of electron withdrawing groups adjacent to the halogen.[115] The radical which forms, therefore, carries a slight positive charge and is able to interact electrostatically with the halide anion released. This is known as the stepwise sticky dissociation model.[115] Percec proposed that this OSET mechanism is the reason re-activation of a propagating PVCl chain can occur at ambient temperature with a Cu(0) catalyst whilst it is not possible at higher temperatures even with the most active Cu(I) ATRP catalysts.[116] Computational techniques demonstrated that the heterolytic bond dissociation energy of an alkyl halide bond was less than that of homolytic bond dissocation.[92] This was cited as the reason for the relative insensitivity of SET-LRP to the alkyl halide bond dissociation energy. Whittaker et al. used the macrobicylic NH_2-Capten ligand for the polymerisation of styrene in toluene using CuBr as a catalyst.[117] The polymerisation was

not controlled, however, it was claimed that the structure formed by the ligand surrounding the copper species would prevent halide bridging and therefore ISET.[117] If this is the case activation can only be possible through an OSET process. Moreover, the ability of non-transition metals OSET donors such as $Na_2S_2O_4$ (which dissociates to form $2SO_2^{-\bullet}$ in water) to catalyse controlled polymerisations provides further evidence for OSET.[82, 118]

By comparing the reaction kinetics of a Cu(I)/TPMA catalysed system, with a polymerisation which was activated using aromatic anions (known OSET donors), Matyjaszewski concluded that OSET occurs at a much slower rate than ISET.[119,120] In his review of CRP techniques in 2007 Matyjaszewski described OSET as a side reaction which may occur in the presence of a large concentration of very active CuBr/Me_6-TREN catalyst.[54] Further work by Guliashivili et al stated that dissociative electron transfer proceeds only via a concerted and not a stepwise process.[121] Moreover, it was concluded that radical anions would not be formed as intermediates because the injection of one electron to an alkyl halide bond gives only a weakly associated radical anion complex.[121] It was argued that for a reasonable reaction rate an OSET donor would need a highly negative potential which is not the case for copper catalysts. Recent Cu(0)-mediated polymerisations of styrene conducted using toluene as a solvent are proposed to react via the ISET mechanism due to the inability of toluene to disproportionate and stabilise free anions.[122,123]

1.5.3.3.4. Principle of microscopic reversibility

The principle of microscopic reversibility dictates that the rate constants of forward and reverse reactions at equilibrium should be equal. For the SET-LRP mechanism, which favours both disproportionation and deactivation by $CuBr_2$, the principle is violated if activation occurs via Cu(0).[54] Percec argued that whilst these rules apply for an isolated homogeneous system, SET-LRP reactions occur via simultaneous heterogeneous activation by Cu(0) and homogeneous deactivation by $CuBr_2$.[82] A change in ligand binding and an exothermic propagation reaction, which may drive certain processes over others, must also be considered. Because of these factors Percec regarded SET-LRP reactions too complex to be considered by this principle.[82]

1.5.4. Reversible Addition Fragmentation Chain Transfer (RAFT) polymerisation

As well as activation-deactivation methods described above, controlled radical polymerisation techniques can also proceed via a degenerative transfer (DT) mechanism. There are two common ways by which these polymerisations occur. Firstly, via atom or group transfer

whereby an atom/group is continually passed back and forth between active and dormant chain ends, for example iodide or tellurium mediated polymerisation. Secondly, and more commonly, an addition-fragmentation mechanism such as Reversible Addition-Fragmentation Chain Transfer (RAFT) polymerisation is used. This method, developed in 1998 by Moad, Rizzardo, Thang et al., was the first reported use of a thiocarbonyl containing molecule as a chain transfer agent (CTA) in order to trap propagating chains in a dormant state.[124] RAFT agents share in common a dithio functionality and can be further sub-divided as one of four groups shown in Figure 25.

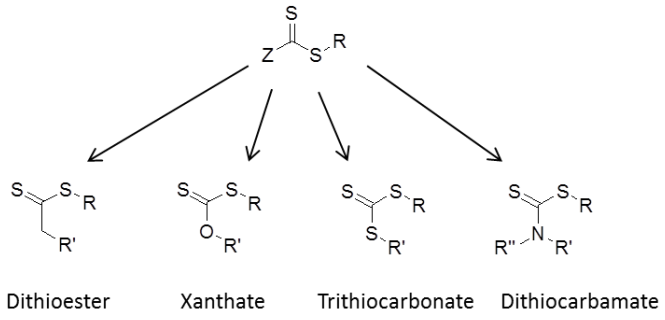

Figure 25: Categories of RAFT agent.

RAFT is a very versatile process and allows polymerisation of a wide range of monomers without the use of a transition metal catalyst. A major drawback is that RAFT agents are not general and for optimum control a specific CTA must be synthesised for individual requirements. Monomers such as such as styrene and (meth)acrylates, which have a conjugated structure, are referred to as "more activated" monomers (MAMs) (Fig. 26a). Polymerisation of these monomers is controlled most effectively using dithioester or trithiocarbonate based RAFT agents. These contain a Z group which stabilises the intermediate radical and increases the reactivity of the C=S bond.[125] Non-conjugated monomers such as vinyl acetate or N-vinyl pyrrolidone are known as "less activated" monomers (LAMs) (Fig. 26b). RAFT agents with electron withdrawing Z moieties (xanthates and dithiocarbamates) are most effective for the control of their polymerisation.[125]

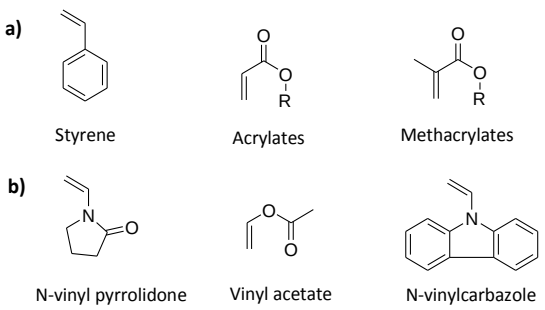

Figure 26: a) More activated monomers (MAMs); **b)** Less activated monomers (LAMs).

Key structural features in the design of RAFT agents are the R and Z groups (Fig. 25) which can be adjusted to finely tune the activity of the molecule. The reactivity of the C=S bond is influenced by the extent of electron donation by the Z groups whilst the R group must fragment easily and be reactive enough to re-initiate further polymer chains. Recently, "switchable" RAFT agents have been developed to control the polymerisation of either MAMs or LAMs using a single chain transfer agent by adjusting the reaction conditions .[126]

RAFT polymerisations are initiated using traditional radical initiators such as azo- or peroxide compounds (Scheme 11a). The radicals generated initiate monomer units which briefly propagate before attacking the reactive C=S bond in a RAFT agent to form an intermediate (b). The intermediate can fragment back to re-release the propagating chain or forward releasing a radical. This radical can further initiate monomer (c) which propagate until they are trapped in the chain equilibration/propagation step (d). This is the key equilibrium in the RAFT process, occurring between a propagating and dormant chain on each side[54, 127]

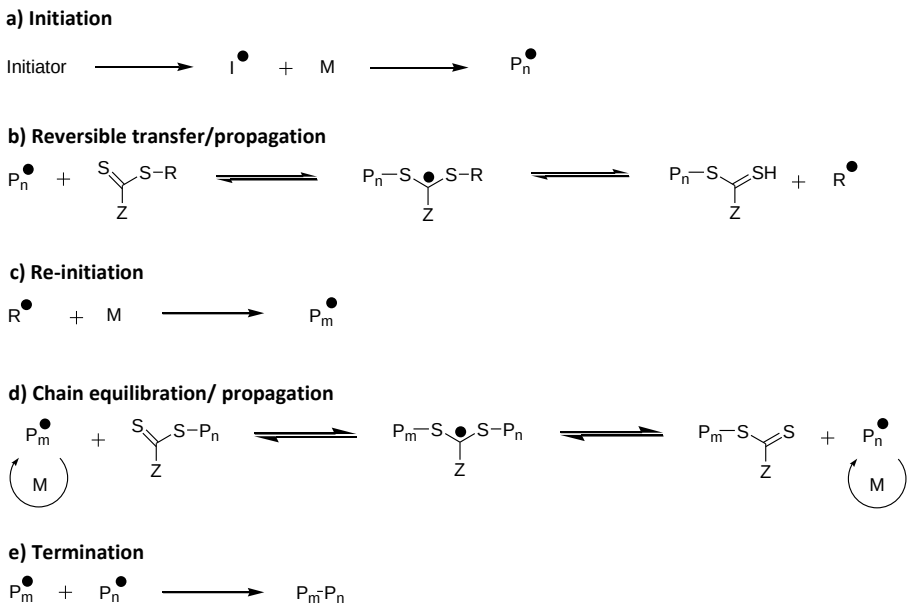

Scheme 11: Mechanism of RAFT polymerisation.

RAFT polymerisation is a very popular technique particularly for aqueous controlled radical polymerisations. It has also been successfully used to synthesise HMW polymers, however, the need for individual synthesis and extensive purification of RAFT agents, usually by column chromatography, limits its use. Moreover, RAFT agents are often coloured (pink or yellow) and strongly odoured. Elevated temperatures are necessary for the use of most radical initiators and long reaction times needed for higher conversions.

Core-first synthesis of star polymers using the RAFT mechanism is more complicated than for NMP, ATRP or SET-LRP. One of two approaches can be used depending on whether core of the RAFT agent attaches to the arms via the R or Z group. With the R group approach, fragmentation of the CTA leaves the propagating radical on the star core and the arms grow from here. When the arms are attached via the Z-group, radicals are released and propagation occurs away from the core before the chains re-attach. The radicals present on the core (R-group approach) allow for the possibility of star-star coupling (i.e. termination). These termination reactions will not occur with the Z-group approach. However, as the propagating chains increase in size, steric effects prevent efficient re-attachment of growing chains to the core.

1.6. Conclusions and thesis aims and objectives

The understanding of drag reduction by dilute polymer solutions in turbulent flow is far from complete. Despite this highly effective polymer systems have been developed based largely on empirical observations which show HMW polymers are necessary for effective drag reduction. PAM and its partially hydrolysed analogues, synthesised using free-radical inverse-emulsion polymerisation, are most commonly used in current commercial applications. Whilst providing efficient DRAs, these systems leave much room for improvement; particularly in terms of environmental impact and mechanical stability. Ashland Inc. currently market a PAM based product, **Praestol**, however, the use of the acrylamide monomer is no longer desirable due to recently introduced legislation. Furthermore, the use of inverse-emulsions, containing oil and surfactant, negatively impacts the environment. The susceptibility of HMW polymers to mechanical degradation in turbulent flow quickly decreases their drag reducing efficiency (DRE); a major problem for current commercial systems. Finally, the ability to degrade the polymer post-use is a desirable property in order to reduce its accumulation.

With these considerations in mind, the aim of this project is the production of an effective water soluble polymer drag reducing agent which has the following properties;

1) Acrylamide free;

2) Environmentally friendly;

3) Oil and surfactant free;

4) Mechanically stable;

5) Economically viable.

Branched polymers show high DRE and enhanced mechanical stability by distributing stresses through the individual polymer arms. Controlled radical polymerisation techniques are useful tools for the synthesis of branched/star polymers with a range of monomer functionalities. Cu(0)-mediated polymerisation reactions allow the synthesis of well-defined polymers, including stars, to HMWs and using ambient reaction temperatures. Furthermore, the technique has been successful using environmentally friendly aqueous solvents. Catalysis using Cu(0) provides many benefits over other transition metal catalysed systems when considering their commercial use. Particularly important is the ease of catalyst handling and recovery from reaction mixture and the extremely low copper contamination in final product. Finally, the introduction of labile functionality in the core of a star polymer may allow degradation post use. In order to achieve these aims, particularly when targeting a material with low environmental impact, the synthesis of a HMW star polymer in aqueous solution via Cu(0)-mediated polymerisation would be a very useful process.

1.7. References

1. Kelland, M. A., *Production Chemicals for the Oil and Gas Industry*. CRC Press: 2009; Vol. 1, p 437.
2. Toms, B. A. *J. Colloid Sci.* **1949,** 4, 511-521.
3. Brostow, W. *Ind Eng. Chem.* **2008,** 14, 409-416.
4. Pritchard; J., P., *Fox and McDonald's Introduction to Fluid Mechanics*. 8 ed.; Wiley: 2011; p 875.
5. Davidson; A., P., *Turbulence: An introduction for scientists and engineers*. Oxford University Press: 2004; p 657.
6. Sreenivasan, K. R.; White, C. M. *J. Fluid Mech.* **2000,** 409, 149-164.
7. White, C. M.; Mungal, M. G., Mechanics and prediction of turbulent drag reduction with polymer additives. In *Annual Review of Fluid Mechanics*, Annual Reviews: Palo Alto, 2008; Vol. 40, pp 235-256.
8. Virk, P. S. *J. Fluid Mech.* **1971,** 45, 417-40.
9. Virk, P. S. *AIChE J.* **1975,** 21, 625-56.
10. Den Toonder, J. M. J.; Hulsen, M. A.; Kuiken, G. D. C.; Nieuwstadt, F. T. M. *J. Fluid Mech.* **1997,** 337, 193-231.
11. Ptasinski, P. K.; Boersma, B. J.; Nieuwstadt, F. T. M.; Hulsen, M. A.; Van Den Brule, B. H. A. A.; Hunt, J. C. R. *J. Fluid Mech.* **2003,** 490, 251-291.
12. Tiederman, W. G.; Luchik, T. S.; Bogard, D. G. *J. Fluid Mech.* **1985,** 156, 419-437.
13. Lumley, J. L. *Annu. Rev. Fluid Mech.* **1969,** 1, 367-384.

14. L'Vov, V. S.; Pomyalov, A.; Procaccia, I.; Tiberkevich, V. *Phys. Rev. Lett.* **2004,** 92, 4.

15. Tabor, M.; De Gennes, P. G. *Europhys. Lett.* **1986,** 2, 519-522.

16. McComb, W. D.; Rabie, L. H. *AIChE J.* **1982,** 28, 547-557.

17. Virk, P., *Aspects of Mechanisms in Type B Drag Reduction*. Springer-Verlag: 1989.

18. Zakin, J. L.; Hunston, D. L. *J. Macromol. Sci. Phy.* **1980,** 18, 795-814.

19. Lumley, J. L. *J. Polym. Sci., Part C: Macromol. Rev.* **1973,** 7, 263-290.

20. McCormick, C. L.; Hester, R. D.; Morgan, S. E.; Safieddine, A. M. *Macromolecules* **1990,** 23, 2132-2139.

21. Gampert, B.; Wagner, P., The influence of molecular weight and molecular weight distribution on drag reduction and mechanical degradation in turbulent flow of highly dilute polymer solutions. In *The Influence of Polymer Additives on Velocity and Temperature Fields*, Gampert, B., Ed. Springer-Verlag: Berlin, 1985; Vol. 1.

22. Dunlop, E. H.; Cox, L. R. *Phys.Fluids* **1977,** 20, 203-213.

23. Liberatore, M. W.; Pollauf, E. J.; McHugh, A. J. *J. Non-Newton Fluid* **2003,** 113, 193-208.

24. McCormick, C. L.; Hester, R. D.; Morgan, S. E.; Safieddine, A. M. *Macromolecules* **1990,** 23, 2124-2131.

25. Shetty, A. M.; Solomon, M. J. *Polymer* **2009,** 50, 261-270.

26. Malik, S.; Shintre, S. N.; Mashelkar, R. A. *Macromolecules* **1993,** 26, 55-59.

27. Zakin, J. L.; Hunston, D. L. *J. Appl. Polym. Sci.* **1978,** 22, 1763-1766.

28. Hlavacek, B.; Rollin, L. A.; Schreiber, H. P. *Polymer* **1976,** 17, 81-86.

29. Brostow, W.; Majumdar, S.; Singh, R. P. *Macromol. Rapid Commun.* **1999,** 20, 144-147.

30. Hoyt, J. W. *Trends Biotechnol.* **1985,** 3, 17-21.

31. Deshmukh, S. R.; Chaturvedi, P. N.; Singh, R. P. *J. Appl. Polym. Sci.* **1985,** 30, 4013-4018.

32. Kim, O. K.; Little, R. C.; Patterson .R. l.; Ting, R. Y. *Nature* **1974,** 250, 408-410.

33. Ohlendorf, D.; Interthal, W.; Hoffmann, H. *Rheologica Acta* **1986,** 25, 468-486.

34. Japper-Jaafar, A.; Escudier, M. P.; Poole, R. J. *J. Non-Newton. Fluid* **2009,** 161, 86-93.

35. Morgan, S. E.; McCormick, C. L. *Prog. Polym. Sci.* **1990,** 15, 507-549.

36. Parker, C. A.; Hedley, A. H. *J. Appl. Polym. Sci.* **1974,** 18, 3403-3421.

37. Kauzmann, W.; Eyring, H. *J. Am. Chem. Soc.* **1940,** 62, 3113-3125.

38. Xue, L.; Agarwal, U. S.; Lemstra, P. J. *Macromolecules* **2005,** 38, 8825-8832.

39. Choi, H. J.; Kim, C. A.; Sohn, J.-I.; Jhon, M. S. *Polym. Degrad. Stab.* **2000,** 69, 341-346.

40. Sim, H. G.; Khomami, B.; Sureshkumar, R. *J. Rheol.* **2007,** 51, 1223-1251.

41. Islam, M. T.; Vanapalli, S. A.; Solomon, M. J. *Macromolecules* **2004,** 37, 1023-1030.

42. Liberatore, M. W.; Baik, S.; McHugh, A. J.; Hanratty, T. J. *J. Non-Newton Fluid* **2004,** 123, 175-183.

43. Kenis, P. R. *J. Appl. Polym. Sci.* **1971,** 15, 607-618.

44. May, P. A.; Moore, J. S. *Chem. Soc. Rev.* **2013,** 42, 7497-7506.

45. Deshmukh, S. R.; Singh, R. P. *J. Appl. Polym. Sci.* **1986,** 32, 6163-6176.

46. Lim, S. T.; Choi, H. J.; Lee, S. Y.; So, J. S.; Chan, C. K. *Macromolecules* **2003,** 36, 5348-5354.

47. Kot, E.; Bismarck, A. *Macromolecules* **2010,** 43, 6469-6475.

48. Inoue, K. *Prog. Polym. Sci.* **2000,** 25, 453-571.

49. Mazur, J.; McCrackin, F. *Macromolecules* **1977,** 10, 326-332.

50. Fetters, L. J.; Kiss, A. D.; Pearson, D. S.; Quack, G. F.; Vitus, F. J. *Macromolecules* **1993,** 26, 647-654.

51. Khanna, K.; Varshney, S.; Kakkar, A. *Polym. Chem.* **2010,** 1, 1171-1185.

52. Szwarc, M.; Levy, M.; Milkovich, R. *J. Am. Chem. Soc.* **1956,** 78, 2656-2657.

53. Eschwey, H.; Burchard, W. *Polymer* **1975,** 16, 180-184.

54. Braunecker, W. A.; Matyjaszewski, K. *Prog. Polym. Sci.* **2007,** 32, 93-146.

55. Cowie, J. M. G., *Polymers: chemistry and physics of modern materials*. 3rd ed ed.; Taylor & Francis: Boca Raton, 2008; Vol. 1.

56. Veregin, R. P. N.; Georges, M. K.; Kazmaier, P. M.; Hamer, G. K. *Macromolecules* **1993,** 26, 5316-5320.

57. Hawker, C. J.; Bosman, A. W.; Harth, E. *Chem. Rev.* **2001,** 101, 3661-3688.

58. Hawker, C. J. *Angew. Chem. Int. Ed.* **1995,** 34, 1456-1459.

59. Paillet, S.; Roncin, A.; Clisson, G.; Pembouong, G.; Billon, L.; Derail, C.; Save, M. *J. Polym. Sci., Part A: Polym. Chem.* **2012,** 50, 2967-2979.

60. Wang, J. S.; Matyjaszewski, K. *J. Am. Chem. Soc.* **1995,** 117, 5614-5615.

61. Kato, M.; Kamigaito, M.; Sawamoto, M.; Higashimura, T. *Macromolecules* **1995,** 28, 1721-1723.

62. Tang, W.; Kwak, Y.; Braunecker, W.; Tsarevsky, N. V.; Coote, M. L.; Matyjaszewski, K. *J. Am. Chem. Soc.* **2008,** 130, 10702-10713.

63. Braunecker, W. A.; Tsarevsky, N. V.; Gennaro, A.; Matyjaszewski, K. *Macromolecules* **2009,** 42, 6348-6360.

64. Horn, M.; Matyjaszewski, K. *Macromolecules* **2013,** 46, 3350-3357.

65. Gromada, J.; Matyjaszewski, K. *Macromolecules* **2001,** 34, 7664-7671.

66. Wang, J. S.; Matyjaszewski, K. *Macromolecules* **1995,** 28, 7572-7573.

67. Matyjaszewski, K.; Jakubowski, W.; Min, K.; Tang, W.; Huang, J. Y.; Braunecker, W. A.; Tsarevsky, N. V. *PNAS* **2006,** 103, 15309-15314.

68. Jakubowski, W.; Min, K.; Matyjaszewski, K. *Macromolecules* **2006,** 39, 39-45.

69. Magenau, A. J. D.; Bortolamei, N.; Frick, E.; Park, S.; Gennaro, A.; Matyjaszewski, K. *Macromolecules* **2013,** 46, 4346-4353.

70. Tasdelen, M. A.; Uygun, M.; Yagci, Y. *Macromol. Chem. Phys.* **2011,** 212, 2036-2042.

71. Mendrek, B.; Trzebicka, B. *Eur. Polym. J.* **2009,** 45, 1979-1993.

72. Angot, S.; Murthy, K. S.; Taton, D.; Gnanou, Y. *Macromolecules* **1998,** 31, 7218-7225.

73. Taton, D.; Gnanou, Y.; Matmour, R.; Angot, S.; Hou, S.; Francis, R.; Lepoittevin, B.; Moinard, D.; Babin, J. *Polym. Int.* **2006,** 55, 1138-1145.

74. McLeod, D. C.; Tsarevsky, N. V. *Polym. Int.* **2014,** 63, 868-875.

75. .

76. Gao, H. F.; Tsarevsky, N. V.; Matyjaszewski, K. *Macromolecules* **2005,** 38, 5995-6004.

77. Burns, J. A.; Houben, C.; Anastasaki, A.; Waldron, C.; Lapkin, A. A.; Haddleton, D. M. *Polym. Chem.* **2013,** 4, 4809-4813.

78. Chan, N.; Cunningham, M. F.; Hutchinson, R. A. *Macromol. Rapid Commun.* **2011,** 32, 604-609.

79. Matyjaszewski, K.; Coca, S.; Gaynor, S. G.; Wei, M. L.; Woodworth, B. E. *Macromolecules* **1997,** 30, 7348-7350.

80. Asandei, A. D.; Percec, V. *J. Polym. Sci., Part A: Polym. Chem.* **2001,** 39, 3392-3418.

81. Percec, V.; Guliashvili, T.; Ladislaw, J. S.; Wistrand, A.; Stjerndahl, A.; Sienkowska, M. J.; Monteiro, M. J.; Sahoo, S. *J. Am. Chem. Soc.* **2006,** 128, 14156-14165.

82. Rosen, B. M.; Percec, V. *Chem. Rev.* **2009,** 109, 5069-5119.

83. Percec, V.; Popov, A. V.; Ramirez-Castillo, E.; Monteiro, M.; Barboiu, B.; Weichold, O.; Asandei, A. D.; Mitchell, C. M. *J. Am. Chem. Soc.* **2002,** 124, 4940-4941.

84. Nguyen, N. H.; Rosen, B. M.; Percec, V. *J. Polym. Sci., Part A: Polym. Chem.* **2010,** 48, 1752-1763.

85. Nguyen, N. H.; Rosen, B. M.; Jiang, X.; Fleischmann, S.; Percec, V. *J. Polym. Sci., Part A: Polym. Chem.* **2009,** 47, 5577-5590.

86. Lligadas, G.; Percec, V. *J. Polym. Sci., Part A: Polym. Chem.* **2008,** 46, 2745-2754.

87. Rosen, B. M.; Percec, V. *J. Polym. Sci., Part A: Polym. Chem.* **2007,** 45, 4950-4964.

88. Nguyen, N. H.; Jiang, X.; Fleischmann, S.; Rosen, B. M.; Percec, V. *J. Polym. Sci., Part A: Polym. Chem.* **2009,** 47, 5629-5638.

89. Lligadas, G.; Rosen, B. M.; Bell, C. A.; Monteiro, M. J.; Percec, V. *Macromolecules* **2008,** 41, 8365-8371.

90. Nguyen, N. H.; Percec, V. *J. Polym. Sci., Part A: Polym. Chem.* **2011,** 49, 4756-4765.

91. Jiang, X.; Rosen, B. M.; Percec, V. *J. Polym. Sci., Part A: Polym. Chem.* **2010,** 48, 2716-2721.

92. Guliashvili, T.; Percec, V. *J. Polym. Sci., Part A: Polym. Chem.* **2007,** 45, 1607-1618.

93. Waldron, C.; Zhang, Q.; Li, Z.; Nikolaou, V.; Nurumbetov, G.; Godfrey, J.; McHale, R.; Yilmaz, G.; Randev, R. K.; Girault, M.; McEwan, K.; Haddleton, D. M.; Droesbeke, M.; Haddleton, A. J.; Wilson, P.; Simula, A.; Collins, J.; Lloyd, D. J.; Burns, J. A.; Summers, C.; Houben, C.; Anastasaki, A.; Li, M.; Becer, C. R.; Kiviaho, J. K.; Risangud, N. *Polym. Chem.* **2014,** 5, 57-61.

94. Zhang, Q.; Li, Z.; Wilson, P.; Haddleton, D. M. *Chem. Comm.* **2013,** 49, 6608-6610.

95. Lligadas, G.; Percec, V. *J. Polym. Sci., Part A: Polym. Chem.* **2008,** 46, 3174-3181.

96. Whittaker, M. R.; Urbani, C. N.; Monteiro, M. J. *J. Polym. Sci., Part A: Polym. Chem.* **2008,** 46, 6346-6357.

97. Boyer, C.; Derveaux, A.; Zetterlund, P. B.; Whittaker, M. R. *Polym. Chem.* **2012,** 3, 117-123.

98. Konkolewicz, D.; Wang, Y.; Krys, P.; Zhong, M.; Isse, A. A.; Gennaro, A.; Matyjaszewski, K. *Polym. Chem.* **2014,** 5, 4396-4417.

99. Pintauer, T.; Braunecker, W.; Collange, E.; Poli, R.; Matyjaszewski, K. *Macromolecules* **2004,** 37, 2679-2682.

100. Matyjaszewski, K.; Paik, H.-j.; Zhou, P.; Diamanti, S. J. *Macromolecules* **2001,** 34, 5125-5131.

101. Peng, C.-H.; Zhong, M.; Wang, Y.; Kwak, Y.; Zhang, Y.; Zhu, W.; Tonge, M.; Buback, J.; Park, S.; Krys, P.; Konkolewicz, D.; Gennaro, A.; Matyjaszewski, K. *Macromolecules* **2013,** 46, 3803-3815.

102. Konkolewicz, D.; Krys, P.; Góis, J. R.; Mendonça, P. V.; Zhong, M.; Wang, Y.; Gennaro, A.; Isse, A. A.; Fantin, M.; Matyjaszewski, K. *Macromolecules* **2014,** 47, 560-570.

103. Harrisson, S.; Couvreur, P.; Nicolas, J. *Macromolecules* **2012,** 45, 7388-7396.

104. Levere, M. E.; Nguyen, N. H.; Sun, H.-J.; Percec, V. *Polym. Chem.* **2013,** 4, 686-694.

105. Jiang, X.; Rosen, B. M.; Percec, V. *J. Polym. Sci., Part A: Polym. Chem.* **2010,** 48, 403-409.

106. Levere, M. E.; Nguyen, N. H.; Leng, X.; Percec, V. *Polym. Chem.* **2013,** 4, 1635-1647.

107. Zhang, Q.; Wilson, P.; Li, Z.; McHale, R.; Godfrey, J.; Anastasaki, A.; Waldron, C.; Haddleton, D. M. *J. Am. Chem. Soc.* **2013,** 135, 7355-7363.

108. Rosen, B. M.; Jiang, X.; Wilson, C. J.; Nguyen, N. H.; Monteiro, M. J.; Percec, V. *J. Polym. Sci., Part A: Polym. Chem.* **2009,** 47, 5606-5628.

109. Wang, Y.; Zhong, M.; Zhu, W.; Peng, C.-H.; Zhang, Y.; Konkolewicz, D.; Bortolamei, N.; Isse, A. A.; Gennaro, A.; Matyjaszewski, K. *Macromolecules* **2013,** 46, 3793-3802.

110. Zhang, Y.; Wang, Y.; Peng, C.-h.; Zhong, M.; Zhu, W.; Konkolewicz, D.; Matyjaszewski, K. *Macromolecules* **2012,** 45, 78-86.

111. Matyjaszewski, K.; Tsarevsky, N. V.; Braunecker, W. A.; Dong, H.; Huang, J.; Jakubowski, W.; Kwak, Y.; Nicolay, R.; Tang, W.; Yoon, J. A. *Macromolecules* **2007,** 40, 7795-7806.

112. Levere, M. E.; Willoughby, I.; O'Donohue, S.; Wright, P. M.; Grice, A. J.; Fidge, C.; Becer, C. R.; Haddleton, D. M. *J. Polym. Sci., Part A: Polym. Chem.* **2011,** 49, 1753-1763.

113. Levere, M. E.; Nguyen, N. H.; Percec, V. *Macromolecules* **2012,** 45, 8267-8274.

114. Konkolewicz, D.; Wang, Y.; Zhong, M.; Krys, P.; Isse, A. A.; Gennaro, A.; Matyjaszewski, K. *Macromolecules* **2013,** 46, 8749-8772.

115. Zhang, N.; Samanta, S. R.; Rosen, B. M.; Percec, V. *Chem. Rev.* **2014,** 114, 5848-5958.

116. Queffelec, J.; Gaynor, S. G.; Matyjaszewski, K. *Macromolecules* **2000,** 33, 8629-8639.

117. Bell, C. A.; Whittaker, M. R.; Gahan, L. R.; Monteiro, M. J. *J. Polym. Sci., Part A: Polym. Chem.* **2008,** 46, 146-154.

118. Percec, V.; Popov, A. V.; Ramirez-Castillo, E.; Coelho, J. F. J.; Hinojosa-Falcon, L. A. *J. Polym. Sci., Part A: Polym. Chem.* **2004,** 42, 6267-6282.

119. Lin, C. Y.; Coote, M. L.; Gennaro, A.; Matyjaszewski, K. *J. Am. Chem. Soc.* **2008,** 130, 12762-12774.

120. Isse, A. A.; Bortolamei, N.; De Paoli, P.; Gennaro, A. *Electrochim. Acta* **2013,** 110, 655-662.

121. Isse, A. A.; Gennaro, A.; Lin, C. Y.; Hodgson, J. L.; Coote, M. L.; Guliashvili, T. *J. Am. Chem. Soc.* **2011,** 133, 6254-6264.

122. Hornby, B. D.; West, A. G.; Tom, J. C.; Waterson, C.; Harrisson, S.; Perrier, S. *Macromol. Rapid Commun.* **2010,** 31, 1276-1280.

123. West, A. G.; Hornby, B.; Tom, J.; Ladmiral, V.; Harrisson, S.; Perrier, S. *Macromolecules* **2011,** 44, 8034-8041.

124. Chiefari, J.; Chong, Y. K.; Ercole, F.; Krstina, J.; Jeffery, J.; Le, T. P. T.; Mayadunne, R. T. A.; Meijs, G. F.; Moad, C. L.; Moad, G.; Rizzardo, E.; Thang, S. H. *Macromolecules* **1998,** 31, 5559-5562.

125. Perrier, S.; Takolpuckdee, P. *J. Polym. Sci., Part A: Polym. Chem.* **2005,** 43, 5347-5393.

126. Keddie, D. J.; Guerrero-Sanchez, C.; Moad, G.; Rizzardo, E.; Thang, S. H. *Macromolecules* **2011,** 44, 6738-6745.

127. Moad, G.; Rizzardo, E.; Thang, S. H. *Aust. J. Chem.* **2012,** 65, 985-1076.

Chapter 2

Synthesis of Initiators

2.1. Introduction

Branched polymers, for example stars, provide efficient drag reducing systems and increase resistance to mechanical degradation, particularly when they contain a small number of high molecular weight (HMW) arms. Cu(0)-mediated polymerisation techniques allow access to HMW star polymers at ambient temperature. Controlled polymerisation reactions can be achieved in aqueous solutions and with low residual copper levels in the product. This technique may therefore be a useful tool in the synthesis of a water-soluble drag reducing agent with enhanced mechanical stability. The core-first strategy is most suited to the synthesis of HMW star polymers. This method requires a multi-functional initiator to grow several arms from a single core. By incorporation of labile functionality in the core molecule, this method may provide the opportunity for degradation of the drag reducing polymer post-use. Several multi-functional initiators are currently available commercially (Fig. 1).

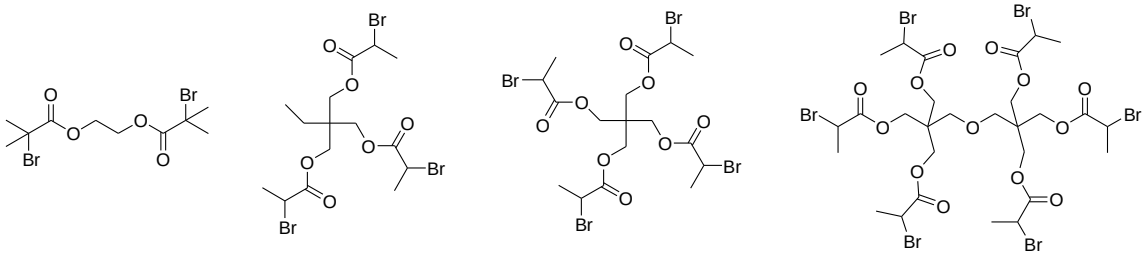

Ethylene bis(2-bromoisobutyrate) | **1,1,1-Tris(2-bromoisobutyryl-oxymethyl)ethane** | **Pentaerythritol tetrakis(2-bromoisobutyrate)** | **Dipentaerythritol hexakis(2-bromoisobutyrate)**

Figure 1: Multi-functional initiators available from Sigma Aldrich.

Several other branched initiators have been studied in order to target specific dendritic materials. Hedrick et al. developed a dimethylolpropionic acid (Bis-MPA) derived branching unit which contained two initiation sites (Scheme 1a).[1, 2] By reaction with different polyols (Scheme 1b), a range of dendritic core molecules were prepared and used in ATRP reactions.

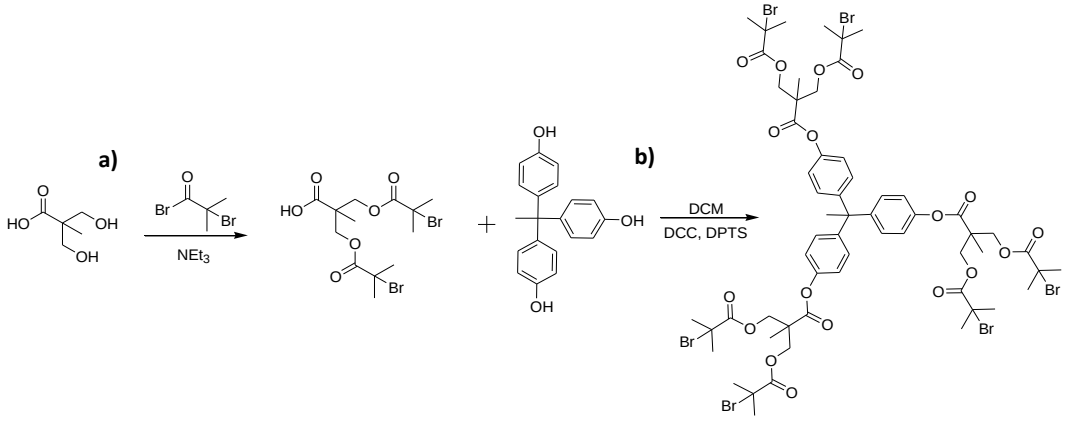

Scheme 1: Synthesis of dendritic initiator via; **a)** Step 1: Synthesis of branched unit; **b)** Step 2: Synthesis of initiator by reaction with polyol.

In order to target aqueous polymerisation, a water soluble initiator is necessary. Though Cu-mediated polymerisation is more common in organic solvents, there are a range of commercially available initiators which have been successfully used for aqueous polymerisation reactions (Fig. 2a).[3,4]

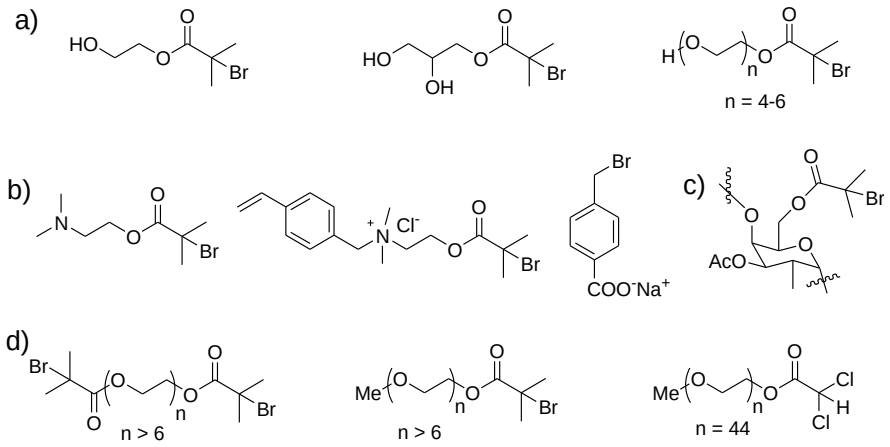

Figure 2: Water soluble initiators; **a)** Commercially available; **b)** Used by Armes et al.[5,6]; **c)** GGM based; **d)** PEG based macro-initiators.

Armes et al., used several water soluble initiators (Fig. 2b) for the aqueous polymerisation of a range of monomers (e.g. oligo(ethylene glycol)methacrylate, OEGMA).[5,6] Albertsson recently used a modified *O*-Acetyl-galactoglucomannan (GGM, Fig. 2c) for aqueous graft co-polymerisation using SET-LRP.[7] The addition of poly(ethylene glycol) (PEG), a water soluble bio-compatible polymer, is a common way to solubilise ATRP/SET-LRP macro-initiators in aqueous systems (Fig. 2d).[8,9,10]

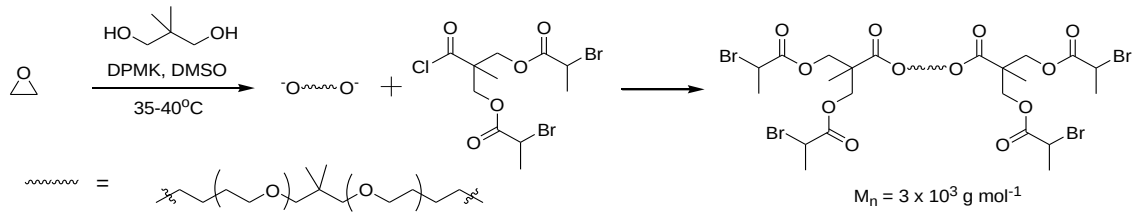

Scheme 2: Synthesis of PEG based macro-initiator via living anionic polymerisation.

Multi-functional water soluble initiators are not common. In order to generate a H-shaped macro-initiator, Gnanou et al. first synthesised a poly(ethylene oxide) (PEO) chain via living anionic polymerisation of ethylene oxide (EO).[11] A branch point was introduced by coupling the anionic chain end with an acyl chloride derivative of the Bis-MPA unit described by Hedrick

(Scheme 2).[1] The resulting macro-initiator was used for the ATRP of styrene in toluene, however, it could potentially be effective for aqueous reactions.[11]

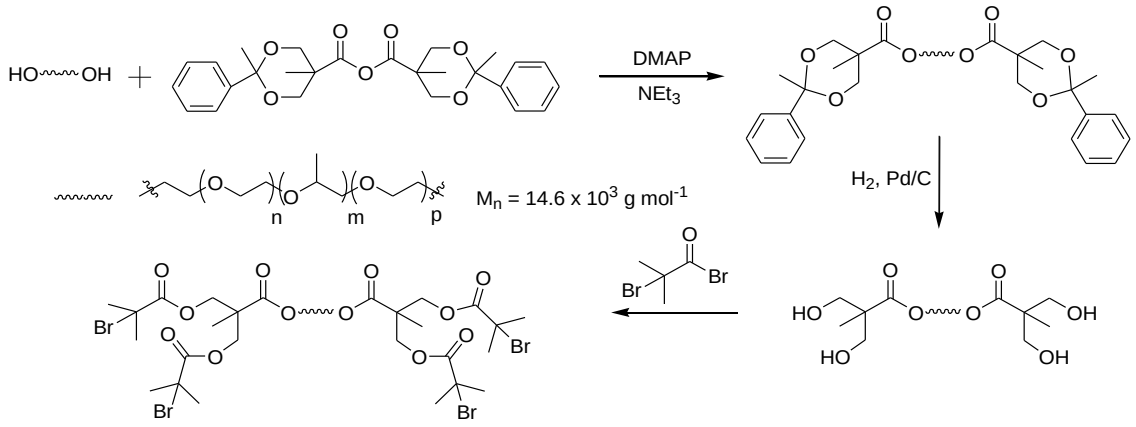

Scheme 3: Synthesis of PEG based macro-initiator using protected Bis-MPA

Izzo et al. followed a separate route to produce a similar macro-initiator (Scheme 3). [12] After co-polymerisation of propylene oxide (PPO) with EO, reaction with acetal protected Bis-MPA introduced the branching point.[12] After de-protection, the free hydroxyl groups were reacted with 2-bromoisobutyryl bromide to produce the final macro-initiator (Scheme 3). These macro-initiators were used for ATRP of methyl methacrylate (MMA) in toluene. Further branched PEG containing initiators were synthesised by Gnanou through anionic polymerisation of EO from tri-functional trimethylol propane (Fig. 3a) [13] This macro-initiator was then used to prepare a co-polymer with poly(acrylic acid) (PAA) via ATRP of *tert*-butyl acrylate (*t*BA) in acetone.[14] Moreover, Frey et al. functionalised branched polyglycerol to produce a macro-initiator which was also used for the polymerisation of *t*BA in acetone using ATRP (Fig. 3b).[15,16] To our knowledge none of these water-soluble multi-functional initiators have been used for aqueous copper mediated polymerisation reactions.

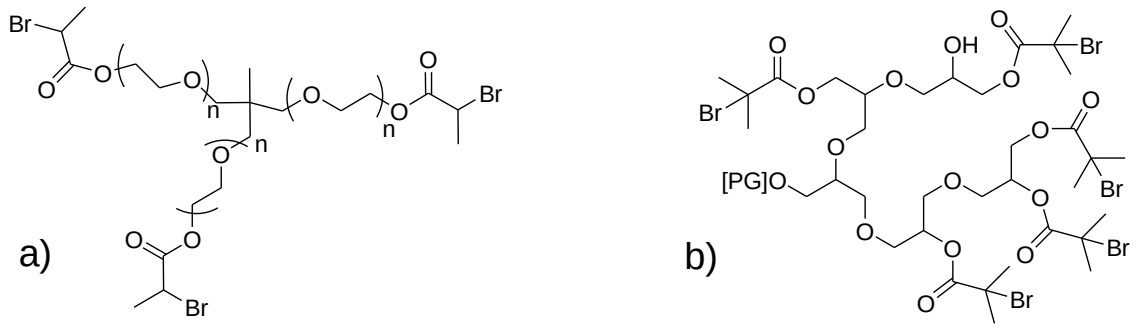

Figure 3: a) Branched PEG based macro-initiator (Gnanou);[14] **b)** Branched polyglycidol based macro-initiator (Frey)[16].

2.2. Experimental

2.2.1. Materials

Triethylamine (NEt_3, ≥ 99.5 %), 2-Bromopropionyl bromide (97 %), α-Bromoisobutyryl bromide (98 %), N,N'-dicyclohexylcarbodiimide (DCC, ≥ 99 %), dimethylolpropionic acid (Bis-MPA, 98 %), poly(ethylene glycol) (M_n ≈ 3350 g mol^{-1}, PEG-3350), mono-methoxy poly(ethylene glycol) (M_n ≈ 2000 g mol^{-1}, OMe-PEG) and magnesium sulfate ($MgSO_4$) were purchased from Sigma Aldrich and used without further purification. DCM, hexane and diethyl ether analytical grade solvents were purchased from Fisher Scientific and used as received. Hydrochloric acid (c.HCl, 37%) and 4-dimethylaminopyridine (DMAP, 99 %) were purchased from Fisher Scientific and used without further purification. Dry DCM wase obtained from the Durham University Chemistry Department solvent purification service (SPS). $CDCl_3$ for NMR analysis was purchased from Apollo Scientific.

2.2.2. Instrumentation

^1H and ^{13}C Nuclear Magnetic Resonance (NMR) spectra were recorded using a Bruker Avance-400, or Varian VNMRS 700 spectrometer operating at 400 and 700 MHz respectively, J values given in Hz. $CDCl_3$ was used as deuterated solvent for NMR analysis and the spectra were referenced to the solvent trace at 7.26 ppm. The following abbreviations are used in describing NMR spectra: s = singlet, d = doublet, t = triplet, m = multiplet, b = broad, dd = doublet of doublets. A ^{13}C Distortion Enhancement by Polarisation Transfer (DEPT) NMR experiment was used to distinguish between –C-, CH/CH_3 and $–CH_2$ carbon environments. The quaternary carbon environments do not appear in the DEPT spectrum, $–CH_2$ carbon resonances are inverted, whilst $-CH/-CH_3$ resonances remain un-inverted as in the ^{13}C NMR spectrum. 2D NMR experiments were also used to fully assign the proton and carbon environments in the products. ^1H-^1H **Co**rrelation **S**pectroscop**y** (COSY) demonstrated proton-proton correlations over two or three bonds. ^1H-^{13}C **H**eteronuclear **S**hift **C**orrelation **S**pectroscopy (HSQC) demonstrated correlation between directly bonded proton and carbons atoms. ^1H-^{13}C **H**eteronuclear **M**ultiple-**B**ond **C**orrelation (HMBC) demonstrated the correlation between proton and carbon environments through several bonds.

A measurement of molecular weight for low mass polymers was obtained using matrix assisted laser desorption/ionisation-time of flight (MALDI-ToF) mass spectrometry. Analysis was carried out using an Autoflex II ToF mass spectrometer (Bruker Daltonik GmBH) using a 337 nm nitrogen laser. Samples were prepared in solution (conc. = 1 mg ml^{-1}) and mixed with matrix

solution (conc. ≈ 50 mg ml^{-1}) in a ratio of 1:9. The mixture (1 μL) was spotted on to a metal target (pre-cleaned using methanol and acetone) and placed into the MALDI ion source. *Trans*-2-[3-*tert*-butylphenyl)-2-methyl-2-propenylidene)malonitrile (DCTB) was used as a suitable matrix. Molecular weight of small molecules was obtained using a Waters AQCUITY TQD (tandem quadrupole) mass spectrometer with an electrospray (ES) ion source for positive ionisation.

Fourier transform-infra-red (FT-IR) spectroscopy was conducted using a Perkin Elmer 1600 series spectrometer. Elemental analysis of small molecules obtained using an Exeter CE-440 elemental analyser.

2.2.3. Synthesis of 2,2-Bis(methyl 2-bromopropionate) propionic acid (BU-S)

2-Bromopropionyl bromide (9.83 ml, 93.9 mmol) was added dropwise to a solution of Bis-MPA (6.00 g, 44.7 mmol) and triethylamine (NEt_3) (13.42 ml, 93.9 mmol) in dry DCM (150 ml) maintained at 0°C, under a flow of nitrogen. The mixture was allowed to warm to room temperature and a white triethylammonium bromide salt precipitate formed. The reaction was stirred for 20 h and the salt was removed by filtration. The DCM was removed under reduced pressure leaving a solid product which was re-dissolved in diethyl ether (100 ml) and washed sequentially with aliquots of 2M HCl (50 ml) and distilled water (50 ml). The organic layer was separated and dried over $MgSO_4$ and the solvent was removed under reduced pressure. The isolated solid was washed with aliquots of hot water (60°C, 4 x 40 ml). The solid was dissolved using diethyl ether (50 ml) and a final aliquot of water added before the organic layer separated and dried over $MgSO_4$. The resulting pale yellow, viscous liquid product (**BU-S**) was isolated by removing the solvent under reduced pressure. Yield 73 % (13.26 g, 32.8 mmol); $C_{11}H_{16}O_6Br_2$; MS: *m/z* ES^+, M + Na^+ = 426 Da; ^{1}H NMR (700 MHz; $CDCl_3$): δ = 1.35 (s, 3H, *4*); 1.82 (d, 6H, *J 6.9*, *7*); 4.36 (m, 6H, *3/6*); 8.92 (br s, 1H, -*COOH*); ^{13}C NMR (176 MHz; $CDCl_3$): δ = 17.88 (*4*); 21.61 (*7*); 39.60 (*6*); 46.56 (*2*); 66.01 (*3*); 169.72 (*5*); 178.55 (*1*); IR = 1708 cm^{-1}, 1734 cm^{-1} (C=O); 2800-3000 cm^{-1} (-C-H/-COOH); CHN: Expected = %C = 32.70, %H = 3.99, %N = 0.00; Measured = %C = 32.52, %H =4.00, %N = 0.00.

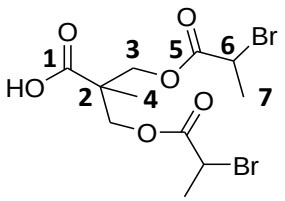

Figure 4: Structure of 2,2-Bis(methyl 2-bromopropionate) propionic acid (**BU-S**) including labelled carbon atoms for reference.

2.2.4. Synthesis of 2,2-Bis(methyl 2-bromoisobutyrate) propionic acid (**BU-T**)

α-Bromoisobutyryl bromide (4.40 ml, 35.7 mmol) was added dropwise to a solution of Bis-MPA (2.00 g, 14.9 mmol) and triethylamine (5.20 ml, 36.6 mmol) in dry DCM (50 ml) at 0°C, under a flow of nitrogen. The mixture was allowed to warm to room temperature and a white triethylammonium bromide salt precipitate formed. The reaction was stirred for 20 h and the salt was removed by filtration. The DCM was removed under reduced pressure leaving a solid product which was re-dissolved in diethyl ether (50 ml) and washed with HCl (2M, 3 x 20 ml). The organic layer was dried over $MgSO_4$, the mixture was filtered, and the solution concentrated under reduced pressure. The residue was washed with hot water (60°C, 3 x 10 ml) before the white solid product (**BU-T**) was re-crystallised from hexane, isolated by filtration and dried under reduced pressure. Yield 83 % (5.30 g, 12.3 mmol); $C_{13}H_{20}O_6Br_2$; MS: *m/z* ES^+, M + Na^+ = 455 Da; ^{1}H NMR (700 MHz; $CDCl_3$): δ = 1.37 (s, 3H, *4*); 1.91 (s, 12H, *7*); 4.36 (q, 4H, J_{AB} *32.2,* J_{AC} *11.1* , *3*); 10.40 (br s, 1H, -COOH); ^{13}C NMR (176 MHz; $CDCl_3$): δ = 17.90 (*4*); 30.76 (*7*); 46.71 (*2*); 55.34 (*6*); 66.12 (*3*); 171.09 (*5*); 178.89 (*1*); IR = 1692 cm^{-1}/ 1730 cm^{-1} (C=O); 2800-3000 cm^{-1} (C-H/-COOH); CHN Expected = %C = 36.14, %H = 4.67 %N = 0.00; Measured = %C = 36.77, %H = 4.78, %N = 0.00.

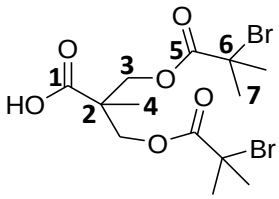

Figure 5: Structure of 2,2-Bis(methyl 2-bromoisobutyrate) propionic acid (**BU-T**) including labelled carbon atoms for reference.

2.2.5. Synthesis of Poly(ethylene glycol)-di-2,2-Bis(methyl 2-bromopropionate) propionate (**I4-S**)

PEG-3350 (9.00 g, 2.69 mmol) was added to a flask fitted with a stirrer bar and a water condenser. To the flask was added **BU-S** (2.70 g, 6.73 mmol) and DCM (90 ml) to dissolve. DCC (1.83 g, 8.88 mmol) and DMAP (0.22 g, 1.78 mmol) were dissolved in DCM (10 ml). This solution was added to the flask to start the reaction and a white dicyclohexyl urea side product precipitated immediately in the solution. The reaction was stirred at room temperature for 24 h before filtering through glass filter paper to remove the urea. The solution was concentrated to around 20 ml before precipitating into cold diethyl ether. The solid was isolated and dried before re-dissolving and re-filtering several times to remove any further urea. The solution was re-precipitated in cold diethyl ether. The product (**I4-S**) was isolated by filtration and dried

under vacuum. Yield 49 % (5.50 g, 1.33 mmol); Average $C_{174}H_{334}O_{87}Br_4$; MS: *m/z* MALDI-ToF $M+H^+$ = 4007 (n = 73), 4051 (n = 74), 4095 (n = 75), 4139 (n = 76), 4183 (n = 77); ^{1}H NMR (700 MHz; $CDCl_3$): δ = 1.29 (s, 6H, *4*); 1.79 (d, 12H, *J 6.9*, *7*); 3.59 (m, 4H, *9'*); 3.61 (s, 4H repeat unit, *8*); 3.67 (t, 4H, *J 5.6*, *10*); 3.69 (m, 4H, *9*); 4.22 – 4.42 (m, 16H*, 3, 6, 10'*); ^{13}C NMR (176 MHz; $CDCl_3$): δ = 17.86 (4); 21.58 (*7*); 39.68 (*6*); 46.61 (*2*); 61.74(*9*); 64.42 (*10'*); 66.19 (3); 68.84 (*10*); 70.61 (*8*); 72.59 (*9'*); 169.60 (*5*); 172.22 (*1*); IR = 1744 cm^{-1} (-C=O stretch), 2882 cm^{-1} (-C-H stretch).

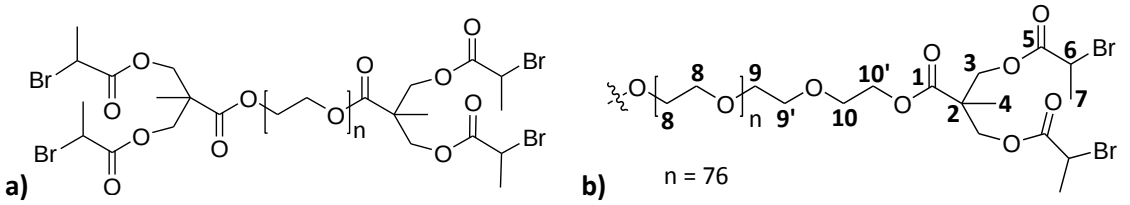

Figure 6: (a) Structure of Poly(ethylene glycol)-di-2,2-Bis(methyl 2-bromopropionate) propionate (**I4-S**). **(b)** Structure including labelled carbon atoms for reference.

2.2.6. Synthesis of Poly(ethylene glycol)-di-(2,2-Bis(methyl 2-bromoisobutyrate) propionate (I4-T)

PEG-3350 (3.00 g, 0.90 mmol) was added to a flask fitted with a stirrer bar and a water condenser. To the flask was added **BU-T** (0.98 g, 2.24 mmol) and DCM (25 ml) to dissolve. DCC (0.61 g, 2.96 mmol) and DMAP (0.72 g, 0.59 mmol) were dissolved in DCM (5 ml). This solution was added to the flask to start the reaction and a white dicyclohexyl urea side product precipitated immediately in the solution. The reaction was stirred at room temperature for 24 h before filtering through glass filter paper to remove the urea. The solution was concentrated to around 5 ml before precipitating in cold diethyl ether. The precipitation process was repeated three times. The product (**I4-T**) was isolated by filtration and dried under vacuum. Yield 70 % (2.65 g, 0.63 mmol); Average $C_{178}H_{342}O_{87}Br_4$ MS: *m/z* MALDI-ToF $M+H^+$ = 4109 (n = 74), 4153 (n = 75), 4197 (n = 76), 4241 (n = 77), 4285 (n = 78); ^{1}H NMR (700 MHz; $CDCl_3$): δ = 1.33 (s, -6H, *4*); 1.90 (s, 24H, *7*); 3.59 (t, 4H, *J 4.9*, *9'*); 3.62 (s, 4H repeat unit, *8*); 3.68 – 3.73 (m, 8*H, 10/9*); 4.28 (t, 4H, *J 4.9*, *10'*); 4.35 (dd, 8H, J_{AB} *42.0* J_{AC} *10.9*, *3*); ^{13}C NMR (176 MHz; $CDCl_3$): δ = 17.98 (*4*); 30.76 (*7*); 46.78 (*2*); 55.50 (*6*); 61.83 (*9*); 64.48 (*10'*); 66.37 (*3*); 68.92 (*10*); 70.68 (*8*); 72.69 (*9'*); 171.04 (*5*); 172.38 (*1*). IR = 1738 cm^{-1} (-C=O stretch), 2890 cm^{-1} (-C-H stretch).

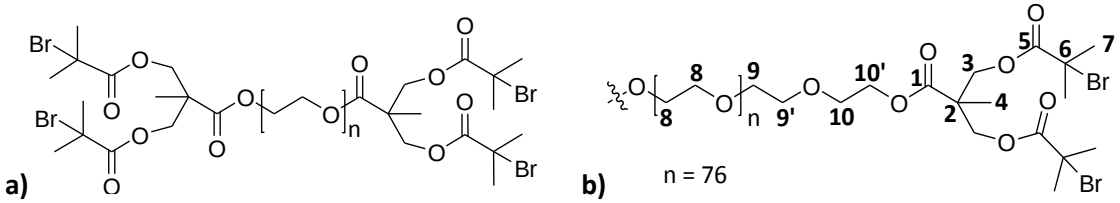

Figure 7: (a) Structure of Poly(ethylene glycol)-di-(2,2-Bis(methyl 2-bromoisobutyrate) propionate (**I4-T**). **(b)** Structure including labelled carbon atoms for reference.

2.2.7. Synthesis of Poly(ethylene glycol) monomethyl ether mono(2,2-Bis(methyl 2-bromopropionate)propionate (I2-S)

OMe-PEG (1.00 g, 0.50 mmol) was added to a flask fitted with a stirrer bar and a water condenser. To the flask was added **BU-S** (0.22 g, 0.55 mmol) and DCM (5 ml) to dissolve. DCC (0.12 g, 0.61 mmol) and DMAP (0.02 g, 0.14 mmol) were dissolved in DCM (5 ml). This solution was added to the flask to start the reaction and a white dicyclohexyl urea side product precipitated immediately in the solution. The reaction was stirred at room temperature for 24 hours before filtering through glass filter paper to remove the urea. The solution was concentrated under reduced pressure and precipitated in cold diethyl ether. The precipitation process was repeated once more. The product (**I2-S**) was isolated by filtration and dried under reduced pressure. Yield 67 % (0.80 g, 0.33 mmol); Average $C_{102}H_{198}O_{51}Br_2$; MS: *m/z* MALDI-ToF M + H^+ = 2313 (n = 43), 2357 (n = 44), 2401 (n = 45), 2445 (n = 46), 2489 (n = 47); ^{1}H NMR (700 MHz; $CDCl_3$): δ = 1.29 (s, 3H, *4*); 1.78 (d, 6H, *J 7.0*, *7*); 3.35 (s, 3H, 12); 3.52 (t, 2H, *J 4.9*, *11'*); 3.58 (t, 2H, *J 4.9*, *9'*); 3.61 (s, 4H repeat unit, *8*); 3.67 (t, 2H, *10*); 3.69 (m, 2H, *9*); 4.00 – 4.50 (m, 7H, *3/6/10'*); ^{13}C NMR (176 MHz; $CDCl_3$): δ = 17.77 (*4*); 21.49 (*7*); 39.63 (*6*); 46.51 (*2*); 58.99 (*12*); 61.66 (*9*); 64.33 (*10'*); 66.21 (*3*); 68.76 (*10*); 70.53 (*8*); 71.90 (11'); 72.51 (9'); 169.48 (*5*); 172.13 (*1*). IR = 1743 cm^{-1} (C=O), 2800–3000 cm^{-1} (C-H).

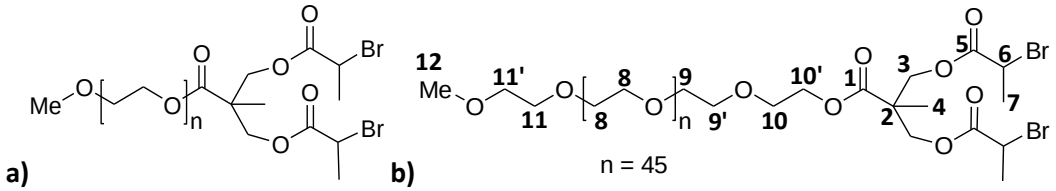

Figure 8: a) Structure of Poly(ethylene glycol) monomethyl ether mono(2,2-Bis(methyl 2-bromopropionate) propionate (**I2-S**). **(b)** Structure including labelled carbon atoms for reference.

2.3. Results and Discussion

A simple two-step process (Scheme 4a) was used to synthesise water soluble, PEG-based macro-initiators (**I4**) for the production of star polymers. By coupling a branching unit (**BU**) at

each end of the PEG chain, four potential initiation sites for copper mediated polymerisation reactions were introduced. The incorporation of ester groups in to the core molecule in this way may provide the opportunity for degradation of any polymers synthesised following their use as drag reducing agents. A literature procedure, with slight modifications to purification, was used to synthesise branching units containing both secondary (**BU-S**) and tertiary (**BU-T**) bromine initiation sites.[1] Commercially available PEG with M_n = 3350 g mol^{-1} (PEG-3350) allowed easy recovery of the macro-initiator by precipitation. The resulting product was readily water soluble. Synthesis of both initiators allows comparison of their suitability for different polymerisation reactions. For illustrative purposes, full discussion of the **I4-S** synthesis is detailed below. The corresponding **I4-T** initiator was evaluated in the same manner and the most important analysis is included. Also synthesised was an analogous macro-initiator with two secondary bromine initiation sites by reaction of the branching unit, **BU-S** with OMe-PEG (M_n = 2000 g mol^{-1}) (**I2-S**) using the same method (Scheme 4b).

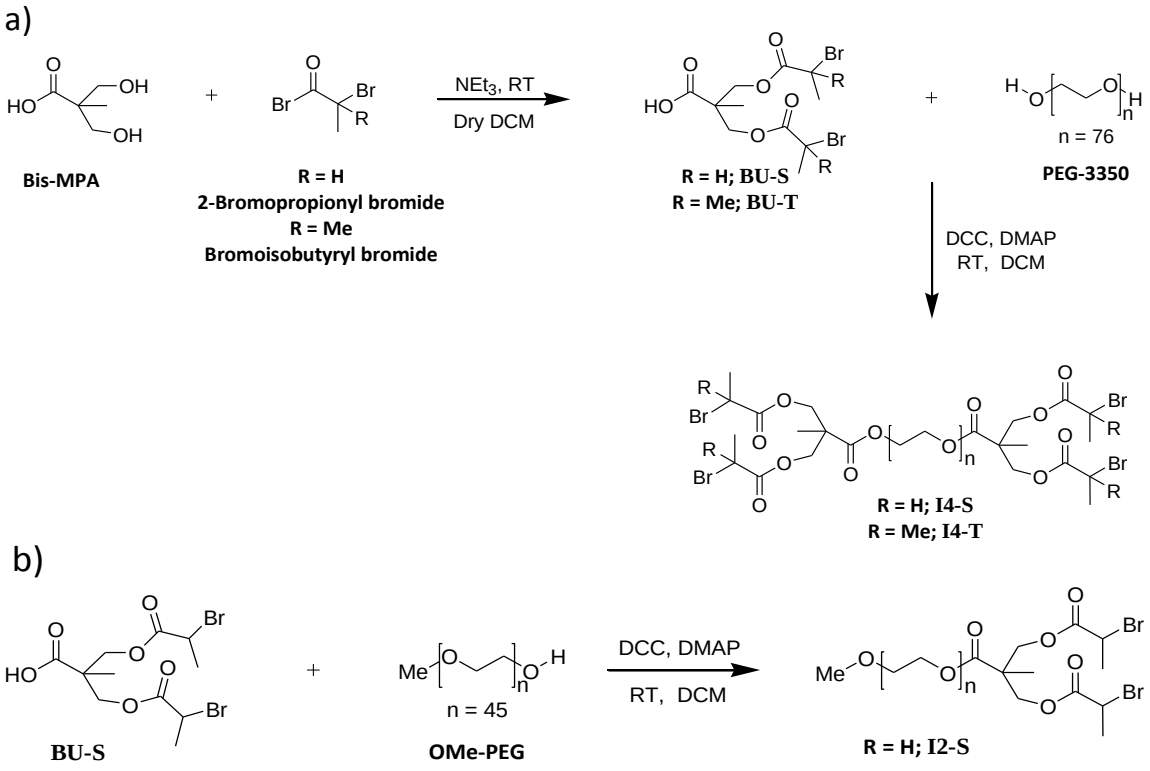

Scheme 4: a) Two step synthesis of; branching unit (**BU-S**, R = H and **BU-T**, R = Me) in the first step; and PEG based tetra-functional macro-initiator (**I4-S**, R = H and **I4-T**, R = Me) in the second step. **b)** Synthesis of PEG based bi-functional macro-initiator, **I2-S**.

2.3.1. Synthesis of 2,2-Bis(methyl 2-bromopropionate) propionic acid (BU-S)

In the first step of Scheme 4a, **BU-S** was synthesised by reacting Bis-MPA and 2-bromopropionyl bromide at room temperature.[17] The two Bis-MPA hydroxyl groups form ester bonds through a nucleophilic addition-elimination reaction with the acyl bromide. The resulting molecule contains a carboxylic acid group which can be coupled to a PEG chain end. The two secondary C-Br bonds can act as initiation sites for polymerisation. Triethylamine (NEt_3) acts as a base and also a scavenger for Br^- released during the reaction; this was observed by the precipitation of NEt_3Br following the addition of 2-bromopropionyl bromide. Furthermore, NEt_3 and DCM are necessary to solubilise Bis-MPA which is insoluble in most common solvents. Starting materials were dried prior to use and the mixture maintained under a flow of N_2 in order to prevent hydrolysis of the acyl bromide bond.

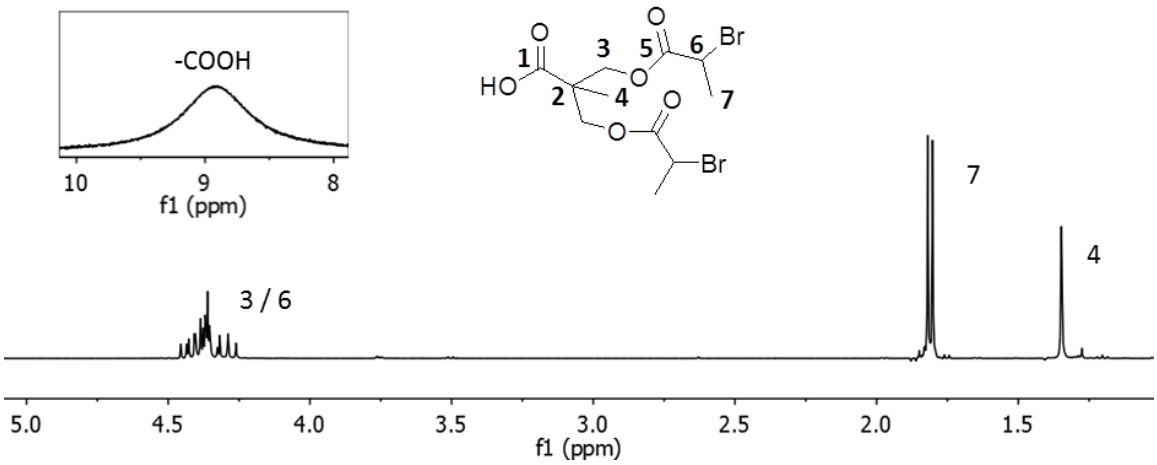

Figure 9: 700 MHz-^{1}H NMR spectrum of **BU-S**. Carboxylic acid -OH resonance shown inset.

The pure product was analysed using ^{1}H and ^{13}C NMR spectroscopy. The ^{1}H NMR spectrum is shown in Figure 9. The singlet at 1.35 ppm is assigned to the methyl group **4**. The doublet at 1.82 ppm is attributed to the two methyl groups (**7**) adjacent to a C-Br bond; the resonance is split due to its proximity to the neighbouring -CH group. Integration of these signals (**4** and **7**) confirms they represent 3 and 6 protons, respectively. The multiplet at 4.36 ppm corresponds to the two methylene groups **3**, and the methine group **6**. The presence of the methine proton (**6**) as part of this multiplet is confirmed using ^{1}H-^{1}H COSY because of its correlation with the resonance of **7** (Fig. 10).

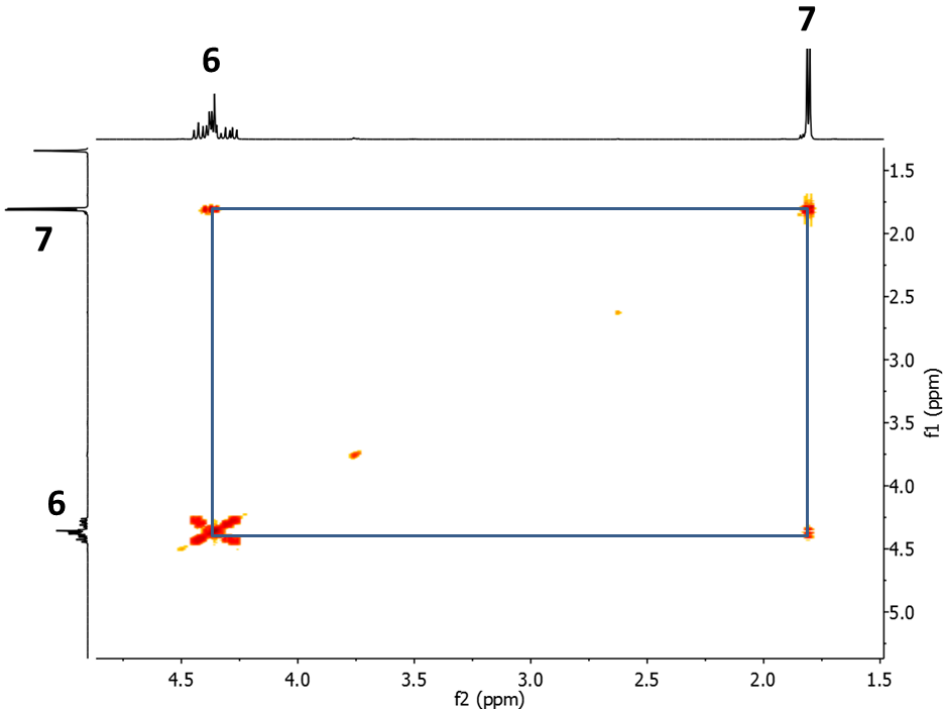

Figure 10: 700 MHz-^{1}H-^{1}H COSY spectrum of **BU-S**, highlighting the correlation between resonance **7** and **6.**

The resonances of **3** and **6** are both split due to the proximity of a methyl group; integration confirms that the multiplet represents 6 protons in total. Importantly, the resonance corresponding to the carboxylic acid –OH can clearly be observed at around 9 ppm and is shown inset in Figure 9.

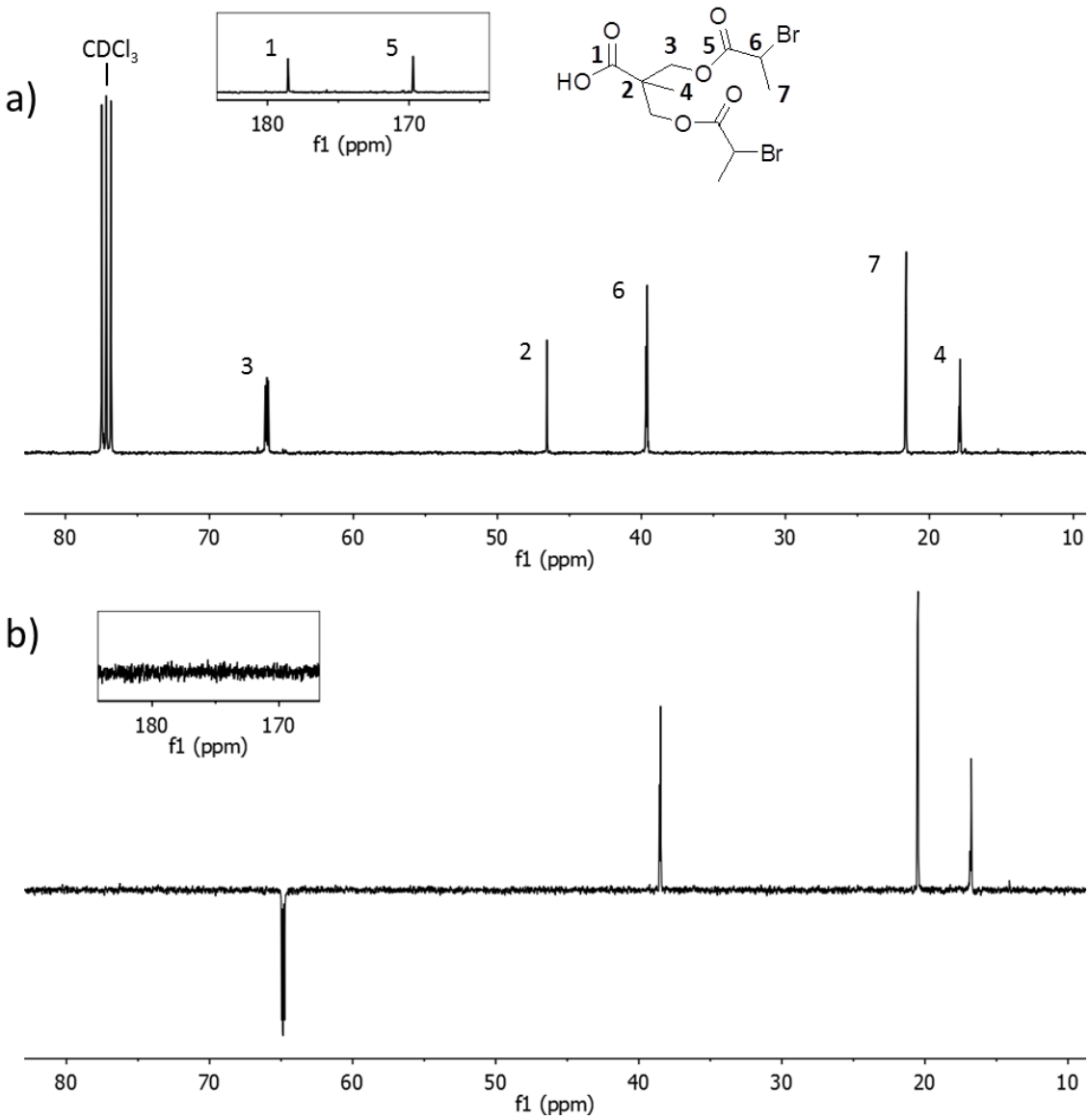

Figure 11: a) 176 MHz-^{13}C NMR spectrum of **BU-S**, carbonyl region shown inset. **b)** 100 MHz-^{13}C DEPT spectrum of **BU-S**, carbonyl region shown inset.

Analysis of the ^{13}C and ^{13}C DEPT NMR spectra allows the respective C, –CH, -CH_2 and –CH_3 carbon environments to be distinguished and assigned. The ^{13}C spectrum of **BU-S** is shown in Figure 11a. The resonances at low shift (17.88 and 21.61 ppm) do not change in the ^{13}C DEPT (Fig. 11b) spectrum and are assigned as the –CH_3 environments **4** and **7**, respectively. This is confirmed using ^{1}H-^{13}C HSQC (Fig 12) which verifies the correlation between these carbon environments and closest proton environments (**4** and **7**).

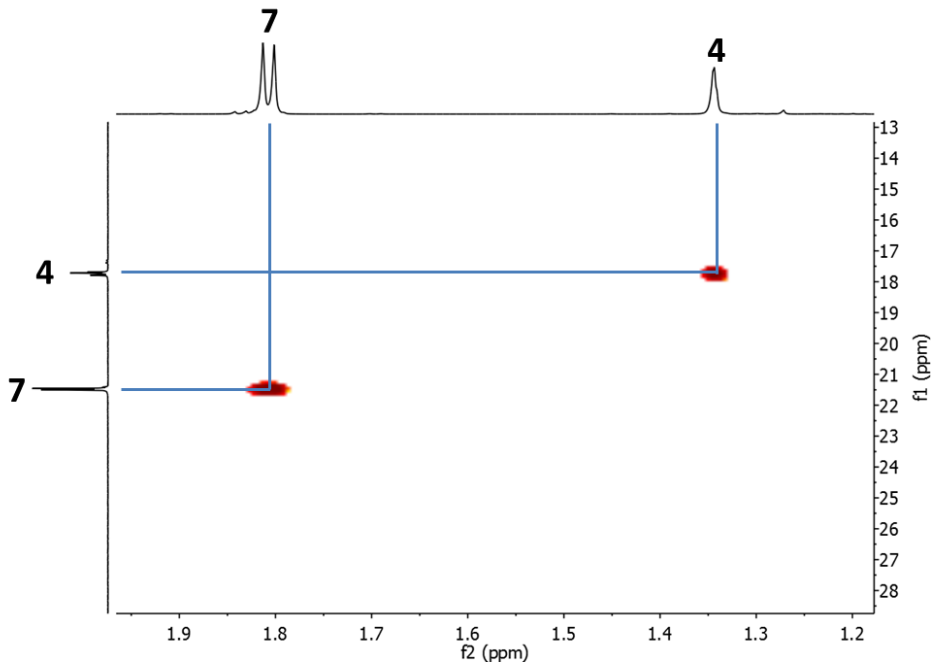

Figure 12: 700 MHz-^{1}H-^{13}C HSQC spectrum of **BU-S**, highlighting the correlation between the proton and carbon resonances of **4** and **7**.

The resonance at 39.60 ppm also remains un-inverted and is therefore assigned to the single methine environment (**6**)**.** The resonance at 66.01 ppm is the only inverted in the ^{13}C DEPT spectrum, demonstrating it represents the only $–CH_2$ environment (**3**). Finally, the disappearance of the resonances at 46.52, 169.72 and 178.55 ppm (Fig. 11a) in the ^{13}C DEPT spectrum (Fig. 11b) reveals they correspond to quaternary carbons. The resonance at 46.52 ppm is assigned as **2**. Through the correlation between the C=O and the closest $–CH_3$ environments (**4** and **7**), determined using ^{1}H-^{13}C HMBC NMR spectroscopy, assignment of the resonances at 169.72 ppm and 178.55 ppm was confirmed as **5** and **1**, respectively (Fig. 13).

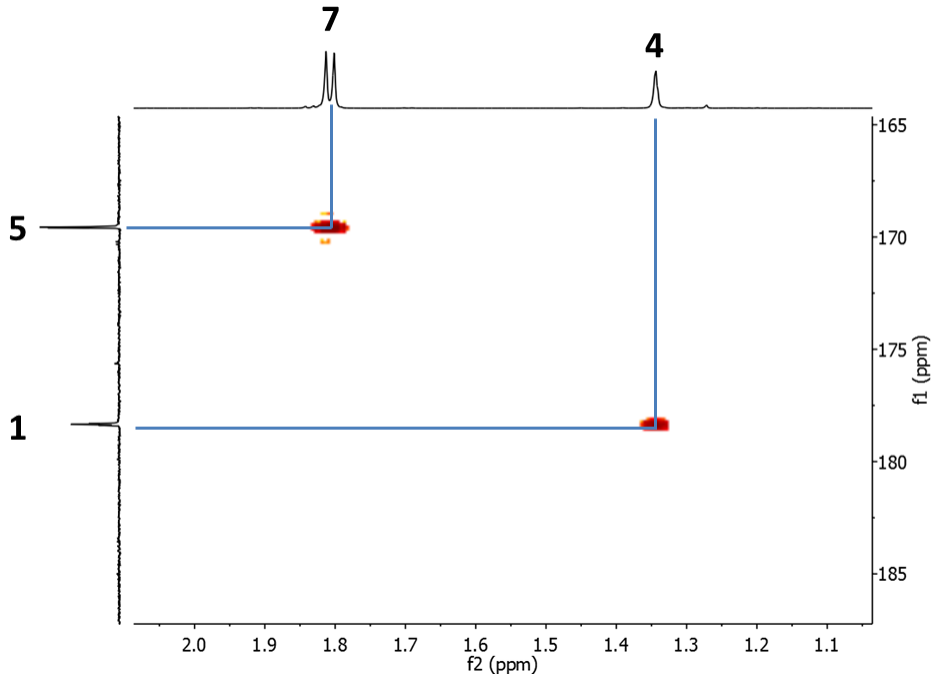

Figure 13: 700 MHz-^{1}H-^{13}C HMBC spectrum of **BU-S**; highlighting the correlation between **7** - **5** and **4** - **1**.

The presence of these two distinct C=O environments was also confirmed using FT-IR spectroscopy shown in Figure 14a (the frequencies between 1600-1800 cm^{-1} are expanded in Figure 14b). The spectrum (Fig. 14b) shows signals at 1708 cm^{-1} (**1**) and 1734 cm^{-1} (**5**), characteristic frequencies for carboxylic acid and ester bond stretches, respectively. The broad signal at 2800-3000 cm^{-1} indicates the presence of alkane –C-H and carboxylic acid –O-H groups in the molecule. Moreover, the correct *m/z* for the product was observed using ESI-MS ($M + Na^{+}$ = 426 Da). Elemental analysis of CHN content closely matches the values expected.

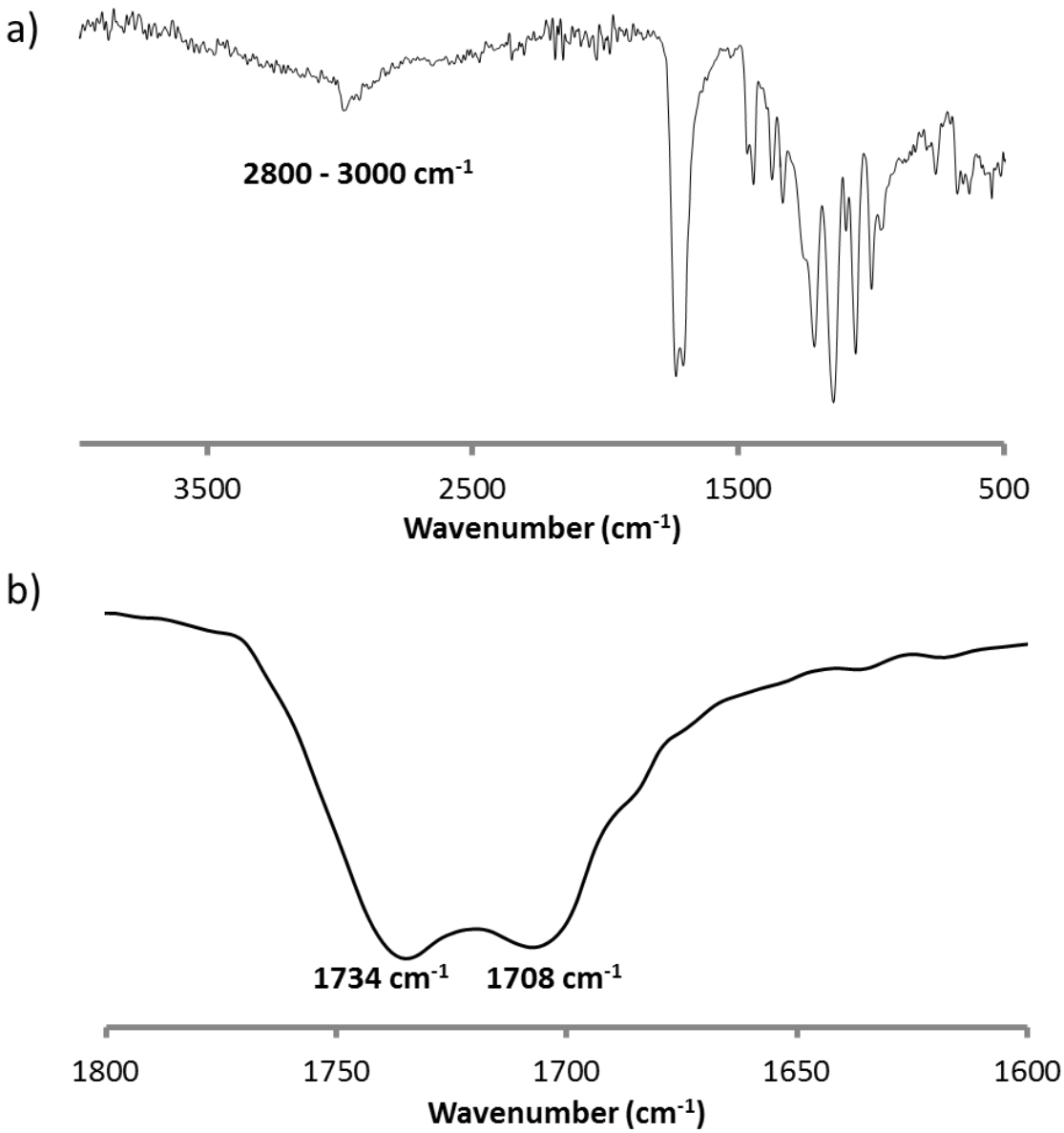

Figure 14: FT-IT spectrum of; **a)** **BU-S**; **b)** **BU-S**, Expanded carbonyl region.

2.3.2. Synthesis of 2,2-Bis(methyl 2-bromoisobutyrate) propionic acid (BU-T)

An equivalent tertiary bromine branching unit (**BU-T**) was synthesised using the same procedure (Scheme 4a, Step 1) by the reaction of Bis-MPA with α-Bromoisobutyryl bromide. The product was again analysed using ^{1}H and ^{13}C NMR spectroscopy. The ^{1}H NMR spectrum is shown in Figure 15 and demonstrates several key differences when compared with that of **BU-S**. Two methyl resonances are again observed, at a shift 1.37 (**4**) and 1.91 (**7**) ppm. By comparing the integration of these resonances, a proton ratio of 3:12 is calculated, due to the presence of the second $–CH_3$ group adjacent to the C-Br bond. Resonance **7** appears as a singlet as this environment is no longer coupled with at –CH proton. The multiplet observed at 4.36 ppm in the **BU-S** ^{1}H NMR spectrum (Fig. 9) simplifies to a quartet, assigned to **3**, and

integration of this resonance confirms it represents four protons. The carboxylic acid –OH resonance is again observed at high shift (Figure. 15, inset).

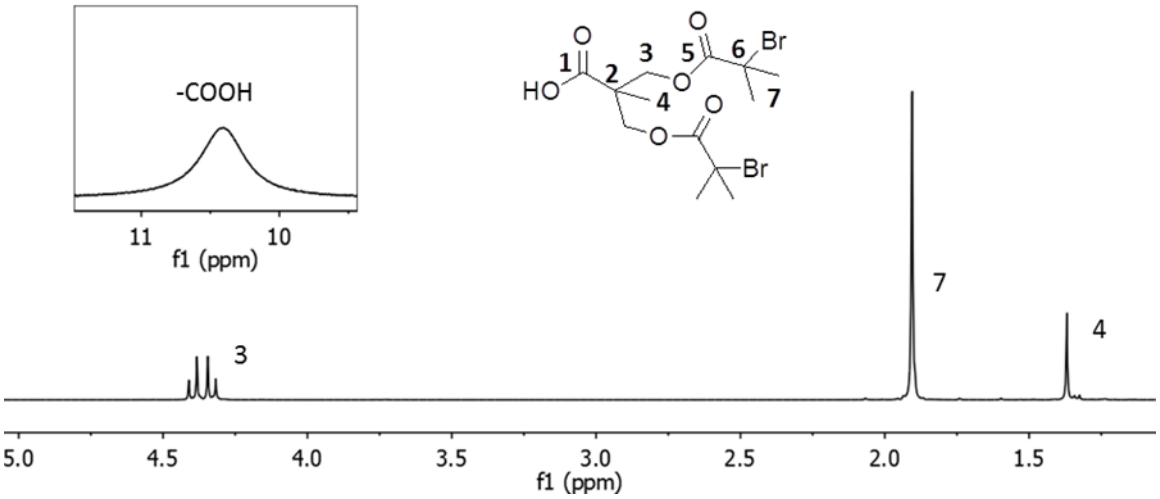

Figure 15: 700 MHz-^{1}H NMR spectrum of **BU-T**. Carboxylic acid -OH resonance shown inset.

Using ^{1}H-^{13}C HSQC NMR spectroscopy (Appendix A, Fig. 1) the methyl carbons are assigned as 17.90 (**4**) and 30.76 (**7**) ppm in the ^{13}C NMR spectrum (Fig. 16). The presence of the second quaternary carbon (**6**) is observed by its disappearance from the ^{13}C DEPT spectrum (Appendix A, Fig. 2) and this allows assignment of the resonance at 55.34 ppm. This resonance demonstrates a downfield shift when compared with peak **6** in the **BU-S** ^{13}C NMR spectrum (Fig. 11a = 39.60 ppm) due to the proximity of a second methyl group. There is no change in carbon environment **2** and this remains almost unchanged at 46.71 ppm. Furthermore, the shift for the methylene carbon **3** remains at around 66 ppm and the ester and carboxylic acid resonances are present at 171.09 (**5**) and 178.89 (**1**) ppm, respectively (Appendix A, Fig. 3). Analysis of the FT-IR spectrum again demonstrates the presence of a carboxylic acid (1692 cm^{-1}, **1**) and ester (1730 cm^{-1}, **5**) group (Appendix A, Fig. 4). A signal corresponding to a –CH and –OH stretch between 2800 and 3000 cm^{-1} is also observed. The correct *m/z* for the product (M + Na^{+} = 455 Da) was measured using ESI-MS and elemental analysis confirms a CHN content closely matching the values anticipated.

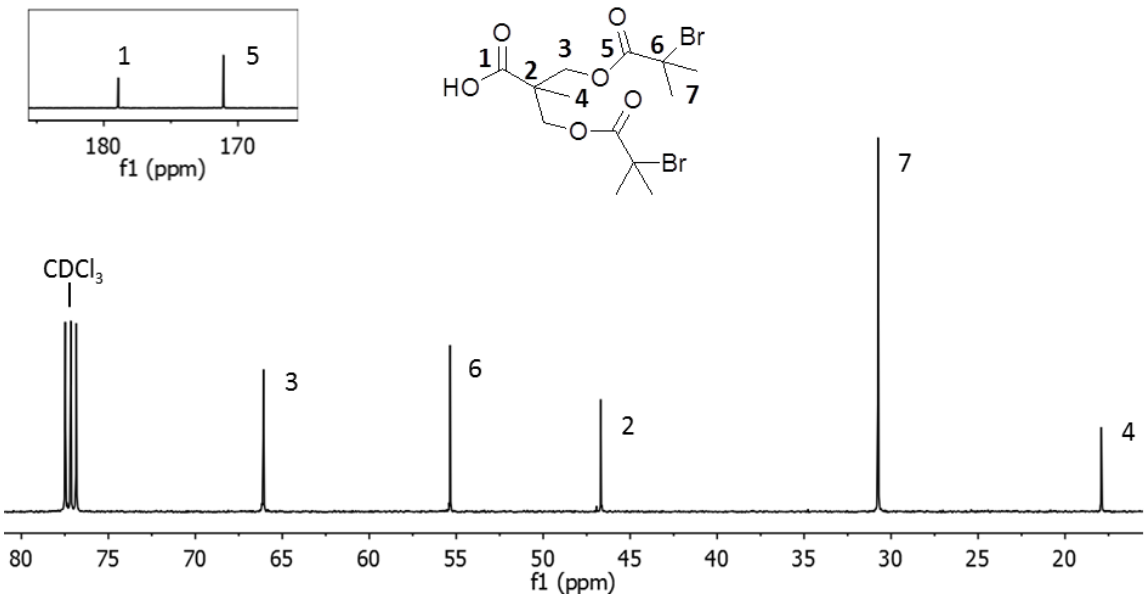

Figure 16: 176 MHz-^{13}C NMR spectrum of **BU-T**, carbonyl region shown inset.

2.3.3. Synthesis of Poly(ethylene glycol)-di-2,2-Bis(methyl 2-bromopropionate) propionate (I4-S)

In the second stage of the synthesis (Scheme 4a), the carboxylic acid group of the branching unit was coupled to the –OH end groups of PEG-3350 in a Steglich esterification reaction. Dicyclohexylcarbodiimide (DCC) was utilised as a coupling agent and 4-dimethylaminopyridine (DMAP) as a base. A dicyclohexylurea precipitate formed almost immediately in the solution demonstrating the fast reaction rate. The pure product was analysed using ^{1}H and ^{13}C NMR spectroscopy and the ^{1}H NMR spectrum is shown in Figure 17a. For comparison, the ^{1}H NMR spectra of **BU-S** and PEG-3350 are shown in Figure 17b and 17c, respectively.

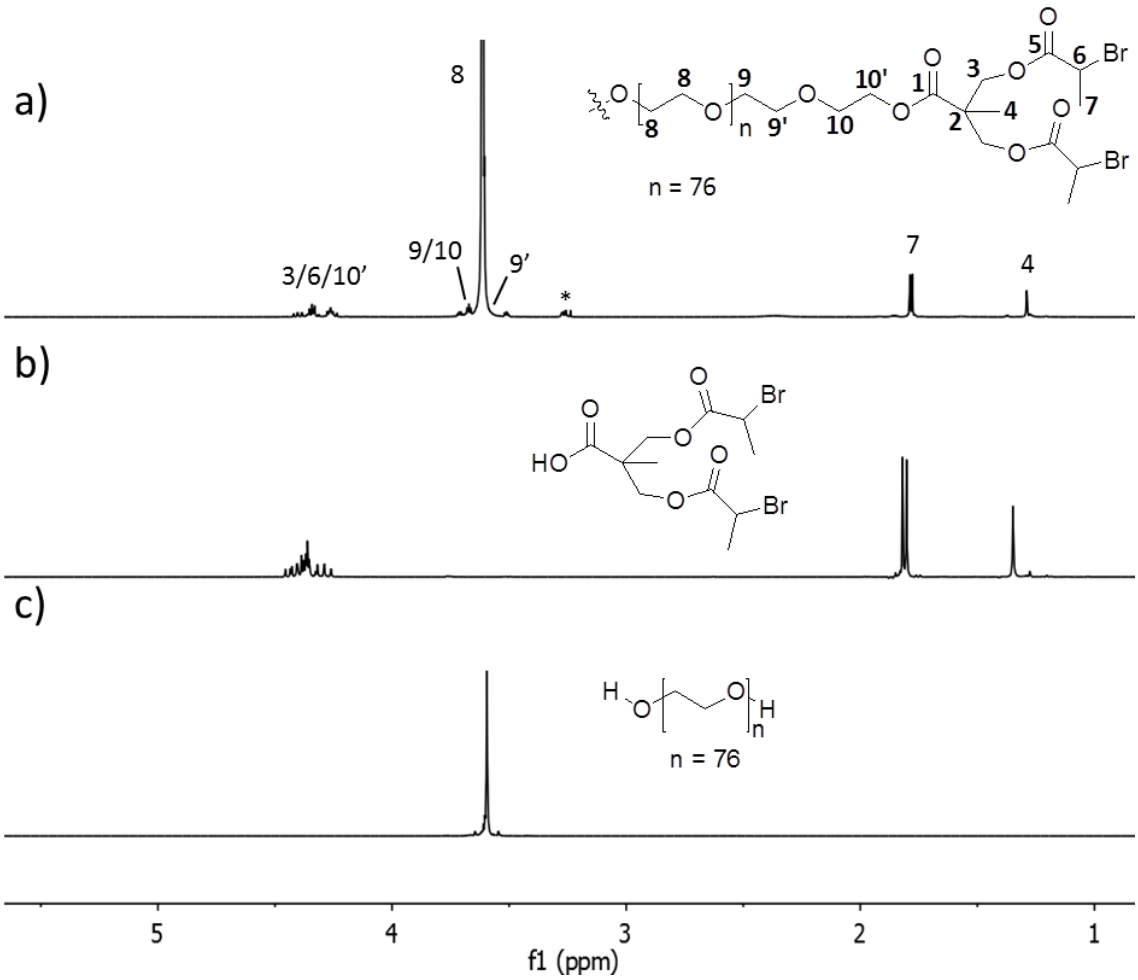

Figure 17:700 MHz-^{1}H NMR spectrum of; **a) I4-S**; **b) BU-S**; **c)** PEG-3350. * = Unidentified peak.

A very intense singlet is observed at 3.61 ppm in the ^{1}H NMR spectrum (Fig. 17a) due to the addition of a large number of PEG –CH_2 protons (**8**). The corresponding carbon environment is also present as an intense resonance at 70.61 ppm in the ^{13}C NMR spectrum (Fig. 18a). The ^{13}C NMR spectra of **BU-S** (b) and PEG-3350 (c) are again included in Figure 18 for comparison. Also visible in both the ^{1}H and ^{13}C NMR spectra are the end group environments; **4** (^{1}H = 1.29 ppm, ^{13}C = 17.86 ppm), **7**, (^{1}H = 1.79 ppm, ^{13}C = 21.58 ppm), **6** (^{1}H = 4.22-4.42 ppm, ^{13}C = 39.68ppm) and **3** (^{1}H = 4.22-4.42 ppm, ^{13}C = 66.19 ppm).

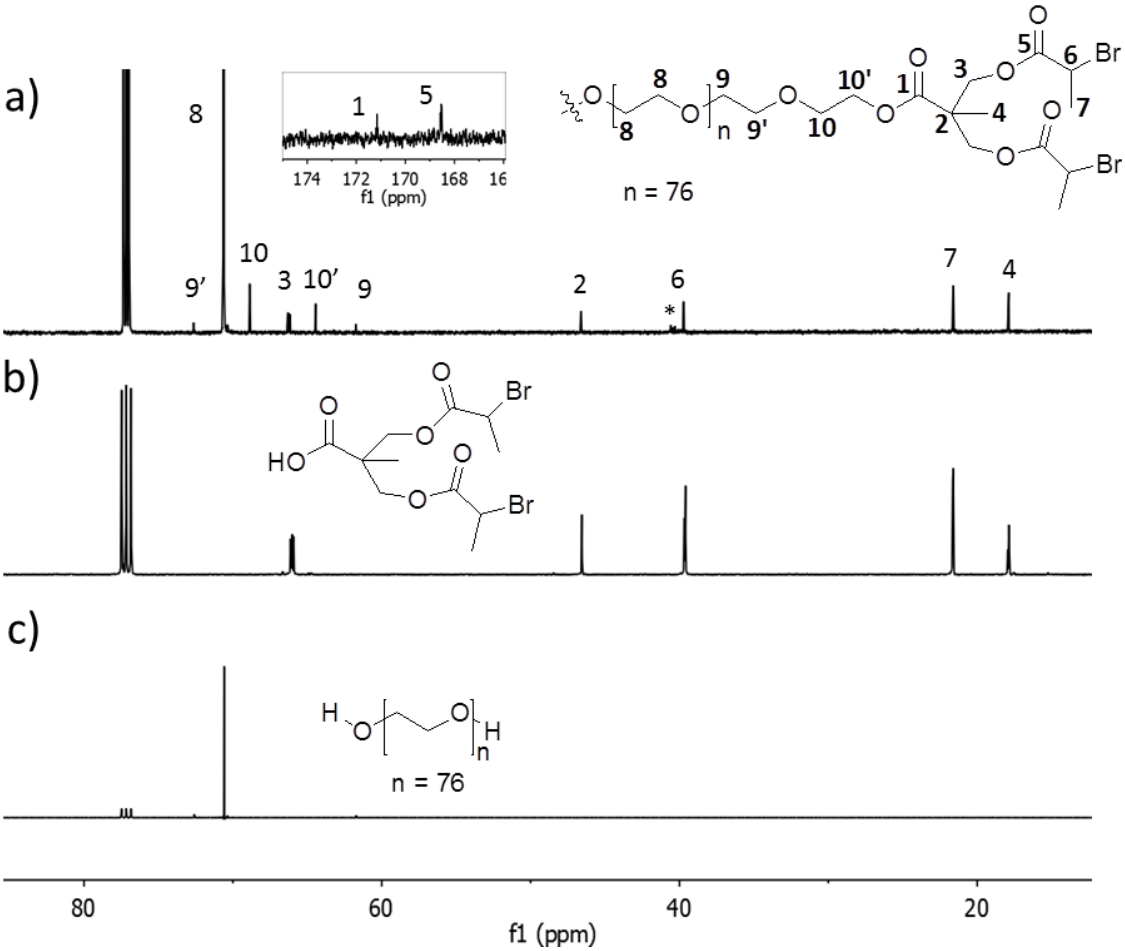

Figure 18: 176 MHz-^{13}C NMR spectrum of; **a) I4-S**, carbonyl region shown inset; **b) BU-S**; **c)** 100 MHz-^{13}C NMR spectrum of PEG-3350. * = Unidentified peak.

The presence of these end groups (**4**, **7**, **6** and **3**) in the product is highlighted by comparison with the ^{1}H NMR spectrum of the **BU-S** starting material (Fig. 17b). Integration of these proton resonances confirms a ratio consistent with the starting material. By comparing the integration of the PEG –CH_2 (**8**) resonance to that of the end group resonance **4** (representing 6 methyl protons), a value of 302 protons is calculated for the PEG backbone. This closely matches the expected value of 304 protons for PEG with an average number of repeat units, n = 76 (M_n ≈ 3350 g mol^{-1}) and supports full incorporation of PEG into the final product. Further important evidence for the attachment of the branched units comes from the appearance of new resonances (**10** and **10'**) in the ^{1}H NMR spectrum corresponding to a change in environment closest to the new chain end groups. In Figure 19 the ^{1}H NMR spectra of **I4-S** (a), **BU-S** (b) and PEG-3350 (c) are compared, with the region around the PEG chain resonance **8** (3.61 ppm) expanded. From this comparison a change in the resonances nearest to the PEG chain end (**10** and **10'**) can be observed. Particularly clear is the resonance at 4.25 ppm which is not present in the either PEG-3350 or **BU-S** spectrum.

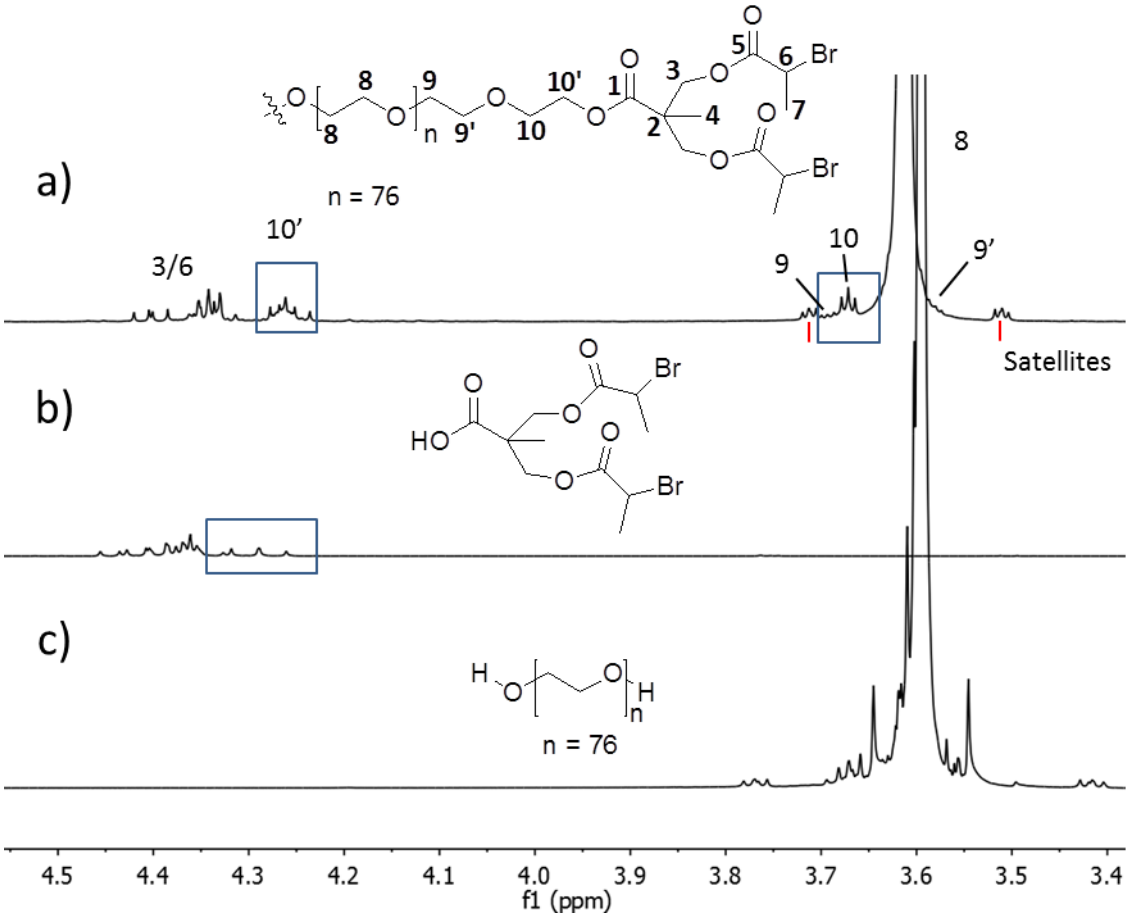

Figure 19: 700 MHz-^{1}H NMR spectrum of: **a) I4-S**, **b) BU-S**, **c)** PEG-3350 expanded to highlight the PEG chain resonances.

Detailed study of ^{1}H-^{1}H COSY, ^{1}H-^{13}C-HSQC and ^{1}H-^{13}C HMBC 2D NMR in combination with the ^{1}H, ^{13}C and ^{13}C DEPT NMR spectra, allows full assignment of both the proton and carbon environments nearest to the PEG chain ends (Fig.17a/18a). Most significant is the proton resonance **10'**, which is shown to correlate through multiple bonds with the carbonyl **1** using ^{1}H-^{13}C HMBC spectroscopy (Fig. 20).

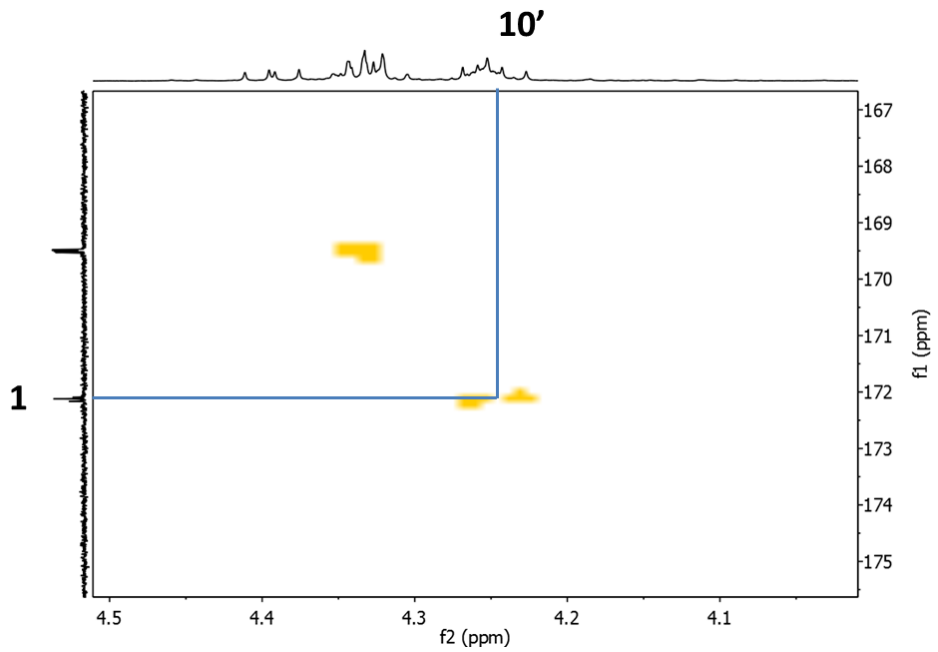

Figure 20: 700 MHz-^{1}H-^{13}C HMBC spectrum of **I4-S** highlighting the correlation between **1** (carbon) and **10'** (proton) environments.

This can be extrapolated to assign the ^{1}H and ^{13}C resonances closest to it using ^{1}H-^{1}H COSY (Fig. 21) and ^{1}H-^{13}C HSQC NMR (Fig. 22).

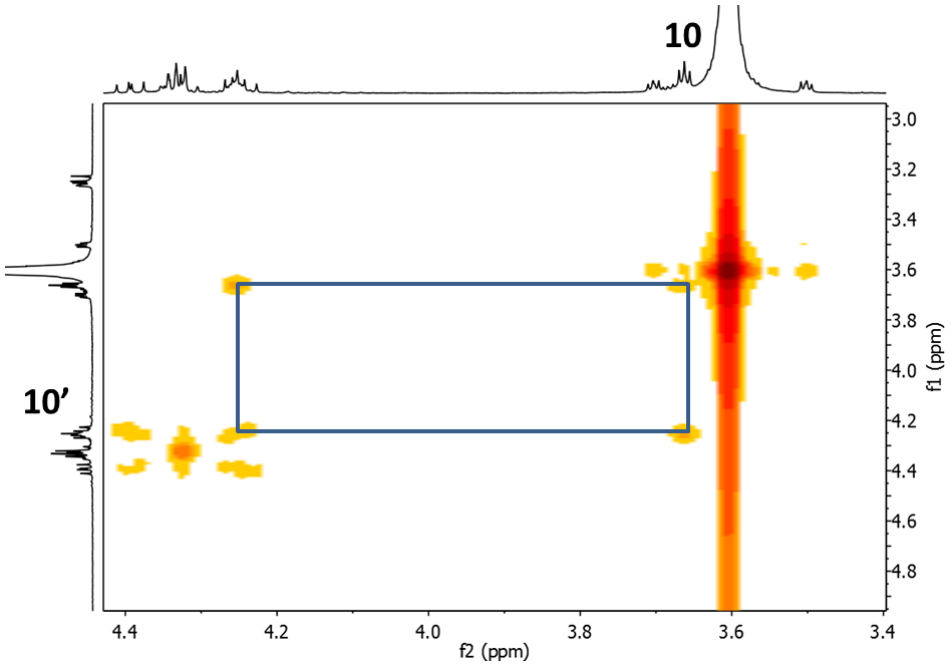

Figure 21: 700 MHz-^{1}H-^{1}H COSY spectrum of **I4-S** highlighting the correlation between **10** and **10'** proton environments.

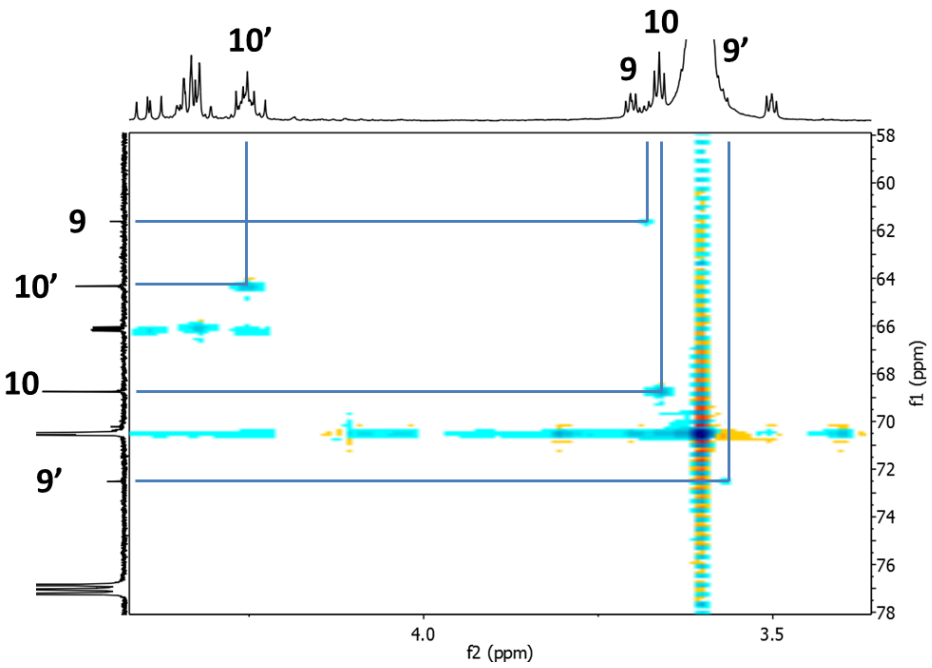

Figure 22: 700 MHz-^{1}H-^{13}C HSQC spectrum of **I4-S** highlighting the correlation between carbon and proton environments of **9** and **10**.

Correlation of the resonance at 3.58 ppm through multiple bonds to the carbon environment **10** using ^{1}H- ^{13}C HMBC (Fig. 23) allows its assignment as **9'.** The resonance at 3.69 ppm therefore corresponds to **9** and ^{1}H-^{13}C HSQC can be used to assign the equivalent carbon environments for both **9** and **9'** (Fig. 22).

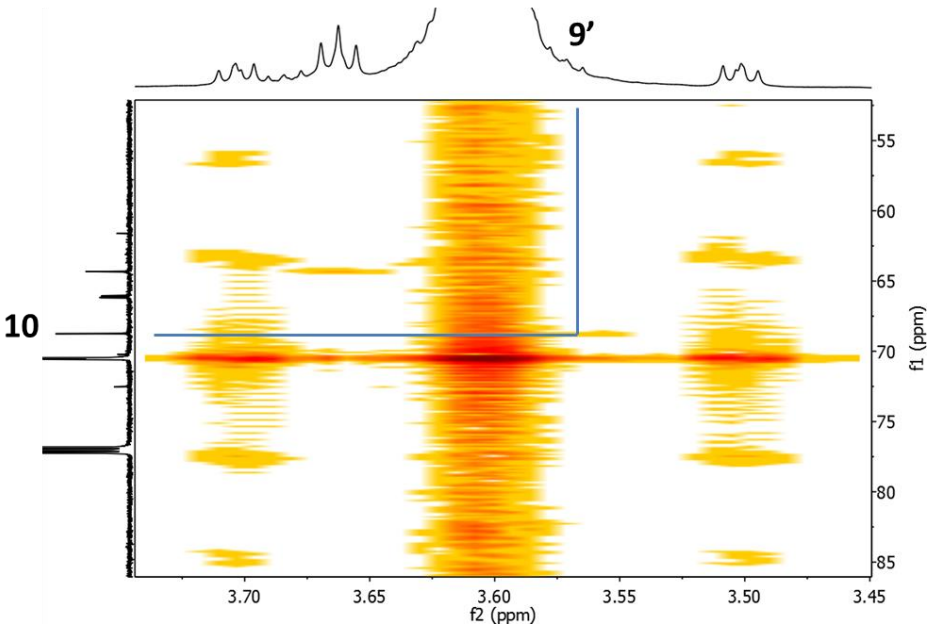

Figure 23: 700 MHz-^{1}H-^{13}C HMBC spectrum of **I4-S** highlighting the correlation between **10** (carbon) and **9'** (proton) environments.

Upon conversion to an ester group in the product, the carboxylic acid -OH resonance of the starting material disappears from the ^{1}H NMR spectrum shown by Figure 24.

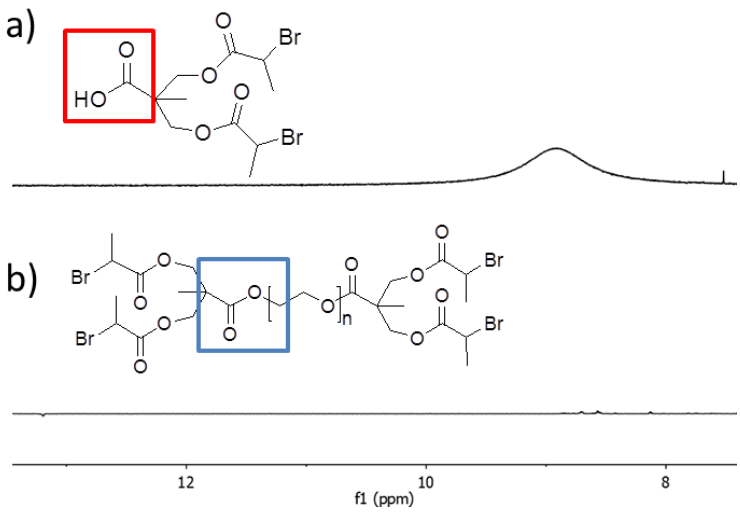

Figure 24: 700 MHz-^{1}H NMR spectrum of: **a) BU-S**, **b) I4-S** highlighting the disappearance of the carboxylic acid resonance.

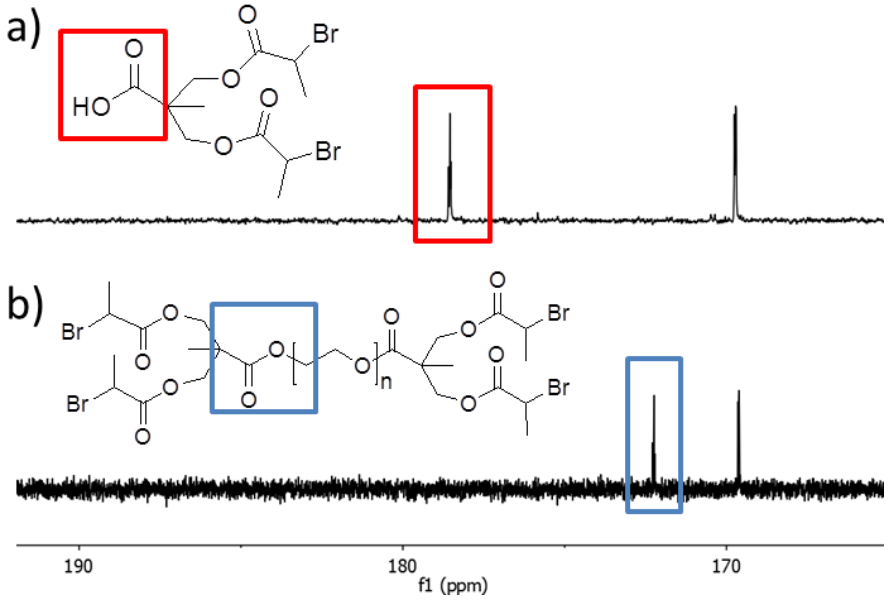

Figure 25: 176 MHz-^{13}C NMR spectrum of; **a) BU-S**; **b) I4-S** highlighting the shift in the C=O resonance as it is converted from a carboxylic acid to an ester group.

This change in carbonyl environment is confirmed by a shift of one of the C=O resonances in the ^{13}C NMR spectrum; the resonance due to **1** moves from 178.89 ppm in the starting material to 172.38 ppm in the product (Fig. 25). The original ester environment (**5**) is effectively unchanged and the chemical shift remains almost constant between starting

material (169.72 ppm) and product (169.60 ppm). Analysis of the FT-IR spectrum (Fig. 26a) also confirms a change in the carbonyl environment. In the product spectrum the carboxylic acid C=O stretch at 1708 cm^{-1} disappears leaving a broader ester resonance at 1744 cm^{-1} (Fig. 26b). A signal corresponding to a C-H stretch (2800-2900 cm^{-1}) dominates the FT-IR spectrum due to the presence of the PEG chain $–CH_2$ groups. Furthermore, there is no observable –OH stretch at around 3200-3600 cm^{-1} which would suggest unreacted PEG chains (Fig. 26a).

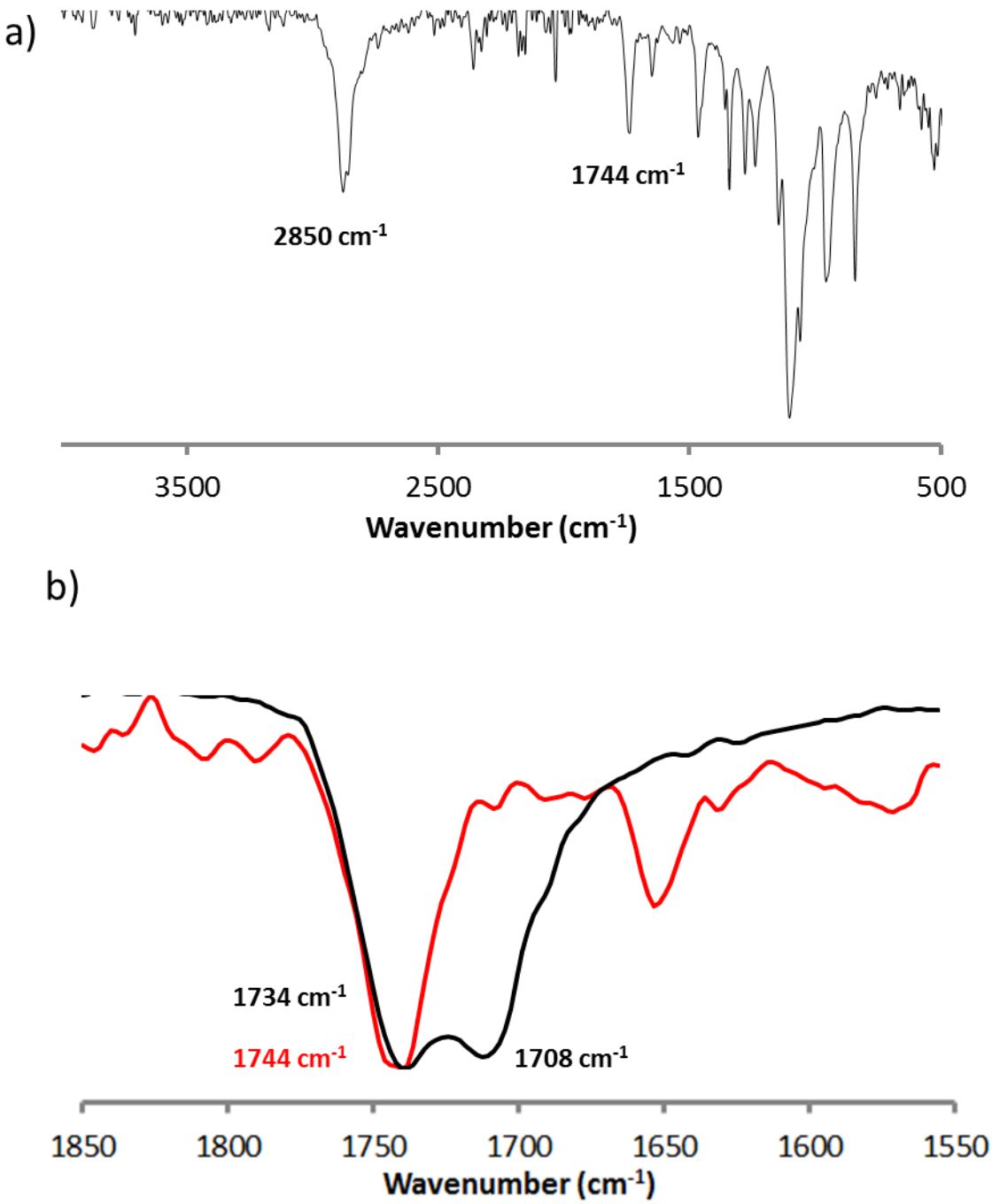

Figure 26: FT-IR spectrum of; **a) I4-S**. **b)** Expanded carbonyl region comparing **I4-S** (red) with **BU-S** (black).

The molecular weight of the product was determined using MALDI-Tof mass spectrometry. As expected for a polymer sample, the spectrum demonstrates a molecular weight distribution (MWD, Fig. 27, blue). A mass difference of 44 g mol^{-1} separating the individual peaks corresponds to an increasing number of ethylene glycol (EG) groups in the polymer chain. Each signal can be divided into the mass of, n, number of EG monomer units with the addition of **BU-S** to each side of the chain. For n = 76 (average for the PEG-3350) a molecular weight of 4139 g mol^{-1} was obtained which correlates to **I4-S** with the addition of a H^+ ion. When the MWD is compared with PEG-3350 (Fig. 27, red) a clear increase in mass can be observed. The difference in m/z between peaks with an equivalent number of EG units is 750 g mol^{-1}. By accounting for the change in counter-ion, the mass difference is 772 g mol^{-1}. This corresponds to the mass of a branched unit (386 g mol^{-1}) at each end of the PEG chain following the loss of H_2O during reaction. The lower intensity secondary MWD of PEG-3350 (red) results from to the polymer with the addition of a H^+ ion. Importantly there is no signal corresponding to unreacted or mono-substituted PEG chains at slightly lower molecular weight (3000 – 4000 g mol^{-1}) in the MALDI spectrum.

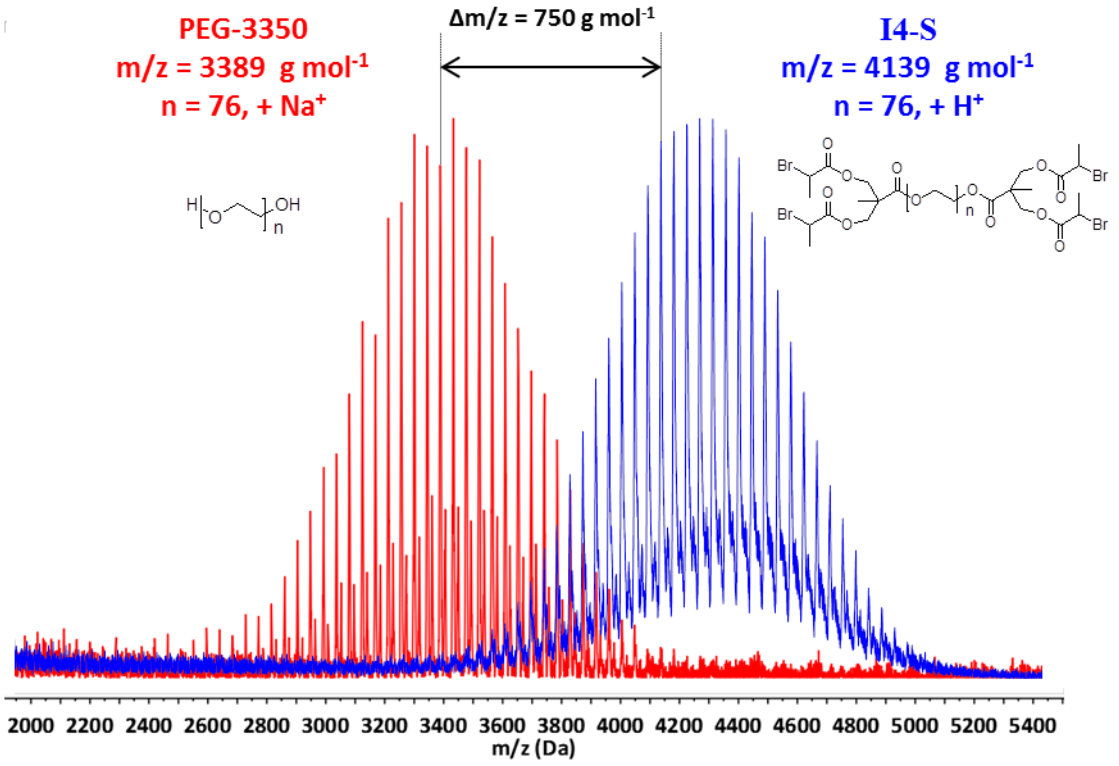

Figure 27: MALDI-MS spectrum comparing PEG-3350 (red) and **I4-S** (blue).

2.3.4. Synthesis of Poly(ethylene glycol)-di-(2,2-Bis(methyl 2-bromoisobutyrate) propionate (I4-T)

Using the same coupling procedure (Scheme 4a, Step 2), PEG-3350 was reacted with **BU-T** to form the tertiary bromine macro-initiator (**I4-T**). Analysis using ^{1}H and ^{13}C NMR spectroscopy again provides evidence for the attachment of the branching unit and the key points are summarised below. The ^{1}H and ^{13}C NMR spectra are shown in Figure 28 and Figure 29, respectively. Resonances due to the PEG chain (**8**), and the end groups (**3, 4, 7**) can be assigned by comparison with the NMR spectra of the starting materials (Appendix A, Fig. 5-7). Distinct resonances corresponding to the $–CH_2$ protons closest to the new chain end groups (**10** and **10'**) were attributed using ^{1}H-^{1}H COSY, ^{1}H-^{13}C-HSQC and ^{1}H-^{13}C HMBC 2D NMR (See Appendix A, Fig. 8-10). Again, it is important to note the disappearance of the starting carboxylic acid -OH resonance and the shift in one carbonyl resonance (**1**) in the ^{13}C NMR spectrum (See Appendix A, Fig. 11-12). FT-IR spectroscopy was used to support this change in carbonyl environment (See Appendix A, Fig. 13).

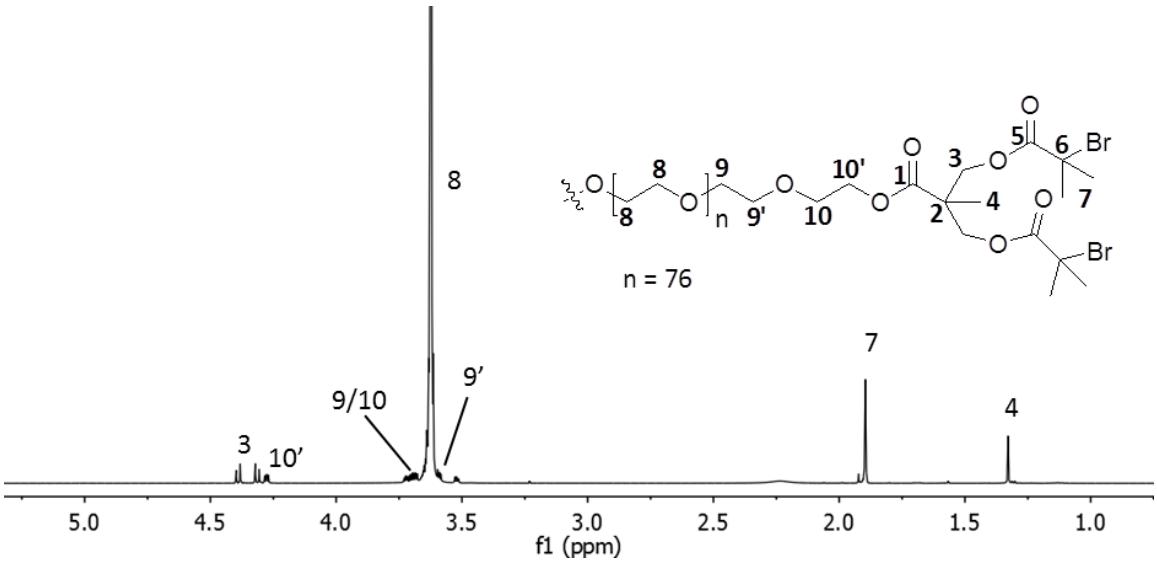

Figure 28: 700MHz-^{1}H NMR spectrum of **I4-T**.

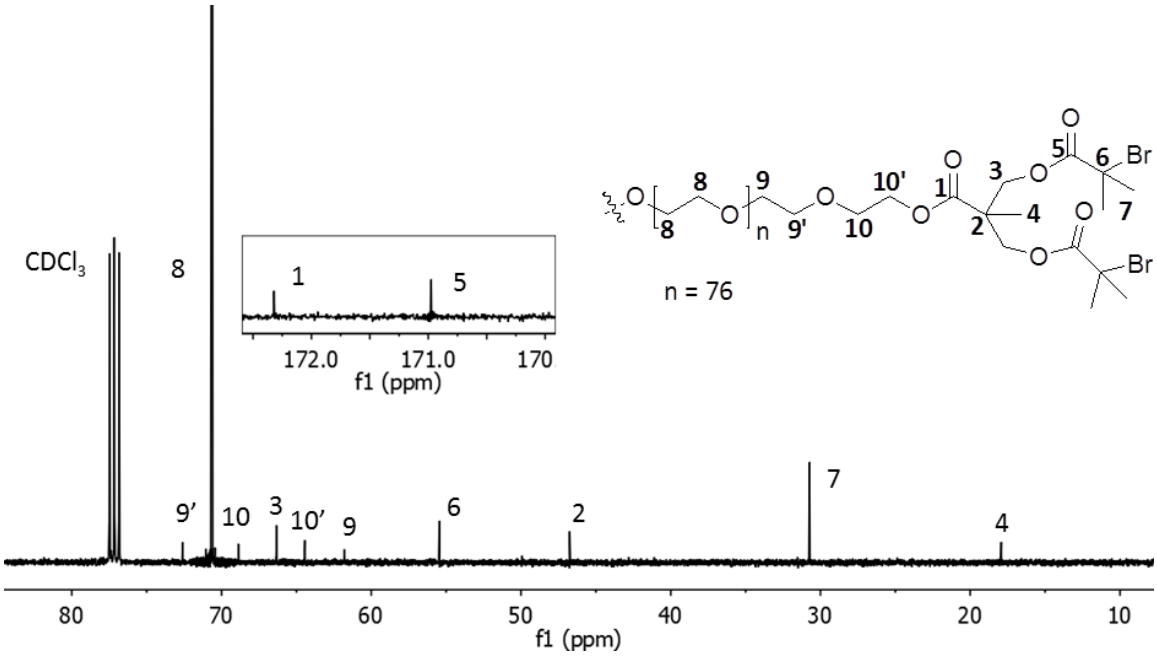

Figure 29: 176 MHz-^{13}C NMR spectrum of **I4-T**, carbonyl region shown inset.

Analysis using MALDI- Tof MS (Fig. 30) once again demonstrates a clear increase in mass between the PEG-3350 starting material and **I4-T** modified at each end. As expected, due to the additional methyl groups in **BU-T**, the difference in mass is larger when compared with **I4-S**. For n = 76, the measured m/z is 4197 g mol^{-1} corresponding to **I4-T** with the addition a H^+ counter-ion. This is 808 g mol^{-1} higher than PEG-3350, which accounts for the addition of two **BU-T** groups, following a change in counter-ion from Na^+ to H^+ and loss of water. No signals are observed which indicate unreacted or partially reacted PEG in the mixture.

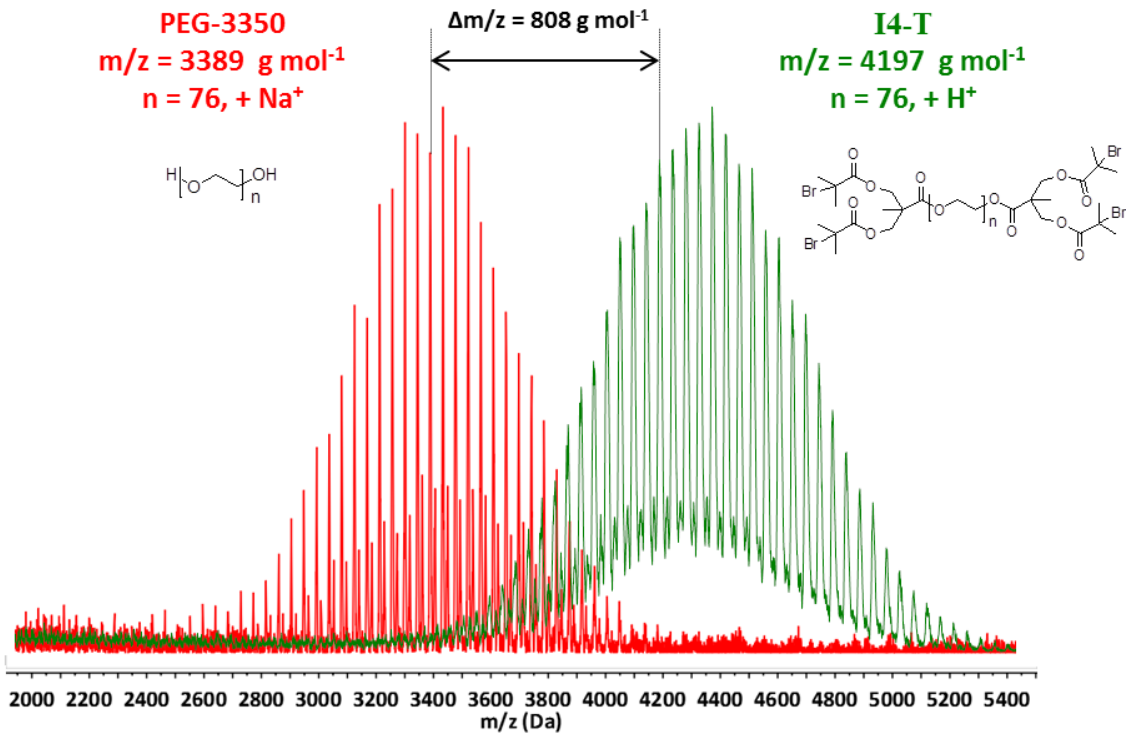

Figure 30: MALDI-MS spectrum comparing PEG-3350 (red) and **I4-T** (green).

2.3.5. Synthesis of Poly(ethylene glycol) monomethyl ether mono(2,2-Bis(methyl 2-bromopropionate)propionate (I2-S)

The **BU-S** branching unit was coupled with a OMe-PEG chain in the same manner to produce a bi-functional macro-initiator (Scheme 4b). The product (**I2-S**) was analysed using ^{1}H and ^{13}C NMR spectroscopy and the assigned spectra are shown in Figure 31 and Figure 32, respectively.

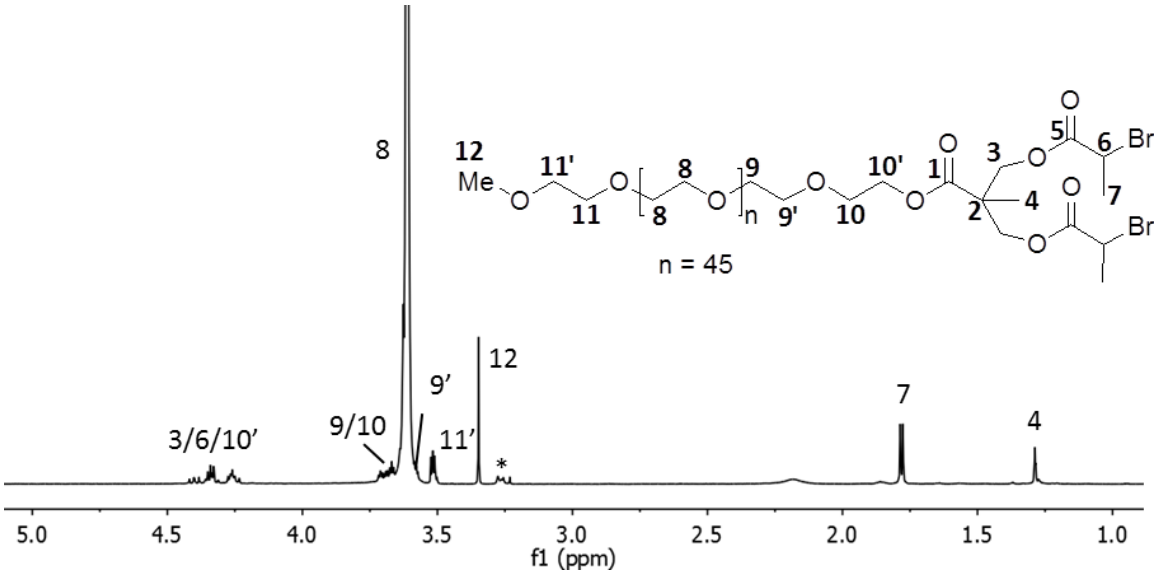

Figure 31: 700 MHz-H NMR spectrum of **I2-S**. *= Unidentified peak.

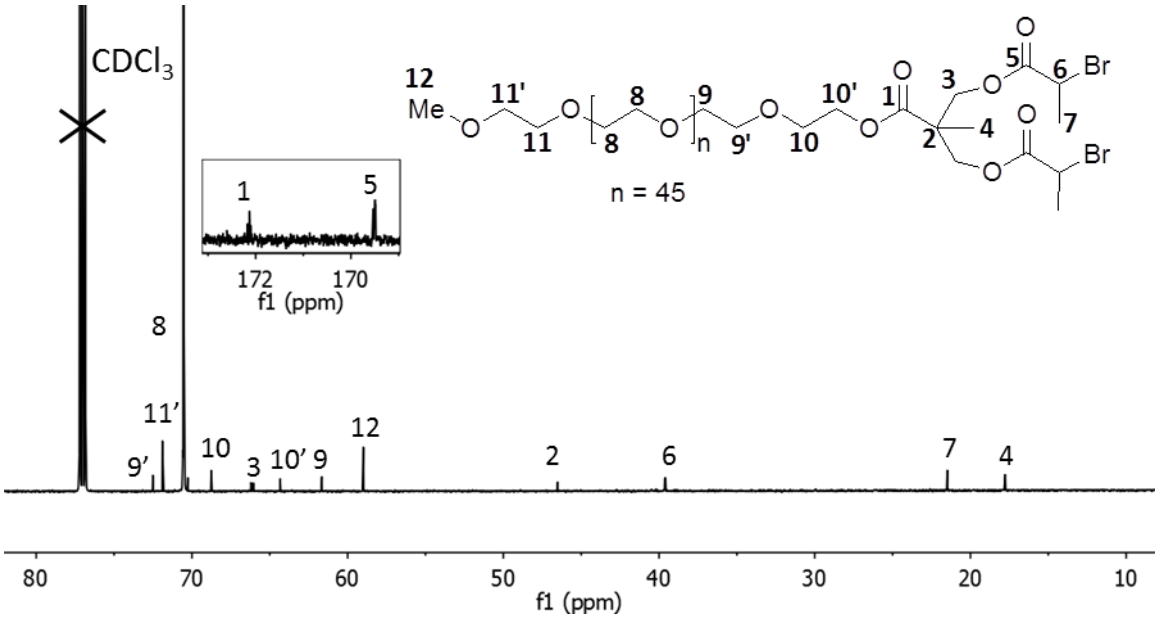

Figure 32: 176 MHz-^{13}C NMR spectrum of **I2-S**, carbonyl region shown inset.

By comparison of the spectra to those of OMe-PEG (Appendix A, Fig. 14-16), a resonance corresponding to the methoxy chain end (**12**) can be assigned at 3.35 ppm and 59.88 ppm in the ^{1}H and ^{13}C NMR spectrum, respectively. As the molecule is non-symmetric there is an increase in the number of resonances in the ^{1}H and ^{13}C spectra due to different environments experienced at each chain end. Using ^{1}H-^{13}C HMBC (Fig. 33) a long range correlation can be observed between the methoxy carbon (**12**) and the protons with a resonance at 3.52 ppm, which is assigned as **11'.** Again, it was necessary to use ^{13}C DEPT, ^{1}H-^{1}H COSY, ^{1}H-^{13}C-HSQC and ^{1}H-^{13}C HMBC NMR to assign the remaining chain end signals (Appendix A, Fig. 17-20) and a change in the carbonyl environment was observed in both the ^{1}H and ^{13}C spectrum (Appendix A, Fig. 21-22)

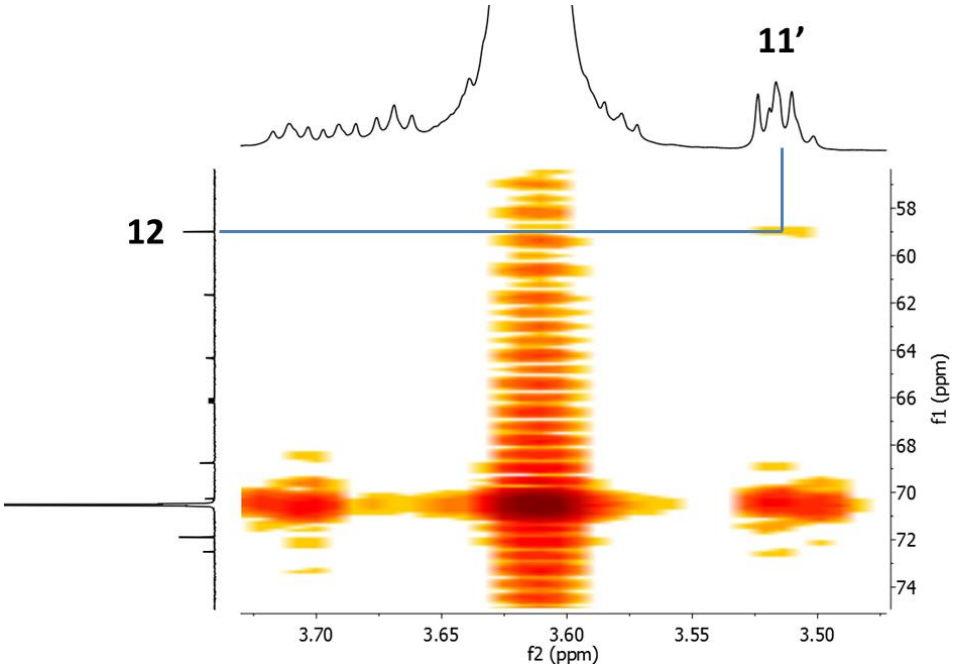

Figure 33: 700 MHz-^{1}H-^{13}C HMBC spectrum spectrum of **I2-S** highlighting the correlation between **12** (carbon) and **11'** (proton) environments.

MALDI-ToF MS was used to compare the mass of the OMe-PEG starting material with the **I2-S** product (Fig. 34). The increase in mass is smaller than for **I4-S**/**I4-T** above. This correlates with the addition of the branched unit to just one chain end. A *m*/*z* of 2401 g mol^{-1} (n = 45, average if M_n = 2000 g mol^{-1}) was measured, which is 386 g mol^{-1} higher than the OMe-PEG taking in to consideration a change in counter-ion from Na^+ to H^+.

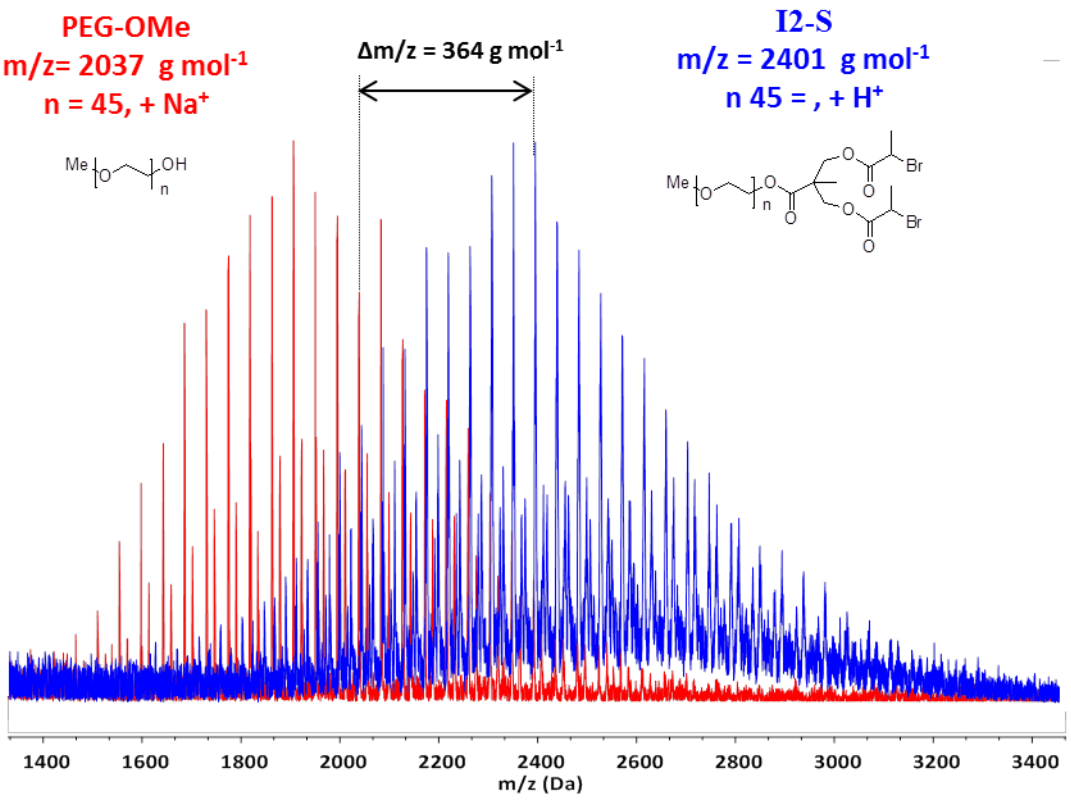

Figure 34: MALDI-MS spectrum comparing OMe-PEG (red) and **I2-S**.

2.4. Conclusion

In conclusion, using a very simple two step strategy, three PEG based water-soluble macro-initiators (**I4-S**, **I4-T**, **I2-S**) have been successfully synthesised. A literature procedure was used to synthesise branching units, **BU-S** and **BU-T**, containing a secondary and tertiary bromine group, respectively.[1] The products were fully characterised using ^{1}H and ^{13}C NMR spectroscopy, IR spectroscopy and mass spectrometry. The branching unit was then coupled with both ends of a PEG chain (M_n= 3350 g mol^{-1}) in order to produce a fully water-soluble macro-initiator (**I4-S** and **I4-T**) with four sites for the initiation of a Cu-mediated polymerisation. Analysis using ^{1}H and ^{13}C NMR spectroscopy as well as MALDI-ToF MS confirmed the attachment of the branching unit to the chain end. The **BU-S** branching unit was also coupled with a mono-methoxy PEG chain (M_n= 2000 g mol^{-1}) to produce an initiator with two initiation sites (**I2-S**).

2.5. References

1. Heise, A.; Hedrick, J. L.; Trollsas, M.; Miller, R. D.; Frank, C. W. *Macromolecules* **1999,** 32, 231-234.

2. Heise, A.; Nguyen, C.; Malek, R.; Hedrick, J. L.; Frank, C. W.; Miller, R. D. *Macromolecules* **2000,** 33, 2346-2354.

3. Konkolewicz, D.; Krys, P.; Góis, J. R.; Mendonça, P. V.; Zhong, M.; Wang, Y.; Gennaro, A.; Isse, A. A.; Fantin, M.; Matyjaszewski, K. *Macromolecules* **2014,** 47, 560-570.

4. Zhang, Q.; Li, Z.; Wilson, P.; Haddleton, D. M. *Chem. Comm.* **2013,** 49, 6608-6610.

5. Wang, X. S.; Jackson, R. A.; Armes, S. P. *Macromolecules* **2000,** 33, 255-257.

6. Wang, X. S.; Armes, S. P. *Macromolecules* **2000,** 33, 6640-6647.

7. Stridsburg, K. M.; Ryner, M.; Albertsson, A. C., Controlled Ring-Opening Polymerization: Polymers with designed Macromolecular Architecture. In *Advances in Polymer Science*, Springer: 2002.

8. Li, Q.; Li, F.; Jia, L.; Li, Y.; Liu, Y.; Yu, J.; Fang, Q.; Cao, A. *Biomacromolecules* **2006,** 7, 2377-2387.

9. Ashford, E. J.; Naldi, V.; O'Dell, R.; Billingham, N. C.; Armes, S. P. *Chem.Comm.* **1999**, 1285-1286.

10. Tang, X.; Liang, X.; Yang, Q.; Fan, X.; Shen, Z.; Zhou, Q. *J. Polym. Sci., Part A: Polym. Chem.* **2009,** 47, 4420-4427.

11. Angot, B.; Taton, D.; Gnanou, Y. *Macromolecules* **2000,** 33, 5418-5426.

12. Gorrasi, G.; Stanzione, M.; Izzo, L. *React. Funct.Polym.* **2011,** 71, 23-29.

13. Francis, R.; Taton, D.; Logan, J. L.; Masse, P.; Gnanou, Y.; Duran, R. S. *Macromolecules* **2003,** 36, 8253-8259.

14. Hou, S. J.; Chaikof, E. L.; Taton, D.; Gnanou, Y. *Macromolecules* **2003,** 36, 3874-3881.

15. Maier, S.; Sunder, A.; Frey, H.; Mulhaupt, R. *Macromol. Rapid Commun.* **2000,** 21, 226-230.

16. Shen, Z.; Chen, Y.; Barriau, E.; Frey, H. *Macromol. Chem. Phys.* **2006,** 207, 57-64.

17. Zagar, E.; Zigon, M.; Podzimek, S. *Polymer* **2006,** 47, 166-175.

Chapter 3

Cu(0)-mediated Polymerisation in Organic Solvent

3.1 Introduction

The tolerance of Cu(0)-mediated polymerisation techniques to impurities and radical inhibitors in starting materials, as well as the ease of recovery and recycling of the catalyst, greatly reduces potential costs when considering the technique for a commercial process.[1,2] Furthermore, the low Cu content in the final product reduces the necessity for specific purification of the polymer. The cost of the current drag reducing systems is very low. In order to maintain an economically viable process, a very simple Cu(0) catalytic system consisting of just Cu(0) wire catalyst and tris(2-aminoethyl)amine (TREN) ligand was chosen for the polymerisation reactions reported here. Several further steps are often taken to allow greater control over the reaction; for example, addition of $CuBr_2$ to the reaction mixture, pre-cleaning of catalyst surface or use of Me_6-TREN ligand. Despite this, perfect control and narrow polymer molecular weight dispersity (*Đ*) is not absolutely vital for this drag reducing application. Instead, a system is required which allows sufficient control for the synthesis of high molecular weight (HMW) star or branched polymers with high conversion, without gelation caused by extensive bimolecular termination reactions. Polymerisation reactions described in this chapter are conducted in organic solvent using *tert*-butyl acrylate (*t*BA) as a protected acrylic acid (AA) monomer. Following full characterisation using triple detection SEC these polymers can be hydrolysed to provide a water-soluble PAA chain. The components used for the Cu(0)-mediated polymerisations are introduced further below.

3.1.1 Initiator

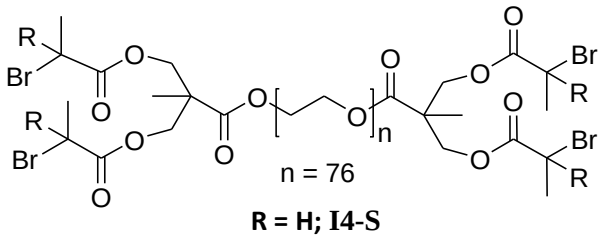

R = H; I4-S
R = Me; I4-T

Figure 1: PEG based macro-initiator.

The **I4-S** and **I4-T** macro-initiators (Fig. 1), discussed in Chapter 2, were synthesised using a poly(ethylene glycol) (PEG) chain (M_n = 3350 g mol^{-1}) in order to generate a water-soluble molecule. Cu-mediated polymerisations using macro-initiators are complicated by an increased steric hindrance and possible trapping of active sites within the polymer random coil.[3] This is most likely to be a problem when using a highly flexible chain such as PEG. Reduced access to active sites disrupts the activation/deactivation process and decreases control over the

polymerisation. In addition, it was also proposed that the PEG backbone may bind Cu species in a similar manner to a crown ether.[3] This would disturb the Cu(I)/Cu(II) ratio and therefore the reaction kinetics. A study by Perrier and Haddleton quantified this effect by analysing the initiator efficiency (I_{eff}) for ATRP reactions (methyl methacrylate (MMA) with CuBr/N-Butyl-2-pyridylmethanimine in toluene at 50, 70 and 90 °C) using mono-methoxy-PEG based macro-initiators of differing lengths (n = 12, 45, 113).[3] The I_{eff} is a measure of the proportion of initiation sites which are converted to growing polymer chains. Theoretically, for a perfectly controlled reaction, this should be 100 % before propagation begins. If the value is below 100 %, the polymer M_n will be higher than theoretically expected at a given monomer conversion; $Đ$ will also increase. The investigation demonstrated that I_{eff} of a PEG macro-initiator decreases as the chain length increases.[3] For the longest PEG chain (n = 113), I_{eff} = 100 % only when the monomer conversion was 80 %. This was monitored using size exclusion chromatography (SEC) which demonstrated a bimodal trace; the higher molecular weight peak due to the growing MMA chains and the lower molecular weight peak due to un-initiated PEG macro-initiator.

3.1.2 Monomer

*t*BA was first polymerised using Cu mediated ATRP by Matyjaszewski in 2000, using CuBr/N,N,N',N",N"-Pentamethyldiethylenetriamine (PMDETA) and methyl 2-bromopropionate (MBP) as an initiator.[4] After observing uncontrolled bulk polymerisation, both benzene and dimethyoxybenzene (DMB) were used as solvents for the reaction. By the addition of $CuBr_2$, 94 % conversion was reached in 3 h (DMB solvent) and M_n close to theoretical was achieved (M_n = 5.8 x 10^3 g mol^{-1}, M_n(Theor) = 6.0 x 10^3 g mol^{-1}).These P*t*BA chains were also combined with divinyl benzene (DVB), 1,4-butanediol diacrylate (BDDA) and ethylene glycol dimethacrylate (EGDMA) to produce more complex star architectures.[5,6]

P*t*BA star polymers (3, 4, 6, 12 and 16 arms) were synthesised by Trzebicka et al. *via* ATRP using a CuBr/PMDETA catalyst system and a range of multi-functional initiators. Reactions were conducted in acetone (60 °C) or anisole (80 °C), allowing control over M_n (4 – 70 x 10^3 g mol^{-1}) and narrow $Đ$ (< 1.20).[7] Using a four site initiator, 4,4'-oxybis(3,3-bis(2-bromopropionate)butane (**4AE**) (in anisole, 100 °C), and a monomer to initiator ratio ($[M]_0$:$[I]_0$) of 16 000, extremely high molecular weight (1.6 – 9.2 x 10^5 g mol^{-1}) star polymers were synthesised.[8] To avoid star-star coupling, conversion was restricted to below 40 %.

P*t*BA has also been combined with PEG on several occasions to form block co-polymers. Huang et al. used Cu(0)-mediated polymerisation (Cu(0)/PMDETA/DMF/RT) in order to polymerise

*t*BA from a functionalised PEG chain end.[9] The same group also polymerised star shaped P*t*BA using ATRP (CuBr/PMDETA/acetone/60°C), following the anionic polymerisation and functionalisation of an ethylene oxide (EO) based star polymer.[10] Gnanou used a tri-functional PEO based macro-initiator for the polymerisation of *t*BA (CuBr/PMDETA/toluene/80°C) to a M_n of 3 x 10^4 g mol^{-1}, although conversion was restricted to ≈ 30 %.[11]

3.1.3 Copper Source

Copper wire is a cheap and easily handled source of Cu(0). Furthermore, it was established that greater control of Đ is possible using wire, due to the particle size dispersity of commercial Cu powder.[12] Percec studied the relationship between Cu surface area (SA) and polymerisation rate by varying the length and gauge of Cu wire.[12] A range of rates between 0.021 min^{-1} (4 cm, 30 gauge, diameter = 0.25 mm) and 0.132 min^{-1} (180 cm, 30 gauge) were examined. An average rate constant (k_p^{app} = 0.044 min^{-1}) was observed using 8.4 cm of 24 gauge wire (diameter = 0.51 mm), therefore, these dimensions were chosen for the catalyst system in the polymerisation reactions described in this chapter.

In Cu(0)-mediated polymerisations, the Cu(0) source can be activated using a reducing agent (e.g. hydrazine,[13] c. HCl[14]) in order to remove Cu_2O accumulated by exposure to air. This has been shown to slightly increase the rate of reaction due to slow activation by Cu_2O, however, non-activated wire has also been used for successfully controlled polymerisations.[15] In the polymerisation reactions described here, no specific purification was carried out on the copper wire before use.

The addition of $CuBr_2$ increases control by allowing immediate deactivation whilst Cu(II) accumulates *via* the persistent radical effect (PRE) or disproportionation; this reduces the levels of termination in a reaction.[16] Despite this, control has been regularly demonstrated without addition of $CuBr_2$, even in the synthesis of HMW star polymers.[15, 17] The addition of $CuBr_2$ increases the handling difficulty and cost of starting materials; it is also likely to increase the copper content of the product, necessitating extra purification steps before use.

3.1.4 Solvent

DMSO is solvent which is commonly used in Cu(0)-mediated polymerisations, providing fast reaction rates and a high degree of control.[15] When used with hydrophobic monomers such as *t*BA and butyl acrylate (*n*BA), a biphasic system is generated as the polymer becomes insoluble above a threshold molecular weight; for example at M_n ≈ 2 – 3 x 10^3 g mol^{-1} for P*n*BA.[18] The mixture contains a polymer rich upper layer and a lower layer containing; monomer, solvent,

ligand and Cu salts.[18] Despite the separation of active chain ends from $CuBr_2$ deactivator, control was still maintained over the polymerisation of *n*BA when targeting a molecular weight of 3 x 10^3 g mol^{-1} (M_n = 4.2 x 10^3 g mol^{-1}, $Đ$ = 1.10) and 12 x 10^3 g mol^{-1} (M_n = 15 x 10^3 g mol^{-1}, $Đ$ = 1.24,).[18] Polymerisation of *t*BA was also controlled, however, a higher dispersity ($Đ$ = 1.42) was observed at an equivalent molecular weight (M_n = 3 x 10^3 g mol^{-1}) which was considered to be a consequence of the increased steric bulk of the monomer. When the system was applied to more hydrophobic, DMSO insoluble, monomers (lauryl acrylate, LA, and 2-ethyl hexyl acrylate, EHA), control over the polymerisation reaction was lost. The resulting polymers demonstrated high dispersity (LA, $Đ$ = 2.23, EHA, $Đ$ = 5.75) and M_n (LA = 22.3 x 10^3 g mol^{-1}, EHA = 4.5 x 10^3 g mol^{-1}) was greater than targeted (3 x 10^3 g mol^{-1}).

A major benefit of this biphasic system was the low Cu loading in the final product. A Cu content of 0.016 wt% (160 ppm) was measured using ICP-MS, without specific purification of the polymer.[18] This is very important for commercial purposes where the release of high levels of copper to the environment is extremely harmful. Furthermore, the biphasic system can have positive implications for the synthesis of star polymers. Bimolecular termination, or star-star coupling, is a major problem when synthesising star polymers to high conversion or molecular weight. Haddleton et al. exploited the heterogeneous system to synthesise a HMW (M_n > 7 x 10^4 g mol^{-1}) 8-arm P*n*BA star to high conversion, without star-star coupling.[13] Parallel homogeneous polymerisation reactions using MA in DMSO or *n*BA in *iso*-propyl alcohol (IPA), both exhibited bimolecular termination at comparable conversions. The suppression of star-star coupling was attributed to the decreased frequency of chain end collisions within the polymer layer.

3.1.5 Ligand

For Cu(0)-mediated polymerisations, ligands which stabilise $CuBr_2$ have been shown to be most successful. In early SET-LRP reactions TREN was used effectively as a ligand, however, Me_6-TREN has recently been widely used for SET-LRP/SARA-ATRP reactions involving acrylates and acrylamides. Although Me_6-TREN is most often used, it is more difficult to synthesise and therefore much more expensive (Price - Sigma Aldrich; TREN = 100 ml - £ 136.50, Me_6-TREN = 1 ml - £ 106.00). The low cost of TREN makes it more suited to commercial applications. For this reason, Percec et al. directly compared the efficacy of TREN and Me_6-TREN for the polymerisation of methyl acrylate (MA) in DMSO, using Cu(0) and a bi-functional initiator (bis(2-bromopropionyl)ethane, BPE).[19] The study demonstrated both ligands could be used for controlled polymerisation reactions. Slightly lower polymerisation rates (k_p^{app}(TREN) = 0.032

min^{-1}, k_p^{app}(Me_6-TREN) = 0.048 min^{-1}) and higher *Đ* (TREN = 1.28, Me_6-TREN = 1.20) were observed using the TREN ligand. This may be due to a slower rate of initiation and slower formation of $CuBr_2$. Despite this, similar conversions (TREN = 88 %, Me_6-TREN = 89 %) and termination levels were also observed and M_n (TREN = 2.05 x 10^4 g mol^{-1}, Me_6-TREN = 2.03 x 10^4 g mol^{-1}) was almost constant for both ligands.[19]

3.2 Experimental

3.2.1 Materials

Dimethyl sulfoxide (DMSO, Anhydrous ≥ 99.9 %), tris(2-aminoethyl)amine (TREN, 97 %), methyl acrylate (MA, 99 %, stabilised with 100 ppm monomethyl ether hydroquinone), methyl 2-bromopropionate (MBP, 98 %), trifluoroacetic acid (TFA, 99 %) and $CuBr_2$ (99 %) were purchased from Sigma Aldrich and used without further purification. Diethyl ether and methanol, analytical grade solvents, were purchased from Fisher Scientific and used as received. *tert*-butyl acrylate (*t*BA, 99 %, stabilised with 15 ppm 4-methoxyphenol) was purchased from Alfa Aesar and used without further purification. Bare copper wire (24 standard wire gauge, diameter = 0.559 mm) was purchased from Fisher Scientific and used without further purification. Deuterated $CDCl_3$ for NMR analysis was purchased from Apollo scientific. The multi-functional initiator, **4AE**, was synthesised by Dr Iain Johnson.[20]

3.2.2 Instrumentation

^1H and ^{13}C NMR spectra were recorded using a Bruker Avance-400, operating at 400 MHz. $CDCl_3$ was used as a solvent and the spectra were referenced to the solvent trace at 7.26 ppm.

Molecular weight analysis of polymer molecules was obtained using size exclusion chromatography (SEC). Specifically a Viscotek TDA 302 using 2 x 300ml PLgel 5µm mixed C columns and THF as the eluent (flow rate of 1 ml min^{-1}) at 35°C. Triple detection using, refractive index (RI), viscosity and light scattering (LS) detectors, was used to determine molecular weights. The detectors were calibrated using narrow molecular weight distribution linear polystyrene as a standard. A value of 0.0539 ml g^{-1} was used for the differential index of refraction (*dn/dc*) of star shaped P*t*BA.[8] A value of 0.0593 ml g^{-1} and 0.068 ml g^{-1} was used for linear P*t*BA and PMA, respectively.[21]

Measurement of copper contamination in polymer samples was conducted in aqueous solution using inductively coupled plasma-optical emission spectrometry (ICP-OES).

Specifically, using a Horiba Ultima 2 at a wavelength of 227.7 and 324.8 nm in comparison with high purity Cu standards (in 1 % v/v nitric acid).

3.2.3 Calculation of monomer to polymer conversion using ^{1}H NMR spectroscopy

The progress of the polymerisation reactions was accurately determined using ^{1}H NMR spectroscopy. By measuring the relative proportions of monomer and polymer in the reaction mixture, monomer conversion could be calculated. An example calculation for the polymerisation of *t*BA is described below.

First, an integral was determined for a resonance due to a monomer vinyl proton (Fig. 2, 5.68 ppm, ∫ = 1, equivalent to 1H). Next, the resonance due to the *tert*-butyl of the polymer side chain was integrated (Fig. 2, 1.42 ppm, ∫ = 89.42, equivalent to 9H) and each integral was divided by the number of protons the resonance represents. This provided the ratio of monomer to polymer (1:9.94) in the reaction mixture. The percentage of monomer converted to polymer was then determined using Equation 1.

$$\frac{9.94}{(1+9.94)} = 0.909 \times 100 = 90.9 \equiv 91\% \qquad \textbf{(Equation 1)}$$

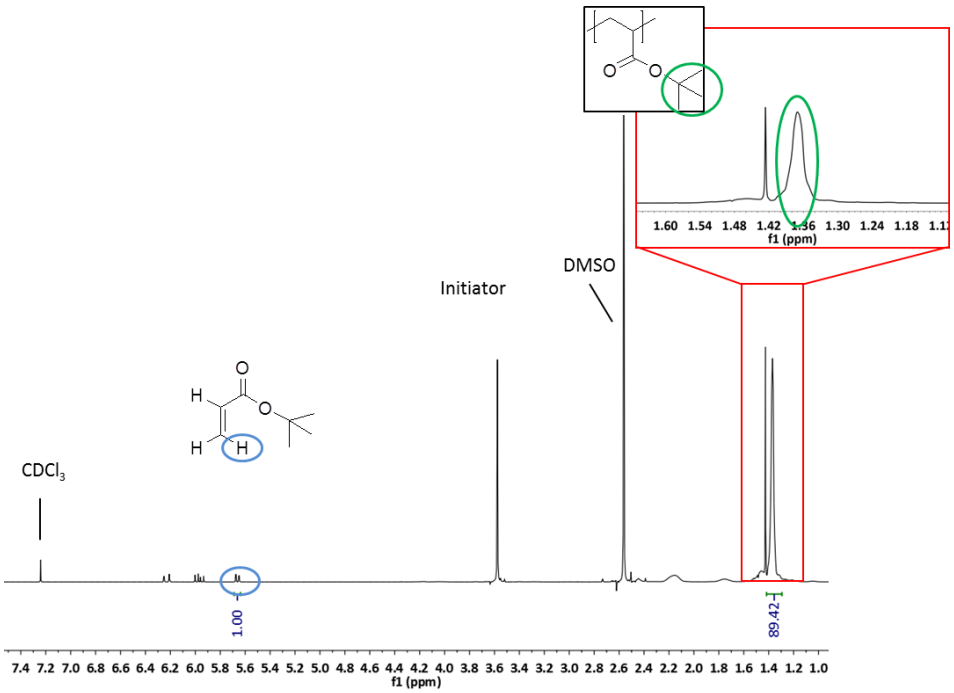

Figure 2: 400-MHz-^{1}H NMR spectrum of P*t*BA highlighting the comparison of intensity of monomer and polymer resonances for monomer conversion analysis.

For polymerisation of MA, the resonance due to a monomer vinyl proton (Fig. 3a) was compared with the resonance representing the single methine proton on the polymer back bone (Fig. 3b), (example spectrum shown in Appendix B, Fig. 1).

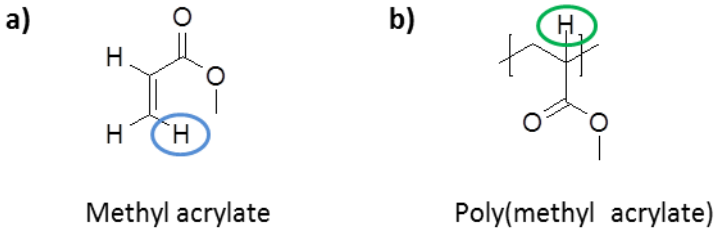

Figure 3: Proton environments for; **a)** methyl acrylate; **b)** Poly(methyl acrylate); compared in ^{1}H NMR spectrum of the polymerisation reaction mixture for conversion analysis.

3.2.4 Typical Polymerisation Procedure

Initiator (**4AE/I4-S/I4-T/I2-S**/MBP) and TREN were weighed into individual vials. DMSO was added to the TREN to give a stock solution. A portion (volume dependent on quantity of TREN) was added to the initiator to dissolve, followed by the addition of monomer (*t*BA/MA) and further DMSO if necessary. The mixture was transferred to a Schlenk tube. Cu(0) wire (8.4 cm, 0.14 g) was wrapped around a magnetic stirrer flea and was held above the reaction mixture using a magnet attached to the wall outside of the flask (Fig. 4a). The flask was sealed using a rubber septum and the mixture deoxygenated. The flask was placed in an oil bath at 25^{o}C and the polymerisation reaction was initiated by submerging the Cu(0)/stirrer (Fig. 4b). The mixture was stirred for an appropriate time and the polymerisation was terminated by removing the Cu(0)/stirrer from the reaction mixture. THF was added to dissolve the resulting product and the conversion was determined using ^{1}H NMR spectroscopy (Section 3.2.3). The solution was diluted with THF and added to a non-solvent (*t*BA = methanol/water (50/50), MA = cool diethyl ether) to precipitate the product which was isolated and dried in an oven under reduced pressure at 40°C.

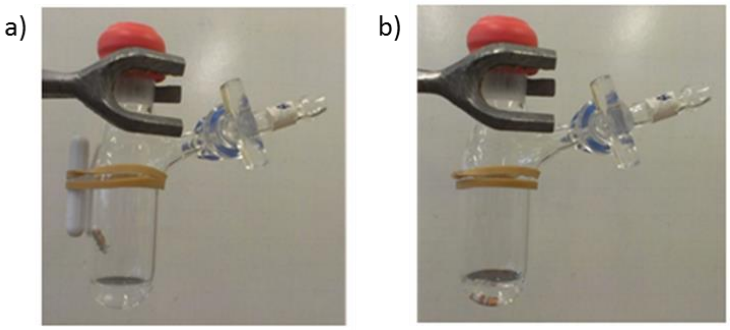

Figure 4: Cu(0)-wire catalyst and stirrer flea; **a)** held above reaction mixture during deoxygenation; **b)** dropped in to reaction mixture to initiate polymerisation.

3.2.5 Control reactions

3.2.5.1 With Cu(0)/TREN but without initiator

Typical procedure (Section 3.2.4) was used with the following modifications:

*t*BA (1.42 g, 11.1 mmol) was added to a Schlenk tube fitted with Cu(0)/stirrer followed by a solution of TREN (0.7 mg, 0.005 mmol) dissolved in DMSO (0.50 ml). The mixture was degassed using 5 freeze-pump-thaw cycles and the flask was backfilled with nitrogen. The reaction was initiated by submerging the Cu(0)/stirrer and stirred for 60 h. The monomer conversion was determined using ^{1}H NMR spectroscopy to be 0 %.

3.2.5.2 With initiator but without Cu(0)/TREN

Typical procedure (Section 3.2.4) was used with the following modifications:

I4-S (0.02 g, 0.005 mmol) was weighed into a vial and DMSO (0.50 ml) was added to dissolve. *t*BA (1.42 g, 11.1 mmol) was added and the mixture was transferred to a Schlenk tube containing a magnetic stirring flea and sealed using a stopper. The mixture was degassed using 5 freeze-pump-thaw cycles and the Schlenk tube was backfilled with nitrogen. The reaction was stirred for 60 h and the monomer conversion was determined using ^{1}H NMR spectroscopy to be 0 %.

3.2.6 Polymerisation of *tert*-butyl acrylate using 4,4'-oxybis(3,3-bis(2-bromopropionate)butane, **4AE**, initiator

3.2.6.1 Kinetic investigation for polymerisation of *tert*-butyl acrylate

3.2.6.1.1 $[M]_0:[I]_0 = 236$

A stock solution of the polymerisation reaction mixture was prepared by mixing: *t*BA (3.55 g, 27.7 mmol), **4AE** (94.8 mg, 0.120 mmol) and TREN (7.0 mg, 0.048 mmol) in DMSO (1.25 ml). Aliquots of the stock solution (1.06 ml) - containing: *t*BA (0.71 g, 0.81 ml, 5.55 mmol), **4AE** (18.6 mg, 0.024 mmol), TREN (1.4 mg, 0.009 mmol), DMSO (0.25 ml) - were transferred to 5 Schlenk tubes. Cu(0) wire (4.2 cm, 0.07 g) was wrapped around a magnetic stirrer flea and held above each mixture. The solutions were deoxygenated by bubbling with nitrogen for 10 min and the Schlenk tube was placed in an oil bath at 25 °C. The reactions were initiated by submerging the Cu(0)/stirrer and terminated after the required time by removing the Cu(0)/stirrer from the mixture. Conversion was determined using ^{1}H NMR spectroscopy.

3.2.6.1.2 $[M]_0:[I]_0 = 2360$

A stock solution of the polymerisation reaction mixture was prepared by mixing: *t*BA (5.68 g, 44.4 mmol), **4AE** (16.0 mg, 0.020 mmol) and TREN (2.8 mg, 0.020 mmol) in DMSO (2.00 ml). Aliquots of the stock solution (2.10 ml) - containing: *t*BA (1.42 g, 1.62 ml, 11.1 mmol), **4AE** (4.0 mg, 0.005 mmol), TREN (0.7 mg, 0.005 mmol), DMSO (0.50 ml) – were transferred to 4 Schlenk tubes. Cu(0) wire (8.4 cm, 0.14 g) was wrapped around a magnetic stirrer flea and held above each mixture. The solutions were deoxygenated by bubbling with nitrogen for 30 min and the Schlenk tube was placed in an oil bath at 25 °C. The reactions were initiated by submerging the Cu(0)/stirrer and terminated after the required time by removing the Cu(0)/stirrer from the mixture. Conversion was determined using ^{1}H NMR spectroscopy.

3.2.7 Polymerisations using Poly(ethylene glycol)-di-(2,2-Bis(methyl 2-bromoisobutyrate) propionate, I4-T, macro-initiator

3.2.7.1 Methyl acrylate

Typical procedure (Section 3.2.4) was used with the following modifications:

I4-T (0.51 g, 0.120 mmol) was weighed into a vial and a solution of TREN (7.0 mg, 0.048 mmol) in DMSO (0.50 ml) was added to dissolve. MA (1.00 ml, 11.1 mmol) was added to the solution and the mixture was transferred to a Schlenk tube fitted with Cu(0)/stirrer. The flask was sealed and the mixture degassed using 4 freeze-pump-thaw cycles before backfilling with nitrogen. The reaction initiated by submerging the Cu(0)/stirrer and stirred for 19 h. Conversion 99.9 %; SEC: M_n = 1.17 x 10^4 g mol^{-1}, M_w = 1.46 x 10^4 g mol^{-1}, $Đ$ = 1.25.

3.2.7.2 *tert*-Butyl acrylate

Typical procedure (Section 3.2.4) was used with the following modifications:

I4-T (0.20 g, 0.047 mmol) was weighed into a vial and a solution of TREN (2.8 mg, 0.019 mmol) in DMSO (0.50 ml) was added to dissolve. *t*BA (1.42 g, 11.1 mmol) was added and the mixture was transferred to a Schlenk tube fitted with Cu(0)/stirrer. The flask was sealed and the mixture degassed using 5 freeze-pump-thaw cycles before backfilling with nitrogen. The reaction was initiated by submerging the Cu(0)/stirrer and stirred for 16 h. Conversion 14 %; SEC: M_n = 1.14 x 10^5 g mol^{-1}, M_w = 4.99 x 10^5 g mol^{-1}, $Đ$ = 4.38.

3.2.8 Polymerisation using Poly(ethylene glycol)-di-2,2-Bis(methyl 2-bromopropionate) propionate, I4-S, macro-initiator

3.2.8.1 Methyl acrylate

Typical procedure (Section 3.2.4) was used with the following modifications:

I4-S (0.51 g, 0.120 mmol) was weighed into a vial and a solution of TREN (7.0 mg, 0.048 mmol) in DMSO (0.50 ml) was added to dissolve. MA (1.00 ml, 11.1 mmol) was added and the mixture was transferred to a Schlenk tube fitted with Cu(0)/stirrer. The flask was sealed and the mixture degassed using 4 freeze-pump-thaw cycles before backfilling with nitrogen. The reaction was initiated by submerging the Cu(0)/stirrer and stirred for 19 h. Conversion 97 %; SEC: M_n = 1.67 x 10^4 g mol^{-1}, M_w = 2.45 x 10^4 g mol^{-1}, $Đ$ = 1.47.

3.2.8.2 *tert*- Butyl acrylate

3.2.8.2.1 $[M]_0:[I]_0 = 78$

Typical procedure (Section 3.2.4) was used with the following modifications:

I4-S (0.61 g, 0.142 mmol) was weighed into a vial and a solution of TREN (8.5 mg, 0.058 mmol) in DMSO (0.50 ml) was added to dissolve. *t*BA (1.42 g, 11.1 mmol) was added and the mixture was transferred to a Schlenk tube fitted with Cu(0)/stirrer. The flask was sealed and the mixture degassed using 5 freeze-pump-thaw cycles before backfilling with nitrogen. The reaction was initiated by submerging the Cu(0)/stirrer and stirred for 16 h. Conversion 72 %; SEC: M_n = 1.51 x 10^4 g mol^{-1}, M_w = 2.87 x 10^4 g mol^{-1}, $Đ$ = 1.90.

3.2.8.2.2 $[M]_0:[I]_0 = 236$

Typical procedure (Section 3.2.4) was used with the following modifications:

I4-S (0.20 g, 0.047 mmol) was weighed into a vial and a solution of TREN (2.8 mg, 0.019 mmol) in DMSO (0.50 ml) was added to dissolve. *t*BA (1.42 g, 11.1 mmol) was added and the mixture was transferred to a Schlenk tube fitted with Cu(0)/stirrer. The flask was sealed and the mixture degassed using 5 freeze-pump-thaw cycles before backfilling with nitrogen. The reaction was initiated by submerging the Cu(0)/stirrer and stirred for 16 h. Conversion 80 %; SEC: M_n = 3.46 x 10^4 g mol^{-1}, M_w = 4.50 x 10^4 g mol^{-1}, $Đ$ = 1.30.

3.2.8.3 Kinetic investigation for polymerisation of *tert*-butyl acrylate

3.2.8.3.1 $[M]_0:[I]_0 = 236$

A stock solution of the polymerisation reaction mixture was prepared by mixing: *t*BA (7.10 g, 55.5 mmol), **I4-S** (1.00 g, 0.235 mmol) and TREN (14.0 mg, 0.096 mmol) in DMSO (2.50 ml). Aliquots of the stock solution (2.1 ml) – containing: *t*BA (1.42 g, 1.62 ml, 11.1 mmol), **I4-S** (0.20 g, 0.047 mmol), TREN (2.8 mg, 0.019 mmol), DMSO (0.50 ml) – were transferred to 5 Schlenk tubes. Cu(0) wire (8.4 cm, 0.14 g) was wrapped around a magnetic stirrer flea and held above each mixture. The flask was sealed using a rubber septum. The solutions were deoxygenated by bubbling with nitrogen for 30 min and the Schlenk tube was placed in an oil bath at 25 °C. The reactions were initiated by submerging the Cu(0)/stirrer and terminated after the required time by removing the Cu(0)/stirrer from the mixture. Conversion was determined using ^{1}H NMR spectroscopy.

3.2.8.3.2 $[M]_0:[I]_0 = 2360$

A stock solution of the polymerisation reaction mixture was prepared by mixing: *t*BA (5.68 g, 44.4 mmol), **I4-S** (80.0 mg, 0.020 mmol) and TREN (2.8 mg, 0.020 mmol) in DMSO (3.00 ml). Aliquots of the stock solution (2.1 ml) – containing: *t*BA (1.42 g, 1.62 ml, 11.1 mmol), **I4-S** (20.0 mg, 0.005 mmol), TREN (0.7 mg, 0.005 mmol), DMSO (0.50 ml) – were transferred to 4 Schlenk tubes. Cu(0) wire (8.4 cm, 0.14 g) was wrapped around a magnetic stirrer flea and held above each mixture. The flask was sealed using a rubber septum. The solutions were deoxygenated by bubbling with nitrogen for 30 min and the Schlenk tube was placed in an oil bath at 25 °C. The reactions were initiated by submerging the Cu(0)/stirrer and terminated after the required time by removing the Cu(0)/stirrer from the mixture. Conversion was determined using ^{1}H NMR spectroscopy.

3.2.9 Polymerisations of *tert*-butyl acrylate using methyl 2-bromopropionate, MBP, initiator

Typical procedure (Section 3.2.4) was used with the following modifications:

MBP (23.8 mg, 0.143 mmol) and TREN (3.5 mg, 0.024 mmol) were weighed into individual vials. DMSO (0.50 ml) was added to the TREN to give a stock solution with a concentration of 0.048 mol dm^{-3}, of which 0.30 ml (TREN = 0.014 mmol) was added to MBP to dissolve. *t*BA (1.42 g, 11.1 mmol) and further DMSO (0.20 ml) were added to prepare the final polymerisation reaction mixture which was transferred to a Schlenk tube fitted with

Cu(0)/stirrer. The flask was sealed using a rubber septum and the solution was deoxygenated by bubbling with nitrogen for 30 min. The reaction was initiated by submerging the Cu(0)/stirrer and stirred for 16 h. Conversion 98 %; SEC: M_n = 3.77 x 10^4 g mol^{-1}, M_w = 40.5 x 10^4 g mol^{-1}, $Đ$ = 10.77.

3.2.9.1 In the presence of $CuBr_2$

Typical procedure (Section 3.2.4) was used with the following modifications:

MBP (23.8 mg, 0.143 mmol) and TREN (8.1 mg, 0.055 mmol) were weighed into individual vials. DMSO (0.50 ml) was added to the TREN to give a stock solution with a concentration of 0.110 mol dm^{-3}, of which 0.12 ml (TREN = 0.014 mmol) was added to the MBP to dissolve. $CuBr_2$ (9.4 mg, 0.042 mmol) was dissolved in DMSO (1.00 ml) to prepare a stock solution with a concentration of 0.042 mol dm^{-3}, of which 0.17 ml ($CuBr_2$ = 0.071 mmol) was added to the TREN/MBP mixture. *t*BA (1.42 g, 11.1 mmol) and further DMSO (0.21 ml) were added to prepare the final polymerisation reaction mixture which was transferred to a Schlenk tube fitted with Cu(0)/stirrer. The flask was sealed using a rubber septum and the solution was deoxygenated by bubbling with nitrogen for 30 min. The reaction was initiated by submerging the Cu(0)/stirrer and stirred for 16 h. Conversion 96 %; SEC: M_n = 4.35 x 10^4 g mol^{-1}, M_w = 37.6 x 10^4 g mol^{-1}, $Đ$ = 8.63.

3.2.9.2 Using reduced monomer concentration

Typical procedure (Section 3.2.4) was used with the following modifications:

MBP (23.8 mg, 0.143 mmol) and TREN (5.7 mg, 0.039 mmol) were weighed into individual vials. DMSO (1.00 ml) was added to the TREN to give a stock solution with a concentration of 0.039 mol dm^{-3}, of which 0.36 ml (TREN = 0.014 mmol) was added to the MBP to dissolve. *t*BA (1.42 g, 11.1 mmol) and further DMSO (1.24 ml) were added to prepare the final polymerisation mixture which was transferred to a Schlenk tube fitted with Cu(0)/stirrer. The flask was sealed using a rubber septum and the solution was deoxygenated by bubbling with nitrogen for 30 min. The reaction was initiated by submerging the Cu(0)/stirrer and stirred for 16 h. Conversion 65 %; SEC: M_n =10.9 x 10^4 g mol^{-1}, M_w = 58.7 x 10^4 g mol^{-1}, $Đ$ = 5.39.

3.2.9.3 Using reduced Cu wire length

Typical procedure (Section 3.2.4) was used with the following modifications:

MBP (23.8 mg, 0.143 mmol) and TREN (3.5 mg, 0.024 mmol) were weighed into individual vials. DMSO (0.50 ml) was added to the TREN to give a stock solution with a concentration of 0.048 mol dm^{-3}, of which 0.30 ml (TREN = 0.014 mmol) was added to the MBP to dissolve. *t*BA (1.42 g, 11.1 mmol) and further DMSO (0.20 ml) were added to prepare the final polymerisation reaction mixture which was transferred to a Schlenk tube. Cu(0) wire (1.6 cm, 0.03 g) was wrapped around a magnetic stirrer flea and was held above the mixture using a magnet attached to the outside wall of the flask. The flask was sealed using a rubber septum and the solution was deoxygenated by bubbling with nitrogen for 30 min. The reaction was initiated by submerging the Cu(0)/stirrer and stirred for 16 h. Conversion 16 %; SEC: M_n = 4.13 x 10^4 g mol^{-1}, M_w = 19.0 x 10^4 g mol^{-1}, $Đ$ = 4.60.

3.2.9.4 Using reduced monomer concentration in the presence of $CuBr_2$

Typical procedure (Section 3.2.4) was used with the following modifications:

MBP (23.8 mg, 0.143 mmol) and TREN (3.1 mg, 0.021 mmol) were weighed into individual vials. DMSO (0.50 ml) was added to the TREN to give a stock solution with a concentration of 0.042 mol dm^{-3}, of which 0.32 ml (TREN = 0.014 mmol) was added to the MBP to dissolve. $CuBr_2$ (1.8 mg, 0.008 mmol) was dissolved in DMSO (0.50 ml) to prepare a stock solution with a concentration of 0.016 mol dm^{-3}, of which 0.45 ml ($CuBr_2$ = 0.071 mmol) was added to the TREN/MBP mixture. *t*BA (1.42 g, 11.1 mmol) and further DMSO (0.83 ml) were added to prepare the final polymerisation reaction mixture which was transferred to a Schlenk tube fitted with Cu(0)/stirrer. The flask was sealed using a rubber septum and the solution was deoxygenated by bubbling with nitrogen for 30 min. The reaction was initiated by submerging the Cu(0)/stirrer and stirred for 16 h. Conversion 88 %; SEC: M_n = 0.70 x 10^4 g mol^{-1}, M_w = 19.5 x 10^4 g mol^{-1}, $Đ$ = 27.84.

3.2.9.5 Using reduced monomer concentration and Cu wire length in the presence of $CuBr_2$

Typical procedure (Section 2.4) was used with the following modifications:

MBP (23.8 mg, 0.143 mmol) and TREN (7.7 mg, 0.053 mmol) were weighed into individual vials. DMSO (0.50 ml) was added to the TREN to give a stock solution with a concentration of 0.106 mol dm^{-3}, of which 0.13 ml (TREN = 0.014 mmol) was added to the MBP to dissolve. $CuBr_2$ (5.4 mg, 0.024 mmol) was dissolved in DMSO (0.50 ml) to prepare a stock solution with a concentration of 0.048 mol dm^{-3}, of which 0.15 ml ($CuBr_2$ = 0.071 mmol) was added to the TREN/MBP mixture. tBA (1.42 g, 11.1 mmol) and further DMSO (1.32 ml) were added to

prepare the final polymerisation reaction mixture which was transferred to a Schlenk tube**.** Cu(0) wire (1.6 cm, 0.03 g) was wrapped around a magnetic stirrer flea and was held above the reaction mixture using a magnet attached to the outside wall of the flask. The flask was sealed using a rubber septum and the solution was deoxygenated by bubbling with nitrogen for 30 min. The reaction was initiated by submerging the Cu(0)/stirrer and stirred for 16 h. Conversion 80 %; SEC: M_n = 0.89 x 10^4 g mol^{-1}, M_w =12.3 x 10^4 g mol^{-1}, $Đ$ = 13.78.

The reaction was then repeated over 30 min, 60 min and 120 min.

3.2.10 Polymerisation of tert-butyl acrylate using Poly(ethylene glycol) monomethyl ether mono(2,2-Bis(methyl 2-bromopropionate)propionate, I2-S, macro-initiator

Typical procedure (Section 3.2.4) was used with the following modifications:

I2-S (10.0 mg, 0.005 mmol) and TREN (1.4 mg, 0.01 mmol) were weighed into individual vials. DMSO (1 ml) was added to the TREN to give a stock solution with a concentration of 0.01 mol dm^{-3}, of which 0.50 ml (TREN = 0.005 mmol) was added to **I2-S** to dissolve. *t*BA (1.42 g, 11.1 mmol) was added to prepare the final polymerisation reaction mixture which was transferred to a Schlenk tube fitted with Cu(0)/stirrer. The flask was sealed using a rubber septum and the solution was deoxygenated by bubbling with nitrogen for 30 min. The reaction was initiated by submerging the Cu(0)/stirrer and stirred for 16 h. Conversion 36 %; SEC: M_n = 4.22 x 10^5 g mol^{-1}, M_w = 6.64 x 10^5 g mol^{-1}, $Đ$ = 1.57.

3.2.11 Large scale polymerisations of *tert*-butyl acrylate

3.2.11.1 Using methyl 2-bromopropionate (MBP) initiator

Typical procedure (Section 3.2.4) was used with the following modifications:

MBP (18.9 mg, 0.118 mmol) was weighed into a vial and TREN (17.3 mg, 0.118 mmol) in DMSO (12.5 ml) was added to dissolve. *t*BA (35.50 g, 278 mmol) was added to prepare the final polymerisation reaction mixture which was transferred to a Schlenk fitted with Cu(0) wire (210 cm, 3.58 g) wrapped around a magnetic stirrer bar. The flask was sealed using a rubber septum and the mixture deoxygenated by bubbling with nitrogen for 45 min. The reaction was initiated by submerging the Cu(0)/stirrer and stirred for 122 h. Conversion 91 %; SEC: M_n = 7.69 x 10^5 g mol^{-1}, M_w = 17.7 x 10^5 g mol^{-1}, $Đ$ = 2.29.

3.2.11.2 Using 4,4'-oxybis(3,3-bis(2-bromopropionate)butane, 4AE, initiator

3.2.11.2.1 $[M]_0:[I]_0 = 2360$

Typical procedure (Section 3.2.4) was used with the following modifications:

4AE (94.0 mg, 0.118 mmol) and TREN (34.6 mg, 0.24 mmol) were weighed into individual vials. DMSO (25.0 ml) was added to the TREN to give a stock solution with a concentration of 0.010 mol dm^{-3}, of which 12.5 ml (TREN = 0.118 mmol) was added to the **4AE** to dissolve. *t*BA (35.50 g, 278 mmol) was added to prepare the final polymerisation reaction mixture which was transferred to a Schlenk tube fitted with Cu(0) wire (210 cm, 3.58 g) wrapped around a magnetic stirrer bar. The flask was sealed using a rubber septum and the mixture deoxygenated by bubbling with nitrogen for 45 min. The reaction was initiated by submerging the Cu(0)/stirrer and stirred for 70 h. Conversion 69 %; SEC: M_n = 3.09 x 10^5 g mol^{-1}, M_w = 4.03 x 10^5 g mol^{-1}, $Đ$ = 1.30.

3.2.11.2.2 $[M]_0:[I]_0 = 7804$

Typical procedure (Section 3.2.4) was used with the following modifications:

4AE (7.90 mg, 0.010 mmol) and TREN (4.2 mg, 0.028 mmol) were weighed into individual vials. DMSO (2.00 ml) was added to the TREN to give a stock solution with a concentration of 0.014 mol dm^{-3}, of which 0.70 ml (TREN = 0.010 mmol) was added to the **4AE** to dissolve. *t*BA (10.00 g, 78.0 mmol) and further DMSO (2.80 ml) were added to prepare the final polymerisation reaction mixture which was transferred to a Schlenk tube fitted with Cu(0) wire (59 cm, 1.00 g) wrapped around a magnetic stirrer bar. The flask was sealed using a rubber septum and the mixture deoxygenated by bubbling with nitrogen for 45 min. The reaction was initiated by submerging the Cu(0)/stirrer and stirred for 24 h. Conversion 85 %; SEC: M_n = 8.61 x 10^5 g mol^{-1}, M_w = 13.9 x 10^5 g mol^{-1}, $Đ$ = 1.61.

3.2.11.3 Using Poly(ethylene glycol)-di-2,2-Bis(methyl 2-bromopropionate) propionate, I4-S, macro-initiator

Typical procedure (Section 3.2.4) was used with the following modifications:

I4-S (42.5 mg, 0.010 mmol) and TREN (3.9 mg, 0.026 mmol) were weighed into individual vials. DMSO (2.00 ml) was added to the TREN to give a stock solution with a concentration of 0.013 mol dm^{-3}, of which 0.75 ml (TREN = 0.010 mmol) was added to the **I4-S** to dissolve. *t*BA (10.00 g, 78.0 mmol) and further DMSO (2.75 ml) were added to prepare the final polymerisation

reaction mixture which was transferred to a Schlenk tube fitted with Cu(0) wire (59 cm, 1.00 g) wrapped around a magnetic stirrer bar. The flask was sealed using a rubber septum and the mixture deoxygenated by bubbling with nitrogen for 45 min. The reaction was initiated by submerging the Cu(0)/stirrer and stirred for 24 h. Conversion 22 %; SEC: M_n = 1.39 x 10^6 g mol^{-1}, M_w = 2.10 x 10^6 g mol^{-1}, $Đ$ = 1.51.

3.2.11.3.1 Using reduced Cu wire length = 29.5 cm

Typical procedure (Section 3.2.4) was used with the following modifications:

I4-S (42.5 mg, 0.010 mmol) and TREN (2.3 mg, 0.015 mmol) were weighed into individual vials. DMSO (1.00 ml) was added to the TREN to give a stock solution with a concentration of 0.015 mol dm^{-3}, of which 0.65 ml (TREN = 0.010 mmol) was added to the **I4-S** to dissolve. *t*BA (10.00 g, 78.0 mmol) and further DMSO (2.85 ml) were added to prepare the final polymerisation reaction mixture which was transferred to a Schlenk tube fitted with Cu(0) wire (29.5 cm, 0.50 g) wrapped around a magnetic stirrer bar. The flask was sealed using a rubber septum and the mixture deoxygenated by bubbling with nitrogen for 45 min. The reaction was initiated by submerging the Cu(0)/stirrer and stirred for 24 h. Conversion 36 %; SEC: M_n = 7.84 x 10^5 g mol^{-1}, M_w = 15.1 x 10^5 g mol^{-1}, $Đ$ = 1.93.

3.2.11.3.2 Using reduced Cu wire length = 14.75 cm

Typical procedure (Section 3.2.4) was used with the following modifications:

I4-S (42.5 mg, 0.010 mmol) and TREN (7.1 mg, 0.048 mmol) were weighed into individual vials. DMSO (2.00 ml) was added to the TREN to give a stock solution with a concentration of 0.024 mol dm^{-3}, of which 0.40 ml (TREN = 0.010 mmol) was added to the **I4-S** to dissolve. *t*BA (10.00 g, 78.0 mmol) and further DMSO (3.10 ml) were added to prepare the final polymerisation reaction mixture which was transferred to a Schlenk tube fitted with Cu(0) wire (14.75 cm, 0.25 g) wrapped around a magnetic stirrer bar. The flask was sealed using a rubber septum and the mixture deoxygenated by bubbling with nitrogen for 45 min. The reaction was initiated by submerging the Cu(0)/stirrer and stirred for 24 h. Conversion 43 %; SEC: M_n = 7.47 x 10^5 g mol^{-1}, M_w = 17.0 x 10^5 g mol^{-1}, $Đ$ = 2.28.

3.2.11.3.3 Using reduced monomer concentration

Typical procedure (Section 3.2.4) was used with the following modifications:

I4-S (42.5 mg, 0.010 mmol) and TREN (7.1 mg, 0.048 mmol) were weighed into individual vials. DMSO (2.00 ml) was added to the TREN to give a stock solution with a concentration of 0.024 mol dm^{-3}, of which 0.40 ml (TREN = 0.010 mmol) was added to the **I4-S** to dissolve. *t*BA (10.00 g, 78.0 mmol) and further DMSO (5.30 ml) were added to prepare the final polymerisation reaction mixture which was transferred to a Schlenk tube fitted with Cu(0) wire (59 cm, 1.00 g) wrapped around a magnetic stirrer bar. The flask was sealed using a rubber septum and the mixture deoxygenated by bubbling with nitrogen for 45 min. The reaction was initiated by submerging the Cu(0)/stirrer and stirred for 24 h. Conversion 26 %; SEC: M_n = 1.88 x 10^6 g mol^{-1}, M_w = 2.68 x 10^6 g mol^{-1}, $Đ$ = 1.43.

3.2.11.4 Using Poly(ethylene glycol) monomethyl ether mono(2,2-Bis(methyl 2-bromopropionate)propionate (I2-S) initiator

Typical procedure (Section 3.2.4) was used with the following modifications:

I2-S (20.0 mg, 0.010 mmol) and TREN (3.1 mg, 0.021 mmol) were weighed into individual vials. DMSO (1.00 ml) was added to the TREN to give a stock solution with a concentration of 0.021 mol dm^{-3}, of which 0.47 ml (TREN = 0.010 mmol) was added to the **I2-S** to dissolve. *t*BA (10.00 g, 78.0 mmol) and further DMSO (3.03 ml) were added to prepare the final polymerisation reaction mixture which was transferred to a Schlenk tube fitted with Cu(0) wire (59 cm, 1.00 g) wrapped around a magnetic stirrer bar. The flask was sealed using a rubber septum and the mixture deoxygenated by bubbling with nitrogen for 45 min. The reaction was initiated by submerging the Cu(0)/stirrer and stirred for 24 h. Conversion 67 %; SEC: M_n = 1.49 x 10^6 g mol^{-1}, M_w = 3.13 x 10^6 g mol^{-1}, $Đ$ = 2.10.

3.3 Results and Discussion

3.3.1 Control reactions

Control reactions were used to confirm the participation of the initiator molecule (**I4-S**) and Cu(0)/TREN catalyst system in the polymerisation reactions. The first included the catalyst but no initiator, whilst the second included the initiator without catalyst. The ^{1}H NMR spectrum of an example reaction mixture in Figure 5 shows the presence of resonances at 1.48 ppm (**5**) and 5.70 – 6.27 ppm (**1** and **2**) due to unreacted monomer in the solution. The absence of characteristic P*t*BA resonances between 1.40 – 2.50 ppm demonstrates that no polymer has formed during the reaction (Fig. 5). This was the case for both control reactions and was taken as a clear indication that the following polymerisation reactions are initiated as the result of a combination of the initiator and Cu(0)/TREN catalyst system.

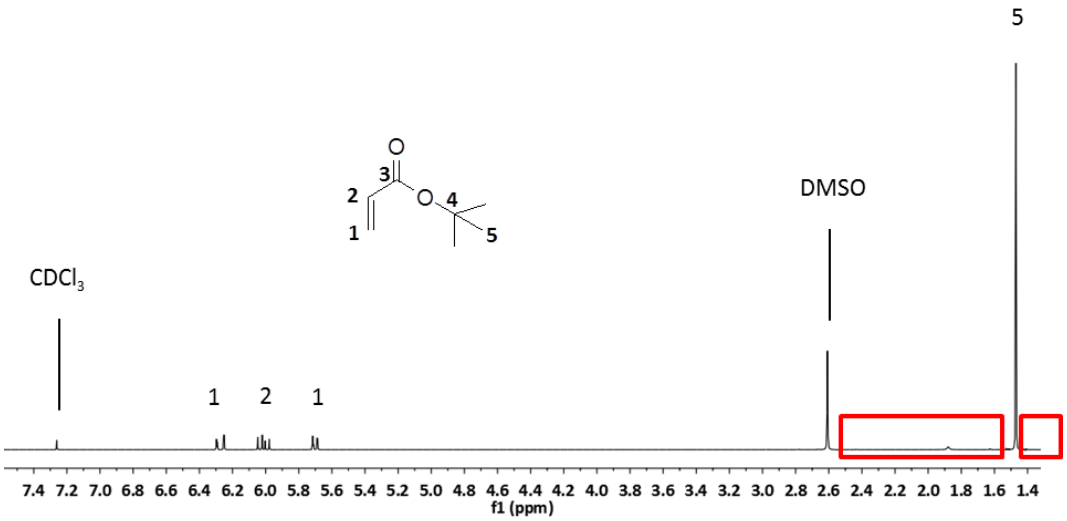

Figure 5: 400 MHz-^{1}H NMR spectrum of control reaction mixture demonstrating no resonances due to P*t*BA.

3.3.2 Polymerisation of *tert*-butyl acrylate using 4,4'-Oxybis(3,3-bis(2-bromopropionate)butane, 4AE initiator

The Cu(0)/TREN catalyst system was first examined for the polymerisation of *t*BA using a small molecule initiator, (**4AE**, Scheme 1) in DMSO. An initial ratio of monomer to initiator and ligand ($[M]_0$:$[I]_0$:$[L]_0$) of 236:1:0.4 was used to target a molecular weight of ≈ 3.1 x10^4 g mol^{-1}.

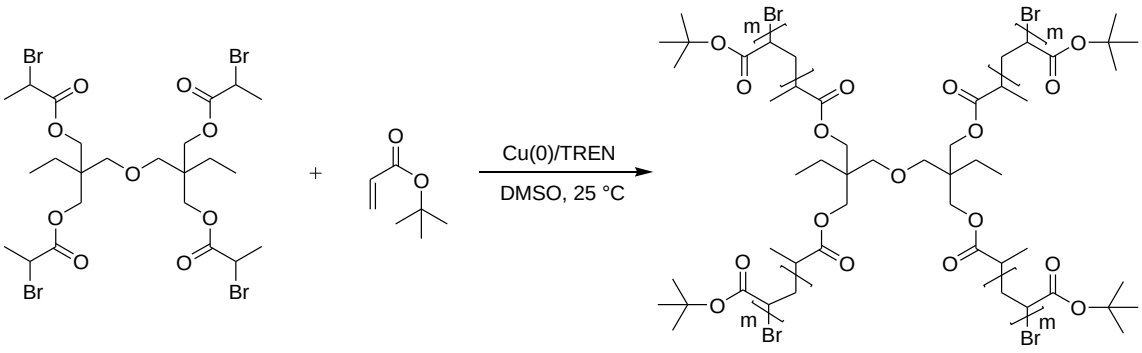

4AE ***t*BA** **4AE-P*t*BA**

Scheme 1: Polymerisation of *t*BA using 4,4'-Oxybis(3,3-bis(2-bromopropionate)butane, **4AE** initiator.

The kinetics of the polymerisation reaction were studied by conducting parallel reactions on a small scale. The evolution of monomer conversion with time is plotted in Figure 6a, (blue axis). The graph demonstrates a linear increase of conversion with time in the early stages of the reaction (< 500 min). At longer reaction times, the graph levels off and the reaction does not progress beyond 80 % conversion, believed to be due to the high viscosity of the mixture. As expected, the reaction mixture became heterogeneous (biphasic) at low conversion due to the

insolubility of P*t*BA in DMSO. The two phases first formed as a stable emulsion with small polymer droplets dispersed in the DMSO/monomer solution. As the reaction progressed, monomer was converted to polymer and the volume of the DMSO/monomer layer decreased. The polymer layer then agglomerated, becoming extremely viscous and as a result the polymerisation became diffusion limited. This is particularly a problem for this heterogeneous reaction where controlled chain extension relies on the interaction between copper activator/deactivator species, monomer and the polymer chain end.

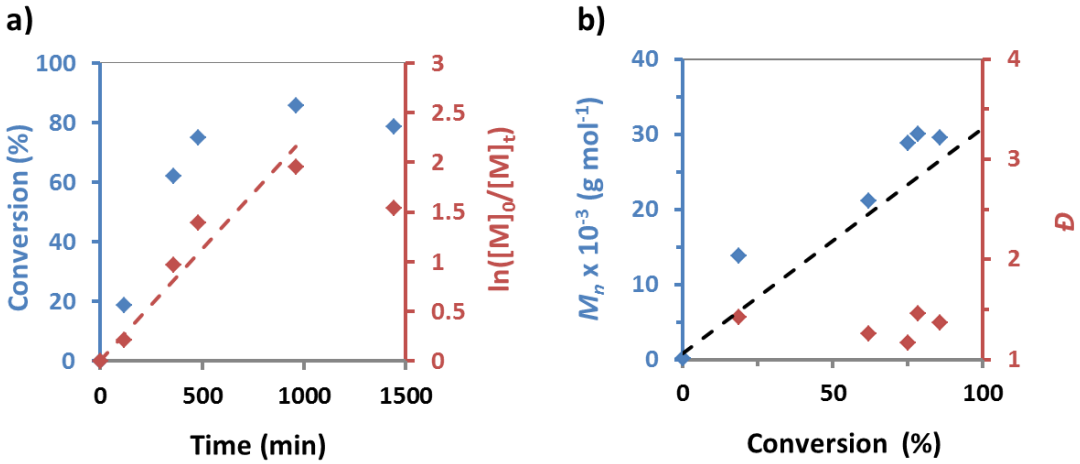

Figure 6: Polymerisation of *t*BA using **4AE**, $[M]_0:[I]_0:[L]_0$ =236:1:0.4; **a)** Conversion (blue axis) and $\ln([M]_0/[M]_t)$ (red axis) vs time; **b)** M_n(SEC) (blue axis) and $Đ$ (red axis) vs conversion. (M_n(Theor) shown by black line).

The kinetic plot of $\ln([M]_0/[M]_t)$ against time is plotted on the secondary axis in Figure 6a (red axis). A linear increase is observed for the first 960 min suggesting a constant concentration of radicals in the solution, a feature of controlled radical polymerisations. The apparent rate constant of propagation (k_p^{app} = 0.0022 min^{-1}) was calculated using the gradient of the kinetic plot. This is comparable to the values obtained by Percec for the polymerisation of *n*BA in a homogeneous mixture of DMSO and tetrafluoropropanol (TFP) (k_p^{app} = 0.0014-0.0061 min^{-1}), suggesting the biphasic system may not significantly affect the rate of this polymerisation.[17] The k_p^{app} is low in comparison to the polymerisation of MA in DMSO, using the same catalyst surface area (k_p^{app} = 0.044 min^{-1}).[12] This is possibly due to the increased steric bulk of the *t*BA monomer. The graphs in Figure 6b relate monomer conversion with M_n(SEC) (blue axis) and $Đ$ (red axis) measured using triple detection SEC in THF. The theoretical molecular weight M_n(Theor) at each conversion was calculated using Equation 2 and is indicated by the black line.

$$M_n(\text{Theor}) = M_{tBA} \times \left(\frac{[\text{Mon}]_0}{[\text{I}]_0} \times \frac{\%\text{Conv}}{100} \right) + M_I \qquad \textbf{(Equation 2)}$$

At low conversion M_n(SEC) is significantly higher than theoretically calculated. This demonstrates a higher rate of propagation than initiation, and may be a consequence of rate acceleration due to phase separation in the early stages of the reaction. As the polymerisation progresses and $CuBr_2$ deactivator forms in more significant quantities, the reaction becomes more controlled. This can be observed by the linear increase of M_n(SEC) at higher conversion and the close correlation with M_n(Theor). Throughout the reaction dispersity remains low ($Đ$ = 1.19, Conv = 60%, Fig. 6b). This compares favourably to polymerisation of *t*BA in DMSO described in the literature using Cu(0)/$CuBr_2$/Me_6-TREN (M_n = 3 x 10^3 g mol^{-1}, $Đ$ = 1.47).[18]

The SEC chromatograms for the reactions (Fig. 7) display a shift towards higher molecular weight with time. At higher conversion, a near symmetrical peak is observed, without a secondary peak or shoulder at HMW to suggest significant star-star coupling. Similar results were reported by the Haddleton group for the synthesis of an 8-arm P*n*BA star in DMSO to high conversion.

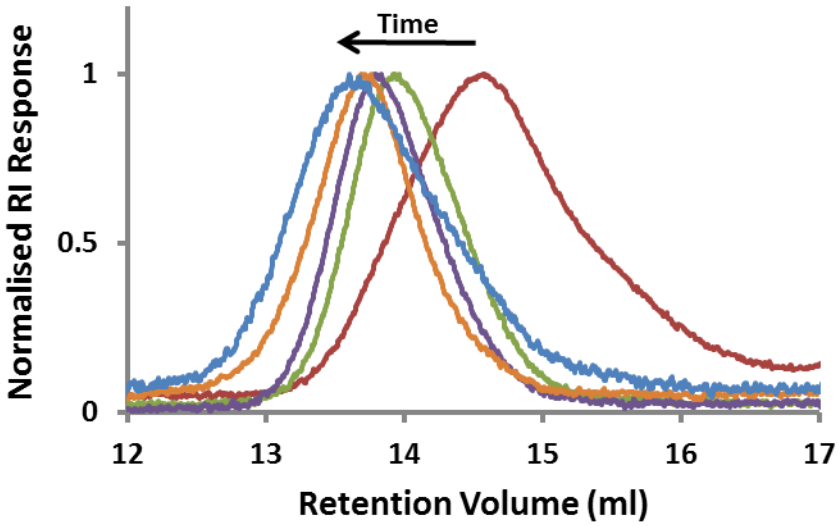

Figure 7: Plot of normalised RI vs retention volume demonstrating shift to higher molecular weight with time for the polymerisation of *t*BA using **4AE**, $[M]_0$:$[I]_0$ = 236. Red line = 120 min; green line = 360 min; purple line = 480 min; orange line = 960 min; blue line = 1440 min.

The ^{1}H NMR spectrum of the pure **4AE-P*t*BA** product is shown in Figure 8. The distinctive broad resonances at 1.4 (**e**), 1.8 (**a**) and 2.2 (**b**) ppm are characteristic of the P*t*BA side chain

and backbone, respectively. At this low molecular weight, resonances corresponding to the core molecule can be clearly seen at 0.9 (**4**), 3.3 (**1**) and 4.0-4.25 (**5**) ppm.

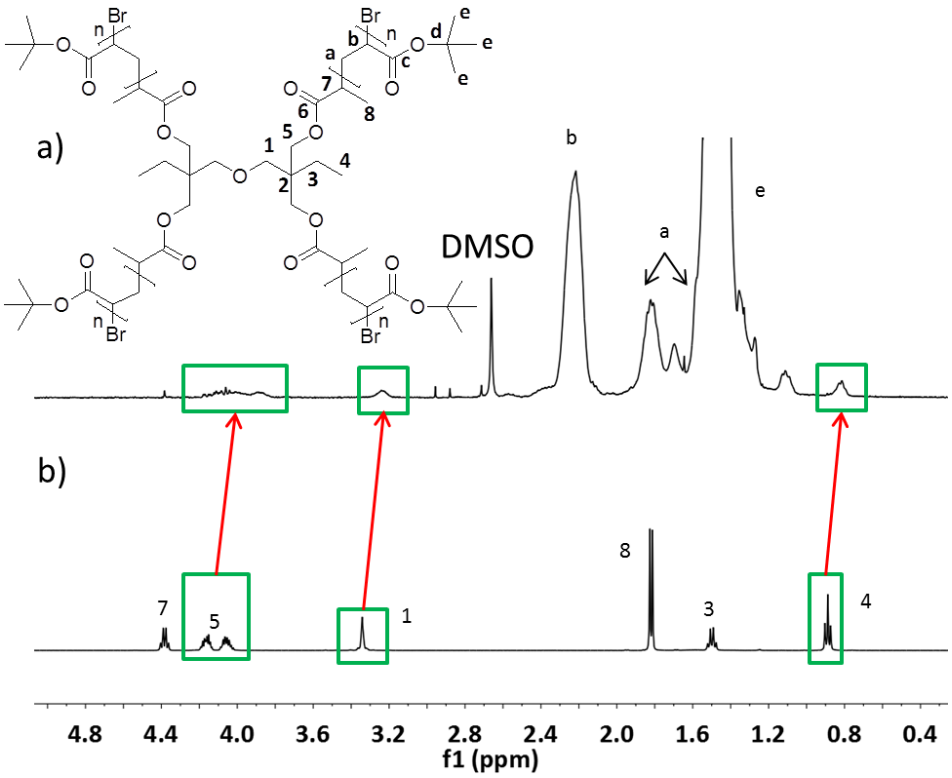

Figure 8: 400 MHz-^{1}H NMR spectrum of; **a)** P*t*BA initiated using **4AE**; **b) 4AE** initiator.

By comparing the integration of the core resonance due to **1** (equivalent to 4H, set to ∫ = 1) with the resonance of **b** for the polymer backbone (1H), an estimate of the polymer molecular weight can be calculated. First the number of *t*BA repeat units is calculated by multiplying the integration due to **b** by 4. To determine the overall mass of P*t*BA this is then multiplied by the mass of a repeat unit (*t*BA = 128.17 g mol^{-1}). Finally, the addition of 790 g mol^{-1} accounts for the mass of the core molecule (**4AE**) in the overall molecular weight. The values estimated are shown in Figure 9 (green) to be in good agreement with M_n(Theor) (black line) and M_n(SEC) (blue).

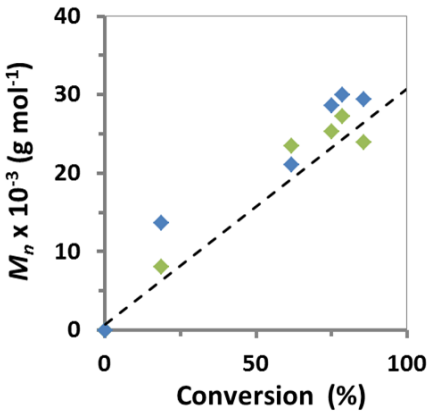

Figure 9: Plot of M_n(NMR) (green) vs monomer conversion. M_n(Theor) (black line) and M_n(SEC) (blue) are included for comparison.

The results described here show that for low molecular weight star polymers, the simple Cu(0)/TREN catalyst system is effective in the controlled synthesis of P*t*BA in DMSO. This also demonstrates control can be maintained over the reaction even following the formation of a biphasic system. HMW polymers are important in order to generate efficient drag reducing agents, therefore, $[M]_0$:$[I]_0$:$[L]_0$ was increased to 2360:1:1 to target a molecular weight of 3.0 x 10^5 g mol^{-1}. The reaction kinetics were examined using the same procedure as above and conversion (blue axis) and $\ln([M]_0/[M]_t)$ (red axis) are plotted against time in Figure 10a. The graph demonstrates a rapid increase in conversion early in the reaction. This is followed by a near linear increase for the remaining reaction time; however, the polymerisation does not progress beyond 50% conversion due to the very high viscosity of the mixture which prevents effective mixing.

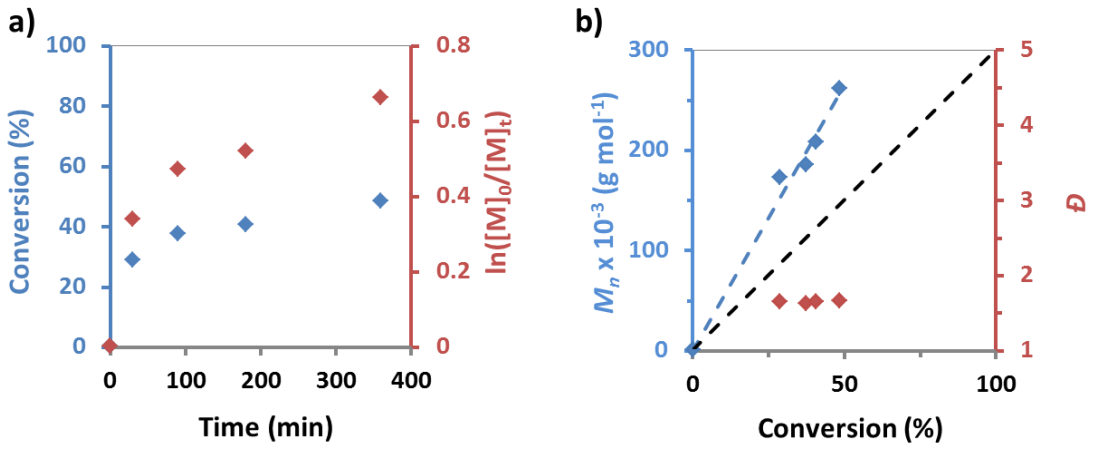

Figure 10: Polymerisation of *t*BA using **4AE**, $[M]_0$:$[I]_0$:$[L]_0$ =2360:1:1; **a)** Conversion (blue axis) and $\ln([M]_0/[M]_t)$ (red axis) vs time; **b)** M_n(SEC) (blue axis) and *Đ* (red axis) vs conversion. (M_n(Theor) shown by black line).

The semi-logarithmic plot of $\ln([M]_0/[M]_t)$ vs time (Fig. 10a, red axis) also demonstrates a rapid increase from 0 before a linear increase between 30 and 360 min. This may suggest that, following the rapid polymerisation in the early stages of the reaction, some termination decreases the initial radical concentration and generates $CuBr_2$ deactivator in the reaction mixture. The polymerisation becomes more controlled and the concentration of radicals remains constant. It is likely that the rapid propagation rate is a consequence of phase separation which occurs at lower conversion (< 1 %) when targeting this higher molecular weight. Furthermore, when the overall number of radicals generated in solution is lower, $CuBr_2$ will take longer to accumulate, which allows the fast rate until sufficient deactivator forms. M_n(SEC) (blue axis) and $Đ$ (red axis) are correlated with monomer conversion in Figure 10b; M_n(Theor) is again indicated by a black line. The linear increase in M_n with conversion suggests that, following the rapid polymerisation at low conversion, the reaction may become controlled. A large discrepancy is consistently observed between M_n(Theor) and M_n(SEC) at each conversion. Generally, this observation comes as a result of low I_{eff}, and a higher rate of propagation than activation. This would be expected if the reaction is not well controlled in the early stages, as in this system due to phase separation. In contrast to the reactions targeting a lower molecular weight above, a higher dispersity ($Đ$ ≈ 1.50) was measured for these HMW polymers. Again, this is likely to be a consequence of the relative rates of activation and propagation. Furthermore, when a low I_{eff} is observed using a multi-functional initiator, it is possible that active chains may grow from all, or just a proportion of the initiation sites on each molecule, resulting in broader $Đ$. The SEC traces are plotted in Figure 11, showing a symmetrical trace with a shift to higher molecular weight as reaction time increases.

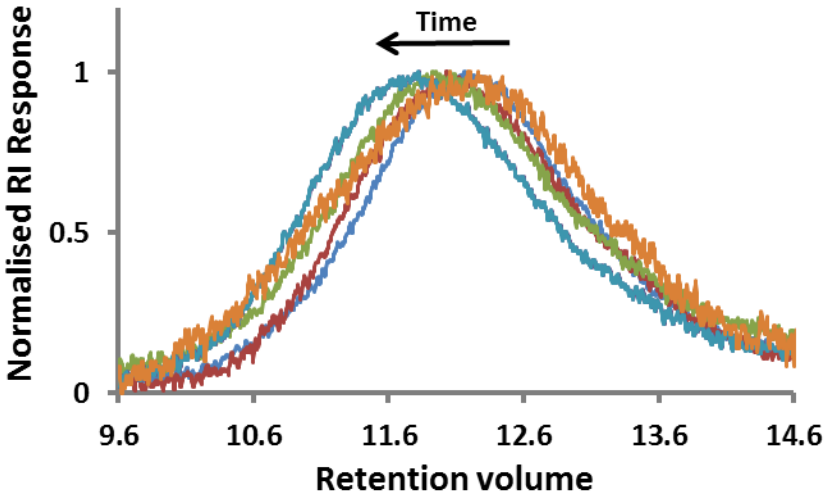

Figure 11: Plot of normalised RI vs retention volume demonstrating shift to higher molecular weight with time for the polymerisation of *t*BA using **4AE**, $[M]_0:[I]_0$ = 2360. Orange line = 30 min; red line = 90 min; green line = 180 min; turquoise line = 360 min.

3.3.3 Polymerisation using PEG based macro-initiators, I4-S, I4-T and I2-S

3.3.3.1 Polymerisation of methyl acrylate

The **I4-S** and **I4-T** macro-initiators were first used for the polymerisation of MA (Scheme 2) to produce a H-shaped, PEG-PMA star block copolymer in a model homogeneous reaction.

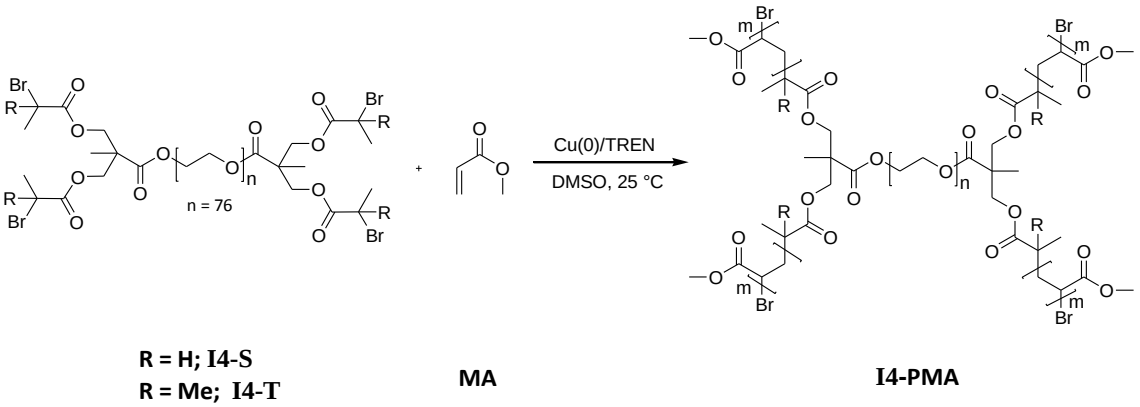

Scheme 2: Polymerisation of MA using **I4-S** or **I4-T** macro-initiators.

Using $[M]_0:[I]_0:[L]_0$ = 92:1:0.4, a molecular weight of around 1.4 x 10^4 g mol^{-1} was targeted. By conducting two parallel reactions for 19 h, the macro-initiators (**I4-S** and **I4-T**) were directly compared. After termination, analysis using ^{1}H NMR spectroscopy demonstrated near total monomer consumption (> 97 %) for both reactions (Table 1, Entry **i** and **ii**). Average molecular weight and *Đ* of each product was evaluated using triple detection SEC.

Table 1: Polymerisation of MA in DMSO using Cu(0)/TREN and **I4-S** or **I4-T** macro-initiator.

Entry	Sample	$[M]_0:[I]_0$	M_n(Target) x 10^{-4} (g mol^{-1})	Time (h)	Conv. (%)	M_n(Theor) x 10^{-4} (g mol^{-1})	M_n (SEC) x 10^{-4} (g mol^{-1})	*Đ*
i	**I4-T-PMA**	92	1.2	19	99.9	1.20	1.17	1.25
ii	**I4-S-PMA**	92	1.2	19	97.0	1.18	1.67	1.47

It is clear from the data in Table 1 that the **I4-T** macro-initiator provides most control over the polymerisation of MA. The dispersity is low (Đ = 1.25) and M_n(SEC) (1.17 x 10^4 g mol^{-1}) is very close to the theoretical value. The small discrepancy in M_n may be the consequence of the compact star structure of the product. This leads to underestimation of molecular weight using SEC, which calculates average molecular weights based on hydrodynamic volume in comparison to linear standards. The secondary bromine macro-initiator (**I4-S**) demonstrated

slightly less control over the reaction. The M_n(SEC) measured (1.67 x 10^4 g mol^{-1}) was higher than theoretical, even considering the underestimation when measuring star polymers, and a higher dispersity (Đ = 1.47) suggests slower initiation relative to propagation and decreased I_{eff}. The normalised RI response for **I4-T-PMA** (red) and **I4-S-PMA** (blue) is plotted against retention volume in Figure 12 and demonstrates the narrower distribution for **I4-T-PMA**. The plot of **I4-S-PMA** exhibits a significant shoulder at low molecular weight, a consequence of incomplete initiation, even at 97 % conversion. The trace of the **I4** macro-initiator is included in green in Figure 12 for comparison. This confirms that the low molecular weight shoulder corresponds to un-reacted macro-initiator. A small shoulder is also observed in the plot of **I4-T-PMA**, though with a much low intensity. Neither graph demonstrates a peak or shoulder at low retention volume suggesting that extensive star-star coupling is avoided for this low molecular weight star polymer, even at high conversion. From these results it was concluded that the more active tertiary bromine group is most suitable for the polymerisation of MA. The faster initiation provided by the tertiary bromine is necessary due to the rapid propagation rate of MA (k_p^{app} ≈20 times faster than *t*BA), but also to counteract the lower I_{eff} for this PEG based macro-initiator.

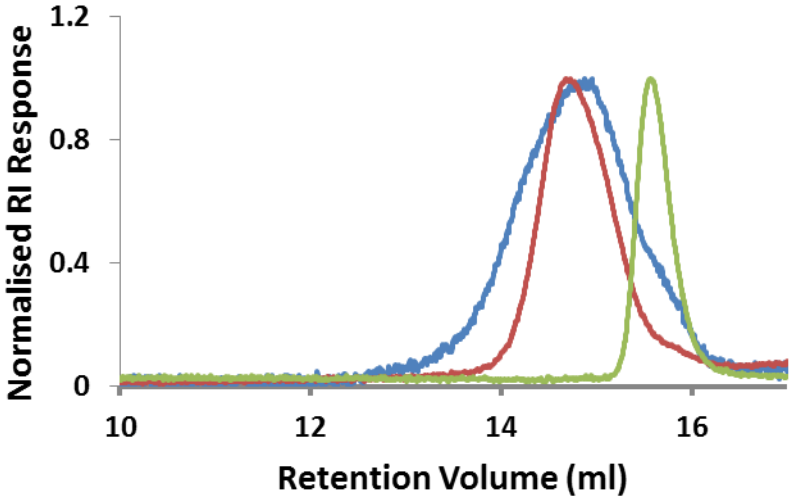

Figure 12: Plot of normalised RI vs retention volume for PMA initiated by **I4-S** (blue)/**I4-T** (red) initiators. Trace for macro-initiator (green) included for comparison.

The ^{1}H NMR spectrum of the pure **I4-T-MA** product is shown in Figure 13. The spectrum demonstrates characteristic proton shifts of the PMA backbone (1.0-2.5 ppm, **a** and **b**) and side chain (3.65 ppm, **d**) which overlaps with the –CH_2 resonance of the PEG core (3.63 ppm, **8**). By expansion of the spectrum in Figure 14a, resonances due to the core end groups are also visible at 1.26 ppm (**4**) and 4.10-4.25 ppm (**3**).

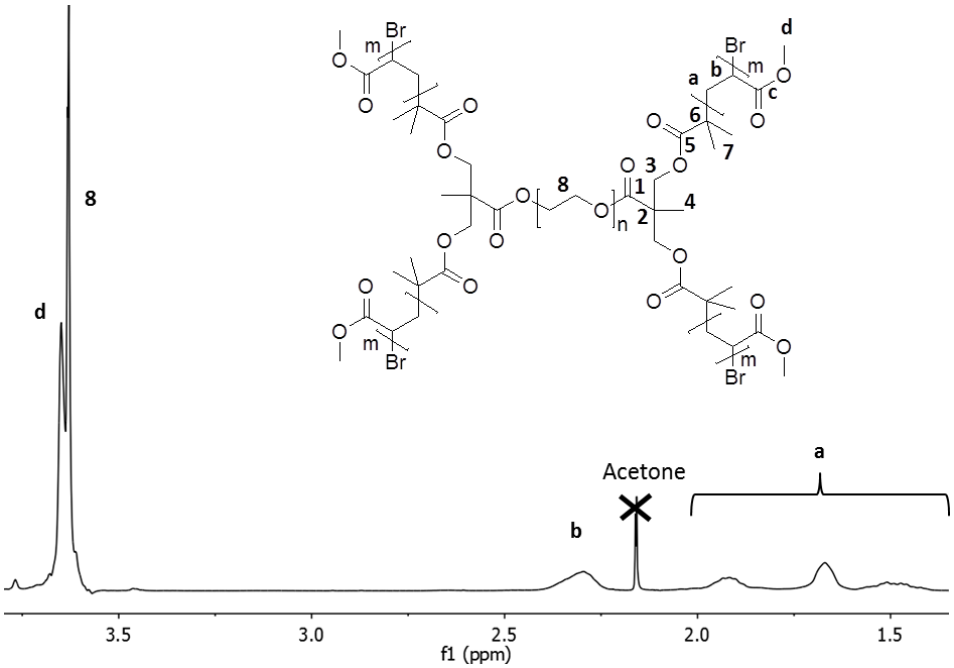

Figure 13: 400 MHz-^{1}H NMR spectrum of **I4-T-PMA**.

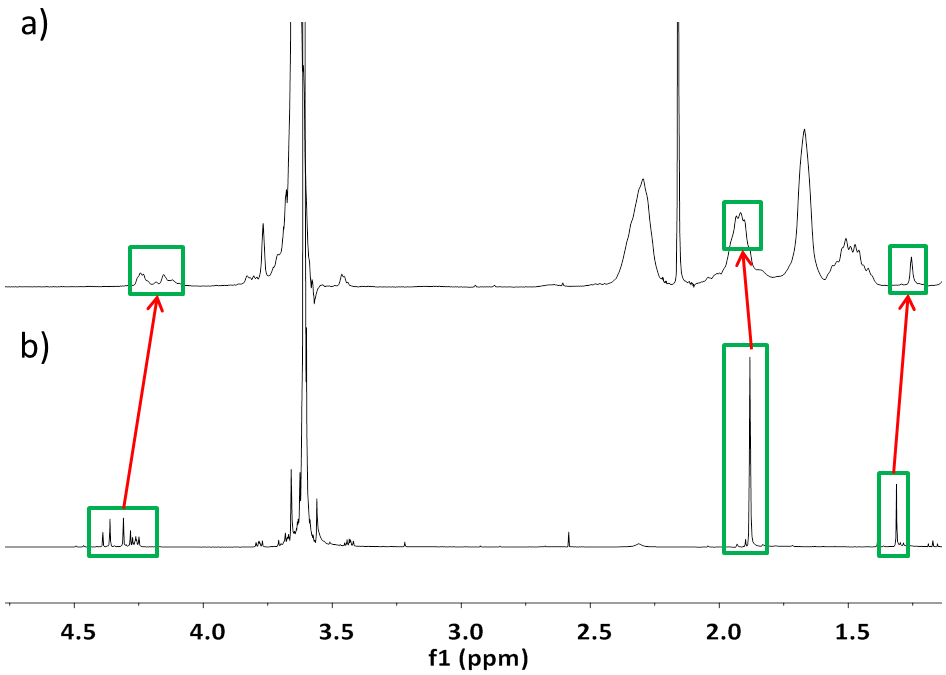

Figure 14: 400 MHz-^{1}H NMR spectrum of; **a**) **I4-T-PMA** expanded to demonstrate presence of core resonances; **b) I4-T.**

3.3.3.2 Polymerisation of tert-butyl acrylate

The **I4-S** and **I4-T** macro-initiators were compared for the heterogeneous polymerisation of *t*BA in DMSO, to produce a H-shaped PEG-P*t*BA star block copolymer (Scheme 3). A ratio of $[M]_0:[I]_0:[L]_0$ = 236:1:0.4 was used to target a molecular weight of 3.4 x 10^4 g mol^{-1} and allow comparison with the **4AE** initiator (Section 3.3.2).

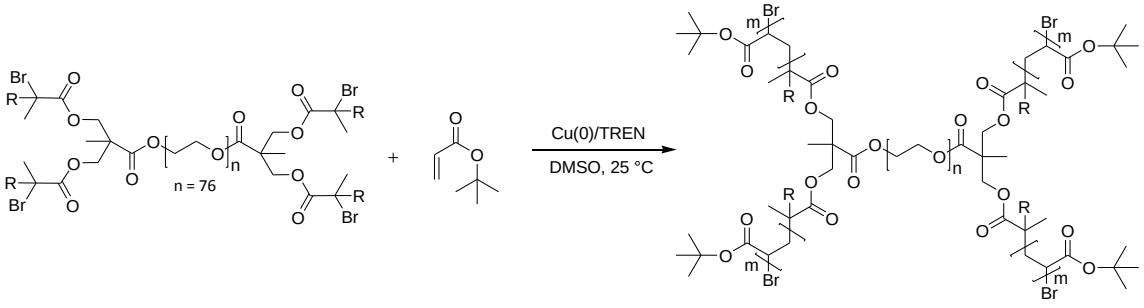

R = H; I4-S
R = Me; I4-T

***t*BA**

I4-P*t*BA

Scheme 3: Polymerisation of *t*BA using **I4-S** or **I4-T** macro-initiator.

After stirring for 16 h, conversion and mass analysis was conducted for the products and is summarised in Table 2. By comparing the data for each macro-initiator, it is clear that **I4-T** (Table 2, Entry **i**) is not an effective initiator for the *t*BA system. Monomer conversion is very low for this reaction (14%) and M_n(SEC) (11.4 x 10^4 g mol^{-1}) is much higher than the theoretical value (0.82 x 10^4 g mol^{-1}). Furthermore, the dispersity is very high ($Đ$ = 4.38), clearly showing that the reaction is uncontrolled. In contrast, the **I4-S** macro-initiator (Table 2, Entry **ii**) demonstrates a much higher conversion (80%). Moreover, M_n(SEC) (3.46 x 10^4 g mol^{-1}) is much closer to theoretical (2.80 x 10^4 g mol^{-1}) and dispersity ($Đ$ = 1.30) is comparable to reactions using **4AE** in Section 3.3.2.

Table 2: Polymerisation of *t*BA in DMSO using Cu(0)/TREN and **I4-S** or **I4-T** macro-initiators.

Entry	Sample	$[M]_0$:$[I]_0$	M_n(Target) x 10^{-4} (g mol^{-1})	Time (h)	Conv. (%)	M_n(Theor) x 10^{-4} (g mol^{-1})	M_n (SEC) x 10^{-4} (g mol^{-1})	$Đ$
i	**I4-T-P*t*BA**	236	3.4	16	14	0.82	11.4	4.38
ii	**I4-S-P*t*BA**	236	3.4	16	80	2.80	3.46	1.30
iii	**I4-S-P*t*BA**	78	1.4	16	72	1.12	1.51	1.90

The SEC chromatogram (normalised RI vs retention volume) of the **I4-S-P*t*BA** product is plotted in Figure 15 (blue4) following recovery by precipitation. A narrow, symmetrical peak can be observed, as well as a clear shift in retention volume when compared with the macro-initiator (**I4**) (Fig. 15, green). The chromatogram of the **I4-T-P*t*BA** sample (Fig. 15, red), is very broad and a secondary peak can be observed at high retention volume, demonstrating unreacted macro-initiator in the mixture even following precipitation.

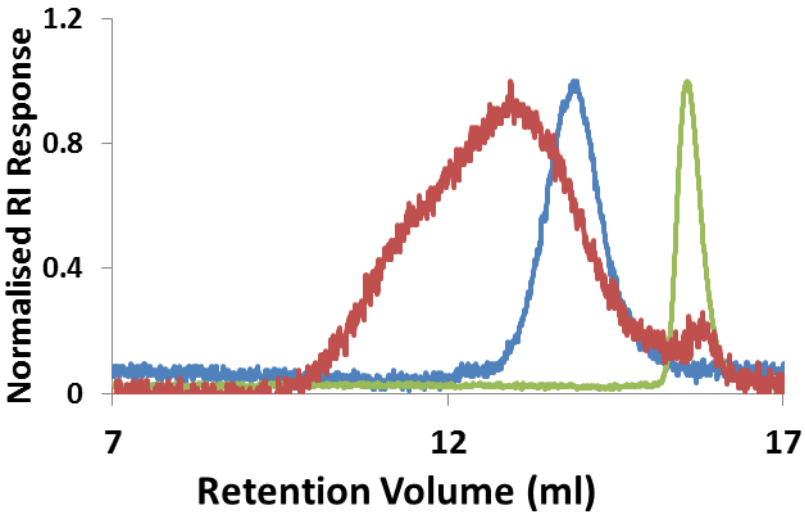

Figure 15: Plot of normalised RI vs retention volume for P*t*BA initiated using **I4-S** (blue), **I4-T** (red) macro-initiators. Trace for macro-initiator (green) included for comparison.

In contrast to the homogeneous polymerisation of MA, **I4-T** appears to be unsuitable for the heterogeneous polymerisation of *t*BA in DMSO. Due to its higher activity, radicals will be produced at a faster rate using this macro-initiator. In this reaction the result was uncontrolled propagation and a product with high M_n and $Đ$; the **I4-S** macro-initiator is not as active which seems to be beneficial here. For a homogeneous system this is counter-intuitive, in general initiation must be faster than propagation to avoid uncontrolled polymerisation. However, in these reactions the situation is complicated by phase separation which may impact the ability to control the reaction, this will be discussed further in Section 3.3.4. The ^{1}H NMR spectrum of the **I4-S-P*t*BA** product (Table 2, Entry **ii**) is shown in Figure 16. The spectrum contains characteristic resonances which represent both the P*t*BA backbone (1.5 – 2.5 ppm, **a** and **b**) and tert-butyl side-chain (1.4 ppm, **e**). Furthermore, an intense resonance at 3.6 ppm demonstrates the presence of PEG chain –CH_2 groups (**8**) in the final polymer.

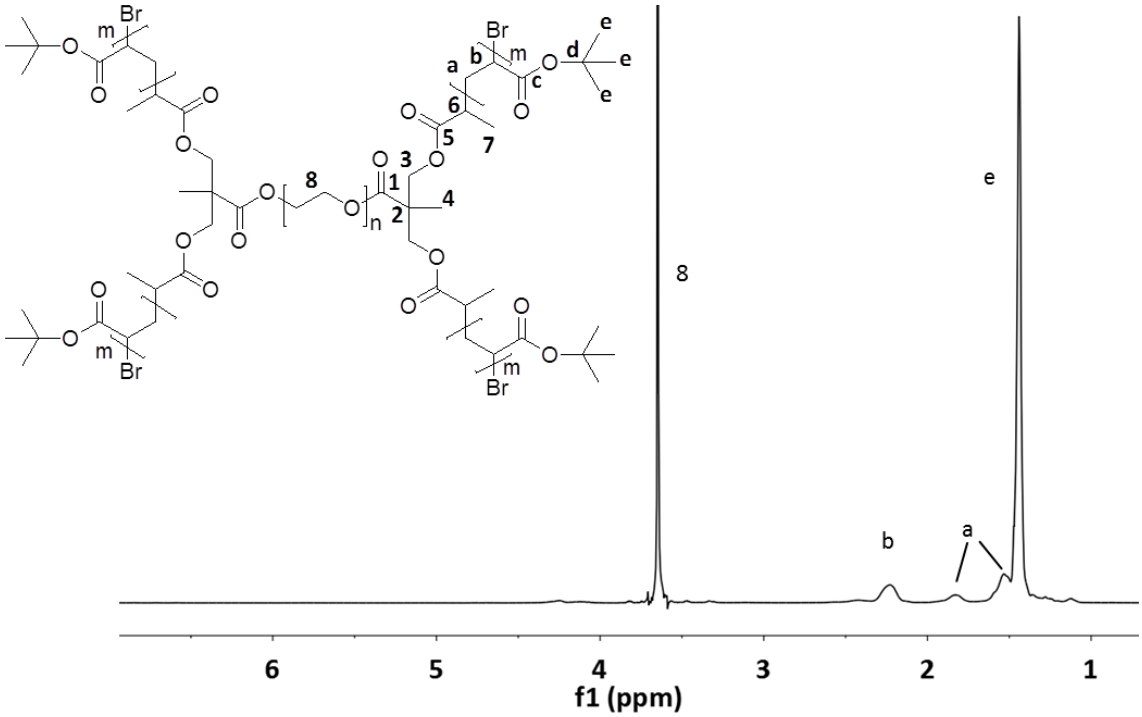

Figure 16: 400 MHz-^{1}H NMR spectrum of **I4-S-P*t*BA**.

Based on the reactions discussed here, the **I4-S** macro-initiator appeared to be the preferred initiator for the polymerisation of *t*BA in DMSO. It was therefore used for the following **I4** polymerisation reactions in this chapter. $[M]_0$:$[I]_0$ was reduced to 78 in order to target a lower molecular weight (1.4 x 10^4 g mol^{-1}, Table 2, Entry **iii**). Analysis using SEC demonstrated much less control over the reaction with M_n(SEC) (1.51 x 10^4 g mol^{-1}) greater than theoretical (1.12 x 10^4 g mol^{-1}) and a very high dispersity ($Đ$ = 1.90). This is likely to be a consequence of low macro-initiator efficiency which means not all of the initiator is consumed even at this conversion (72 %). This is supported by a comparison of the SEC traces for **I4-S** (green) and low molecular weight **I4-S-P*t*BA** (purple) in Figure 17. A significant RI response can be observed in the **I4-S-P*t*BA** trace at the same retention volume as the macro-initiator.

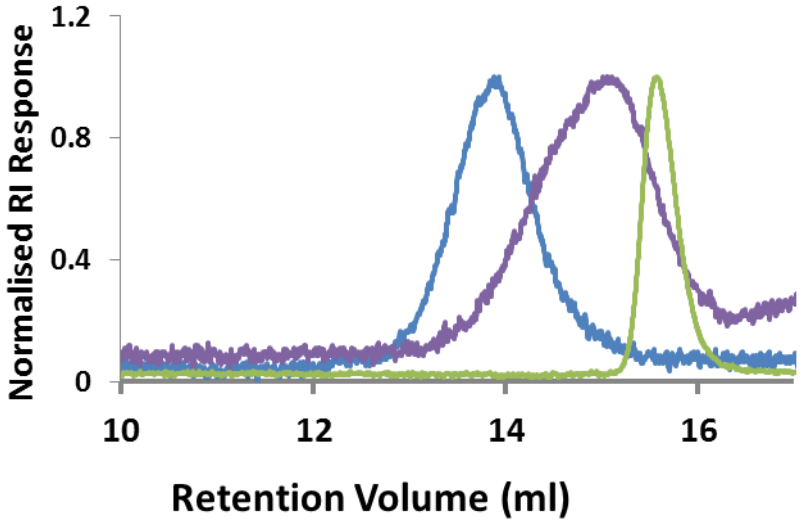

Figure 17: Plot of normalised RI vs retention volume for P*t*BA initiated using **I4-S;** M_n(target)= 1.4 x 10^4 g mol^{-1} (purple), M_n(target) = 3.4 x 10^4 g mol^{-1} (blue). Trace for macro-initiator (green) included for comparison.

Following the preliminary investigations, the kinetics of *t*BA polymerisation using **I4-S** were studied using several parallel reactions with a ratio of $[M]_0:[I]_0:[L]_0$ = 236:1:0.4 to target a molecular weight of ≈ 3.4 x 10^4 g mol^{-1}. The evolution of conversion with time is plotted in Figure 18a (blue axis) which shows a linear increase reaching 80 % after 960 min. There is, however, a non-linear correlation in the kinetic plot of $\ln([M]_0/[M]_t)$ vs time (Fig. 18a, red axis), which suggests that the radical concentration is not constant across the individual reactions.

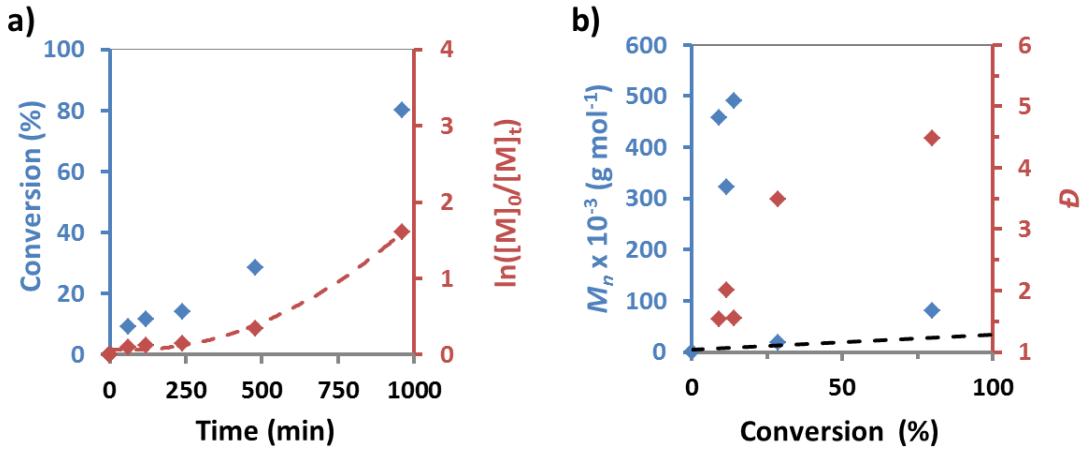

Figure 18: Polymerisation of *t*BA using **I4-S**, $[M]_0:[I]_0:[L]_0$ =236:1:0.4; **a)** Conversion (blue axis) and $\ln([M]_0/[M]_t)$ (red axis) vs time; **b)** M_n(SEC) (blue axis) and *Đ* (red axis) vs conversion. (M_n(Theor) shown by black line).

Whilst this information suggests the polymerisation may be controlled, the plot of M_n(SEC) (blue axis) and *Đ* (red axis) against conversion (Fig. 18b) clearly demonstrates that the reaction

is not a controlled radical process. The decrease in M_n(SEC) with conversion is typical of a uncontrolled free radical polymerisation where propagation is faster than initiation and the values are much higher than those theoretically calculated at a given conversion. Dispersity increases from 1.54 at 9.2 % conversion to reach a value of 4.48 (conv. = 80 %) as the reaction progresses. These results are different to those observed for the initial polymerisation of *t*BA using **I4-S** (Table 2. Entry **ii**), which demonstrated good control over the reaction. The lack of control is similar to that observed using **I4-T**; although the conversion is still much higher for the **I4-S** macro-initiator. It is possible that this unreliability is a result of the heterogeneous reaction conditions and will be discussed further in Section 3.3.4. The plots of Wf/dlogM vs logM for these reactions are shown in Appendix B, Fig. 2.

The kinetics of *t*BA polymerisation with an increased ratio of $[M]_0$:$[I]_0$:$[L]_0$ = 2360:1:1 targeting a molecular weight of ≈ 3 x 10^5 g mol^{-1} were also studied. The evolution of conversion (blue axis) and $\ln([M]_0/[M]_t)$ (red axis) is plotted against time in Figure 19a. Both of these graphs show a linear increase demonstrating a constant concentration of radicals in the system. The final experiment was conducted until mixing was no longer possible and a conversion of 80 % was reached in 960 min, higher than observed when targeting the same molecular weight using the **4AE** initiator (Section 3.3.2), possibly a due to more effective stirring for this reaction. A value of k_p^{app} = 0.0016 min^{-1} was calculated from the gradient of the kinetic plot (Fig. 19a, red axis) which is comparable to the rate (k_p^{app} = 0.0022 min^{-1}) measured when using the **4AE** initiator.

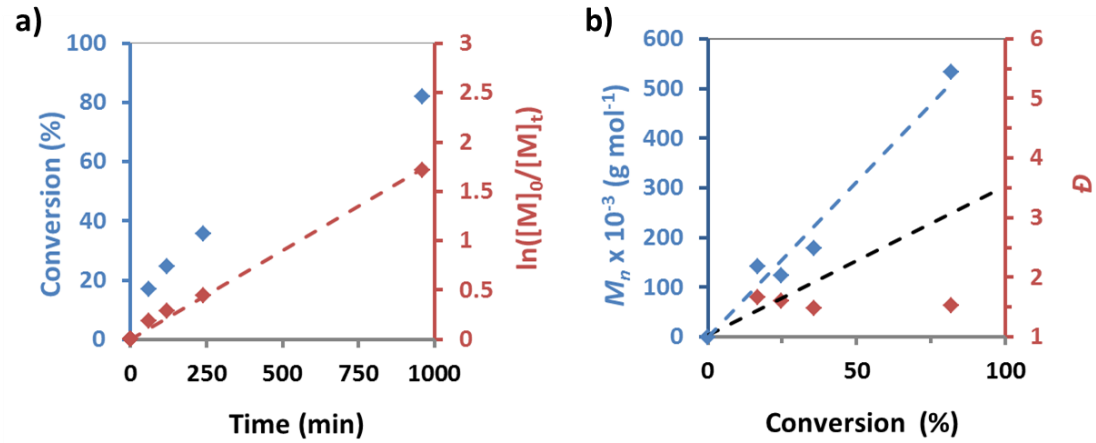

Figure 19: Polymerisation of *t*BA using **I4-S**, $[M]_0$:$[I]_0$:$[L]_0$ =2360:1:1; **a)** Conversion (blue axis) and $\ln([M]_0/[M]_t)$ (red axis) vs time; **b)** M_n(SEC) (blue axis) and *Đ* (red axis) vs conversion. (M_n(Theor) shown by black line).

The plot of M_n(SEC) (blue axis) against conversion is shown in Figure 19b demonstrating a positive linear correlation. A large discrepancy between M_n(SEC) and M_n(Theor) (Fig. 19b, black line) is observed, highlighting the low I_{eff} for the macro-initiator in this system. A steady decrease of dispersity (Fig. 19b, red axis) is indicative of a controlled polymerisation and $Đ$ < 1.30 was obtained at the highest conversion. By plotting Wf/dlogM vs logM (Fig. 20) for each time, a shift to higher molecular weight is observed as the reaction time increases.

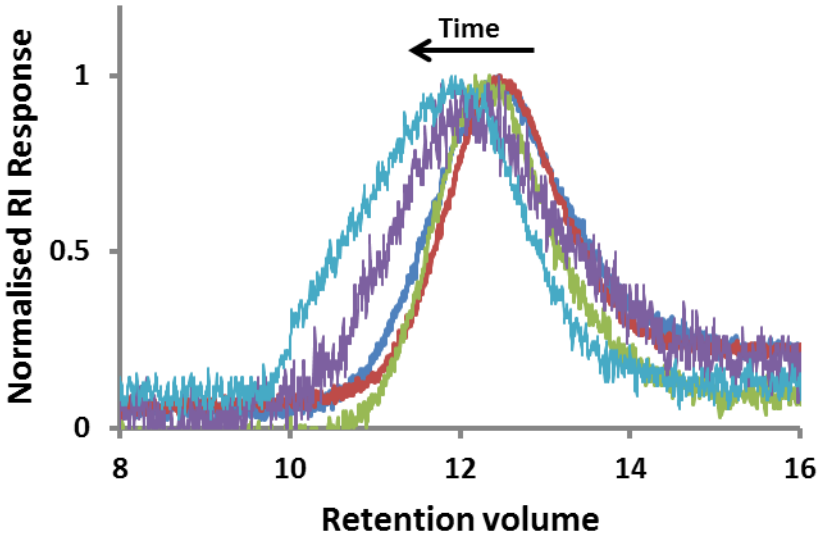

Figure 20: Plot of normalised RI vs retention volume demonstrating shift to higher molecular weight with time for the polymerisation of *t*BA using **I4-S**, $[M]_0:[I]_0$ = 2360. Blue line = 60 min; red line = 120 min; green line = 240 min; turquoise line = 960 min.

An example ^{1}H NMR spectrum for HMW **I4-S-P*t*BA** is shown in Figure 21. Despite the dominance of the P*t*BA chain, a resonance can still be observed at 3.61 ppm, corresponding to the PEG environments (**8**) in the core molecule. This resonance has a much lower intensity than the characteristic P*t*BA signals present between 1.4 and 2.5 ppm (**a**, **b** and **e**). By integrating the signal due to **8** (304 H, n = 76), and comparing this with a resonance of the P*t*BA backbone (**b**, 2.16 ppm, 1H), the polymer molecular weight can be estimated. As the P*t*BA signal, **b**, represents 1 proton of the *t*BA repeat unit, the number of repeat units is calculated by multiplying the integration of **b** by 304. This value is then multiplied by the molar mass of *t*BA (128.17 g mol^{-1}) to determine the overall molecular weight of the P*t*BA block; addition of 4 x 10^3 g mol^{-1} accounts for the mass of the core molecule.

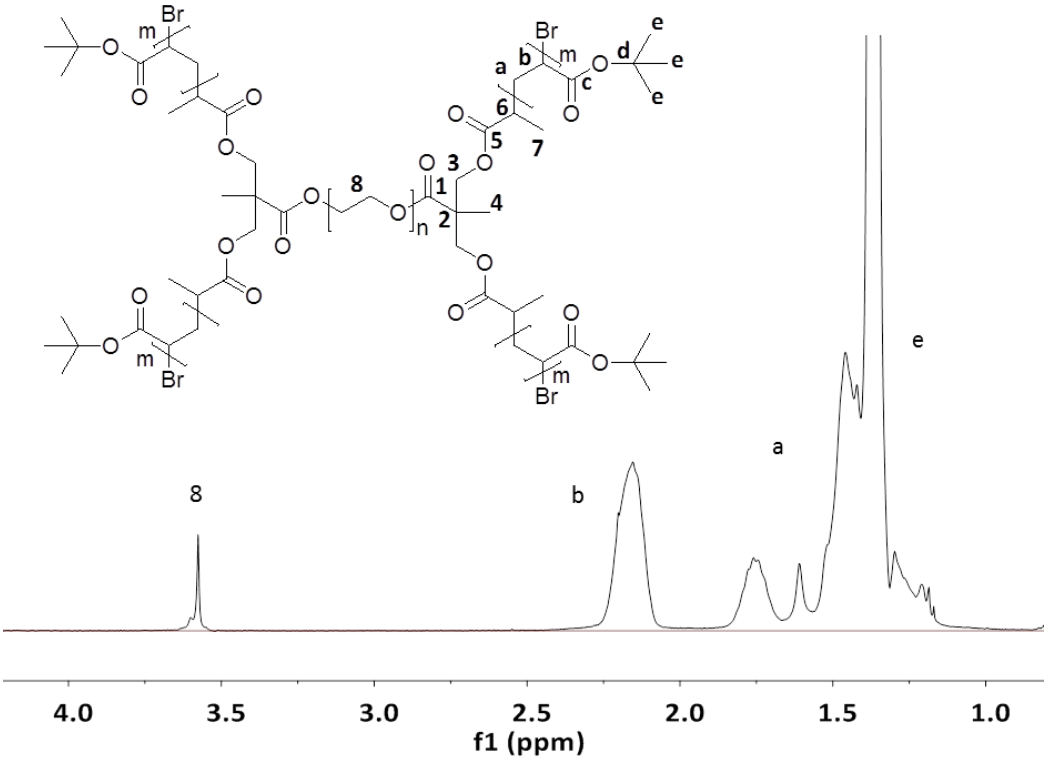

Figure 21: 400 MHz-^{1}H NMR spectrum of HMW **I4-S-P*t*BA**.

By performing this calculation for the reaction mixture after 960 min (Fig. 19a, conv. = 80 %) a molecular weight of 3.0 x 10^5 g mol^{-1} was estimated. This value is close to M_n(Theor), however, does not match the value measured using SEC (M_n = 5.4 x 10^5 g mol^{-1}). The ^{1}H NMR spectrum of the reaction mixture is compared with the same polymer sample after re-precipitation in Figure 22a and b, respectively. The unreacted monomer (vinyl proton resonances observed at 5.5-6.5 ppm) is clearly removed by this purification. Moreover, the intensity of the PEG resonance (**8**) also decreases relative to P*t*BA, increasing the estimated molecular weight. The decrease in the intensity of **8** is due to a loss of unreacted **I4-S**, which may be expected, due to the low I_{eff} for this reaction. The polymer sample was re-precipitated until a constant intensity of resonance **8** relative to **b** of the P*t*BA backbone was reached.

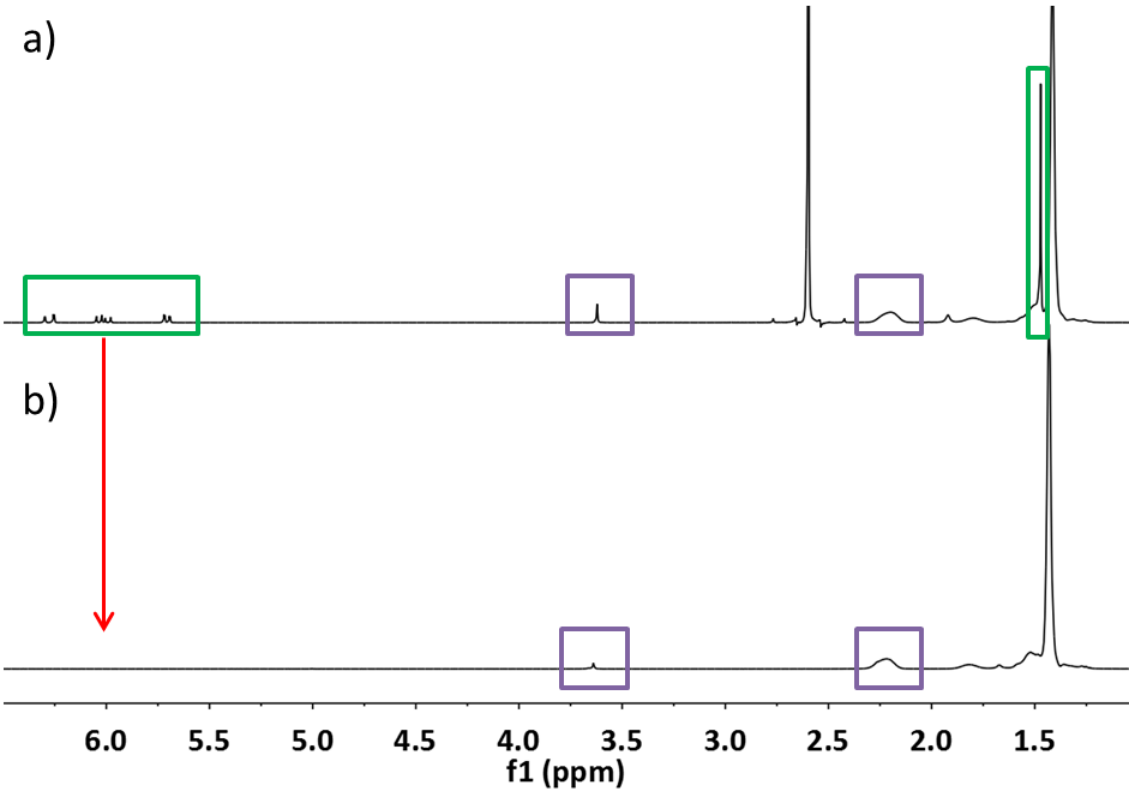

Figure 22: 400 MHz-^{1}H NMR spectrum of HMW **I4-S-P*t*BA**; **a)** Reaction mixture; **b)** Purified polymer.

In Figure 23 the change in estimated M_n(NMR) is plotted following these consecutive re-precipitations. It shows an initial increase in the molecular weight before a consistent level is reached after 4-5 re-precipitations. This demonstrates a constant level of PEG in the system confirming the incorporation of **I4-S** in to the P*t*BA polymer. The final value calculated for molecular weight is approximately 5.0 x 10^5 g mol^{-1} which is close to the value obtained using SEC (5.4 x 10^5 g mol^{-1}, Fig. 23, red).

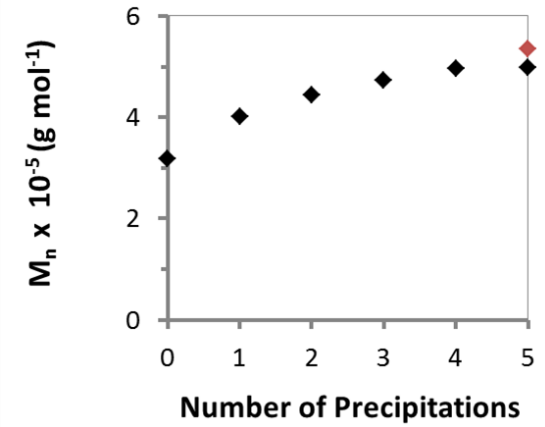

Figure 23: Plot of M_n after successive re-precipitations HMW **I4-S-P*t*BA**, estimated from analysis of ^{1}H NMR spectra. M_n(SEC) shown in red.

The **I2-S** macro-initiator was used on a small scale with $[M]_0:[I]_0:[L]_0$ = 2360 in order to target a molecular weight of 3 x 10^5 g mol^{-1} (Scheme 4). This macro-initiator allows the synthesis of a Y-shaped PEG-P*t*BA block co-polymer; however, due to the relative size of the PEG chain in comparison to the P*t*BA section, the polymer characteristics should be similar to that of linear P*t*BA.

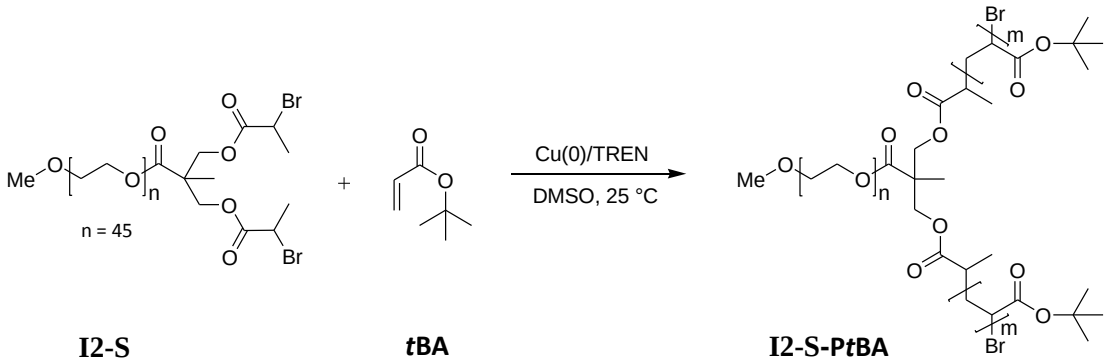

Scheme 4: Polymerisation of *t*BA using **I2-S** macro-initiator.

Whilst the conversion was low (Table 3, Entry 1), possibly due to the high viscosity of the polymer layer, the dispersity is also relatively low (Đ = 1.57). The M_n(SEC) (4.22 x 10^5 g mol^{-1}) is much higher than theoretical (1.12 x 10^5 g mol^{-1}) demonstrating a low I_{eff} when using this macro-initiator for the polymerisation of *t*BA in DMSO.

Table 3: Polymerisation of *t*BA in DMSO using Cu(0)/TREN and **I2-S** macro-initiator,

Entry	Sample	$[M]_0:[I]_0$	M_n(Target) x 10^{-5} (g mol^{-1})	Time (h)	Conv. (%)	M_n(Theor) x 10^{-5} (g mol^{-1})	M_n (SEC) x 10^{-5} (g mol^{-1})	Đ
i	**I2-T-PtBA**	2360	3.0	16	36	1.12	4.22	1.57

3.3.4 Polymerisation of *tert*-butyl acrylate using methyl 2-bromopropionate, MBP, initiator

During the kinetic study for the polymerisation of *t*BA using the **I4-S** macro-initiator (Section 3.3.3.2), uncontrolled polymerisation was observed ($[M]_0:[I]_0$ = 236). Methyl 2-bromopropionate (MBP, Scheme 5) was therefore chosen as a model initiator in order to investigate the polymerisation of *t*BA in DMSO further. MBP is a single site initiator commonly used in copper mediated polymerisations, therefore avoiding the complications experienced when using multi-functional or macro-initiators. A ratio of $[M]_0:[I]_0$ = 78 was used to target a low molecular weight (1 x 10^4 g mol^{-1}) maintaining the same reactions conditions (Cu(0) = 8.4 cm/TREN/*t*BA/DMSO = 0.5 ml) as for the polymerisations described above. The reaction

reached almost complete monomer conversion (Table 4, Entry **i**), however, no control over the polymerisation was observed (*Đ* = 10.77). The reaction mixture quickly separated in the two phases and the polymer layer became a very viscous within a few minutes. Analysis of molecular weight demonstrated M_n(SEC) (3.8 x 10^4 g mol^{-1}) was much higher than targeted (1 x 10^4 g mol^{-1}).

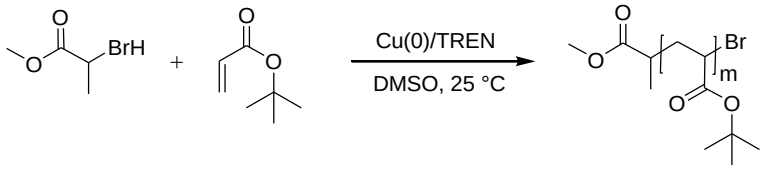

MBP ***t*BA** **MBP-P*t*BA**

Scheme 5: Polymerisation of *t*BA using MBP initiator.

Haddleton et al. demonstrated control over the polymerisation of *n*BA and *t*BA using a system consisting of; ethylene bis(2-bromoisobutyrate), Cu(0)-wire (1.6 cm), Me_6-TREN ligand, DMSO (1.6 ml) and $CuBr_2$.[18] Both a lower catalyst surface area and lower monomer concentration were used when compared to the reactions described above (Table 4, Entry **i**). The addition of $CuBr_2$ is known to improve control by allowing immediate deactivation of chains at the beginning of the reaction. To investigate the impact of these changes on this polymerisation reaction, the reaction conditions were altered systematically (using TREN ligand) (Table 4, Entry **ii**-**vi**).

Table 4: Polymerisation of *t*BA using MBP initiator and a range of reaction conditions, $[M]_0$:$[I]_0$ = 78, M_n(Target) = 1 x 10^4 g mol^{-1}, t = 16 h

Entry	Conditions	Conv. (%)	M_n(Theor) x 10^{-4} (g mol^{-1})	M_n (SEC) x 10^{-4} (g mol^{-1})	*Đ*
i	**Cu(0) catalyst**	98	0.98	3.77	10.77
ii	**Addition of $CuBr_2$**	96	0.98	4.35	8.63
iii	**Decr. [M]**	65	0.65	10.9	5.39
iv	**Decr. Cu(0) length**	16	0.16	4.13	4.60
v	**$CuBr_2$ and Decr. [M]**	88	0.88	0.70	27.84
vi	**$CuBr_2$, Decr. [M] and Decr. Cu(0)**	80	0.80	0.89	13.78

NB: Decr. Cu(0) length to 1.6 cm, Decr. [M] - solvent volume increased to 1.6 ml.

The traces in Figure 24 show the SEC chromatogram measured for each reaction as the reaction conditions were altered. The SEC trace using the original catalyst system is shown in Figure 24a. No significant impact was observed when $CuBr_2$ was added (Fig. 24b), the monomer concentration decreased (Fig. 24c) or catalyst length decreased (Fig. 24d) individually.

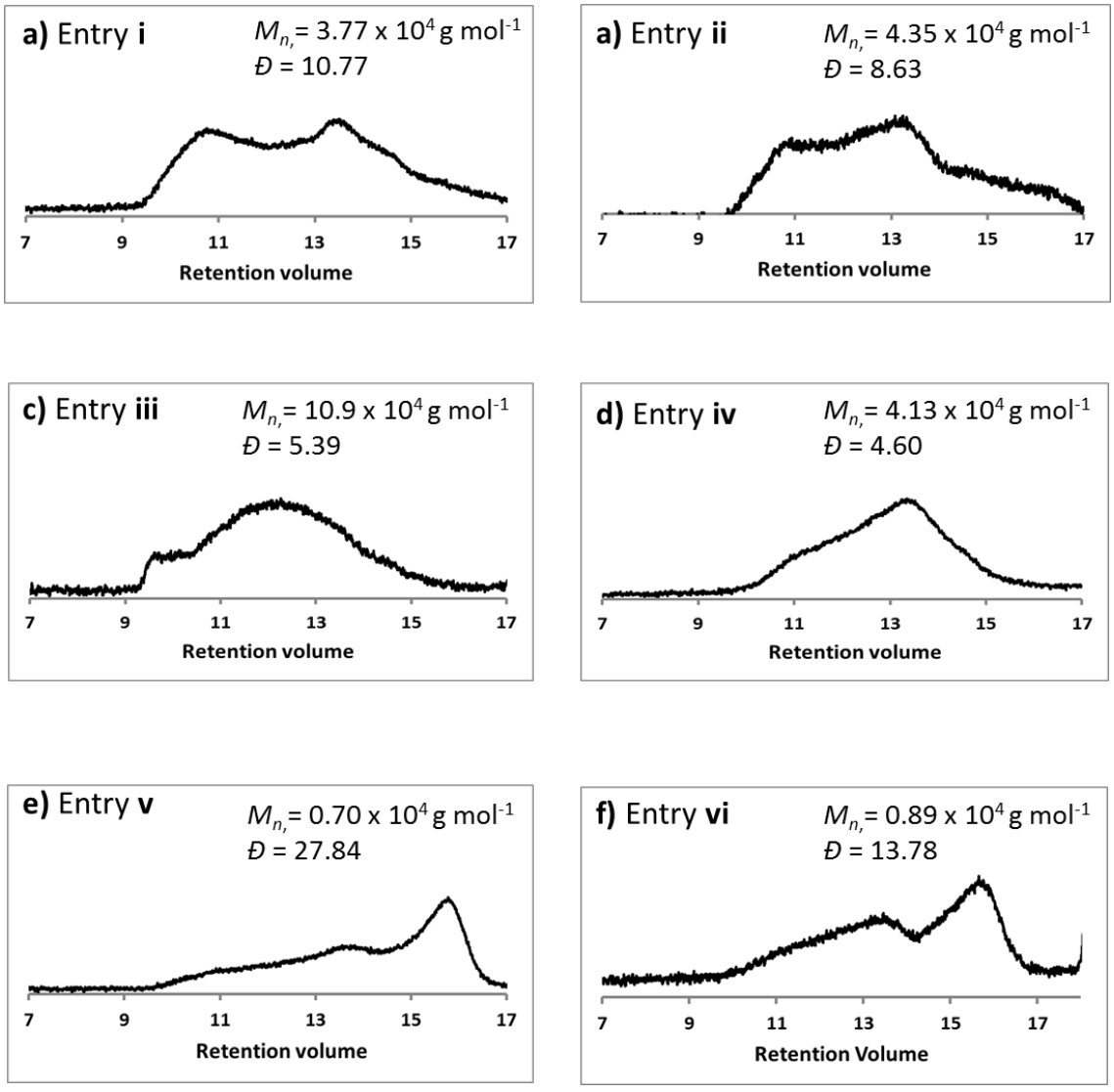

Figure 24: SEC traces as reaction conditions are changed for the polymerisation of *t*BA using MBP; **a)**-**f)** correspond to Table 4, Entry **i**-**vi**.

By simultaneously adding $CuBr_2$ and decreasing monomer conversion (Table 4, Entry **v**), a large increase in dispersity was measured (*Đ* = 27.84). The chromatogram (Fig. 24e) demonstrates, relatively, a higher proportion of the sample at lower retention volume, nearer to the targeted molecular weight. A slightly narrower dispersity (*Đ* = 13.78) was observed when the presence of $CuBr_2$, monomer concentration and Cu(0) length were altered simultaneously (Table 4, Entry **vi**). The chromatogram (Fig. 24f) again shows that a high proportion of the sample is low

molecular weight. The final reaction (Table 4, Entry **vi**); in the presence of $CuBr_2$, decreased monomer concentration and Cu(0) length was conducted over shorter reaction times (30, 60, 120 min) and the development of the SEC chromatograms was monitored (Fig. 25a-d). After 30 min, a monomer conversion of 24% (Fig. 25a) and a near symmetrical SEC trace was observed. However, a small shoulder ($M_p > 3 \times 10^4$ g mol^{-1}) can be seen developing at low retention volume. At longer reaction times, as the conversion increases (80 % after 960 min) the HMW shoulder increases in intensity and broadens whilst the original low molecular weight peak remains (Fig. 25b-d). This suggests two competing polymerisation mechanisms in the system. When the M_p of the low molecular weight peak (Fig. 25a) is analysed, a value of $\approx 3.1 \times 10^3$ g mol^{-1} is obtained. This seems likely that the polymerisation is initiated and proceeds *via* a controlled mechanism, due to the high concentration of $CuBr_2$, up to a molecular weight of 3.1×10^3 g mol^{-1}. At this point the P*t*BA chain becomes insoluble in DMSO. In this reaction, the biphasic system rapidly forms a very viscous, polymer layer. Despite its high concentration, the $CuBr_2$ deactivator cannot access the active polymer chains and the polymerisation continues to propagate through a free radical mechanism due to the presence of monomer in the polymer layer. After 960 min (Fig. 25d) the peak is extremely broad suggesting high levels of termination and chain transfer. The change in shape of the SEC chromatogram observed following the addition of $CuBr_2$ (Fig. 24e-f) may be due to a higher proportion of dormant chains which do not participate in the second free radical polymerisation mechanism.

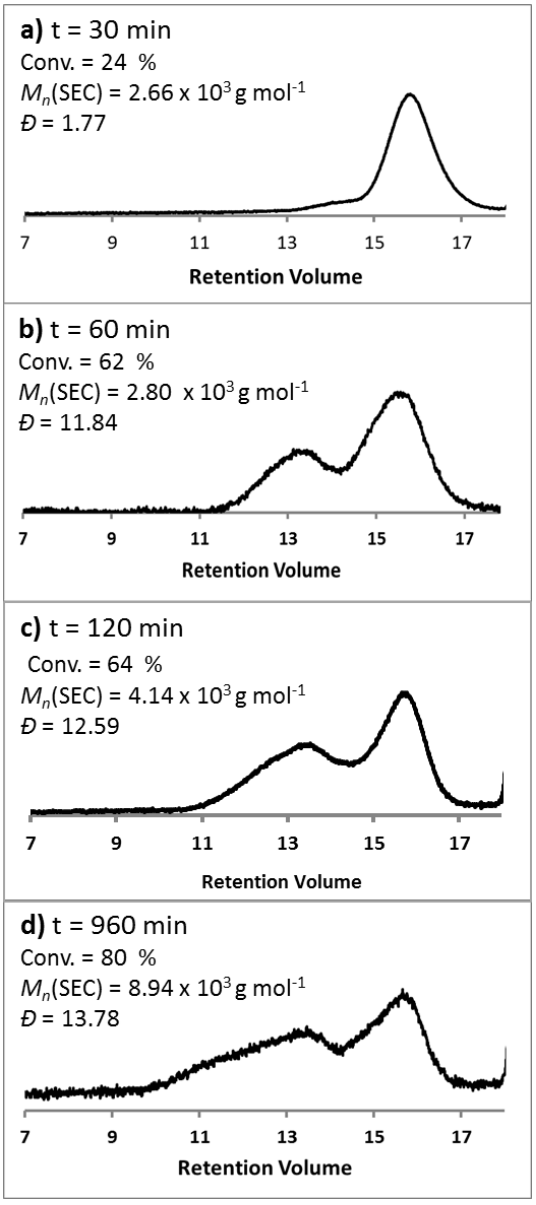

Figure 25: SEC chromatograms at increasing times for polymerisation of *t*BA using MBP in the presence of $CuBr_2$ with decreased Cu(0) length and monomer concentration.

The results described here for the polymerisation of *t*BA using MBP demonstrate that control over this polymerisation is problematic when targeting a low molecular weight. They also confirm that the ability of the $CuBr_2$ deactivator to access the active chain ends is key to avoiding uncontrolled free radical polymerisation. Whilst the biphasic system initially forms as a stable emulsion, allowing access of $CuBr_2$ due to high surface area of the polymer droplets, the polymer layer was then observed to rapidly agglomerate and $CuBr_2$ access was prevented. The polymer layer is swollen by DMSO and so there is the potential for some $CuBr_2$ to be incorporated in to this phase. It is clear, however, that this does not occur in sufficient quantities during this rapid polymerisation.

Despite these observations, control was shown for the polymerisation of *t*BA using the multi-functional **4AE** initiator (Section 3.3.2). In these reactions the agglomeration of the polymer layer was observed to be a much slower process; possibly a consequence of increased steric hindrance when combining the bulky *t*BA monomer with an initiator which has four initiation sites in close proximity. This should decrease the rate of polymerisation, and the longer the time before the polymer layer agglomerates, the more easily $CuBr_2$ can access the active chain ends. Furthermore, there is more opportunity for $CuBr_2$ to diffuse into the polymer phase. The **I4** macro-initiator is more hindered toward *t*BA than MBP and less hindered than **4AE** due to the presence of the PEG chain separating two sets of initiation sites. No control was observed during the kinetic investigations targeting a molecular weight of 3 x 10^4 g mol^{-1}. When the target molecular weight was increased (3 x 10^5 g mol^{-1}) there was a linear increase in conversion with time and analysis of M_n and $Đ$ suggested a much more controlled polymerisation. This may also be a consequence of the rate of agglomeration of the polymer layer. The ratio of $[M]_0$:$[I]_0$ is reduced when targeting a higher molecular weight and consequently, fewer polymer chains are initiated at the start of the reaction. Though the individual chains quickly become insoluble, the lower concentration of polymer chains may reduce the chance of the polymer layer agglomerating. Furthermore, the apparent improvement when using the less active **I4-S** macro-initiator may be explained by the lower rate at which radicals are formed, again possibly reducing the rate of polymer layer agglomeration. However, the subsequent kinetic investigation demonstrated the same lack of control for **I4-S** as for **I4-T,** therefore, further study is necessary before a definite conclusion regarding the relative effectiveness of each initiator can be made.

3.3.5 Large scale polymerisation reactions

To synthesise sufficient polymer sample for drag reduction testing, the scale of the *t*BA polymerisation reactions was increased. For comparison of the drag reducing properties of linear and star polymers, reactions were conducted using MBP and **I2-S** as well as **4AE** and **I4-S** initiators (Table 5). In order to avoid auto-acceleration, a major risk when increasing the scale of exothermic polymerisations, efficient mixing and heat transfer was necessary. Due to the high viscosity of the heterogeneous reaction mixture it was not possible to sample the reaction to monitor monomer conversion. The reaction was stopped after the polymer layer had completely solidified.

Table 5: Large scale polymerisation of *t*BA in DMSO using MBP, **4AE**, **I4-S** and **I2-S** initiators.

Entry	Sample Code	M_n(Target) x 10^{-5} (g mol^{-1})	Time (h)	Conv. (%)	M_n(Theor) x 10^{-5} (g mol^{-1})	M_n (SEC) x 10^{-5} (g mol^{-1})	*Đ*	IV (dL g^{-1})
i	**MBP-A**	3.0	44	91	2.73	7.69	2.29	3.70
ii	**4AE-A**	3.0	70	69	2.08	3.09	1.30	0.76
iii	**4AE-B**	10.0	24	85	8.50	8.61	1.61	2.16
iv	**I4-S-A**	10.0	24	22	2.20	13.9	1.51	3.25
v	**I4-S-B**	10.0	24	36	3.60	7.84	1.93	2.55
vi	**I4-S-C**	10.0	24	43	4.30	7.47	2.28	2.98
vii	**I4-S-D**	10.0	24	26	2.60	18.8	1.43	3.88
viii	**I2-S-A**	10.0	24	70	7.00	14.9	2.10	5.01

NB: Quantity of Monomer **i-ii** = 35.5 g, **iii**-**viii** = 10 g; Entry: **v** Cu(0) length = 29.5 cm; **vi** Cu(0) length = 14.75 cm; **vii** Monomer conc = 64 wt%. SEC traces for samples are shown in Appendix B, Fig. 3**i**-**viii**.

The first scale-up polymerisation used the MBP initiator (**MBP-A**, Table 5, Entry **i**) and targeted a molecular weight of 3 x 10^5 g mol^{-1} ($[M]_0$:$[I]_0$ = 2360:1) on a 35 g scale. M_n(SEC) was found to be much higher than the theoretical, however, a narrower molecular weight distribution (*Đ* = 2.29) was observed in comparison to those observed for lower molecular weights (Section 3.3.4).

The reaction was repeated using the **4AE** initiator (**4AE-A,** Table 5, Entry **ii**). A higher conversion (69 %) was reached compared to the small scale kinetic reactions (≈ 50%, Section 3.3.2). Following purification, M_n and *Đ* were determined using SEC. As observed for the small scale reactions, M_n(SEC) was significantly higher than M_n(Theor) however the narrow dispersity (*Đ* = 1.30) suggested control was maintained over the polymerisation. By increasing $[M]_0$:$[I]_0$ to 7804, a molecular weight of 1 x 10^6 g mol^{-1} was targeted using **4AE** (**4AE-B**, Table 5, Entry **iii**). ^{1}H NMR spectroscopy demonstrated that a conversion of 85 % was reached after 24 h despite the extremely high viscosity of the system, due to more effective mixing on a slightly smaller scale (10 g monomer). For this reaction M_n(SEC) closely matched M_n(Theor) and the dispersity was relatively narrow (*Đ* = 1.61) considering the high molecular weight.

The same reaction was repeated using the **I4-S** macro-initiator (**I4-S-A**, Table 5, Entry **iv**). Analysis using ^{1}H NMR spectroscopy demonstrated a very low conversion (22%) for this reaction after 24 h. The viscosity of the polymer layer was observed to increase much more quickly than for reaction with **4AE** and entirely surrounded the Cu(0) wire/stirrer, preventing further initiation. The molecular weight measured (M_n(SEC) = 14 x 10^5 g mol^{-1}) was extremely high relative to theoretical (2.2 x 10^5 g mol^{-1}) due to the low I_{eff} in this system. This leads to the production of HMW chains early in the reaction and may contribute to the increased viscosity. Despite this the dispersity measured remains low ($Đ$ = 1.49).

In order to improve the conversion of this large scale polymerisation**,** subsequent reactions were conducted under slightly altered reaction conditions (**I4-S-B/C/D**, Table 5, Entry **iv**-**vii**). The length of copper wire catalyst was first reduced by half (29.5 cm, **I4-S-B**, Table 5, Entry **iv**). By decreasing the catalyst surface area, the rate of the reaction should decrease and the effect on conversion could be examined. The reduction of the wire length from 59 cm to 29.5 cm provided a small increase in conversion (36%). The length of the wire was therefore halved again (14.75 cm, **I4-S-C,** Table 5, Entry **v**) and a conversion of 43% was attained. As the catalyst length was decreased M_n(SEC) became much closer to theoretical value (Table 5, Entry **iv-vi**), however, there was also a simultaneous increase in $Đ$; 1.49, 1.93, 2.28 for **I4-S-A**, **I4-S-B and I4-S-C**, respectively. This suggests that whilst the rate of propagation is reduced, the rate of initiation is decreased by a greater amount.

P*t*BA becomes insoluble in DMSO during the polymerisation of *t*BA, however, it has been shown that the polymer layer is swollen by the solvent. An increase in the solvent content may increase the swelling of the polymer layer, decreasing viscosity and increasing monomer conversion. The polymerisation of *t*BA was carried out using the same catalyst length as for **I4-S-A** (Table 5, Entry **iii**) but with a higher quantity of solvent (5.7 ml, **I4-S-D,** Table 5, Entry **vi**). In conventional free radical polymerisation this should decrease the propagation rate by reducing the concentration of radicals in solution; however, the situation is complicated for some Cu-mediated polymerisations, as polar solvents can act to increase the rate of propagation. Analysis of the reaction mixture using ^{1}H NMR spectroscopy demonstrated that the monomer conversion was not significantly increased using higher solvent levels. Moreover, the M_n(SEC) was increased by a large amount. This suggests that higher DMSO levels may increase the transport of monomer to the growing chain ends, therefore, increasing the propagation rate of the polymerisation. In addition to these adjusted reaction conditions, mechanical stirring was also used to introduce an efficient mixing and heat transfer and attempt to improve the conversions of these reactions. Unfortunately, these attempts were

unsuccessful as it was difficult to exclude oxygen from the reaction mixture during the polymerisation reaction.

The **I2-S** macro-initiator was also used for the large scale polymerisation of *t*BA (**I2-S-A**, Table 5, Entry **viii**) targeting a molecular weight of 1 x 10^6 g mol^{-1} was targeted on a 10 g scale. This allows further comparison of linear and star PEG containing drag reducing agents. A monomer conversion of 70 % was reached for the polymerisation though SEC analysis demonstrated a product with high dispersity ($Đ$ = 2.1) and M_n(SEC) much higher value than theoretically calculated.

The intrinsic viscosity (*IV*) of the polymer samples was measured as part of triple detection SEC analysis. It is known that increasingly branched polymers have lower intrinsic viscosities when compared with linear analogues of equivalent molecular weight. Comparison of the IV of the polymers synthesised using the MBP or **I2-S** initiators, to those synthesised using **4AE** or **I4-S** should give some information regarding the relative levels of branching in each of the systems. The plot of *IV* against log(M_w) for the linear (red) and star (blue) polymers is shown in Figure. 26. Whilst there are only a small number of linear samples for comparison, a higher IV is observed when compared with polymers synthesised using a multi-functional initiator (**4AE** or **I4-S**). The difference approaches zero at higher molecular weight, this is expected as the length of the polymer arms increases and the properties of the star polymer more closely match those of the linear analogue. This clearly indicates the difference in the amount of branching between the linear polymers and those synthesised here using multi-functional initiators. A more effective way to study the topology of these HMW polymer samples may be to use atomic force microscopy (AFM) which will be a part of further studies.

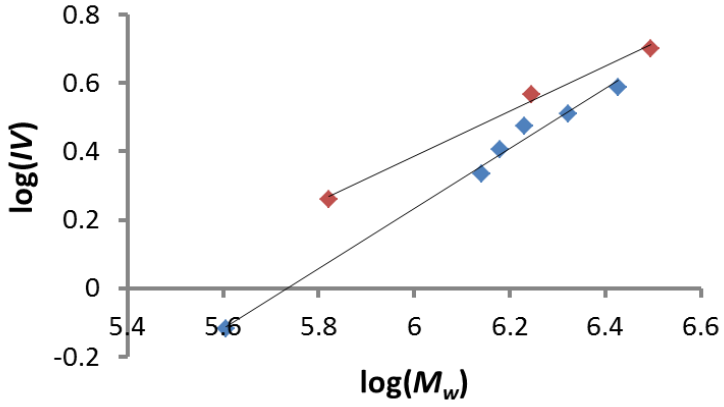

3

Figure 26: Plot of Log(*IV*) vs Log(M_w) for large scale reactions. Linear polymers (synthesised using MBP and **I2-S**) shown in red. Branched polymers (synthesis using **4AE** and **I2-S**) shown in blue.

Low copper content is very important for commercial use due to its toxicity. In order to determine the level of contamination in these systems, a sample of **4AE-B** was hydrolysed using trifluoroacetic acid (TFA) and analysed by ICP-OES. A value of 0.36 mg l^{-1} (0.36 ppm) was measured. This level is low when compared with other Cu-mediated polymerisation techniques such as ATRP (Cu = 50 – 10 000 ppm). It should be noted that measurement taken following isolation of the polymer by precipitation.

3.4 Conclusion

This chapter described the application of Cu(0)/TREN for the synthesis of star polymers in DMSO, using *t*BA as a protected AA monomer. P*t*BA becomes insoluble in DMSO at ≈ 3 x 10^3 g mol^{-1} and through the formation of this biphasic system, low copper contamination can be achieved in the product. The frequency of star-star coupling can also be reduced, allowing higher conversions to be targeted in the synthesis of star polymers. Kinetic evaluation of the polymerisation reaction using the **4AE** initiator (M_n(Target) = 3 x 10^4 g mol^{-1}) demonstrated good control. When the target MW was increased to 3 x 10^5 g mol^{-1}, conversion was restricted to 50 % due to the high viscosity of the mixture.

The PEG based macro-initiators, **I4-S** and **I4-T**, were used for the homogeneous polymerisation of MA (M_n(Target) = 1.4 x 10^4 g mol^{-1}), both demonstrating good control ($Đ$ < 1.50). When these macro-initiators were used to polymerise *t*BA (M_n(Target) = 3.4 x 10^4 g mol^{-1}), control ($Đ$ = 1.30) was observed for **I4-S** whilst a high dispersity was measured using **I4-T** ($Đ$ = 4.38). The **I4-S** initiator was chosen for use in subsequent polymerisations in the chapter; however, kinetic investigation of the same reaction later demonstrated uncontrolled polymerisation. By increasing the target molecular weight to 3 x 10^5 g mol^{-1}, a linear increase of M_n(SEC) with conversion was attained, as well a low dispersity throughout the reaction.

MBP was used in a model system to investigate the effect of changing reaction conditions on the control of the polymerisation of *t*BA in DMSO. Control could not be achieved over the reaction even following the addition of $CuBr_2$ and analysis of the SEC chromatograms suggested two radical polymerisation mechanisms were occurring simultaneously. It was concluded that rapid formation of the insoluble polymer layer prevented access of $CuBr_2$ to the active chain ends. Control when using **4AE** was attributed to the increased steric hindrance experienced in this system.

The scale of the polymerisation of *t*BA (10/35 g monomer) and the target MW (3 x10^5/1 x 10^6 g mol^{-1}) were increased to generate HMW samples for drag reduction testing. Whilst good

control was observed with **4AE**, the equivalent polymerisation using **I4-S** was restricted to low conversion due to the high viscosity of the mixture. The conversion was increased following the reduction of catalyst surface area, however, a simultaneous increase in dispersity was observed. Linear polymers were also synthesised on a large scale using MBP and **I2-S** initiators. The lower IV of the **4AE** and **I4-S** star polymers when compared with the linear analogues demonstrated the higher levels of branching for these polymers. When the copper contamination of the **4AE-B** polymer was measured using ICP-OES, a very low value, less than 1 ppm was obtained.

3.5 References

1. Lligadas, G.; Percec, V. *J. Polym. Sci., Part A: Polym. Chem.* **2008,** 46, , 3174-3181.
2. Waldron, C.; Zhang, Q.; Li, Z.; Nikolaou, V.; Nurumbetov, G.; Godfrey, J.; McHale, R.; Yilmaz, G.; Randev, R. K.; Girault, M.; McEwan, K.; Haddleton, D. M.; Droesbeke, M.; Haddleton, A. J.; Wilson, P.; Simula, A.; Collins, J.; Lloyd, D. J.; Burns, J. A.; Summers, C.; Houben, C.; Anastasaki, A.; Li, M.; Becer, C. R.; Kiviaho, J. K.; Risangud, N. *Polym. Chem.* **2014,** 5, 57-61.
3. Perrier, S.; Haddleton, D. M. *Eur. Polym. J.* **2004,** 40, 2277-2286.
4. Davis, K. A.; Matyjaszewski, K. *Macromolecules* **2000,** 33, 4039-4047.
5. Zhang, X.; Xia, J. H.; Matyjaszewski, K. *Macromolecules* **2000,** 33, 2340-2345.
6. Gao, H. F.; Matyjaszewski, K. *Macromolecules* **2006,** 39, 3154-3160.
7. Mendrek, B.; Trzebicka, B. *Eur. Polym. J.* **2009,** 45, 1979-1993.
8. Mendrek, B.; Trzebicka, B.; Walach, W.; Dworak, A. *Eur. Polym. J.* **2010,** 46, 2341-2351.
9. Jing, R. K.; Wang, G. W.; Zhang, Y. N.; Huang, J. L. *Macromolecules* **2011,** 44, 805-810.
10. Li, P. P.; Li, Z. Y.; Huang, J. L. *Macromolecules* **2007,** 40, 491-498.
11. Hou, S. J.; Chaikof, E. L.; Taton, D.; Gnanou, Y. *Macromolecules* **2003,** 36, 3874-3881.
12. Nguyen, N. H.; Rosen, B. M.; Lligadas, G.; Percec, V. *Macromolecules* **2009,** 42, 2379-2386.
13. Waldron, C.; Anastasaki, A.; McHale, R.; Wilson, P.; Li, Z.; Smith, T.; Haddleton, D. M. *Polym. Chem.* **2014,** 5, 892-898.
14. Zhang, Y.; Wang, Y.; Peng, C.-h.; Zhong, M.; Zhu, W.; Konkolewicz, D.; Matyjaszewski, K. *Macromolecules* **2012,** 45, 78-86.
15. Percec, V.; Guliashvili, T.; Ladislaw, J. S.; Wistrand, A.; Stjerndahl, A.; Sienkowska, M. J.; Monteiro, M. J.; Sahoo, S. *J. Am. Chem.Soc.* **2006,** 128, 14156-14165.
16. Ren, W. Y.; Jiang, L.; Wang, W. W.; Dan, Y. *J. Polym. Sci., Part A: Polym. Chem.* **2010,** 48, 2793-2797.

17. Samanta, S. R.; Percec, V. *Polym. Chem.* **2014,** 5, 169-174.

18. Boyer, C.; Atme, A.; Waldron, C.; Anastasaki, A.; Wilson, P.; Zetterlund, P. B.; Haddleton, D.; Whittaker, M. R. *Polym. Chem.* **2013,** 4, 106-112.

19. Nguyen, N. H.; Levere, M. E.; Percec, V. *J. Polym. Sci., Part A: Polym. Chem.* **2012,** 50, 35-46.

20. Johnson, I., Synthesis and Characterisation of Polymeric Materials via RAFT Polymerisation. Durham University, Durham, 2013.

21. Podzimek, S., *Light Scatterting, Size Exclusion Chromatography and Asymmetric Flow Field Flow Fractionation: Powerful Tools for the Characterisation of Polymers, Proteins and Nanoparticles*. Wiley: New Jersey, 2011.

Chapter 4

Aqueous Cu(0)-mediated Polymerisation

4.1. Introduction

Water is a cheap and abundant solvent for chemical reactions. Furthermore, it has a low environmental impact and is less hazardous than most organic solvents. These benefits make aqueous polymerisation reactions highly appealing for commercial processes. Controlled radical polymerisation in aqueous systems allows the direct synthesis of interesting hydrophilic or ionic polymers. Rates of Cu mediated polymerisations are accelerated in polar solvents, particularly in water where disproportionation is heavily favoured, due to the relative stability of Cu(II) over Cu(I).[1,2] This shifts the activation/deactivation equilibrium and increases the concentration of radicals in the system (Scheme 1). The propagation rate increases as well as the frequency of termination reactions.[3]

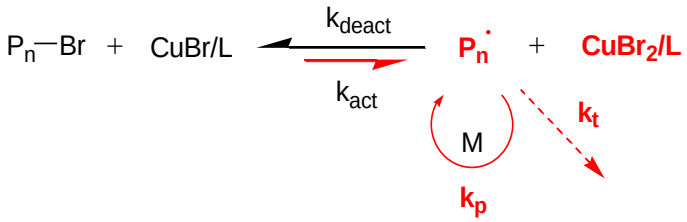

Scheme 1: Activation/Deactivation equilibrium shifted towards active species (red) in polar solvents increasing concentration of radicals in solution.

A series of side reactions can also contribute to the loss of active species, further increasing termination.[4] Substitution of N-ligands by H_2O, or hydrolysis of the C-Hal bond in the initiator or dormant chain, reduces the efficiency of the catalyst and initiator, respectively. Moreover, $CuBr_2$ can be hydrolysed to $CuBr^+$ which is no longer able to deactivate active polymer chains, therefore, reducing the concentration of deactivator in solution. For these reasons much focus on aqueous controlled radical polymerisations has centred on NMP and RAFT techniques.[5,6]

The tolerance of ATRP to protic solvents was first demonstrated by Matyjaszewski through the polymerisation of oligo(ethylene glycol)methacrylate (OEGMA) in a 50 % v/v aqueous solution (CuCl/Bipy/90 °C).[7] The reaction reached 87 % conversion and a narrow dispersity ($Đ$ = 1.34, M_n = 1.47 x 10^4 g mol^{-1}) demonstrated control over the polymerisation. Moreover, Haddleton and Perrier used a stable CuBr/*N*-(n-alkyl)-2-pyridylmethamine catalyst to polymerise mono-methoxy poly(ethylene glycol) methacrylate (OMe-PEGMA) to low degree of polymerisation (DP = 10) in water. High conversion (97 %) and good control (Đ = 1.13) was achieved through addition of $CuBr_2$ ($CuBr/CuBr_2$ = 0.1).[8]

The increased stability of a C-Cl bond over C-Br results in lower reaction rates when using a CuCl catalyst for ATRP. The C-Cl bond is also less prone to hydrolysis and, therefore, is often

considered more effective for an aqueous reactions;[9] CuCl systems have been used successfully for the controlled polymerisation OEGMA[10] and also acrylamide.[11] When using acrylamide based monomers, coordination of the side chain to the copper metal centre can occur, displacing ligand or halide ions from the catalyst.[12,13]

This can also happen during the polymerisation of acidic monomers such as acrylic acid (AA) or methacrylic acid (MAA).[14] Furthermore, when using these acidic monomers, protonation of the N-ligand is possible, poisoning the catalyst.[15] Acidic monomers are therefore polymerised, either in organic solvents using protecting groups, or in their salt form. Armes was the first to use aqueous ATRP (CuBr/bpy/90 °C) to directly react an acidic monomer in salt form. Sodium methacrylate was polymerised at a pH of 8-9 to ensure full deprotonation of the MAA monomer.[16] The reaction reached 80 % conversion with M_n (2.9 x 10^3 g mol^{-1}) very close to theoretical (2.8 x 10^3 g mol^{-1}). A narrow dispersity ($Đ$ = 1.27) demonstrated good control. Despite improved polymerisation of this ionic monomer, interaction between the carboxylate group and the metal centre may still occur.[17,18] Lui et al. used $CuCl_2$/Bipy in combination with a radical initiator (AIBN) to polymerise sodium acrylate (NaA) without an alkyl halide initiator.[19] The high dispersity ($Đ$ = 2.37) of the final product demonstrated that the reaction was not controlled, however, the polymer could be used for chain extension reactions with N-isopropylacrylamide (NIPAM), suggesting high chain end retention. Several other ionic monomers have been polymerised in aqueous Cu mediated systems including; 4-styrene sulfonate,[20,21] sodium 4-vinyl benzoate[22] and amino acid based monomers.[18] Using surface mediated processes, Kilbey II et al. polymerised both itaconic acid and methacrylic acid in their salt form and Ober et al. synthesised PAA *via* direct polymerisation of NaA.[17,23]

Cu(0)-mediated polymerisations in aqueous systems have also been reported. Percec et al. used a Cu(0)-wire catalyst and Me_6-TREN ligand to polymerise mono-methoxy oligo(ethylene glycol) methacrylate (OMe-OEGMA) in water, observing good control (M_n = 1.72 x 10^4 g mol^{-1}, $Đ$ = 1.26) even without the addition of $CuBr_2$.[24] Albersson et al. used a hemi-cellulose based initiator for the Cu(0)-mediated polymerisation of a zwitterionic carboxybetaine monomer.[25] Whilst the reaction demonstrated linear kinetics, molecular weight data was not recorded. More recently, Haddleton et al. used the pre-disproportionation of CuBr/Me_6-TREN in water for the highly controlled polymerisation of acrylamide/acrylate monomers with very high conversions (N,N-Dimethylacrylamide (DMA), conv = 99 %, M_n = 9.7 x 10^3 g mol^{-1}, $Đ$ = 1.18; hydroxyethyl acrylate (HEA), conv = 97 %, M_n = 8.8 x 10^3 g mol^{-1}, $Đ$ = 1.07).[26] The fast reaction rates were attributed to nascent Cu(0) formed in the reaction mixture; the good control due to the high levels of $CuBr_2$ in the early stages of the reaction.

4.2. Experimental

4.2.1. Materials

Tris(2-aminoethyl)amine (TREN, 97%), acrylic acid, (99 %, stabilised with 180-200 ppm monomethyl ether hydroquinone) and sodium hydroxide (pellets, ≥ 97 %) were purchased from Sigma Aldrich and used without further purification. CuBr (99.999 %) was purchased from Sigma Aldrich and first purified by sequential washing with acetic acid and ethanol; the pure CuBr was separated by filtration and dried under reduced pressure at room temperature. Glacial acetic acid (≥ 99.7 %) and ethanol and acetonitrile analytical grade solvents were purchased from Fisher Scientific and used as received. Bare copper wire (24 standard wire gauge, diameter = 0.559 mm) was purchased from Fisher Scientific and used without further purification. D_2O for NMR analysis was purchased from Goss Scientific.

4.2.1.1. Preparation of sodium acrylate monomer

AA was purified by distillation under reduced pressure at 40°C to remove diacrylate impurities. The pure AA was transferred to a flask fitted with magnetic stirrer bar and dissolved in distilled water to give a solution with a concentration of 50 wt%. The solution was cooled to 0°C before a NaOH (aq) solution (57 wt%) was added dropwise to the AA with continuous cooling. Measurement of pH, using pH paper, confirmed neutralisation.It is important to note that this purification also removes mono-methyl ether hydroquinone (MEHQ) radical stabiliser. In the previous chapter, for the polymerisation of methyl acrylate (MA) and *tert*-butyl acrylate (*t*BA), the monomer was used without removal of radical inhibitor.

4.2.2. Instrumentation

$^{1}H/^{13}C$ NMR spectra were recorded using a Bruker Avance-400 spectrometer operating at 400 MHz. D_2O was used as solvent and the spectra were referenced to the solvent trace (4.79 ppm).

PNaA samples were sent to Ashland Inc, Bradford for molecular weight analysis using aqueous size exclusion chromatography (SEC). Specifically an Agilent 1200 system was used with a Tosoh TSK gel G3000/G6000 column set (flow rate of 0.5 ml min^{-1} at 40 °C). The samples were prepared at concentrations of 0.15 % and 0.2 M NaCl (aq) with 0.05 M dibasic potassium phosphate was used as the mobile phase. Single detection using a refractive index (RI) detector was used to determine the molecular weights by conventional calibration using linear poly(sodium acrylate) (PNaA) standards.

4.2.3. Calculation of monomer to polymer conversion using ^{1}H NMR spectroscopy

Monomer conversion was calculated using ^{1}H NMR spectroscopy via the method described in Chapter 3, Section. 3.2.3. For polymerisation of NaA, the resonance due to a monomer vinyl proton (Fig. 1, 5.65 ppm, 1H) was compared with the resonance representing the single methine proton on the polymer back bone (Fig. 1, 2.08 ppm, 1H).

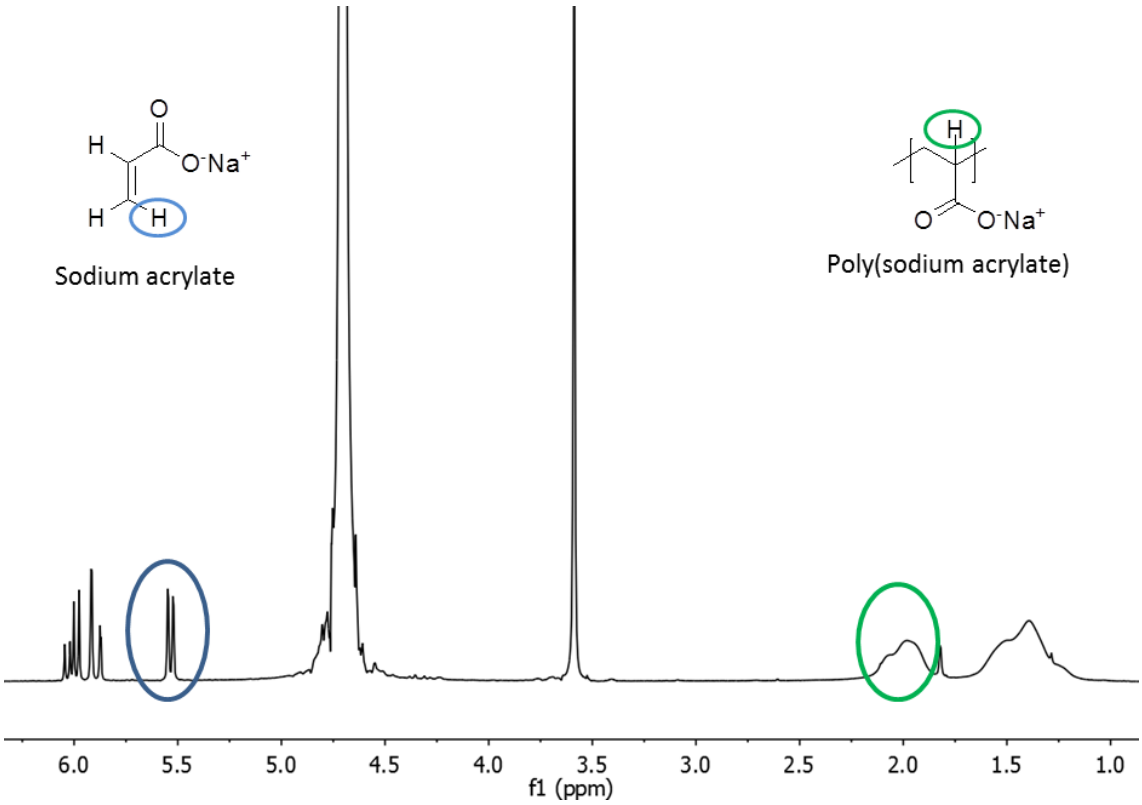

Figure 1: Proton environments compared for conversion analysis using ^{1}H NMR spectroscopy for the polymerisation of NaA.

4.2.4. Typical polymerisation procedure

Initiator (**I4-S/I4-T**) was weighed in to a vial and a solution of TREN in H_2O (0.50 ml) and NaA (aq) (1.92 ml, 5.78 mol dm^{-3}, 11.1 mmol) was added to dissolve. The polymerisation mixture was transferred to a Schlenk tube and the pH was tested using pH paper. Cu(0) wire (8.4 cm, 0.14 g) was wrapped around a magnetic stirrer flea and was held above the reaction mixture using a magnet attached to the wall outside of the flask. The flask was sealed using a rubber septum and the mixture was deoxygenated. The flask was placed in an oil bath at 25 ^{o}C and the polymerisation reaction was initiated by submerging the Cu(0)/stirrer. The mixture was stirred for an appropriate time (15-1440 min) and the polymerisation was terminated by removing the Cu(0)/stirrer from the reaction mixture. Further H_2O was added to dissolve the resulting product and the conversion was determined by ^{1}H NMR spectroscopy in D_2O. The solution was

added to MeCN to precipitate the product which was isolated and dried in an oven under reduced pressure at 40°C.

4.2.5. Control Reactions

4.2.5.1. With Cu(0)/TREN but without initiator

Typical procedure (Section 4.2.4) was used with the following modifications:

NaA (aq) (1.92 ml, 11.1 mmol) was added to a Schlenk tube fitted with Cu(0)/stirrer followed by a solution of TREN (2.0 mg, 0.012 mmol) dissolved in water (0.50 ml). The mixture was degassed using 5 freeze pump-thaw-cycles and the flask was backfilled with nitrogen. The reaction was initiated by submerging Cu(0)/stirrer and stirred for 16 h. The monomer conversion was determined using ^{1}H NMR spectroscopy to be 22-26 %.

4.2.5.2. With initiator but without Cu(0)/TREN

Typical procedure (Section 4.2.4) was used with the following modifications:

I4-T (0.14 g, 0.032 mmol) was weighed in to a vial and H_20 (0.50 ml) was added to dissolve. NaA (aq) (1.92 ml, 11.1 mmol) was added to prepare the final polymerisation mixture which was transferred to a Schlenk tube containing a magnetic stirrer flea. The mixture was degassed using 4 freeze pump-thaw-cycles and the flask was backfilled with nitrogen. The reaction was stirred for 16 h and the monomer conversion was determined using ^{1}H NMR spectroscopy to be 0 %.

4.2.6. Polymerisation of sodium acrylate using Poly(ethylene glycol)-di-2,2-Bis(methyl 2-bromopropionate) propionate, I4-S, initiator

Typical procedure (Section 4.2.4) was used with the following modifications:

I4-S (0.14 g, 0.032 mmol) was weighed in to a vial and a solution of TREN (1.9 mg, 0.013 mmol) in H_20 (0.50 ml) was added to dissolve. NaA (aq) (1.92 ml, 11.1 mmol) was added to the solution and the mixture was transferred to a Schlenk tube fitted with Cu(0)/stirrer. The mixture was degassed using 4 freeze pump-thaw-cycles and the flask was backfilled with nitrogen. The reaction initiated by submerging the Cu(0)/stirrer and stirred for 16 h. Conversion 17 %.

4.2.7. Polymerisation of sodium acrylate Poly(ethylene glycol)-di-(2,2-Bis(methyl 2-bromoisobutyrate) propionate, I4-T, initiator

Typical procedure (Section 4.2.4) was used with the following modifications:

I4-T (0.14 g, 0.032 mmol) was weighed in to a vial and a solution of TREN (1.9 mg, 0.013 mmol) in H_20 (0.50 ml) was added to dissolve. NaA (aq) (1.92 ml, 11.1 mmol) was added to the solution and the mixture was transferred to a Schlenk tube fitted with Cu(0)/stirrer. The mixture was degassed using 4 freeze pump-thaw-cycles and the flask was backfilled with nitrogen. The reaction initiated by submerging the Cu(0)/stirrer and stirred for 16 h. Conversion 81 %.

4.2.7.1. Optimisation of pH

Procedure in Section 4.2.7 was repeated two more times with pH was adjusted to 6 and 11 by altering the quantity of NaOH added to the reaction mixture.

4.2.7.2. Optimisation of monomer concentration

Procedure in Section 4.2.7 was repeated at reduced monomer concentration by increasing the total amount of H_2O (3, 5, 10 ml) in the reaction mixture.

4.2.7.3. Kinetic Investigation

4.2.7.3.1. $[M]_0:[I]_0 = 348$

A stock solution of the polymerisation reaction mixture was prepared by mixing: NaA (aq) (13.44 ml, 77.7 mmol), **I4-T** (0.98 g, 0.224 mmol) and TREN (13.3 mg, 0.091 mmol) in H_2O (3.50 ml). Aliquots of the stock solution (2.42 ml) –containing: NaA (aq) (1.92 ml, 11.1 mmol), **I4-T** (0.14 g, 0.032 mmol), TREN (1.9 mg, 0.013 mmol), H_2O (0.50 ml) - were transferred to 7 Schlenk tubes. Cu(0) wire (8.4 cm, 0.14 g) was wrapped around a magnetic stirrer flea and held above each mixture. The pH of each solution was monitored using pH paper and the flask was sealed using a rubber septum. The solutions were deoxygenated by bubbling with nitrogen for 30 min and the Schlenk tube was placed in an oil bath at 25°C. The reactions were initiated by submerging the Cu(0)/stirrer and terminated after the required time by removing the Cu(0)/stirrer from the mixture. Conversion was determined using ^{1}H NMR spectroscopy.

4.2.7.3.2. $[M]_0:[I]_0 = 3480$

A stock solution of the polymerisation reaction mixture was prepared by mixing: NaA (aq) (9.60 ml, 55.5 mmol), **I4-T** (68.3 mg, 0.016 mmol) and TREN (2.3 mg, 0.016 mmol) in H_2O (2.50 ml).

Aliquots of the stock solution (2.42 ml) - containing: NaA (aq) (1.92 ml, 11.1 mmol), **I4-T** (13.7 mg, 0.003 mmol) TREN (0.5 mg, 0.003 mmol), H_2O (0.50 ml) - were transferred to 5 Schlenk tubes. Cu(0) wire (8.4 cm, 0.14 g) was wrapped around a magnetic stirrer flea and held above each mixture. The pH of each solution was monitored using pH paper and the flask was sealed using a rubber septum. The solutions were deoxygenated by bubbling with nitrogen for 30 min and the Schlenk tube was placed in an oil bath at 25 °C. The reactions were initiated by submerging the Cu(0)/stirrer and terminated after the required time by removing the Cu(0)/stirrer from the mixture. Conversion was determined using ^{1}H NMR spectroscopy.

4.2.7.4. By pre-disproportionation of CuBr

TREN (12.0 mg, 0.082 mmol) was weighed in to a vial and H_2O (1.00 ml) was added to give a stock solution with a concentration of 0.082 mol dm^{-3}. An aliquot (0.60 ml) of TREN/H_2O (TREN = 0.050 mmol) was diluted in further H_2O (1.90 ml) and the solution was transferred to a Schlenk tube fitted with a stirrer bar. The flask was sealed with a rubber septum and deoxygenated by bubbling with nitrogen for 15 min. CuBr (14.7 mg, 0.103 mmol) was transferred to the Schlenk tube under a flow of nitrogen. Within 1 min the solution turned a deep blue colour and a red-brown precipitate was observed at the bottom of the flask. The flask was lowered into an oil bath at 25°C and the solution degassed for a further 15 min.

Simultaneously, **I4-T** (0.14 g, 11.1 mmol) was weighed into a second Schlenk tube and NaA (aq) (1.92 ml, 11.1 mmol) and H_2O (3.00 ml) were added. The flask was sealed using a rubber septum and the solution was deoxygenated by bubbling with nitrogen for 15 min. The solution was transferred to the first Schlenk tube (containing Cu(0)/$CuBr_2$/TREN) *via* a cannula to initiate the reaction. The mixture was stirred at 25 °C for 1 h before a sample was taken under a flow of nitrogen and monomer conversion was analysed using ^{1}H NMR spectroscopy. The reaction was stirred for a further 15 h before a second sample was removed for conversion analysis. The reaction terminated by filtering the mixture through an alumina plug and a sample was taken for molecular weight analysis using aqueous SEC. Conversion 72 %; SEC: M_n = 2.98 x 10^4 g mol^{-1}, M_w = 5.30 x 10^4 g mol^{-1}, $Đ$ = 1.78.

4.3. Results and Discussion

4.3.1. Control Reactions

Control reactions were conducted to determine the participation of the macro-initiator and Cu(0)/TREN during the aqueous polymerisation of NaA. The first control reaction was carried out using **I4-T** macro-initiator in the absence of Cu(0)/TREN. Analysis of the reaction mixture

using ^{1}H NMR spectroscopy (Fig. 2a) demonstrates resonances due to vinyl groups of unreacted monomer at 5.65, 6.02 and 6.12 ppm. Moreover, resonances due to **I4-T** are present at 1.40, 1.93 and 3.70 ppm. However, characteristic resonances due to the PNaA polymer backbone (between 1.0-2.5 ppm) are absent demonstrating no monomer conversion.

The second control reaction was performed in the presence of Cu(0)/TREN but without a macro-initiator. In this case polymerisation was observed by the formation of a heterogeneous mixture and accumulation of a small amount of solid PNaA on the wall of the Schlenk tube. This necessitated the addition of further H_2O to homogenise the mixture before analysis of monomer conversion. Analysis of the reaction mixture using ^{1}H NMR spectroscopy (Fig. 2b) again demonstrates intense resonances due to vinyl protons of unreacted monomer. However, the spectrum also contains polymer backbone resonances at 1.0-2.5 ppm due to the formation of PNaA in the mixture (Fig. 2b). This result was unexpected, however, the control reaction was repeated and a consistent monomer conversion up to 26% was observed.

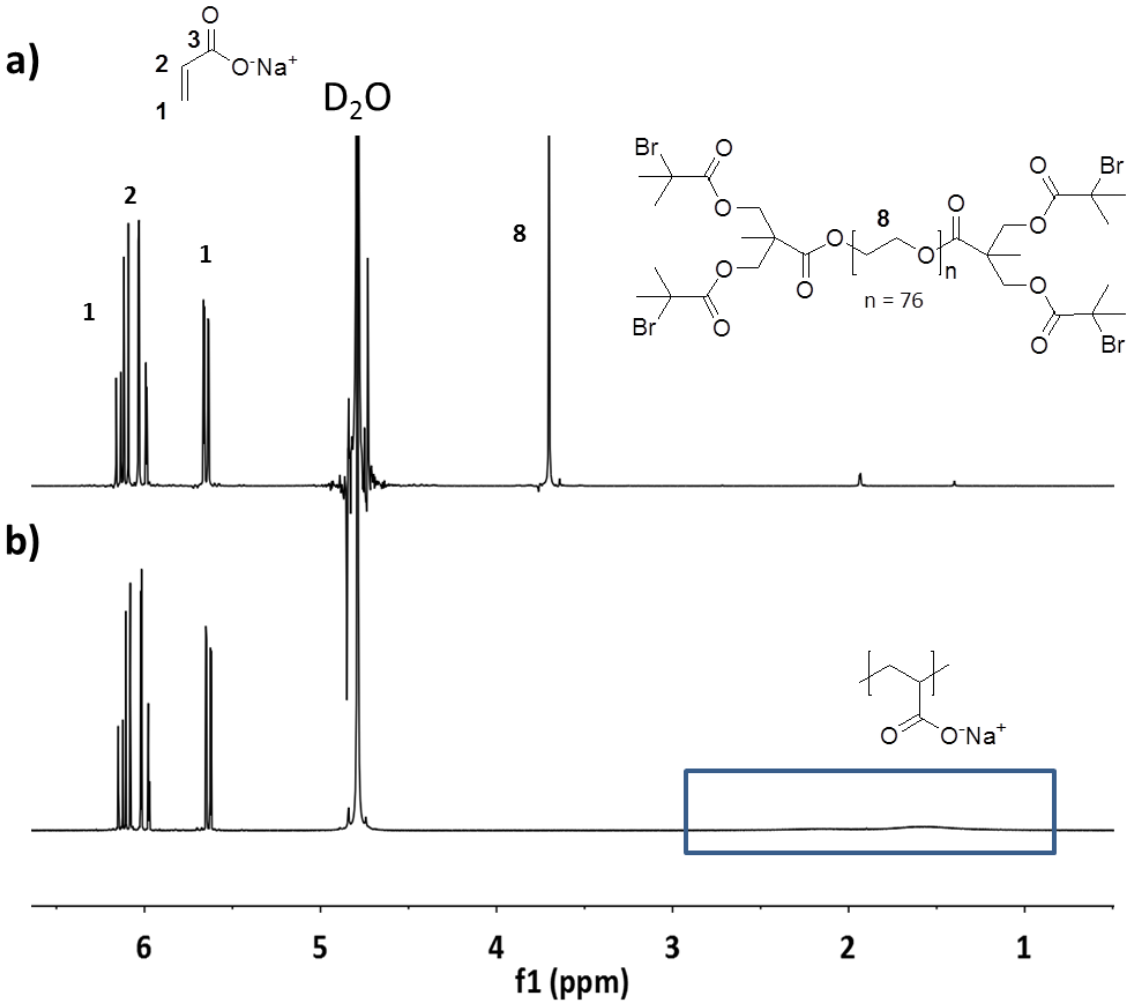

Figure 2: 400 MHz-^{1}H NMR spectra of control reaction; **a)** with macro-initiator but without Cu(0)/TREN; **b)** with Cu(0)/TREN but without initiator.

From this it was concluded that, following the removal of radical inhibitor and thorough de-oxygenation, free radical polymerisation occurred in this system due to the presence of Cu(0)/TREN. Whilst Cu(0)/TREN can generate radicals in the reaction mixture, active chains cannot be reversibly deactivated without the bromine containing initiator (**I4-T**). For this reason, and without the continuous generation of radicals as in traditional free radical polymerisation, the polymer chains quickly terminate and monomer conversion is low.

Armes et al. also observed monomer conversion (44 %) for the polymerisation of sodium methacrylate, in the presence of CuBr/Bipy but without the mono-methoxy PEG based macro-initiator.[16] In the absence of both CuBr/Bipy and initiator, a conversion of 80 % was attained, demonstrating a contribution from the catalyst system. When the catalyst and initiator were both included, good control (M_n = 2.9 x 10^3 g mol^{-1}, $Đ$ = 1.27) was observed over the polymerisation reaction.[16] Armes attributed the monomer conversion to free radical polymerisation initiated due to the high temperature (90 °C) of the reaction. The reactions described here use a low temperature (25 °C) which makes thermal auto-initiation much less likely. The primary amine TREN ligand, however, is known to undergo Michael addition reactions (Scheme 2), which may initiate polymerisation of activated olefins as a side reaction. The exothermic nature of this Michael addition could also promote thermal auto-initiation. The likelihood of a Michael addition reaction decreases upon formation of $CuBr_2$ in the solution due to the stability of the $CuBr_2$/TREN complex [27]

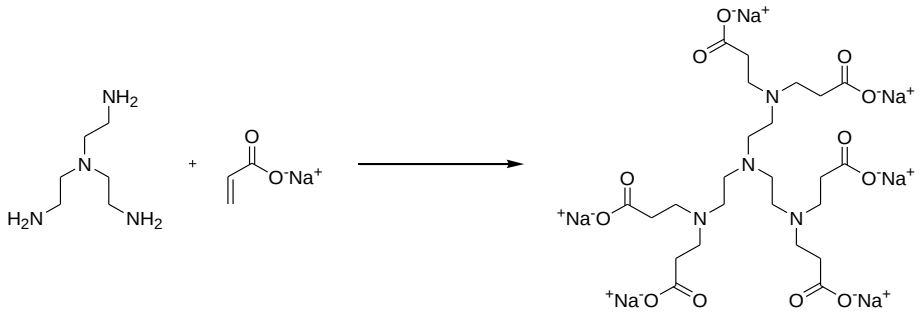

Scheme 2: Possible Michael addition of TREN to sodium acrylate.

4.3.2. Polymerisation of sodium acrylate using PEG based macro-initiator, I4

The polymerisation of NaA using a PEG -based macro-initiator (**I4)** and a Cu(0)/TREN catalyst system is described in Scheme 3.

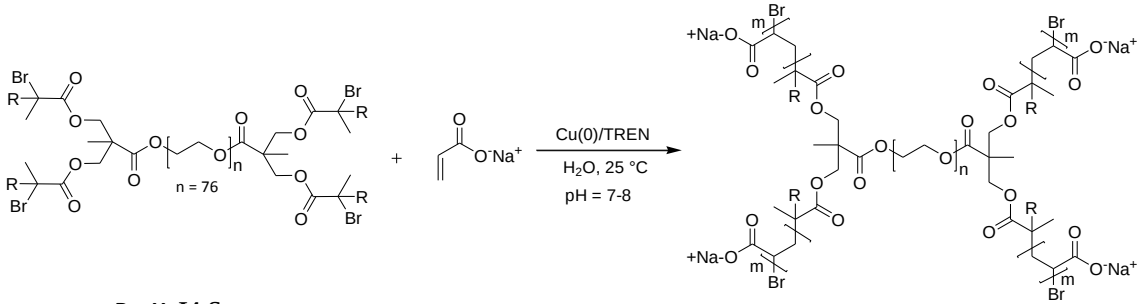

Scheme 3: Polymerisation of NaA using **I4-S** or **I4-T** macro-initiator.

In order to compare the suitability of each macro-initiator (**I4-S**/**I4-T**), parallel reactions were conducted using a ratio of $[M]_0:[I]_0:[L]_0$ = 348:1:0.4 to target a molecular weight of approximately 3.7 x 10^4 g mol^{-1}. A slightly basic pH (7-8) was used for the reaction, as well as a monomer concentration of 40 wt% to avoid a saturated solution and allow full dissolution of the macro-initiator. Monomer conversion was measured for each reaction in order to compare the efficacy of the respective macro-initiators. The reaction using **I4-S** demonstrated a very low conversion of just 17 % after 16 h. This conversion is consistent with the auto-initiated polymerisation observed for the initiator free control reaction (Section 4.3.1). Furthermore, the reaction mixture was heterogeneous, comprising a non-viscous liquid and PNaA collected on the wall of the flask in a similar manner to the control reaction. This suggests that the **I4-S** macro-initiator may not have any influence over the polymerisation reaction. In contrast, **I4-T** allowed a monomer conversion of 80 % over the same reaction time. The solution became very viscous, though some solid was observed around the walls of the flask. The reaction mixture was green/blue in colour suggesting the presence of $CuBr_2$ in the solution. This monomer conversion is significantly higher than obtained in any of the control reactions (Section 4.3.1) and is taken as clear evidence for the contribution of the macro-initiator in this polymerisation reaction. The increased conversion when compared with the **I4-T** initiator is thought to be due to the presence of the more reactive tertiary bromine group. Following these preliminary results the **I4-T** macro-initiator was used for all remaining polymerisation reactions in this chapter.

The ^{1}H NMR spectrum of the pure **I4-T-PNaA** product is shown in Figure 3. Characteristic resonances of the PNaA backbone are observed at 1.49 ppm (**a**) and 2.08 ppm (**b**). Furthermore, peaks corresponding to resonances of the **I4-T** core PEG chain (**8**) can be observed at 3.68 ppm.

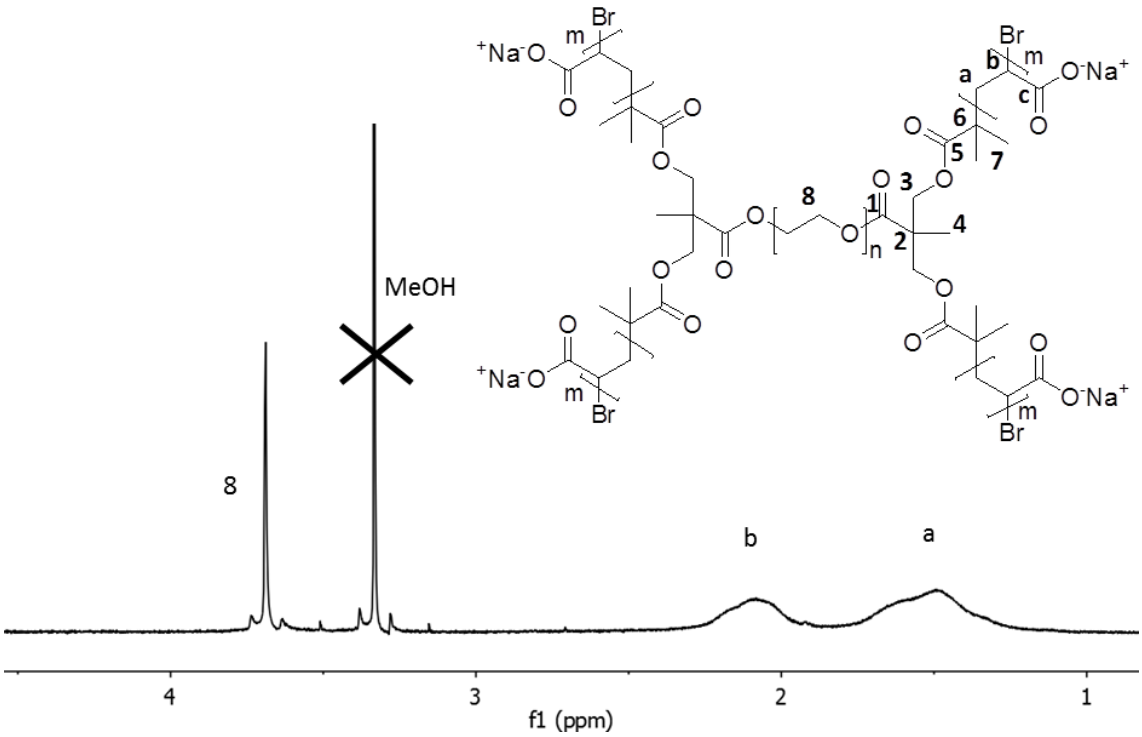

Figure 3: 400 MHz-^{1}H NMR spectrum of **I4-T-PNaA**.

By comparing the integral of the resonance due to the PEG core (**8**) with that of the resonance, **a**, for the polymer backbone, an estimate can be made of molecular weight for the PEG-PNaA co-polymer. A value was calculated after three re-precipitations and the change in molecular weight with each precipitation is plotted in Figure 4. There is a large initial increase as unreacted macro-initiator is removed from the solution; however, the value remains constant after further precipitations. The final value estimated is around 2.3 x 10^5 g mol^{-1} which is much higher than the target molecular weight (3.7 x 10^4 g mol^{-1}). The reasons for this will be discussed further in Section 4.3.2.1. The quantity of unreacted **I4-T** removed suggests a very low I_{eff} for the macro-initiator in this reaction. Despite this, the continued presence of the PEG resonance confirms the incorporation of **I4-T** in to the final polymer.

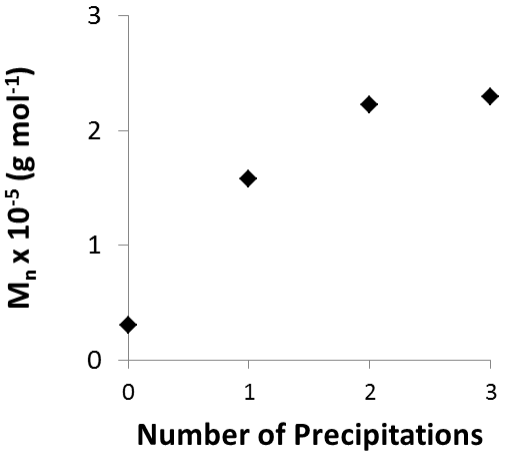

Figure 4: Plot of M_n after successive re-precipitations for PNaA initiated using **I4-T** initiator, estimated from analysis of ^{1}H NMR spectra.

The use of correct solution pH is important for the aqueous polymerisation of acidic monomers. The mixture must be slightly basic to avoid protonation of the TREN ligand; however, if the pH becomes too basic there is an increased risk of C-Br bond hydrolysis in the initiator or dormant polymer chains. Furthermore, as degree of ionisation increases, the rate of propagation decreases significantly due to the repulsion between the monomer and the active polymer chain end.[28] A pH of 7-8 was therefore used in the initial reactions described. To confirm that this was optimum, the polymerisation of NaA using **I4-T** ($[M]_0$:$[I]_0$:$[L]_0$ = 348:1:0.4) was repeated with solution pH adjusted to be slightly acidic (pH 6) and slightly more basic (pH 11). In each reaction negligible levels of monomer conversion were observed following analysis of the reaction mixture using ^{1}H NMR spectroscopy (pH 6 = 0 %, pH 11 = 3 %). This greatly contrasted the conversion of 80 % at a pH of 7-8.

After observing a heterogeneous reaction mixture during the preliminary experiments, the impact of decreasing monomer concentration was also investigated. The initial **I4-T** reaction (monomer conc = 40 wt%) was repeated (pH 7-8, $[M]_0$:$[I]_0$:$[L]_0$ = 348:1:0.4) at a reduced monomer concentration of 25 wt%, 17 wt% and 9 wt%. Unfortunately, during each of these reactions the formation of a gel layer was observed surrounding the Cu(0) catalyst surface (Fig. 5). This prevented access of the polymerisation mixture to the catalyst and therefore prevented the initiation of further polymerisation. The low monomer conversion confirms the necessity of the Cu(0) catalyst for the production of radicals in the system. Similar observations were made by Percec et al. when using a Cu(0) wire catalyst for the polymerisation of HEA in water.[29] Percec attributed this gelation to the high polarity of the solvent which promotes non-polar interactions between the polymer backbone and Cu(0).[29] The growing polymer chains

accumulate at the Cu(0)-surface and the high local radical concentration leads to extensive coupling reactions and the formation of insoluble gel. In the system described here, when the monomer concentration is decreased the migration of the non-polar polymer backbones to the copper wire is promoted. The gelation could also be accelerated due to an increased propagation rate as the the polarity of the reaction mixture increases.

Figure 5: Gel layer surrounding Cu(0) wire.

4.3.2.1. Kinetic Investigation

The kinetics of the aqueous polymerisation of NaA using **I4-T** ($[M]_0$:$[I]_0$:$[L]_0$ = 348:1:0.4) were then studied using parallel runs over a range of reaction times. The evolution of conversion (blue axis) and $\ln[M]_0/[M]_t$ (red axis) are plotted against time in Figure 6a. The plot of conversion demonstrates two clear regions. In the first region, there is a fast increase of monomer conversion from 0 to ≈20 % within the first 15 min of the reaction. The second region (15 – 1440 min), demonstrates a much slower linear increase, reaching a monomer conversion of over 70 % after 960 min. The kinetic plot (Fig. 6a, red) also shows a rapid increase early in the reaction, however, at longer reaction times a linear trend suggests a relatively consistent concentration of radicals. Molecular weight analysis demonstrates a relatively low dispersity ($Đ$ = 1.45) at low conversion (Fig 6b, red axis). Despite this, the high M_n(SEC) measured, which then decreases continuously throughout the reaction (Fig. 6b, blue axis), is typical for a free radical polymerisation mechanism where the rate of propagation is faster than initiation. Furthermore, there is a simultaneous increase in dispersity ($Đ$ = 1.45 → 2.05), which also suggests an uncontrolled polymerisation reaction. SEC traces for the reactions are shown in Appendix C, Fig. 1.

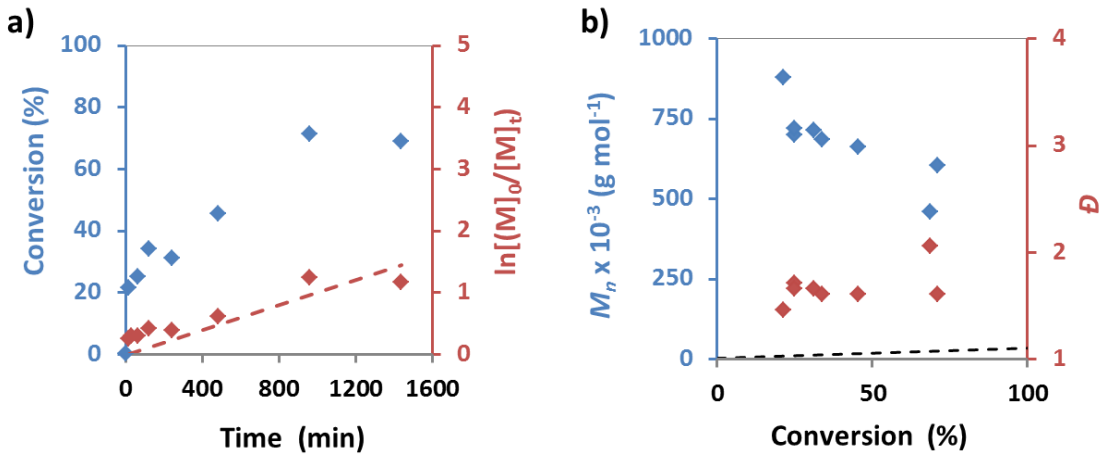

Figure 6: Polymerisation of NaA using **I4-T**, $[M]_0:[I]_0:[L]_0$ =348:1:0.4**; a)** Conversion (blue) and $\ln([M]_0/[M]_t)$ (red) vs time; **b)** M_n(SEC) (blue) and $Đ$ (red) vs conversion, (M_n(Theor) shown by black line)

It is likely that this lack of control is a consequence of the low concentration of $CuBr_2$ early in the reaction. This is particularly a problem for aqueous Cu(0)-mediated polymerisations where propagation rate is accelerated and $CuBr_2$ deactivator is unstable toward halide displacement. Polymer chains initiated at low conversion will propagate in an uncontrolled manner until sufficient $CuBr_2$ is generated. The problem may be further exacerbated by the low I_{eff} often observed macro-initiators, which decreases the rate at which $CuBr_2$ can be formed, either through disproportionation or the persistent radical effect (PRE). It may also be important to consider the reduced rate of termination during the synthesis of ionic polymers due to repulsion of like charges between polymer chains.[28] This will also decrease the rate of $CuBr_2$ formation through the PRE and may contribute to the propagation of chains to high molecular weights before they are terminated.

In conventional free radical polymerisation techniques, a high monomer conversion is achieved using a radical source, for example, a radical initiator with a suitably long half-life. Radicals are formed throughout the reaction and new polymer chains are initiated. In the reaction described here, the only radical source is *via* homolytic cleavage of a C-Br bond in the **I4-T** macro-initiator using Cu(0) as a catalyst. Although the reaction is not controlled, it could be viewed as an analogous technique to ceric ammonium nitrate (CAN) redox polymerisation. CAN polymerisation reactions can be initiated by the formation of an alkyl radical adjacent to a hydroxyl group on an organic initiator molecule; with simultaneous reduction of a cerium metal centre (Scheme 4a).[30] Free-radical polymerisation then propagates from this point forming a polymer branch on the original initiator (Scheme 4b). In this instance the Cu(0)/TREN catalyst generates radicals on the **I4-T** macro-initiator and from these sites free-radical

polymerisation can occur. As discussed in Chapter 1, the ceric ammonium nitrate (CAN) redox polymerisation method has been used in order to synthesise branched polymer drag reducing agents with enhanced mechanical stability.[31,32]

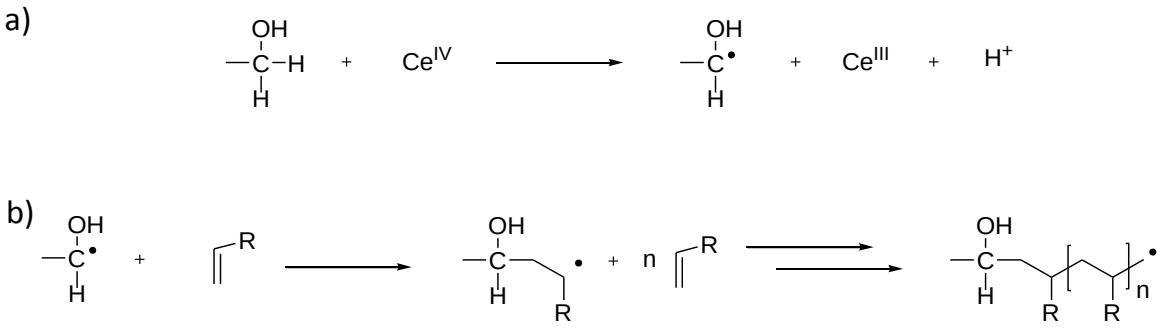

Scheme 4: Redox polymerisation initiated using Ceric Ammonium Nitrite (CAN); **a)** Production of radical on initator molecule with reduction of Ce^{IV}; **b)** Free radical polymerisation of vinyl monomer.

Similarly uncontrolled Cu(0)-mediated polymerisation was observed by Matyjaszewski et al. during the polymerisation of MA in DMSO using ARGET ATRP. A linear plot of $\ln[M]_0/[M]_t$ vs time was shown, however, the same decrease in molecular weight and increase in dispersity with conversion was also observed.[27] In this example, control was achieved over the polymerisation following the addition of $CuBr_2$. When studying the polymerisation of MMA and MA in toluene using a Cu(0) catalyst, Perrier et al. also observed uncontrolled polymerisation early in the reaction.[33] In this non-polar solvent, Cu(I) disproportionation cannot occur and CuBr generated by activation further initiates a second polymer chain. $CuBr_2$ deactivator is generated only after the formation of a second radical. Uncontrolled polymerisation therefore occurs at low conversions (< 10 %) with control gained when the deactivator concentration begins to increase. At low monomer conversion M_n was much higher than theoretical; however, as control was gained over the reaction, M_n decreased to closely match the theoretical value and $Đ$ began to decrease with conversion. [33]

The reactions described in this work do not suggest control was gained over the polymerisation of NaA. This may be a consequence of the instability of $CuBr_2$ in aqueous solutions. The investigations of Matyjaszewski and Perrier both suggest that higher levels of $CuBr_2$ should allow better control over the polymerisation of NaA using **I4-T**. This is investigated further in Section 4.3.2.2.

By adjusting $[M]_0:[I]_0:[L]_0$ to 3480:1:1, a higher molecular weight (3 x 10^5 g mol^{-1}) was targeted and the reaction kinetics were studied. The evolution of conversion (blue) and $\ln[M]_0/[M]_t$

(red) with time are plotted in Fig. 7a. In contrast to the lower molecular weight reactions, there is a single linear region in the plot of conversion vs time. This may be due to the lower initiator concentration, which will therefore generate fewer radicals in the system at the beginning of the reaction. A monomer conversion of 80 % was reached within 1000 min, before the reaction terminated due to the high viscosity of the reaction mixture. The kinetic plot is also linear suggesting a constant concentration of radicals in the system. In Figure 7b, M_n(SEC) (blue) and $Đ$ (red) are plotted against monomer conversion and similar results to the lower molecular weight reactions are observed. M_n(SEC) is significantly higher than theoretically expected at low conversion (Fig. 7b, black line), again decreasing with conversion. In this case the dispersity remains between 1.5-1.6 for all samples. SEC traces for the reactions are shown in Appendix C, Fig. 2.

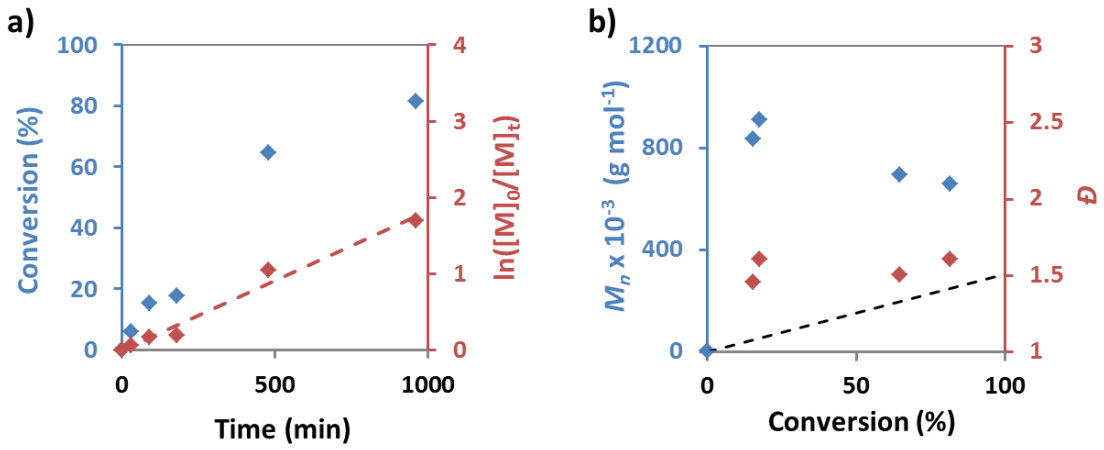

Figure 7: Polymerisation of NaA using **I4-T**, $[M]_0:[I]_0:[L]_0$ =3480:1:1**; a)** Conversion (blue) and $\ln([M]_0/[M]_t)$ (red) vs time; **b)** M_n(SEC) (blue) and $Đ$ (red) vs conversion, (M_n(Theor) by shown black line) (NB: For conversion of 6.1 % insufficient polymer recovered for SEC analysis).

The product of the reaction over 960 min (Fig. 7a, conv. = 82 %) was re-precipitated and analysis of the ^{1}H NMR spectrum was used to make an estimate of polymer molecular weight as described in Section 4.3.2. The change in molecular weight with consecutive precipitations is plotted in Figure 8 showing a consistent value following two re-precipitations. This demonstrates a consistent quantity of PEG in the solution which was again considered as evidence of incorporation of the **I4-T** macro-initiator in to the final product. The final value of ≈ 5.00 x 10^5 g mol^{-1} is in reasonable agreement with that obtained using single detection SEC (6.56 x 10^5 g mol^{-1}). The discrepancy observed may be a consequence of the low intensity of the PEG resonance in the ^{1}H NMR spectrum which decreases the precision of the estimate of

molecular weight using this method. Moreover, the use of aqueous SEC with just a single mode of detection may reduce the accuracy of these measurements of molecular weight.

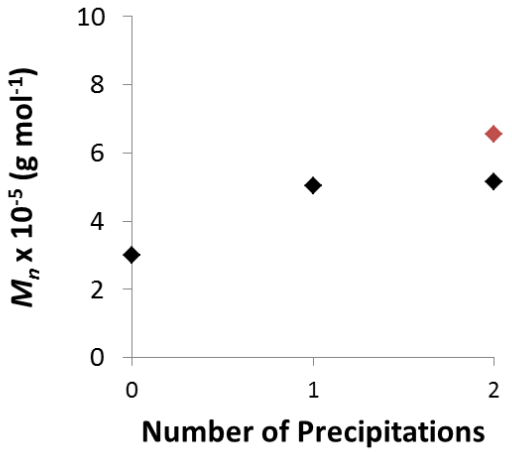

Figure 8: Plot of M_n after successive re-precipitations for PNaA initiated using **I4-T** initiator, estimated from analysis of ^{1}H NMR spectra. M_n(SEC) shown in red.

4.3.2.2. Polymerisation of sodium acrylate by pre-disproportionation of CuBr

From the evidence described above, the Cu(0)/TREN catalyst system is not sufficient to control the aqueous polymerisation of NaA using the **I4-T** macro-initiator. It was proposed that this is due to the low concentration of $CuBr_2$ deactivator in the reaction mixture. A high $CuBr_2$ concentration allows immediate deactivation of the rapidly propagating chains and compensates for the instability of $CuBr_2$ in water. By decreasing the rate of propagation relative to initiation, control over the polymerisation reaction should be attained.

In several recent publications, Haddleton et al. demonstrated highly controlled aqueous polymerisation by exploiting the disproportionation of CuBr in water in the presence of N-ligands (e.g. Me_6-TREN).[13,26,34] By allowing complete disproportionation of CuBr to Cu(0) and $CuBr_2$ prior to the addition of monomer and initiator, the polymerisation reaction begins in the presence of a very high concentration of deactivator ($CuBr_2$). In order to investigate the effect of this on the polymerisation of NaA using **I4-T**, the pre-disproportionation method was applied to this system (Scheme 5-6).[26] To allow comparison with Cu(0) wire catalyst, a $[M]_0$:$[I]_0$:$[L]_0$ of 348:1:0.4 was used for this reaction with a monomer concentration of 14 wt%, following the literature procedure.[26] As the technique forms nascent Cu(0) activator in situ, gelation on the copper surface is no longer a concern for this reaction allowing the lower monomer concentration to be used.

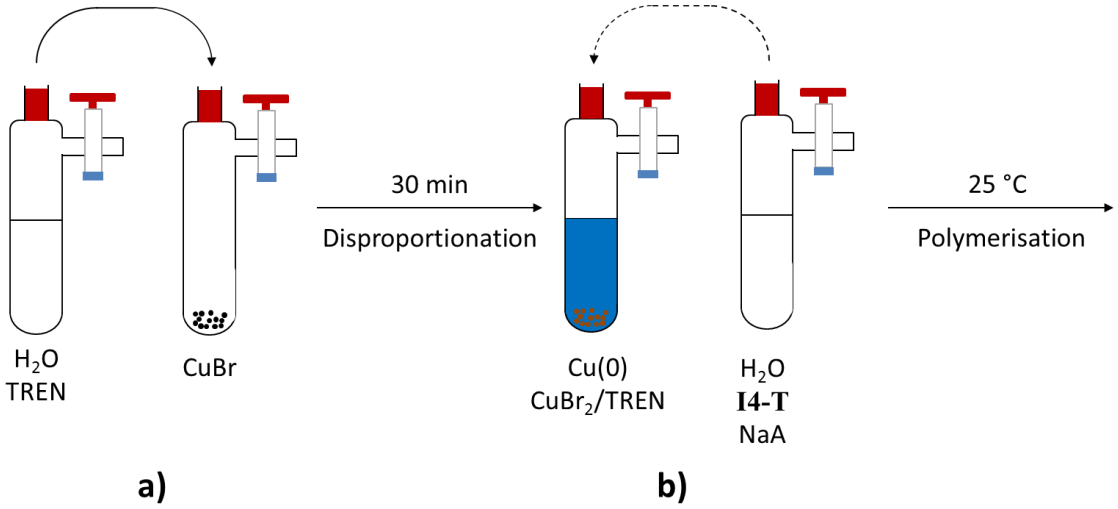

Scheme 5: Schematic diagram demonstrating order of addition for polymerisation; **a)** Pre-disproportionation of CuBr in H_2O with TREN; **b)** Initiation of polymerisation reaction by addition of monomer and initiator.[26]

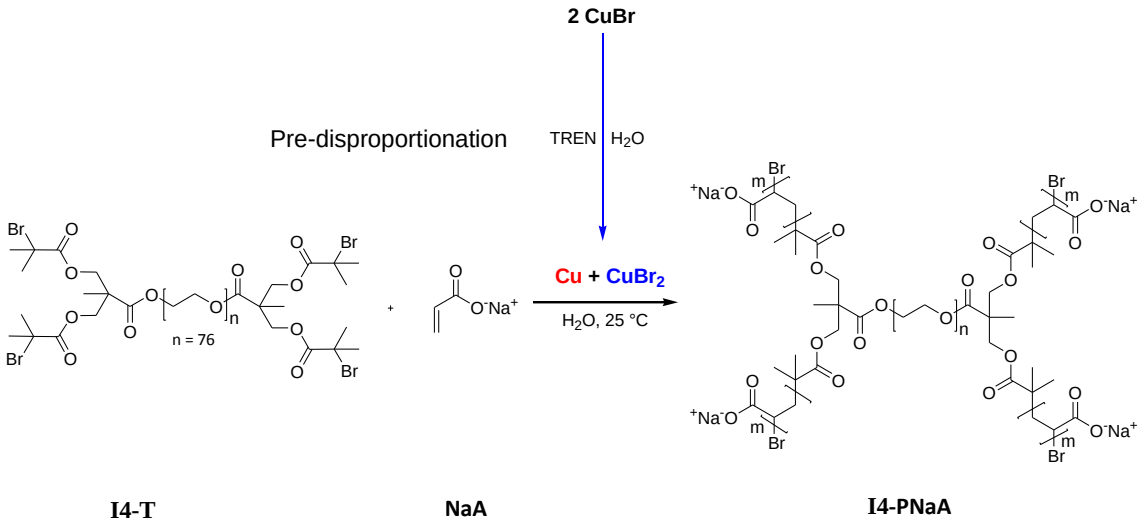

Scheme 6: Polymerisation of NaA using **I4-T** initiator and catalyst generated in situ by the pre-disproportionation of CuBr.

After the addition of CuBr to water in the presence of TREN (Scheme 5a), almost immediate disproportionation was observed by the blue colour of the reaction mixture and the formation of a red-brown Cu(0) suspension (Fig. 9). The reaction was then initiated by the addition of monomer, initiator and further solvent *via* cannula (Scheme 5b). The reaction was sampled after 60 min which showed a monomer conversion of 70 %, demonstrating a much higher rate of polymerisation when compared to the Cu(0) wire polymerisation reactions. This may be due to the high activity of nascent Cu(0) formed through disproportionation, or rate acceleration due to the higher water content. After 960 min, the reaction was again sampled and no further

increase in conversion was observed. Analysis using SEC demonstrated that M_n (2.98 x 10^4 g mol^{-1}) very closely matched the theoretical value (2.99 x 10^4 g mol^{-1}), particularly when compared with the copper wire reactions discussed above. The dispersity of the polymer was high (Đ = 1.78), possibly a consequence of slow initiation using **I4-T**, however, it seems clear that uncontrolled polymerisation is avoided early in the reaction due to the presence of $CuBr_2$ salts.

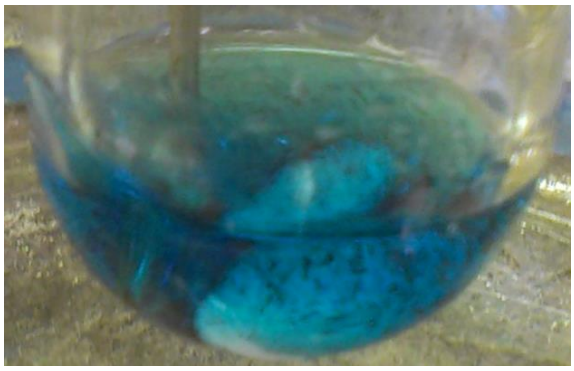

Figure 9: Pre-disproportionation of CuBr observed by the blue colour of the reaction mixture ($CuBr_2$) and red-brown suspension of Cu(0)

The SEC traces in Figure 10 compare the product of the pre-disproportionation reaction (green) with the trace of PNaA synthesised using the Cu(0) wire system in Section 4.3.2.1 (Fig. 6a, 960 min, conv. = 71 %) shown in blue. There is a clear difference in retention volume for the two chromatograms. The product synthesised using the pre-disproportionation method is symmetrical without a tail at low retention volume. This suggests that, using this method, high molecular weight polymer is not generated *via* an uncontrolled polymerisation mechanism.

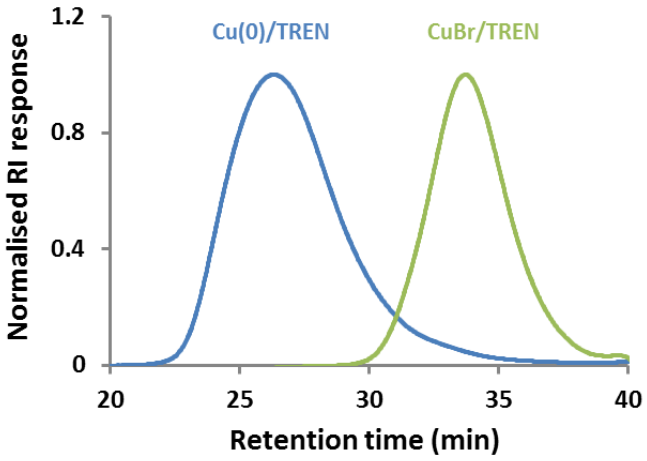

Figure 10: Plot of normalised RI response vs retention time comparing polymers synthesised using Cu(0) wire method (blue) and pre-disproportionation of CuBr method (green).

4.4. Conclusion

In this chapter, the **I4-S** and **I4-T** macro-initiators were compared for the aqueous polymerisation of NaA using a Cu(0)/TREN catalyst system. Due to its higher activity, **I4-T** was shown to be most suitable for this reaction allowing much higher conversions (80 % in 16 h). Kinetic investigations demonstrated that control over the polymerisation of NaA using Cu(0)/TREN was difficult due to insufficient $CuBr_2$ in the reaction mixture. Despite this, the reactions proceeded to high conversion and generated high molecular weight polymers. Furthermore, analysis using ^{1}H NMR spectroscopy confirmed the incorporation of the macro-initiator in to the final product. A method exploiting the pre-disproportionation of CuBr to generate a high $CuBr_2$ deactivator concentration in-situ, prior to the addition of monomer and initiator, was investigated. This method prevented the uncontrolled polymerisation at low conversion and there was a close agreement between measured and theoretical molecular weight.

4.5. References

1. Rosen, B. M.; Percec, V. *Chem. Rev.* **2009,** 109, 5069-5119.

2. Konkolewicz, D.; Krys, P.; Góis, J. R.; Mendonça, P. V.; Zhong, M.; Wang, Y.; Gennaro, A.; Isse, A. A.; Fantin, M.; Matyjaszewski, K. *Macromolecules* **2014,** 47, 560-570.

3. Rosen, B. M.; Jiang, X.; Wilson, C. J.; Nguyen, N. H.; Monteiro, M. J.; Percec, V. *J. Polym. Sci., Part A: Polym. Chem.* **2009,** 47, 5606-5628.

4. Tsarevsky, N. V.; Matyjaszewski, K. *Chem. Rev.* **2007,** 107, 2270-2299.

5. Xu, X.; Smith, A. E.; Kirkland, S. E.; McCormick, C. L. *Macromolecules* **2008,** 41, 8429-8435.

6. Smith, A. E.; Xu, X.; Kirkland-York, S. E.; Savin, D. A.; McCormick, C. L. *Macromolecules* **2010,** 43, 1210-1217.

7. Coca, S.; Jasieczek, C. B.; Beers, K. L.; Matyjaszewski, K. *J. Polym. Sci., Part A: Polym. Chem.* **1998,** 36, 1417-1424.

8. Perrier, S.; Armes, S. P.; Wang, X. S.; Malet, F.; Haddleton, D. M. *J. Polym. Sci., Part A: Polym. Chem.* **2001,** 39, 1696-1707.

9. Tsarevsky, N. V.; Braunecker, W. A.; Brooks, S. J.; Matyjaszewski, K. *Macromolecules* **2006,** 39, 6817-6824.

10. Wang, X. S.; Armes, S. P. *Macromolecules* **2000,** 33, 6640-6647.

11. Jewrajka, S. K.; Mandal, B. M. *Macromolecules* **2002,** 36, 311-317.

12. Wever, D. A. Z.; Raffa, P.; Picchioni, F.; Broekhuis, A. A. *Macromolecules* **2012,** 45, 4040-4045.

13. Alsubaie, F.; Anastasaki, A.; Wilson, P.; Haddleton, D. M. *Polym.Chem.* **2015**, Advance Article.

14. Patten, T. E.; Matyjaszewski, K. *Adv. Mater.* **1998,** 10, 901-915.

15. Bergenudd, H.; Coullerez, G.; Jonsson, M.; Malmström, E. *Macromolecules* **2009,** 42, 3302-3308.

16. Ashford, E. J.; Naldi, V.; O'Dell, R.; Billingham, N. C.; Armes, S. P. *Chem. Comm.* **1999**, 1285-1286.

17. Sankhe, A. Y.; Husson, S. M.; Kilbey, S. M. *Macromolecules* **2006,** 39, 1376-1383.

18. Chung, I.-D.; Britt, P.; Xie, D.; Harth, E.; Mays, J. *Chem. Comm.* **2005**, 1046-1048.

19. Jin, S.; Liu, M.; Chen, S.; Gao, C. *Macromol. Chem. and Phys.* **2008,** 209, 410-416.

20. Choi, C. K.; Kim, Y. B. *Polym. Bull.* **2003,** 49, 433-439.

21. Iddon, P. D.; Robinson, K. L.; Armes, S. P. *Polymer* **2004,** 45, 759-768.

22. Wang, X. S.; Jackson, R. A.; Armes, S. P. *Macromolecules* **2000,** 33, 255-257.

23. Dong, R.; Krishnan, S.; Baird, B. A.; Lindau, M.; Ober, C. K. *Biomacromolecules* **2007,** 8, 3082-3092.

24. Nguyen, N. H.; Kulis, J.; Sun, H. J.; Jia, Z. F.; Van Beusekom, B.; Levere, M. E.; Wilson, D. A.; Monteiro, M. J.; Percec, V. *Polym. Chem.***2013,** 4, 144-155.

25. Edlund, U.; Rodriguez-Emmenegger, C.; Brynda, E.; Albersson, A.-C. *Polym. Chem.* **2012,** 3, 2920-2927.

26. Zhang, Q.; Wilson, P.; Li, Z.; McHale, R.; Godfrey, J.; Anastasaki, A.; Waldron, C.; Haddleton, D. M. *J. Am. Chem.Soc.* **2013,** 135, 7355-7363.

27. Kwak, Y.; Magenau, A. J. D.; Matyjaszewski, K. *Macromolecules* **2011,** 44, 811-819.

28. Barth, J.; Buback, M. *Macromolecules* **2012,** 45, 4152-4157.

29. Leng, X.; Nguyen, N. H.; van Beusekom, B.; Wilson, D. A.; Percec, V. *Polym. Chem.***2013,** 4, 2995-3004.

30. Matsuda, T.; Saito, N.; Sugawara, T. *Macromolecules* **1996,** 29, 7446-7451.

31. Singh, R. P.; Singh, J.; Kumar, A.; Deshmukh, S. R., The Effect of Grafted and Ungrafted Guargum on Turbulent Flow of Water and on Hydraulic. In *The Influence of Polymer Additives on Velocity and Temperature*, Gampert, B., Ed. Springer-Verlag: Berlin, 1985; p131.

32. Kim, O. K.; Little, R. C.; Patterson.R.l.; Ting, R. Y. *Nature* **1974,** 250, 408-410.

33. West, A. G.; Hornby, B.; Tom, J.; Ladmiral, V.; Harrisson, S.; Perrier, S. *Macromolecules* **2011,** 44, 8034-8041.

34. Anastasaki, A.; Haddleton, A. J.; Zhang, Q.; Simula, A.; Droesbeke, M.; Wilson, P.; Haddleton, D. M. *Macromol. Rapid Comm.* **2014,** 35, 965-970.

Chapter 5

Measurement of Drag Reducing Properties and Resistance to Mechanical Degradation

5.1. Introduction

Drag reducing efficiency (DRE) and resistance to mechanical degradation are crucial features of any drag reducing polymer. A range of methods have been used to test these properties, and to probe the mechanism of drag reduction. DRE is often expressed in terms of %drag reduction (*%DR*), which is a measure of the difference in flow rate of a drag reducing polymer solution when compared with that of a pure solvent. Capillary rheometers (Fig. 1a) were particularly important in early studies. In these systems a polymer solution is forced through a narrow tube generating turbulent flow (high Reynolds number, *Re*).[1,2] Drag reduction is calculated by comparing the pressure drop between two points along the tube, with that shown by pure solvent. A capillary rheometer (diameter, d = 0.1575 cm) was used by Little et al. to compare the DRE of poly(ethylene oxide) (PEO) and polyacrylamide (PAM) and examine the relative mechanical stability of a branched PAM analogue.[2] During the first pass, a percentage drag reduction (*%DR*) of 60 – 70 % was measured for all polymers (*Re* 5.7 – 9.0 x 10^3, conc. = 100 ppm). The polymer solutions were passed through the rheometer 13 further times and a decrease in *%DR* (PEO = 10-25 %, PAM = 10-20 %, branched PAM = 5-10 %) was observed due to mechanical degradation of the polymer chain. These results clearly indicated an increased mechanical stability for a branched polymer.[2]

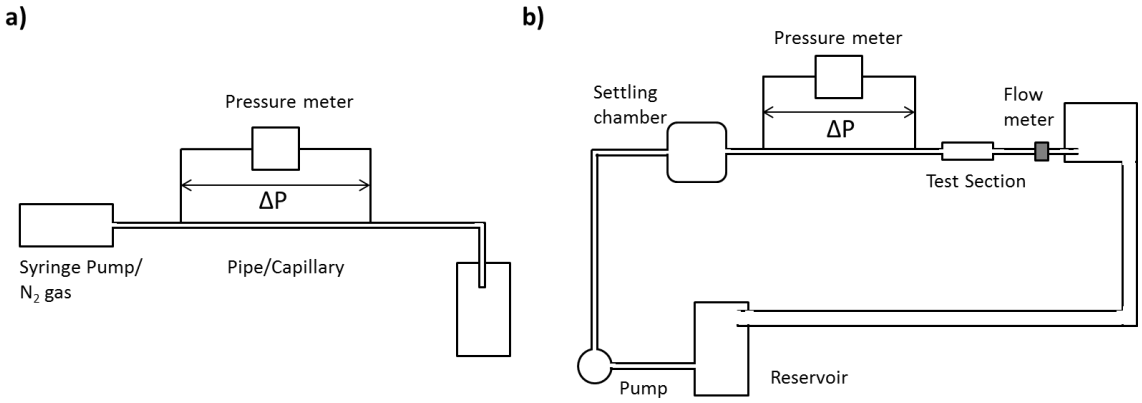

Figure 1: Schematic diagram demonstrating pipe flow apparatus; **a)** open capillary rheometer system; **b)** close loop system.

Kulik used a pipe flow method to compare DRE of PEO with a range of molecular weights (M_n = 0.3 - 3.5 x 10^6 g mol^{-1}).[3] Polymer solutions (conc. = 50 ppm) were driven through a straight, stainless steel pipe (length, L = 0.125 – 4 m, d = 2 mm) at high pressure (16 MPa) providing *Re* up to 8 x 10^4. The time taken for 0.6 l of solution to be transferred was recorded, allowing the measurement of *%DR* (30-90 %). Most effective drag reduction was observed for the highest molecular weight PEO sample, at highest Re. A more simple method based on flow through a

plastic pipe (*L* = 3 m) under gravity also provided reproducible measurements of *%DR*.[4] Using a solution volume of 10 l, and by varying pipe diameter (*d* = 1/16 – ½ in), *Re* could be adjusted between 0.5 and 10 x 10^3. This system allowed the comparison of *%DR* for PAM samples with a range of molecular weights (8-14 x 10^6 g mol^{-1}).

Solomon et al. used an open pipe flow apparatus (*L* = 0.3-3 m, *d* = 10.9 mm) to measure the effect of mechanical degradation on the DRE of PEO (5 x 10^6 g mol^{-1}).[5] The flow was driven by nitrogen gas (5-150 psi, *Re* = 1– 25 x 10^4) to avoid polymer degradation caused when a solution passes through a mechanical pump.[5]A *%DR* of 75 % was measured at a polymer concentration of 100 ppm; this reduced to 50 % following twelve passes through the system. A narrow capillary system (*L* = 10-30 cm, *d* = 125 μm) was used by Al-Hashmi et al. to compare the *%DR* and mechanical stability of a hydrolysed PAM co-polymer (M_w ≈ 18.5 x 10^6 g mol^{-1}).[6] Extremely high shear rates (1.5 x 10^6 s^{-1}) were generated in this system and *%DR* up to 80 % was measured.[6]

Looped pipe flow systems (Fig. 1b) are particularly useful when studying polymer degradation and turbulent flow properties as they allow solutions to be cycled indefinitely through an apparatus. Den Toonder et al. used a flow loop (*L* = 34 m, d = 40 mm) to measure *%DR* (70 %) of a commercial PAM product 'Superfloc' (conc. = 20 ppm), whilst also visualising the flow using laser Doppler velocimetry.[7] With a similar system (*L* = 13.35 m, *d* = 10 cm), Escudier et al. compared *%DR* of carboxymethylcellulose (CMC), xanthan gum (XG) and PAM at *Re* > 2 x 10^4.[8] The DRE of XG (conc. = 20 - 200 ppm) was also studied by Liberatore et al. at *Re* of 5 – 70 x 10^3 using copper pipe system (*L* = 25 ft, *d* = ¼ - 1 inch).[9] Chun et al. compared the DRE of PEO (0.2 - 4 x 10^6 g mol^{-1}, conc. = 1-20 ppm) at *Re* between 3 – 6 x 10^4 with a flow loop system (*L* = 2 m, *d* = 17.1 mm) measuring a *%DR* up to 50 %.[10] Finally, Zhou et al. used a closed loop to compare the measurement of *%DR* for high molecular weight (HMW) poly(2-acrylamido-2-methyl-1-propanesulfonic acid) (PolyAMPS) in straight and coiled pipes (*Re* 2 – 11 x10^4).[11] The friction experienced by fluids in coiled tubing is increased due to a secondary perpendicular flow caused by centrifugal forces. Three distinct coiled test sectios allowed coil size and number to be varied; the results demonstrated a lower *%DR* for a more coiled system (*%DR*; straight = 75 %, coiled = 65 %).

Pipe flow systems are the most effective and realistic way to test drag reduction, however, they are often time consuming and require voluminous samples. To conduct quicker, smaller scale experiments, rotational rheometers have proven to be very useful. Calculation of *%DR* in these systems is possible by comparing the torque necessary to rotate in a dilute polymer

solution and pure solvent. A range of rheometer geometries have been used for this purpose (Fig. 2). Choi et al. used a rotating disk apparatus (Fig. 2a) to measure the DRE of polyisobutylene in cyclohexane.[12] Furthermore, *%DR* of XG,[13] guar gum,[14] PAM and PEO were measured in aqueous solutions.[15,16] A similar system has also been used in the work of McCormick for the study of PAM based polyampholytes.[17,18] Although this geometry provides a measurement of drag reduction, it most accurately describes drag flow around a body rather than pipe flow.

Concentric cylinder geometries more closely mimic pipe flow as they enclose the flow between two surfaces. The rotating outer cylinder design (Fig. 2b) has been used to measure DRE of both PEO and PAM.[19,20] A double gap geometry (Fig. 2c) has proven most suitable for DR measurements as the surface area in contact with the fluid is maximised, which increases sensitivity for low viscosity solutions. Nakken et al. used this geometry to measure DRE of poly α-olefins in Varsol 80 and polystyrene in toluene.[21,22] Bismarck and Kot also used the system to the test the DRE of a novel PAM drag reducing agent (M_w = 2.8 x 10^6 g mol^{-1}) in aqueous solution.[23] During this test extremely high rotation speeds (2 x 10^3 rpm, shear rate = 1 x 10^4 s^{-1}) were necessary to generate a sufficiently turbulent system, and *%DR* up to 55 % was measured over a range of concentrations (25-300 ppm). Furthermore, Pereira and Soares used the double gap geometry at even higher rotational speed (3 x 10^3 rpm) when analysing the DRE of PEO (0.3 - 5.0 x 10^6 g mol^{-1}, *%DR* 6 -26 %) and PAM (5 x 10^6 g mol^{-1}, *%DR* = 24 %) at a concentration of 100 ppm.[24] This work was then extended to the measurement of XG (*%DR* = 20 %).[24,25]

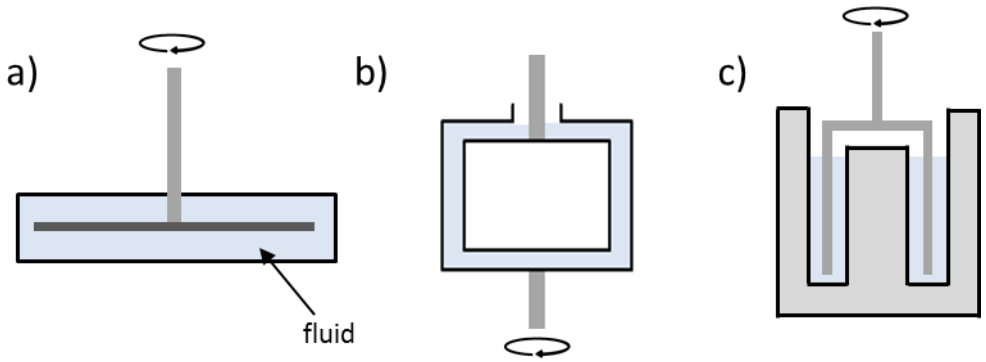

Figure 2: Rotational rheometer geometries; **a)** Rotating disk; **b)** Concentric cylinders, rotating outer cylinder; **c)** Concentric cylinders, double gap geometry.

5.2. Experimental

5.2.1. Materials

Trifluoroacetic acid (TFA, 99 %) was purchased from Sigma Aldrich and used without further purification. Dichloromethane (DCM) was purchased from Fisher Scientific and used as received. $CDCl_3$ and D_2O for NMR analysis were purchased from Apollo Scientific and Goss Scientific, respectively.

Testing of drag reduction efficiency was conducted using tap water from Shipley/Bingley, Bradford zone. The supply is classified as 'moderately soft' and typically has; pH = 7.61, Ca content 27.63 mg Ca/l, magnesium content of 1.84 mg Mg/l, and sodium content of 7.56 mg Na/l.

Praestol (PAM) for drag reduction testing was provided by Ashland Inc and used as received as an inverse-emulsion (0.5 wt% polymer). Stock solutions of HMW polymer samples for drag reduction testing were prepared at a concentration of 0.5 wt% by stirring in distilled water for several days to provide a fully homogeneous solution. The solutions were further diluted to the required to dose during testing. Polyacrylamide (M_w = 5 – 6 x 10^6 g mol^{-1}, **PAM-6M**) was purchased from Acros Organics whilst Poly(ethylene oxide) ($M_v \approx 8 \times 10^6$ g mol^{-1}, **PEO-8M**) and Poly(acrylic acid) ($M_v \approx 1.25 \times 10^6$ g mol^{-1}, **PAA-1M**) were purchased from Sigma Aldrich; all polymers were used as received. The data for the samples tested following synthesis in this work is summarised in Table 1. Degree of polymerisation (DP) is included for direct comparison of molecular weights. The P*t*BA samples (Table 1, Entry **i**-**viii**) were taken from the large scale polymerisation reactions described in Chapter 3, Section 3.3.5. The PNaA samples (Table 1, Entry **ix**-**xiv**) were taken from the aqueous polymerisation kinetic investigations described in Chapter 4, Section 4.3.2.1.

Table 1: Summary of samples synthesised in Chapter 3 and 4 tested for drag reducing properties.

Entry	Sample Code	Polymer Type	M_n(Target) x 10^{-5} (g mol^{-1})	Reaction Time (h)	Conv. (%)	M_n(SEC) x 10^{-5} (g mol^{-1})	*DP* x 10^{-3}	*Đ*
i	**4AE-A**	P*t*BA	3.0	44	91	3.09	2.41	1.30
ii	**4AE-B**	P*t*BA	3.0	70	69	8.61	6.71	1.61
iii	**I4-S-A**	P*t*BA	10.0	24	85	13.9	10.8	1.51
iv	**I4-S-B**	P*t*BA	10.0	24	22	7.84	6.09	1.93
v	**I4-S-C**	P*t*BA	10.0	24	36	7.47	5.79	2.28
vi	**I4-S-D**	P*t*BA	10.0	24	43	18.8	14.6	1.43
vii	**MBP-A**	P*t*BA	10.0	24	26	7.69	6.00	2.29
viii	**I2-S-A**	P*t*BA	10.0	24	70	14.9	11.6	2.10
ix	**I4-T-A**	PNaA	0.3	2	34	6.83	7.26	1.60
x	**I4-T-B**	PNaA	0.3	8	45	6.61	7.03	1.60
xi	**I4-T-C**	PNaA	0.3	16	71	6.01	6.39	1.60
xii	**I4-T-D**	PNaA	0.3	24	69	4.58	4.87	2.05
xiii	**I4-T-E**	PNaA	3.0	8	65	6.94	7.38	1.50
xiv	**I4-T-F**	PNaA	3.0	16	82	6.56	6.98	1.60

5.2.2. Instrumentation

^{1}H NMR spectra were recorded using a Bruker Avance-400, spectrometer operating at 400 MHz. $CDCl_3$ and D_2O were used as deuterated solvent for NMR analysis and the spectra were referenced to the solvent trace at 7.26 ppm and 4.79 ppm, respectively.

A measurement of molecular weight for low mass polymers was obtained using matrix assisted laser desorption/ionisation-time of flight (MALDI-ToF) mass spectrometry. Analysis was carried out using an Autoflex II ToF mass spectrometer (Bruker Daltonik GmBH) using a 337 nm nitrogen laser. Samples were prepared in solution (conc. = 1 mg ml^{-1}) and mixed with matrix

solution (conc. ≈ 50 mg ml^{-1}) in a ratio of 1:9. The mixture (1 µL) was spotted on to a metal target (pre-cleaned using methanol and acetone) and placed into the MALDI ion source. *Trans*-2-[3-*tert*-butylphenyl)-2-methyl-2-propenylidene)malonitrile (DCTB) was used as a suitable matrix.

5.2.2.1. Drag Reduction Rig

A test rig owned by Ashland Inc. (Fig. 3) was used to measure the *%DR* of polymer solutions. The rig is used routinely by Ashland to determine the *%DR* of **Praestol** (PAM) commercial products. It allows a simple and effective method to calculate *%DR* of a dilute polymer solution experienced during pipe flow. The rig comprises a pressure chamber into which the polymer solution is loaded and pressurised using nitrogen gas. The solution is released in to the Teflon tube (l = 219 cm, d = 0.4 cm) and collected in a measuring cylinder. To calculate *%DR*, the time is recorded for a known volume of dilute polymer solution (500 ml) to travel through the length of pipe. The flow rate is compared with a pure water control sample (See Section 5.2.5).

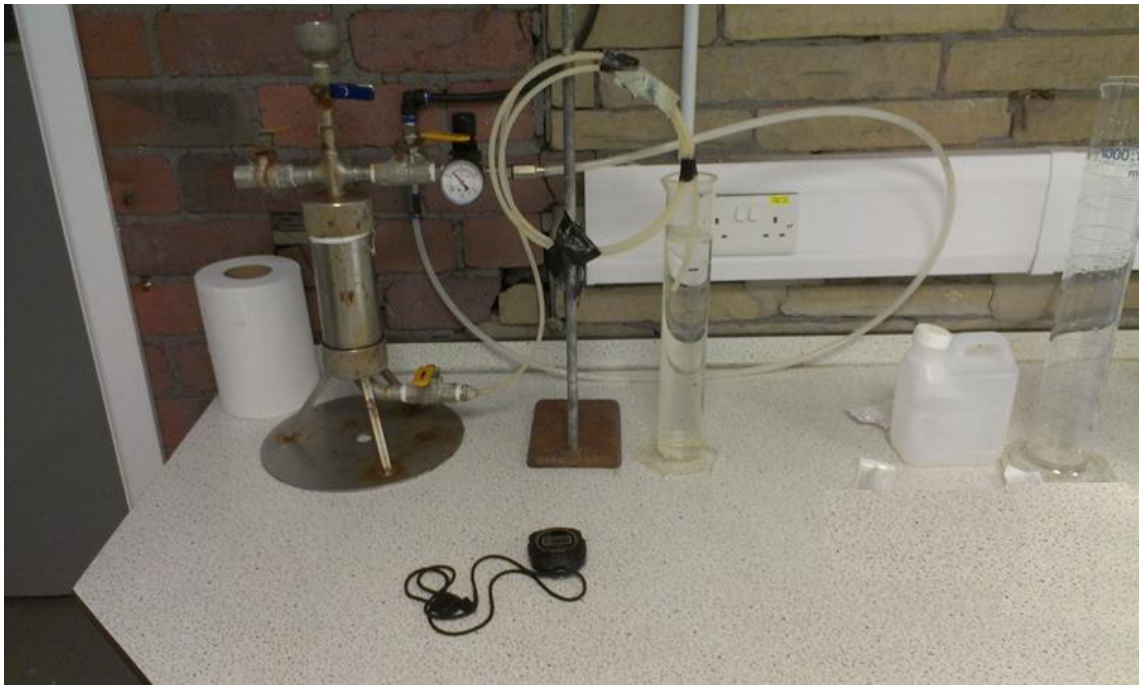

Figure 3: Drag reduction test rig.

5.2.3. Hydrolysis of poly(*tert*-butyl acrylate) to poly(acrylic acid)

Poly(*tert*-butyl acrylate) (P*t*BA) (50 mg, 1.0 µmol, 0.4 mmol *tert*-butyl groups) was dissolved in $CDCl_3$ (0.9 ml) and transferred to an NMR tube. The sample was analysed using ^1H NMR spectroscopy before trifluoroacetic acid (TFA) (0.1 ml, 0.15 mg, 1.3 µmol) was added to begin the hydrolysis reaction. The reaction mixture was analysed at regular time intervals using ^1H NMR spectroscopy.

The reaction was then repeated on a larger scale for each sample, an example is described below;

P*t*BA (0.25 g, 5.0 µmol, 2.0 mmol *tert*-butyl groups), was transferred to a round bottomed flask fitted with a magnetic stirrer bar and water condenser. DCM (9 ml) was added to the flask and the mixture stirred for 3 h until fully homogeneous. TFA (0.77 ml, 1.14 g, 10.0 mmol) was injected in to the flask and stirred at room temperature for 40 h. The reaction mixture became heterogeneous and the solid polymer was isolated by removal of DCM/TFA solution. The solid poly(acrylic acid) (PAA) product was dried under a flow of nitrogen and analysed by ^1H NMR spectroscopy in D_2O.

5.2.4. Examination of macro-initiator (I4) stability

I4-S and **I4-T** (0.10 g, 2.5 µmol) were weighed in to separate round bottomed flasks fitted with a magnetic stirrer bar and water condenser and DCM (5.00 ml) was added to each flask and stirred to dissolve. TFA (0.50 ml, 0.74 g, 7.0 µmol) was injected in to each flask and the mixtures stirred for 40 h at room temperature. The resulting solution was analysed using ^1H NMR spectroscopy and MALDI-ToF mass spectrometry.

5.2.5. Testing of drag reduction efficiency

The drag reduction test rig is represented schematically in Figure 4. An example procedure for the determination of *%DR* of a dilute polymer solution is detailed below. A data set recorded for a **Praestol** (PAM) sample is used to demonstrate the procedure to convert the raw data to *%DR* values.

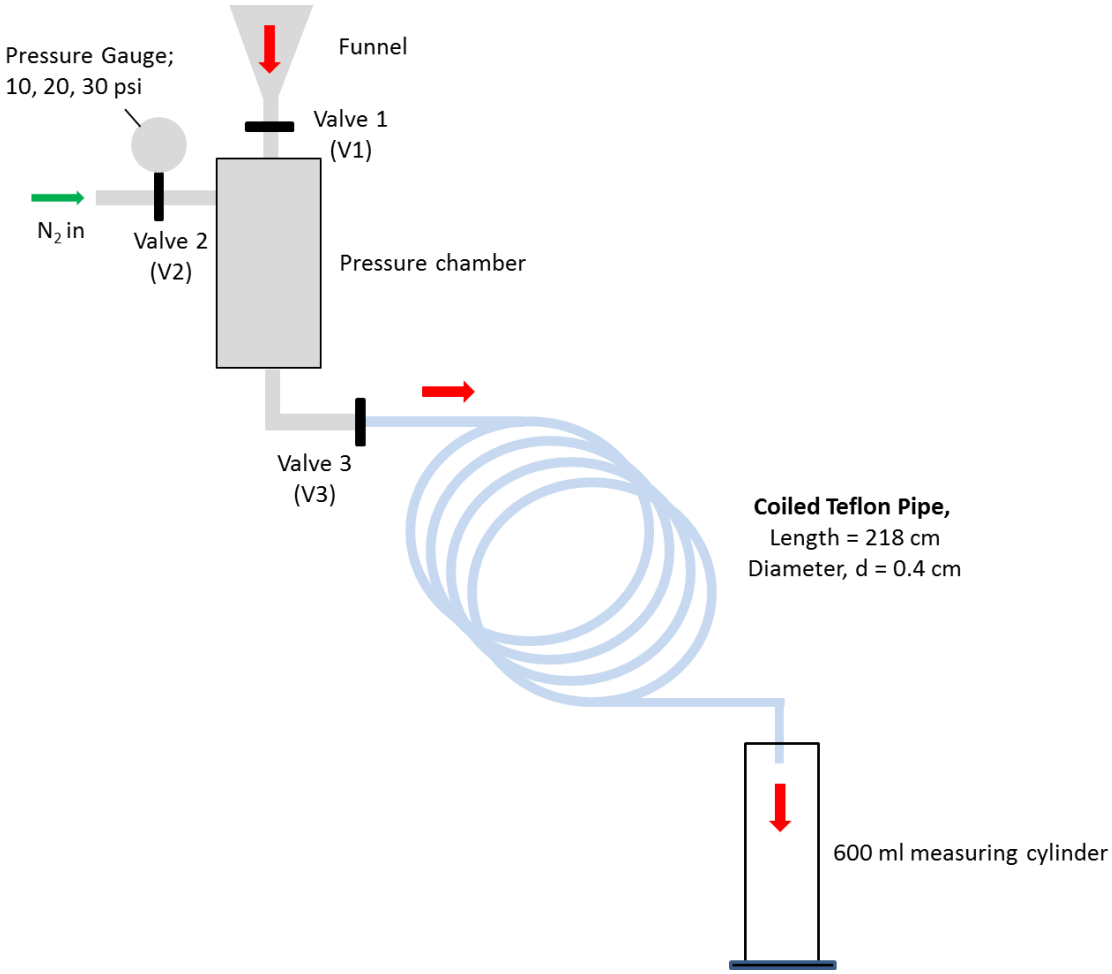

Figure 4: Schematic representation of drag reduction test rig.

5.2.5.1. General procedure

A pure water control sample was first tested as follows:

1. Valve 1 (V1) (Fig. 4) was opened and water (600 ml) was loaded to the pressure chamber via the funnel; the chamber was sealed by closing V1.
2. V2 (leading to the nitrogen line) was opened and the chamber was pressurised to 10 psi.
3.
4. V3 was opened and a small amount of water (≈ 100 ml) was run through the pipe into the measuring cylinder. This allowed fine tuning of the pressure (via the gauge) and loaded the pipe with sample in order to accurately measure the time for 500 ml of sample to be dispensed.
5. The water was returned to the chamber, which was re-pressurised.

6. V3 was opened and a stopwatch was used to measure the time taken for 500 ml of water to flow in to the measuring cylinder.

7. The remaining water was then evacuated from the pipe.

8. The measurement was repeated at 10 psi before the same procedure was conducted at a pressure of 20 and 30 psi. The average time for 500 ml of liquid to flow in to measuring cylinder at each pressure is shown in Table 2.

Table 2: Average time for transfer of 500 ml of water at increasing pressure.

	Dose (ppm)	Pressure (Psi)	Ave. Time (s)
Water control	0	10	14.97
		20	10.41
		30	8.16

Following the blank water measurement, a dilute polymer solution was prepared by adding the stock solution (0.5 wt%, volume dependent on required dose) via syringe to a flask containing tap water (600 ml). The flask was shaken thoroughly for 1 min to allow complete mixing of polymer solution. The procedure described above was repeated for the polymer solution. Following measurement at 10, 20 and 30 psi, the solution was fully evacuated from the pipe and further stock solution was added to increase the dose. The process was repeated with increasing dose until all required doses had been tested. The raw data set for a **Praestol** sample is shown in Table 3.

Table 3: Average time for transfer of 500 ml of **Praestol** polymer solution at a range of pressures and increasing dose.

Dose (ppm)	Total volume of stock solution added (ml)	Pressure (Psi)	Time (s)
1.25	0.15	10	14.16
		20	9.66
		30	7.43
2.5	0.30	10	13.34
		20	9.00
		30	6.91
5.0	0.60	10	12.44
		20	8.00
		30	6.15
10	1.20	10	13.07
		20	8.22
		30	6.12

5.2.5.2. Calculation of *%DR*

Following the measurements taken for pure water and the polymer solution, *%DR* was calculated as follows:

1. The time for the transfer of 500 ml of polymer solution at each dose and pressure was converted to flow rate using Equation 1. This information, for each pressure at a dose of 1.25 ppm, is summarised in Table 4.

$$\text{Flow rate } (Q) = \frac{\text{volume (500 ml)}}{\text{time (s)}} \qquad \textbf{(Equation 1)}$$

Table 4: Flow rate for **Praestol**, dose = 1.25 ppm at increasing pressure.

Dose (ppm)	Pressure (Psi)	Time (s)	Flow Rate (ml s^{-1})
1.25	10	14.16	35.31
1.25	20	9.66	51.76
1.25	30	7.43	67.29

2. Re for each dose and pressure (dependent on the flow rate, pipe dimensions and solution properties) was then calculated using Equation 2. This gives a measure of turbulence in each system.

$$Re = \frac{d\,\mu\,\rho}{\zeta} \quad \text{where} \quad \mu = \frac{4Q}{\pi d^2} \qquad \textbf{(Equation 2)}$$

d = inner diameter of tube (0.4 cm), ***Q*** = flow rate (ml s^{-1}), ***ρ*** = solution density ≡ 1, ζ = solution viscosity in Poise (1 cP = 0.01 P). For these ultra-dilute systems ***ρ*** and ***ζ*** assumed to be equal to pure water.

A friction factor (*F*), a measure of the friction a fluid experiences as it flows through a pipe, was also calculated for each polymer solution at increasing pressure using Equation 3. *Re* and *F* is summarised for a dose of 1.25 ppm at each pressure in Table 5.

$$F = \frac{d^5 \Delta P\, \pi^2}{32\, L\, \rho\, Q^2} \qquad \textbf{(Equation 3)}$$

Δ*P* = pressure drop from the pressure chamber (10, 20 or 30 Psi) to 0 Psi at end of pipe (convert pressure from Psi to pressure in dynes cm^{-1} by multiplying by 68985), ***L*** = length of tube = 219 cm, ***ρ*** = density ≡ 1

Table 5: Summary of *Re* and *F* at each pressure for **Praestol** dose = 1.25 ppm

Dose (ppm)	Pressure (Psi)	Time (s)	Flow Rate (ml s^{-1})	R_e x 10^{-4}	Friction Factor (*F*) x 10^{3}
1.25	10	14.16	35.31	1.124	8.0
1.25	20	9.66	51.76	1.648	7.4
1.25	30	7.43	67.29	2.142	6.6

3. *Re* was then plotted vs *F* and the equation of the trendline was calculated (Fig. 5).

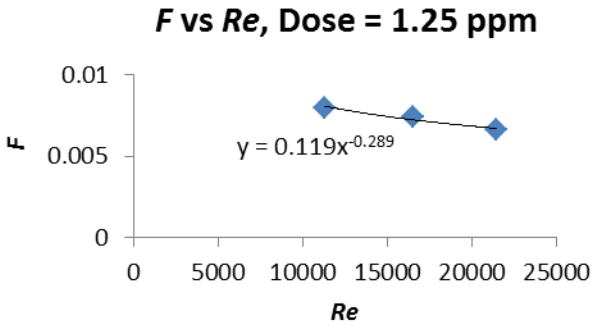

Figure 5: Plot of *Re* vs *F* for **Praestol** dose = 1.25 ppm with equation of trendline included.

This equation ($F = 0.119Re^{-0.289}$) allowed *Re* to be standardised and *F* could be calculated at three specifically chosen *Re* values (Table 6). This is important as *Re* varies for every solution, even at the same pressure, depending on the exact solution properties. It is necessary to determine *F* at a specific *Re* value in order to directly compare with the control water sample.

Table 6: *F* calculated at specific *Re* for **Praestol** dose = 1.25 ppm.

Dose (ppm)	Chosen *Re* x 10^{-4}	*F* x 10^{3}
1.25	1.0	8.3
1.25	1.5	7.4
1.25	2.0	6.8

4. Steps 1-4 were then used to determine *F* for pure water (at *Re* = 1.0, 1.5 and 2.0 x 10^{4}). The *%DR* at each *Re* was calculated from the difference between *F* of the polymer solution and

pure water sample (Equation 4). The *%DR* at each *Re* is summarised for dose = 1.25 ppm in Table 7.

$$\%DR = 100 - \left(\frac{(F(\text{polymer solution})}{F(\text{pure water})} \times 100 \right) \quad \textbf{(Equation 4)}$$

Table 7: Summary of *%DR* at increasing *Re* for **Praestol** dose = 1.25 ppm.

Dose (ppm)	Chosen *Re* x 10^{-4}	*F* (Polymer solution) x 10^{3}	*F* (Pure water) x 10^{3}	*%DR*
1.25	1.0	8.3	9.1	8.8
1.25	1.5	7.4	8.4	11.9
1.25	2.0	6.8	8.0	15.0

5. The same analysis (Steps 1-5) was repeated for each increasing dose (2.5-10 ppm) and is summarised in Table 8. From this data a graph was then plotted demonstrating the change in drag reduction with polymer dose (Fig. 6).

Table 8: Summary of *%DR* for **Praestol**, calculated at each dose and Re.

Dose (ppm)	Chosen *Re* x 10^{-4}	*F* (Polymer solution) x 10^{3}	*F* (Pure water) x 10^{3}	*%DR*
1.25	1.0	8.3	9.1	8.8
	1.5	7.4	8.4	11.9
	2.0	6.8	8.0	15.0
2.5	1.0	7.6	9.1	16.5
	1.5	6.6	8.4	21.4
	2.0	6.0	8.0	24.6
5	1.0	6.9	9.1	25.3
	1.5	5.8	8.4	31.0
	2.0	5.1	8.0	36.2
10	1.0	7.6	9.1	16.5
	1.5	6.1	8.4	27.4
	2.0	5.2	8.0	35.0

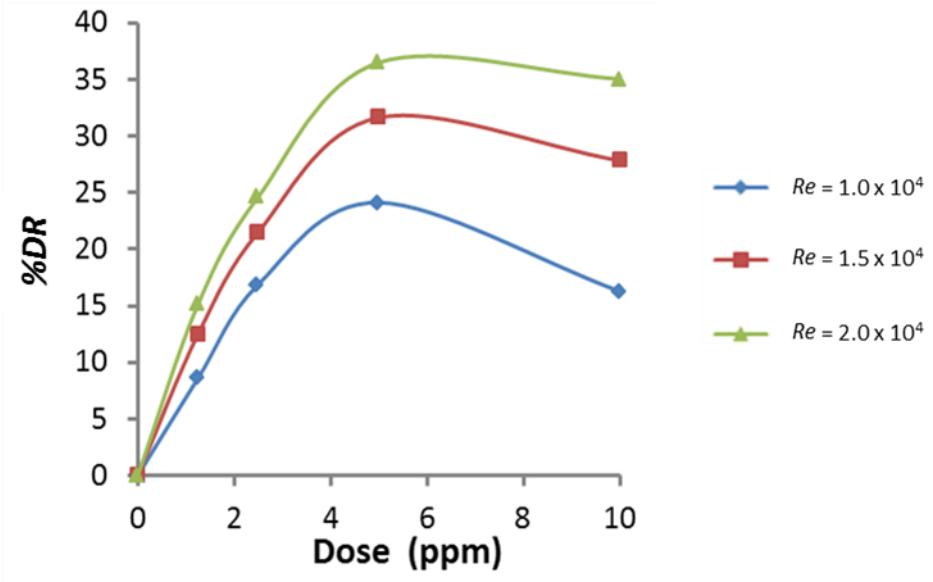

Figure 6: Change of *%DR* with polymer dose for **Praestol** at three *Re* values.

5.2.6. Measurement of polymer mechanical stability

To study the resistance of a polymer sample to mechanical degradation, the *%DR* was first measured for the sample as described above (Section 5.2.5-5.2.6). The polymer solution was then cycled through the drag reduction test rig for 30 runs (pressure = 30 Psi) and the flow rate recorded for each run. The *%DR* then measured again for the resulting solution.

5.3. Results and Discussion

5.3.1. Hydrolysis of poly(*tert*-butyl acrylate)

HMW poly(*tert*-butyl acrylate) (P*t*BA) samples were prepared in Chapter 3 using a variety of initiators (MBP, **4AE**, **I4-S**, **I2-S**). To convert these to water soluble samples for drag reduction testing, the polymer side chain was hydrolysed using TFA to prepare PAA (Scheme 1).

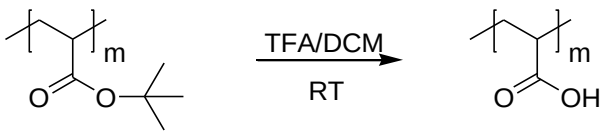

Scheme 1: Hydrolysis of PtBA to PAA using TFA/DCM.

TFA is commonly used as a strong acid to convert PtBA to PAA.[26,27] In particular, it has been useful to selectively cleave *tert*-butyl ester groups, whilst leaving other esters (e.g. methyl ester) unaffected within the same molecule.[28] This is important for the PEG-based branched

systems described here, as the ester bonds in the core of the macro-molecule (Fig. 7) must remain intact to maintain the star structure of the polymers.

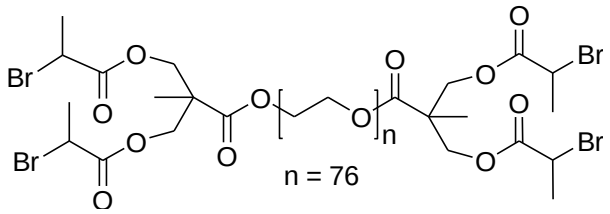

Figure 7: PEG based macro-initiator, **I4-S**, containing several ester groups which is incorporated in to P*t*BA core.

The hydrolysis reaction was first conducted in an NMR tube using $CDCl_3$ as deuterated solvent. ^1H NMR spectroscopy (Fig. 8) was used to monitor the reaction progress by following the decrease in intensity of the resonance due to the *t*BA side chains (**1**, 1.42 ppm, Fig. 8a). Moreover, the increase in the intensity of the resonance corresponding to *tert*-butyl fluoroacetate released in solution (**2**, 1.58 ppm, Fig. 8b-d) can be observed as the reaction progresses. Integration of the two resonances allows the ratio of *tert*-butyl fluoroacetate to *tert*-butyl side chains to be calculated. Within 5 min (Fig. 8b), a ratio of 0.17 indicated that hydrolysis began immediately in the system. After 360 min (Fig. 8d) a ratio of 65.97 demonstrated almost complete cleavage of the polymer side groups. Finally, at 24 h (Fig 8e) no resonance could be observed due to polymer side chain, illustrating that the *tert*-butyl groups had been entirely removed

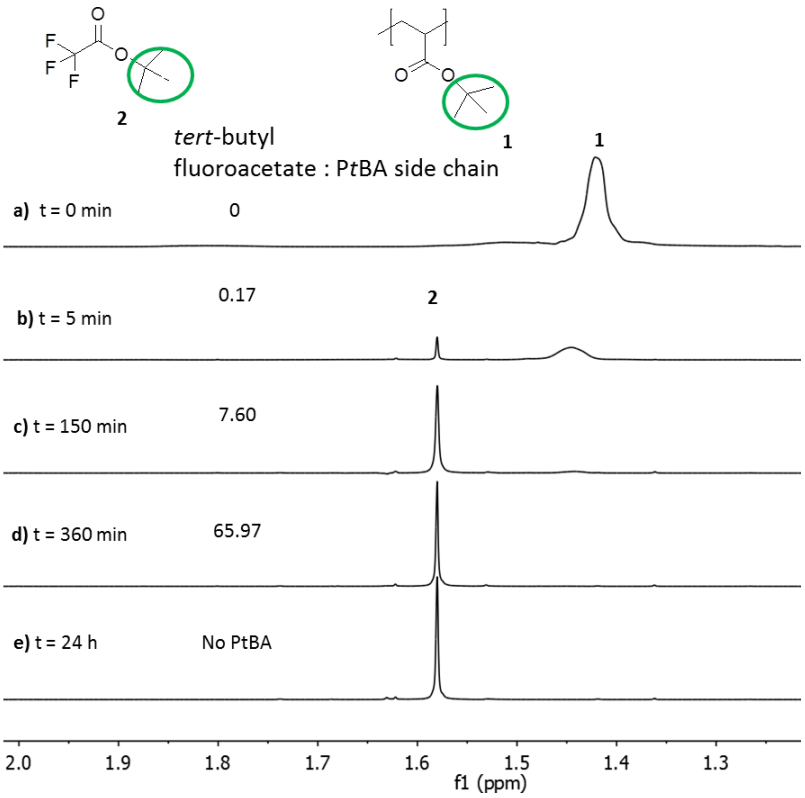

Figure 8: 400 MHz-^{1}H NMR spectra showing small scale hydrolysis reaction at increasing time from **a)** - **e)**.

The scale of the reaction was increased in order to prepare samples for *%DR* testing. To ensure full de-protection on this scale, the reaction time was increased to 40 h. Comparison of the ^{1}H NMR spectrum before (Fig. 9a) and after (Fig. 9b) the reaction demonstrated complete hydrolysis providing a fully water soluble PAA sample.

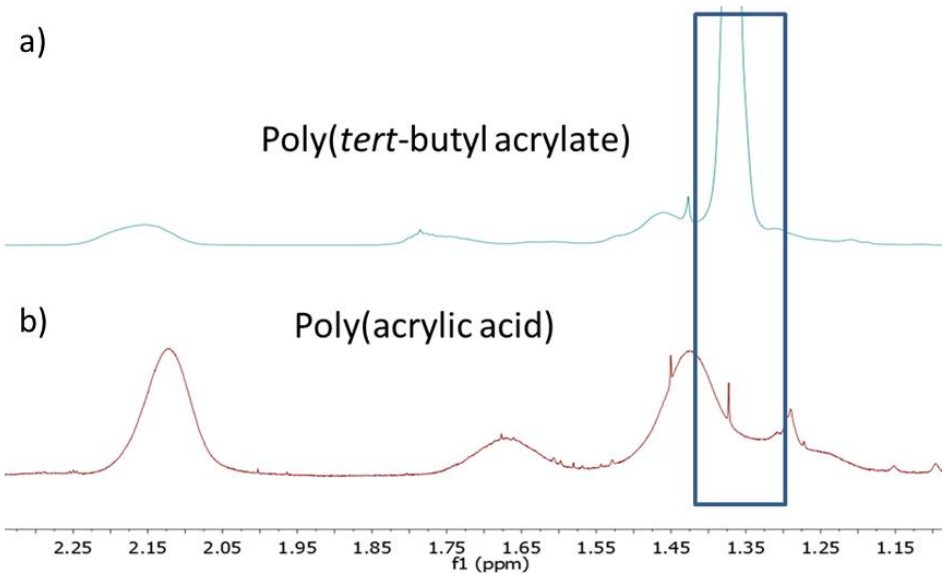

Figure 9: 400 MHz-^{1}H NMR spectrum of; **a)** P*t*BA before hydrolysis (in $CDCl_3$); **b)** PAA following hydrolysis (in D_2O).

The **I4-S** and **I4-T** initiator molecules (Fig. 7) were both exposed to the same hydrolysis conditions to probe the stability of the ester groups within the polymer core. After stirring the macro-initiators in DCM/TFA for 40 h, ^{1}H NMR spectroscopy and MALDI-ToF MS were used to analyse the solution. Analysis of the ^{1}H NMR spectrum confirmed the presence of both the PEG chain and branched end groups (Appendix D, Fig. 1) In Figure 10 and 11 the MALDI-Tof mass spectra of **I4-S** and **I4-T** are compared before (a) and after (c) stirring with DCM/TFA. Also included in Figure 11b and Figure 12b is the spectrum of PEG (M_n = 3350 g mol^{-1}) . From this comparison it can be clearly observed that there is no reduction in mass of the macro-initiators following treatment with DCM/TFA, even after 40 h. No peaks are observed in the spectrum corresponding to PEG-3350 which is taken as strong evidence that the chain end ester groups have not been cleaved within the macro-initiator.

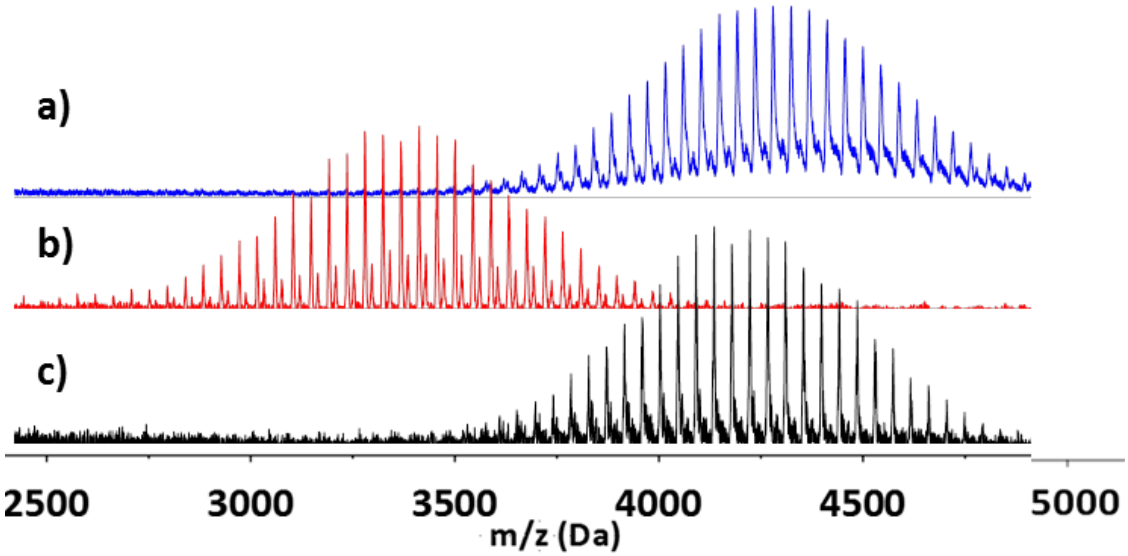

Figure 10: MALDI-ToF MS spectra of**; a)** **I4-S**; **b)** PEG-3350; **c)** **I4-S** after stirring with DCM/TFA for 40 h.

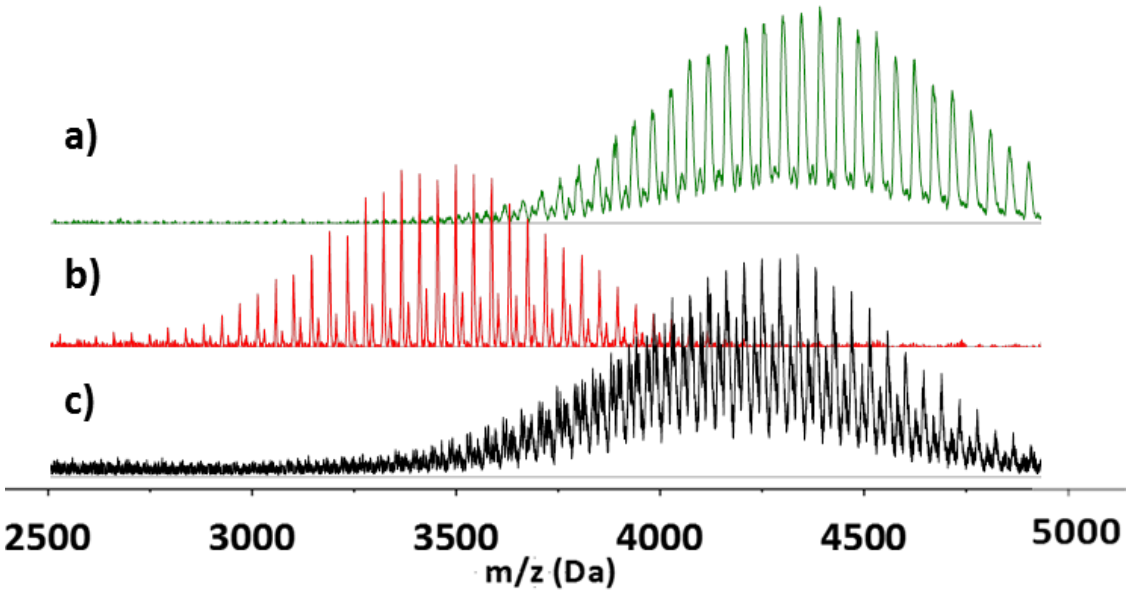

Figure 11: MALDI-ToF MS spectra of**; a)** **I4-T**; **b)** PEG-3350; **c)** **I4-T** after stirring with DCM/TFA for 40h.

5.3.2. Measurement of drag reduction efficiency

The molecular weight and drag reduction measurements for all of the samples tested are summarised in Table 9. Due to the diverse range of techniques, conditions and polymers studied in the literature, a direct comparison with the polymers described here is not possible. Therefore, in addition to the samples synthesised in Chapters 3 and 4, four commercially available polymers were also examined (Table 9, Entry **i**-**iv**) allowing some comparisons to be made. By studying polymers with known drag reducing properties, the suitability of the test rig for measurement of *%DR* can be confirmed. The reproducibility of results obtained using the drag reduction test rig was first examined by repeating three separate measurements using the same polymer solution (**4AE-B**). The results are plotted for *Re* of 1.0 x 10^4, 1.5 x 10^4 and 2.0 x 10^4 in Fig. 12a, b and c, respectively. At low *Re* (Fig. 12a) there is a slight difference between the values recorded for Run 2 at low dose. When *Re* is increased (Fig. 12b-c) the results were closely reproduced across the three runs. A clear increase in *%DR* is observed as the turbulence of the system is increased.

Table 9: Summary of molecular weight and DRE data for polymer samples tested using drag reducing rig.

Entry	Sample Code	Polymer Type	M_n x 10^{-5} (g mol^{-1})	*DP* x 10^{-3}	*Đ*	$\%DR_{MAX}$	Dose (ppm)	*%DR* at 190 ppm
i	**Praestol**	PAM	~200*		N/A	36.5	5.0	N/A
ii	**PAM-6M**	PAM	50-60*		N/A	32.6	20.0	22.6
iii	**PEO-8M**	PEO	80*		N/A	57.0	10.0	22.0
iv	**PAA-1M**	PAA	13*		N/A	1.2	2.5	-2.4
v	**4AE-A**	PAA+	1.77	2.41	1.30	3.20	330	1.2
vi	**4AE-B**	PAA+	4.84	6.71	1.60	34.5	190	34.5
vii	**I4-S-A**	PAA+	7.84	10.8	1.51	32.2	330	29.3
viii	**I4-S-B**	PAA+	4.43	6.09	1.93	12.4	190	12.4
ix	**I4-S-C**	PAA+	4.21	5.79	2.28	19.6	100	19.1
x	**I4-S-D**	PAA+	10.58	14.6	1.43	24.6	190	24.6
xi	**MBP-A**	PAA+	4.32	6.00	2.29	23.6	100	22.7
xii	**I2-S-A**	PAA+	8.38	11.6	2.10	31.4	190	24.6
xiii	**I4-T-A**	PNaA	6.83	7.26	1.60	31.6	190	31.6
xiv	**I4-T-B**	PNaA	6.61	7.03	1.60	32.9	190	32.9
xv	**I4-T-C**	PNaA	6.01	6.39	1.60	28.9	320	9.5
xvi	**I4-T-D**	PNaA	4.58	4.87	2.05	31.4	270	20.5
xvii	**I4-T-E**	PNaA	6.94	7.38	1.50	30.4	270	19.9
xviii	**I4-T-F**	PNaA	6.56	6.98	1.60	7.2	270	0.7

.* = M_w based on suppliers intrinsic viscosity measurements; + = M_n values measured for P*t*BA samples using THF SEC and adjusted assuming full hydrolysis of P*t*BA to PAA.

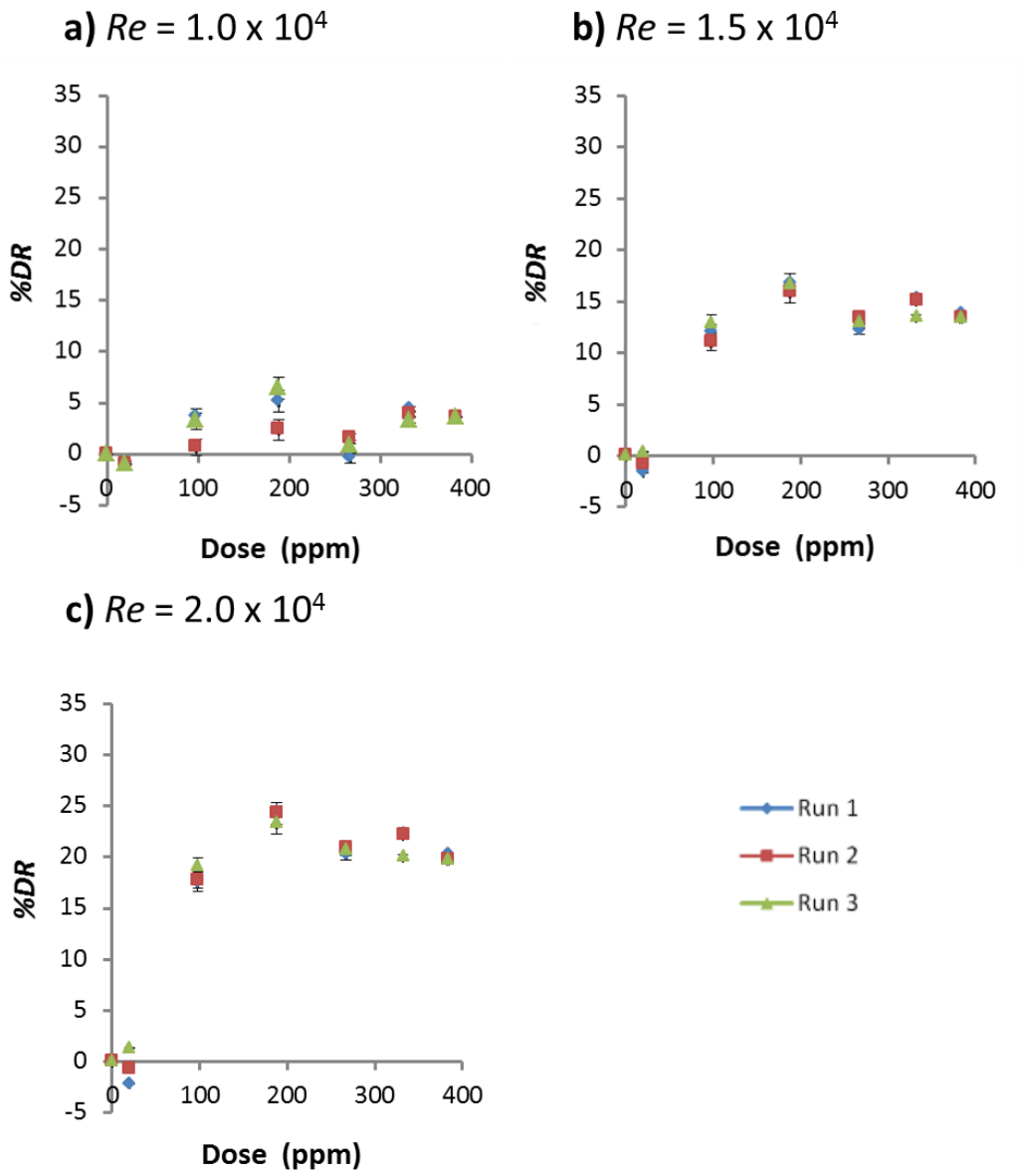

Figure 12: *%DR* vs Dose (ppm) for **4AE-B** repeated three times at**; a)** *Re* = 1 x 10^4; **b)**; *Re* = 1.5 x 10^4 **c)** *Re* = 2.0 x 10^4.

The evolution of *%DR* with polymer dose for each commercially available polymer (Table 9, Entry **i-iv**) is plotted in Figure 13a-d. The graph for the **Praestol** sample (Table 9, Entry **i**) in Figure 13a demonstrates a sharp increase in *%DR* with dose up to 5 ppm. At 5 ppm a maximum *%DR* ($\%DR_{MAX}$ = 36.5 %) is reached before *%DR* decreases as dose further increases. This is a common trend observed when measuring drag reducing efficiency. As the polymer dose increases, *%DR* rises with the concentration of HMW polymer which is able to contribute to drag reduction. However, the introduction of HMW polymer also increases the viscosity of the solution. As the drag reducing effect is counterbalanced by the increased solution viscosity, *%DR* levels off and begins to decrease (Fig. 13a).

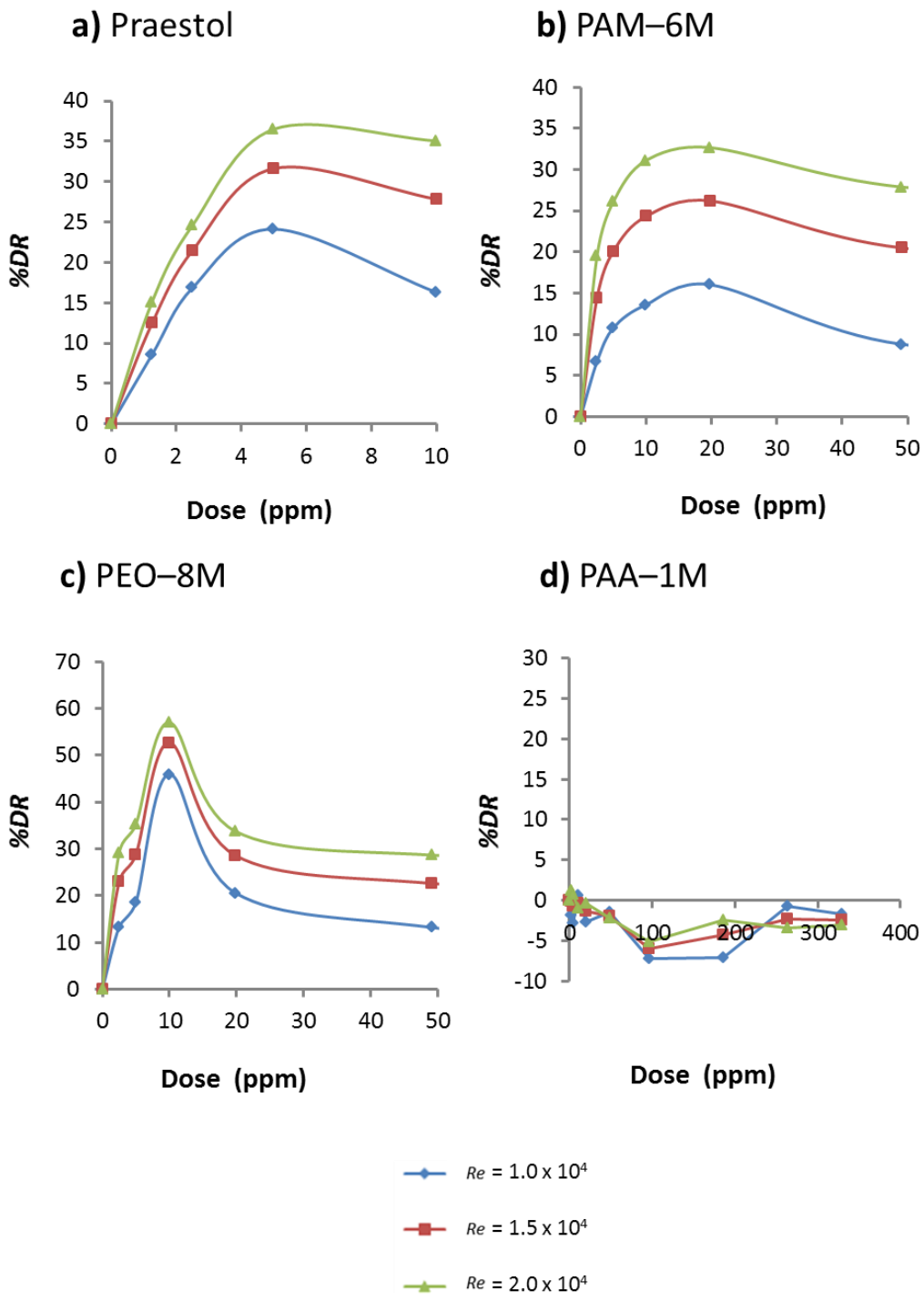

Figure 13: Plot of *%DR* vs Dose for**; a) Praestol; b) PAM-6M; c) PEO-8M; d) PAA-1M**.

The **PAM-6M** sample (Table 9, Entry **ii**) has a lower molecular weight and, therefore, a higher dose (10-20 ppm) was required to reach the maximum level of *%DR* (Fig. 13b, $\%DR_{MAX}$ = 32.6 %). Despite this, the value is comparable to the higher molecular weight **Praestol** sample. The most effective drag reducing polymer measured was **PEO-8M** (Table 9, Entry **iii**), which demonstrated $\%DR_{MAX}$ of 57 % at 10 ppm (Fig 13c); this high DRE is believed to due to the flexibility of the PEO chain. The plot of *%DR* vs dose for this polymer in Figure 13c

demonstrates a sharp peak after which the *%DR* decreases rapidly with increasing dose. The results described for these PAM/PEO samples confirm the suitability of the test rig for comparison for polymer drag reducing properties. The final sample was a linear PAA sample with $M_v \approx 1.25 \times 10^6$ g mol^{-1} (**PAA-1M**, Table 9, Entry **iv**). This polymer demonstrated no drag reducing effect at any dose (Fig. 13d). This may be a result of the of the high solution viscosity which counter-balances drag reduction, however, further study is necessary in order to determine this.

The P*t*BA samples synthesised in Chapter 3 were then tested for their DRE following hydrolysis to PAA (Table 9, Entry **v**-**xii**). The two samples synthesised using the **4AE** initiator provided both low (**4AE-A**. Table 9, Entry **v**) and high (**4AE-B**. Table 9, Entry **vi**) molecular weight polymers for direct comparison of *%DR*. The graphs of *%DR* vs dose for **4AE-A** and **4AE-B** are plotted in Figure 14a and 14b, respectively. From Figure 14a it is clear that the lower molecular weight star polymer is ineffective as a drag reducing agent. The $\%DR_{MAX}$ does not reach above 5 %, even at high dose, whilst at lower dose the flow rate of the solution decreases, demonstrated by the negative *%DR* value. In contrast, when the molecular weight of the star polymer is increased (Fig. 14b), a significant $\%DR_{MAX}$ of 24.3 % is observed. This value is comparable to $\%DR_{MAX}$ observed for the HMW PAM test samples (30-40 %, Table 9, Entry **i**-**ii**). Though a higher dose of 190 ppm was required to reach $\%DR_{MAX}$, this result is a clear indication that high molecular weight star polymers can be effective drag reducing agents.

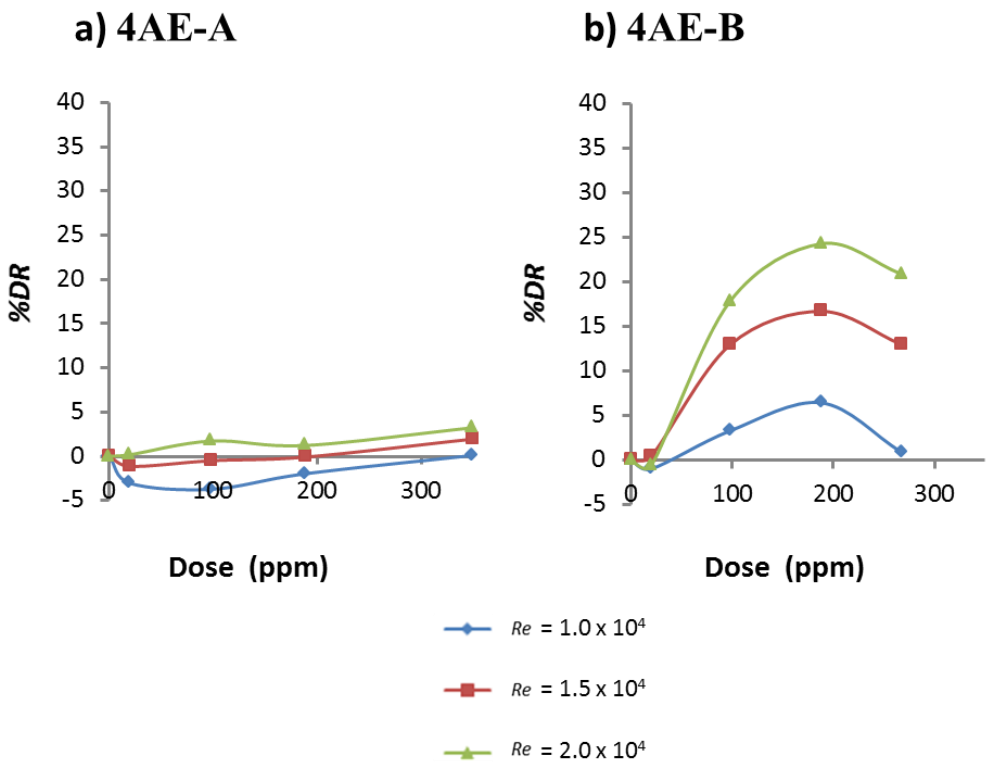

Figure 14: Plot of *%DR* vs Dose for; **a) 4AE-A; b) 4AE-B**.

The pH of the solution was monitored during the testing of these PAA samples and the change with increasing dose is plotted in Figure 15. The graph shows that the solution becomes steadily more acidic as dose increases above ≈ 10 ppm.

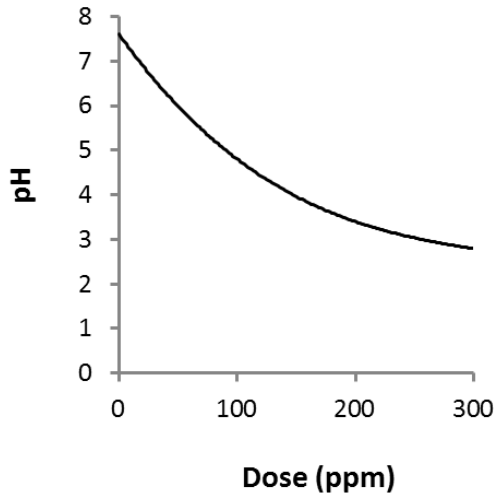

Figure 15: Plot of pH with increase polymer dose during the testing of PAA samples.

The graphs of *%DR* vs dose for the PEG containing star polymers **I4-S-A** - **D** (Table 9, Entry **vii**-**x**) are plotted in Figure 16a-d. In Figure 16a, a high *%DR* response ($\%DR_{MAX}$ = 32.2 %) is observed as dose is increased for **I4-S-A**. Again, this value is comparable to the commercial drag

reducing agent (**Praestol**). The **I4-S-B** (Fig. 16b) and **I4-S-C** (Fig. 16c) samples have a slightly lower molecular weight and *%DR* is decreased for these polymers *(%DR*$_{MAX}$ = 12.4 and 19.6 %). A higher *%DR*$_{MAX}$ of 24.6 % was measured for **I4-S-D** (Fig. 16d) due to its increased molecular weight.

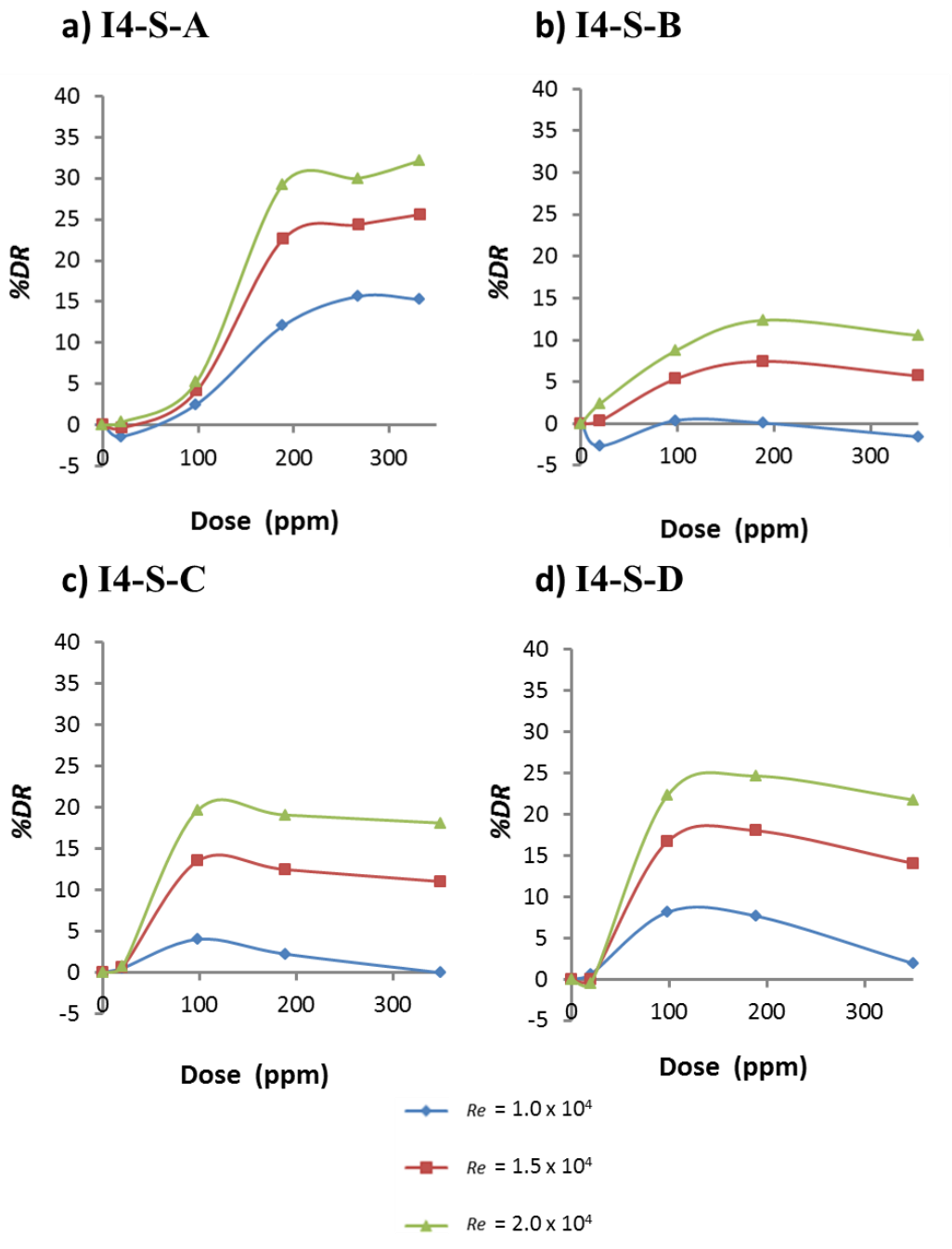

Figure 16: Plot of *%DR* vs Dose for; **a) I4-S-A; b) I4-S-B**; **c) I4-S-C**; **d) I4-S-D**.

The *%DR*$_{MAX}$ for these branched PAA samples (Table 9, Entry **v**-**x**) is plotted against M_n and M_w in Figure 17a and b, respectively. A positive correlation is observed between the molecular weight of the polymer and DRE. A similar trend is shown for both M_n and M_w, suggesting that

the polymer molecular weight dispersity (Đ) does not have a significant impact on the DRE of the polymer. Due to the time intensive nature of the experiment, testing is restricted to a discrete number of doses for each polymer. Unfortunately, this means that the true $\%DR_{MAX}$ may be missed if it lies between doses. A closer correlation between $\%DR_{MAX}$ and M_n or M_w may be expected with a greater number of doses tested.

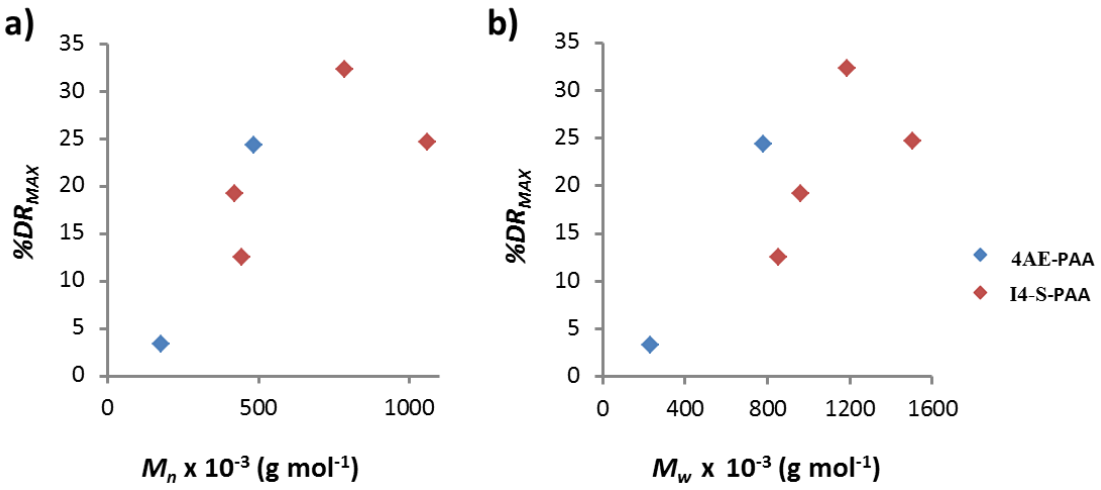

Figure 17: Plot of $\%DR_{MAX}$ vs; **a)** M_n; **b)** M_w. For PAA samples synthesised using **4AE** (blue) and **I4-S** (red) initiators.

Finally, two linear PAA samples **MBP-A** (Table 9, Entry **xi**) and **I2-S-A** (Table 9, Entry **xii**) were tested and the correlation between *%DR* and dose is shown in Figure 18a and 18b, respectively. From these diagrams a similar $\%DR_{MAX}$ (**MBP-A** = 22.7 % at 100 ppm, **I2-S-A** 31.4 % at 100 ppm) can be observed as for the star polymers described above.

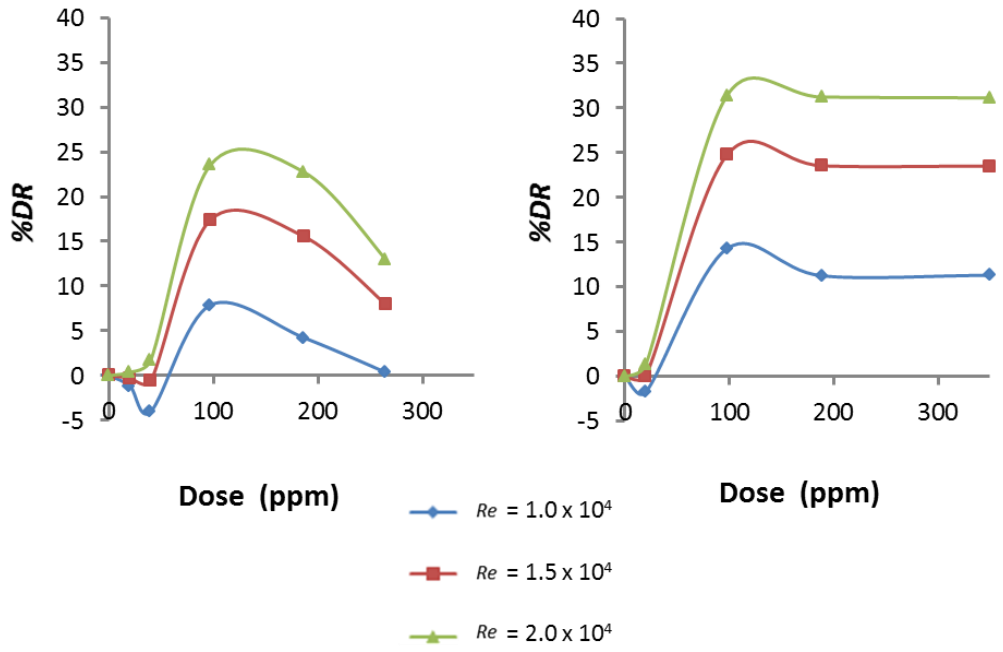

Figure 18: Plot of *%DR* vs Dose for; **a) MBP-A; b) I2-S-A**.

When these values are plotted against M_n and M_w along with the star polymers in Figure 19, a similar trend is followed. This suggests that the polymer topology does not have a significant impact on the DRE of the system. If the linear polymers were much more effective as drag reducing agents it may be expected that there would be a significantly higher *%DR* at equivalent molecular weight.

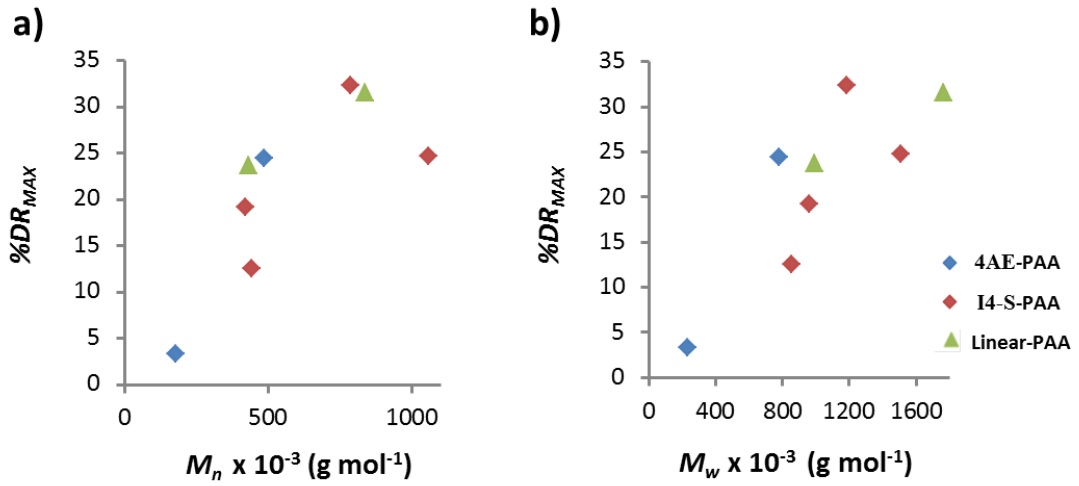

Figure 19: Plot of $\%DR_{MAX}$ vs; **a)** M_n; **b)** M_w. For PAA samples synthesised using **4AE** (blue), **I4-S** (red) and **MBP/I2-S** (green) initiators.

The DRE of the PNaA samples, synthesised using the **I4-T** macro-initiator, was also tested (Table 9, Entry **xiii**-**xviii**). The change in pH with dose was again monitored (Fig. 20), demonstrating that these polymer samples will be ionised during testing. The negative charge

on the polymer backbone will cause the chain to expand in to a more extended, rod-like conformation which may impact the ability of the polymer to reduce drag in turbulent flow.

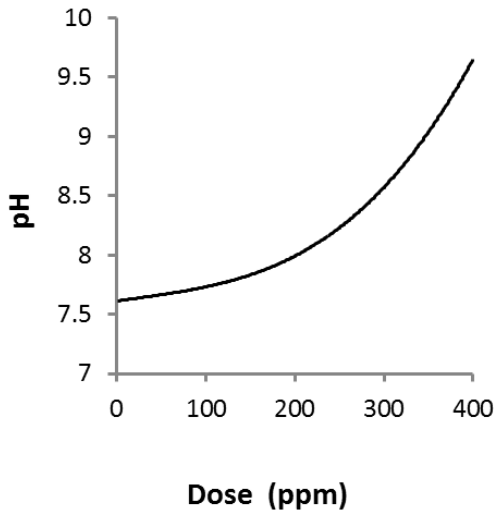

Figure 20: Plot of pH with increased polymer dose during the testing of PNaA samples.

The correlation of *%DR* with dose for each PNaA sample is shown in Figure 21a-f. The graphs for samples **I4-T-A-E**, (Fig 21.a-e) all demonstrate a high *%DR* (*%DR*$_{MAX}$ = 28.9- 32.9 %) which is comparable to the **Praestol** test polymer and the PAA samples. A dose of between 190-330 ppm was necessary to generate these drag reducing effects.

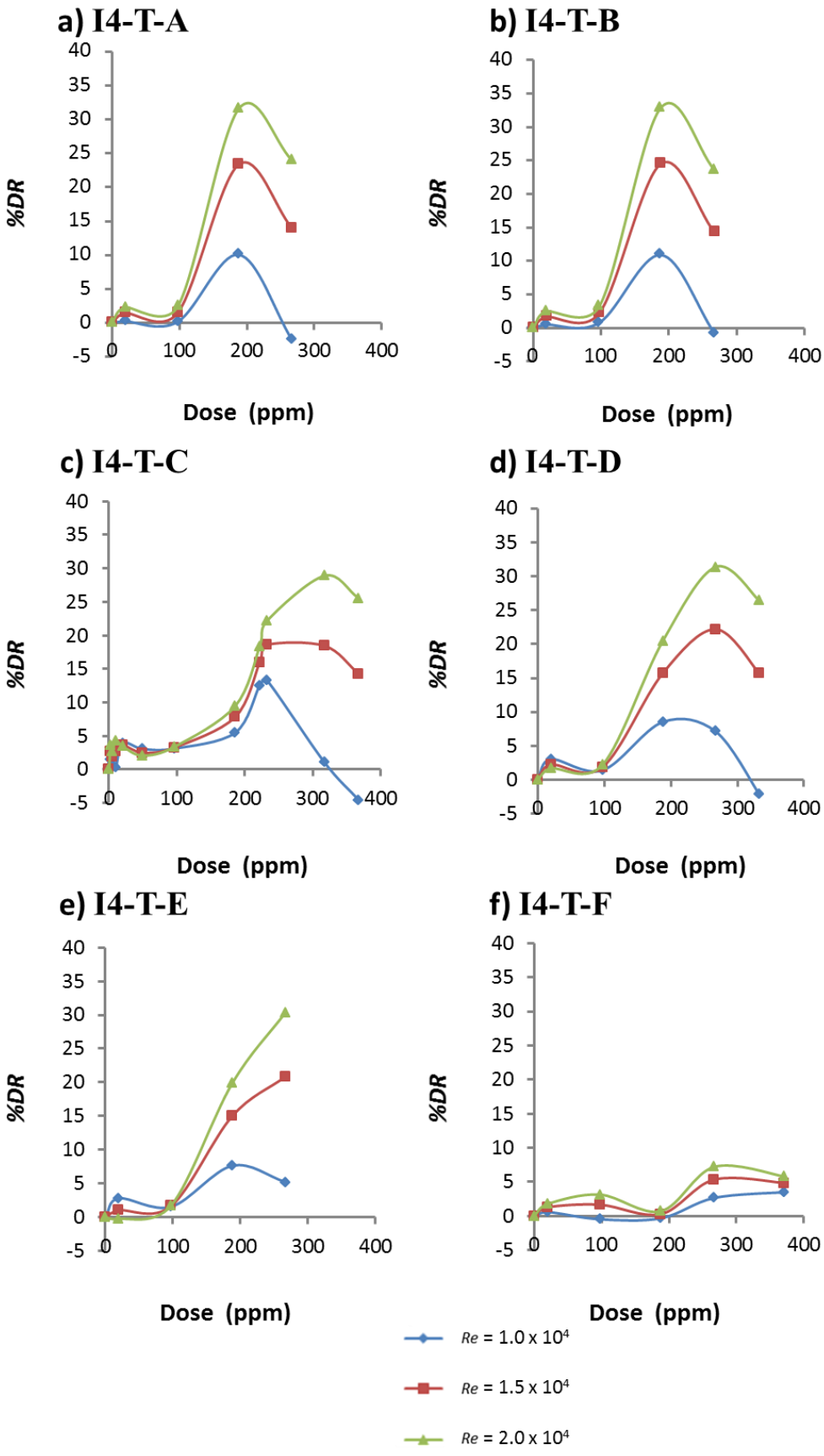

Figure 21: Plot of *%DR* vs Dose for; **a) I4-T-A; b) I4-T-B**; **c) I4-T-C**; **d) I4-T-D**; **e) I4-T-E; f) I4-T-F.**

Despite a having a similar molecular weight, the plot of **I4-T-F** (Fig. 21f, Table 9, Entry **xviii)** demonstrates a much lower *%DR* (*%DR*$_{MAX}$ = 7.2 %) compared with the other PNaA samples, even at high dose. In Figure 22a and 22b, *%DR*$_{MAX}$ is plotted against M_n and M_w for each sample. No correlation can be observed for either graph; this is different to the PAA samples where DRE increased with molecular weight (Fig. 17) as it is expected to for polymer drag reducing systems.

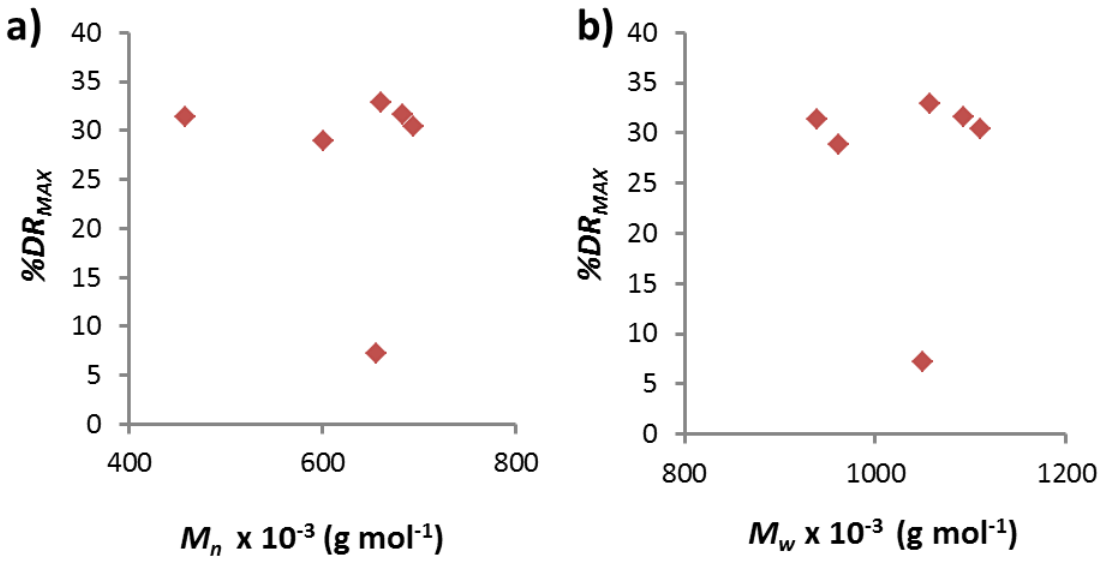

Figure 22: Plot of *%DR*$_{MAX}$ vs; **a)** M_n; **b)** M_w. For PNaA samples synthesised using **I4-T** macro-initiator

It is believed that the lack of correlation between molecular weight and *%DR* may be a consequence of inaccurate measurements using single detection aqueous SEC. When the monomer conversion for the polymerisation reaction for each sample, **I4-T-A-F**, is plotted against *%DR*$_{MAX}$ in Figure 23a, a clear drop in DRE is observed above a conversion of 75 %. Furthermore, when the *%DR* for each sample measured at a dose of 190 ppm, is plotted against conversion in Figure 23b, a linear decrease is observed. Finally, in Figure 23c the dose necessary for *%DR*$_{MAX}$ is plotted against conversion showing a positive correlation. To explain these correlations the uncontrolled nature of the aqueous polymerisation must be considered. In the kinetic investigations described in Chapter 4 (Section 4.3.2.1), HMW polymer chains were produced early in the polymerisation reaction at low conversion. As conversion increased the polymer molecular weight decreased. From these plots it is clear than the highest molecular weight polymer generated early in the reaction is necessary to cause drag reduction. At higher conversions the proportion of the highest molecular weight fraction decreases in the stock solution; therefore decreasing DRE of the polymer sample. It seems that the single detection aqueous SEC may be providing an over-estimate of the polymer molecular weight at

higher reaction conversions. This correlates with discrepancy between M_n measured using NMR and SEC described in Chapter 4 (Section 4.3.2.1), where a lower value was estimated using NMR (M_n(NMR) ≈ 5.00 x 10^5 g mol^{-1} when compared with that of SEC (M_n(SEC) = 6.56 x 10^5 g mol^{-1}).

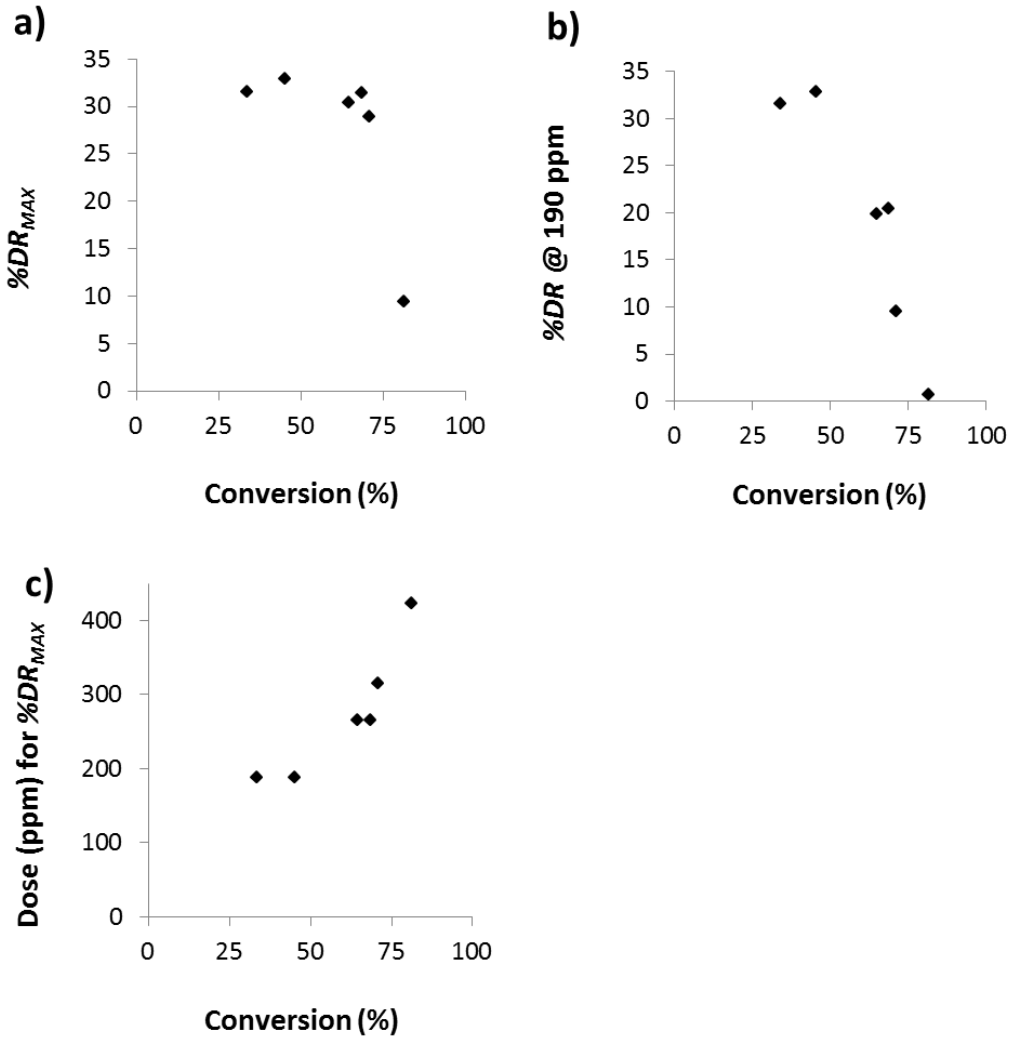

Figure 23: Plot of conversion vs; **a)** *%DR*$_{MAX}$; **b)** *%DR* at a dose of 190 ppm; **c)** Dose (ppm) for *%DR*$_{MAX}$. For the PNaA polymer samples **I4-T-A-F**.

5.3.3. Measurement of polymer mechanical stability

A number of polymer samples with high DRE were selected for testing of their mechanical stability. The tests were conducted by following the change in flow rate and *%DR* over 30 runs through the test rig; the data is summarised in Table 10.

Table 10: Summary of drag reduction and mechanical stability data.

Entry	Sample Code	$\%DR_{MAX}$	Dose (ppm)	*%DR* at 190 ppm	Rate of change of flow rate (ml s^{-1} run^{-1})	% Change of flow rate	Ave. Change in *%DR*
i	**Praestol**	36.5	5.0	N/A	-0.28	-10.2	-12
ii	**PAM-6M**	32.6	20.0	22.6	-0.16	-6.0	-9
iii	**PEO-8M**	57.0	10.0	22.0	-0.26	-8.2	-9
iv	**4AE-B**	24.3	190	24.3	-0.03	-0.5	+3
v	**I4-S-D**	24.6	190	24.6	-0.07	-1.8	-2
vi	**MBP-A**	23.6	100	22.7	-2.90	-12.8	-10
vii	**I4-T-D**	31.4	270	20.5	-0.04	-2.5	-1

`

The commercial polymers; **Praestol**, **PAM-6M** and **PEO-8M** (Table 10, Entry **i-iii**) were first tested and the trend in flow rate for each sample is plotted in Figure 24 (raw data shown in Appendix D, Fig. 2-4). Measurements were conducted at the dose corresponding to $\%DR_{MAX}$ which was 5 ppm (**Praestol**), 20 ppm (**PAM-6M)** and 10 ppm (**PEO-8M**). The graph of each sample demonstrates a clear decrease in flow rate. The gradient of each trend line gives the rate of decrease. The **Praestol** sample (Fig. 24, red), shows a change in flow rate of -0.28 ml s^{-1} run^{-1}. The rate is lower for **PAM-6M** (-0.16 ml s^{-1} run^{-1}, Fig. 24, green) possibly due to the lower molecular weight which decreases its susceptibility to mechanical degradation. A rate of -0.26 ml s^{-1} run^{-1} was measured for **PEO-8M** (Fig. 24, blue), which is comparable to the higher molecular weight **Praestol** sample. The high rate of degradation is believed to be due to the absence of side-groups in the PEO chain. By comparing the flow rate of the first and thirtieth runs, a decrease of 6-10 % was observed for each sample (Table 10, Entry **i-iii**). This further confirms the high level of degradation for these commercial polymers.

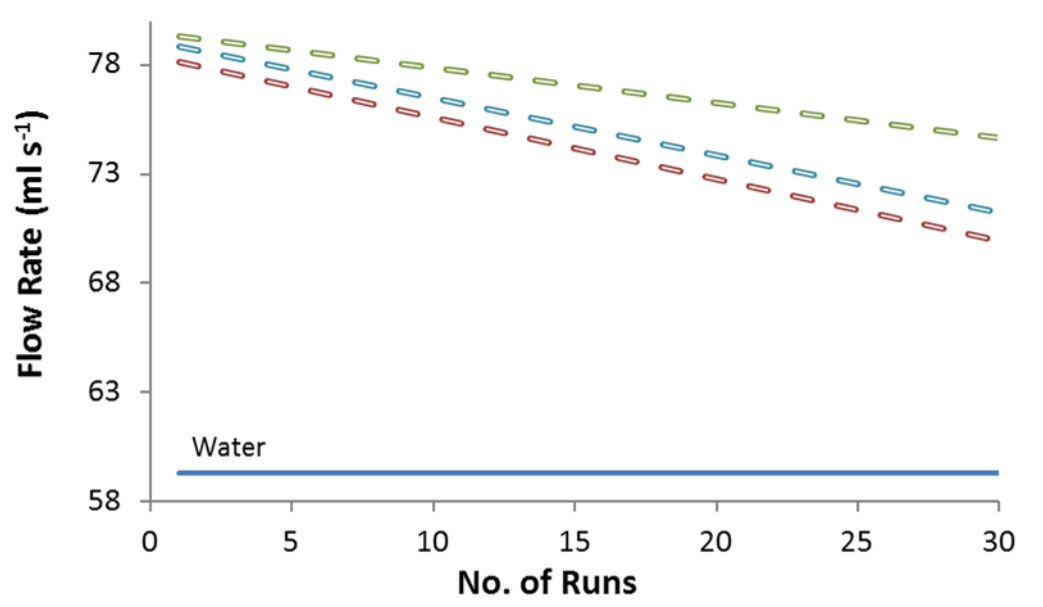

Figure 24: Change in flow rate over consecutive runs through the test rig for; **Praestol** (red); **PAM-6M** (green); **PEO-8M** (blue). Solid blue line corresponds to flow rate of pure water.

The PAA samples synthesised using the **4AE**, **I4-S** and MBP initiators (Table 10, Entry **iv**-**vi**) were then tested at a dose of 190 ppm. The change in flow rate for the star polymers **4AE-B** (black) and **I4-S-D** (red) is plotted in Figure 25 (raw data shown in Appendix D, Fig. 5-6). These samples were chosen for their DRE and also their high molecular weight which should make them most susceptible to mechanical degradation. The graph clearly shows that the decrease in flow rate for these star polymers is much slower in comparison with the test polymers; -0.03 ml s^{-1} run^{-1} and **=** -0.07 ml s^{-1} run^{-1} for **4AE-B** and **I4-S-D**, respectively. These values are ≈ 4-7 times lower than the **Praestol** sample described earlier (Table 10, Entry **i**). The slower decrease in flow rate observed for **4AE-B** *versus* **I4-S-D** may be due to the less flexible core structure, although it may also be a consequence of the slightly lower DP of the polymer (**4AE-B** = 6.7 x 10^3, **I4-S-D** = 14.6 x 10^3). The flow rate for both samples decreased by less than 2 % between the first and thirtieth runs; this is in contrast to 10 % for **Praestol**.

The change in flow rate for the linear PAA analogue, **MBP-A** (Table 10, Entry **vi**), synthesised using the same Cu(0)-mediated polymerisation method, is also shown in Figure 25 (yellow, raw data shown in Appendix D, Fig. 7). A much higher, exponential, decrease in flow rate is observed, with an initial rate of -2.9 ml s^{-1} run^{-1} which is 10 times faster than for **4AE-B** despite a similar DP for these samples (**4AE-B** = 6.7 x 10^3, **MBP-A** = 6.0 x 10^3). For this polymer a decrease in flow rate of 12.8 % was observed between the first and thirtieth run. The comparison between linear and branched molecules is considered to be evidence that the mechanical stability of PAA is improved as a result of branching in its structure. The higher

strength of a star polymer is thought to be a result of the distribution of strain through multiple polymer arms. In addition, the slower decrease in DRE may result from the individual removal of polymer arms. This greatly reduces the impact of polymer chain scission upon the overall molecular weight and hence DRE.

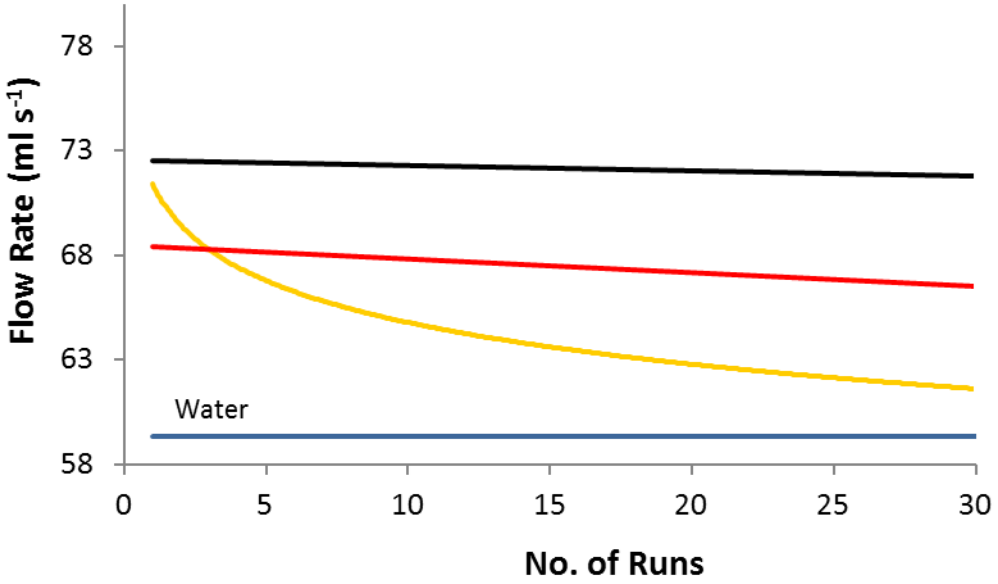

Figure 25: Change in flow rate over consecutive runs through the test rig for; **4AE-B** (black); **I4-S-D** (red); **MBP-A** (yellow). Solid blue line corresponds to flow rate of pure water.

Finally, the PNaA sample, **I4-T-D**, was tested in the same manner (Table 10, Entry **vii**) and the results are plotted in Figure 26 (green, raw data shown in Appendix D, Fig. 8). The slow rate of degradation observed for this polymer (-0.04 ml s^{-1} run^{-1}) is much lower than the test polymers (-0.16—0.28 ml s^{-1} run^{-1}) and linear PAA analogue (-2.9 ml s^{-1} run^{-1}). Whilst the result is comparable to the PAA stars (**4AE-B** and **I4-S-D**), the expanded polymer structure and shielding by counter-ions, due to the high degree of ionisation, may also be a factor in the mechanical stability of this polymer.

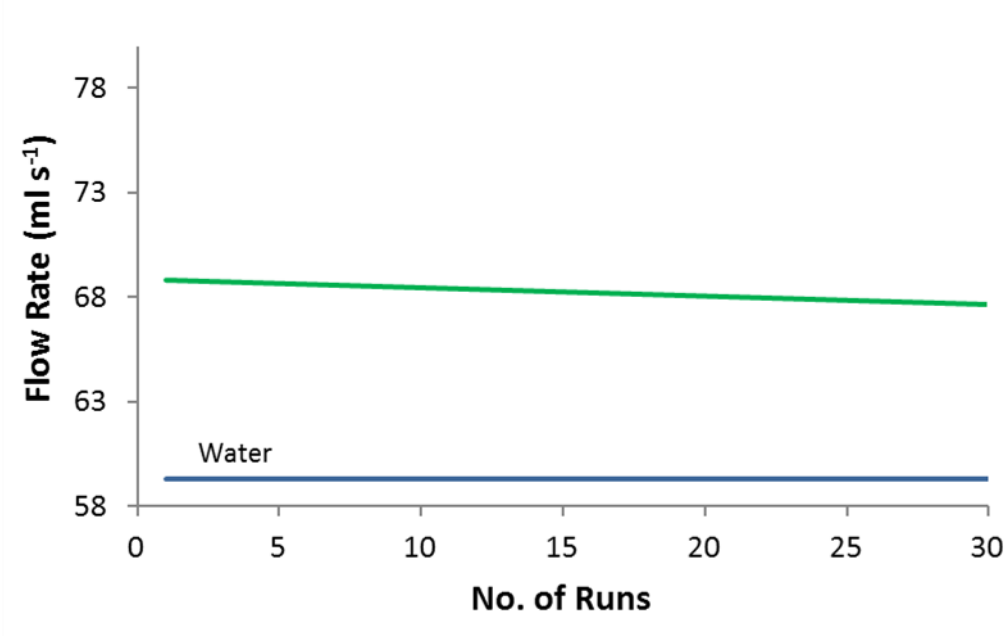

Figure 26: Change in flow rate over consecutive runs through the test rig for; **I4-T-D** (green). Solid blue line corresponds to flow rate of pure water.

Furthermore, *%DR* measured before and after the 30 runs was also compared for each sample. The average difference in *%DR* (measured over three *Re* as described in Section 5.2.5) is plotted as a bar chart in Figure 27. The linear samples (blue) and demonstrate a large decrease for each polymer between 8-12 %. In contrast, the star/branched polymers (red) show a much smaller decrease in *%DR* of less than 2 % after 30 circulations. The **4AE-B** star sample demonstrates a small increase in *%DR* (+3 %).

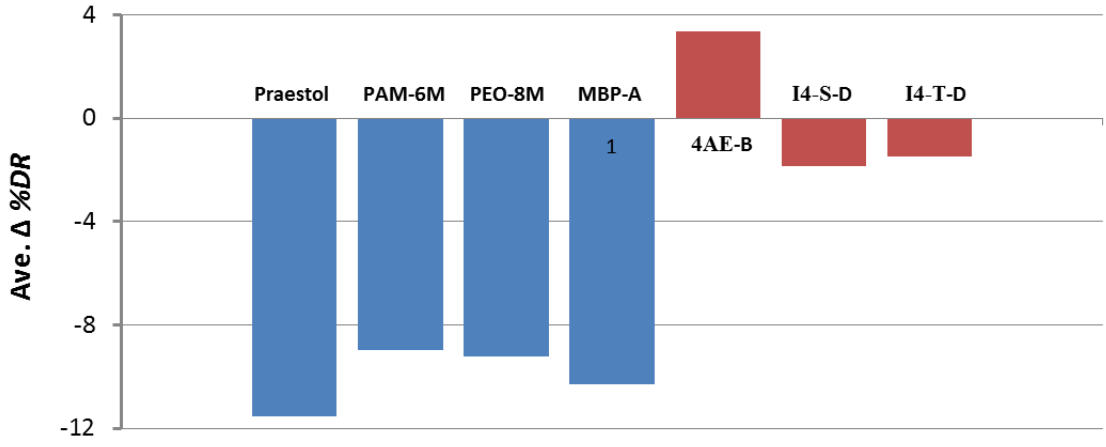

Figure 27: Bar chart plotting the charge in *%DR* before and after 30 runs through the test rig. Linear samples = blue, branched/star samples = red.

The commercial polymers were tested at a dose of 5-20 ppm as these concentrations corresponded to $\%DR_{MAX}$. The PAA/PNaA samples, however, were tested at a higher dose of 190 ppm. In order to investigate the effect of dose on the degradation, the **PEO-8M** sample was repeated at a dose of 190 ppm and the change in flow rate over 30 runs is plotted in Figure 28 (blue, raw data shown in Appendix D, Fig. 9). Due to increased viscosity of the solution at higher concentration, the initial flow rate is lower (71.7 ml s^{-1}) than at $\%DR_{MAX}$ (78.0 ml s^{-1}, Fig. 24, blue). However, in contrast to at lower concentration, flow rate increases with consecutive passes through the test rig (Fig. 28, blue).

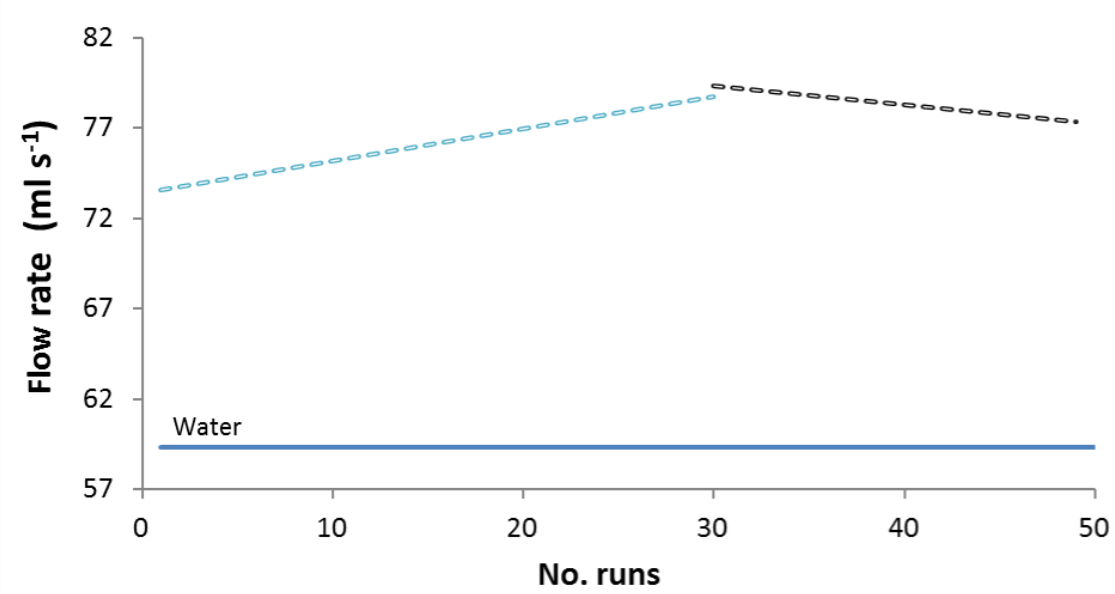

Figure 28: Change in flow rate over consecutive runs through the test rig for **PEO-8M** at dose = 190 ppm; 0-30 runs (blue); 30-50 runs (black) Solid blue line corresponds to flow rate of pure water.

This effect may also be explained as a consequence of chain degradation. For drag reduction to occur, a sufficient quantity of HMW polymer chains is required in the solution. At low dose, corresponding to $\%DR_{MAX}$ (**PEO-8M**, dose = 10 ppm), these HMW chains are degraded as the solution is passed through the test rig and hence DRE decreases. At a dose of 190 ppm the concentration of HMW polymer chains is high. When the solution is passed through the test rig some chains are broken, however, there is still a sufficient number to cause drag reduction. The breaking of these chains also leads to a decrease in solution viscosity and an increase in flow rate. In the example here (**PEO-8M**, Fig. 28 blue), the flow rate increased by 0.17 ml s^{-1} run^{-1} over the first 30 runs; this suggests significant chain degradation in the sample. It was predicted that if the solution was cycled further times, the flow rate would eventually decrease as all the HMW chains are broken. To examine this, the solution was cycled for a further 20

runs and a decrease in flow rate was observed as anticipated (Fig. 28, black, raw data shown in Appendix D, Fig. 9).

Although the aim of the test was to examine mechanical degradation under the turbulent pipe flow conditions, the polymer solution will also experience a large extensional stress as it passes from the pressure tank to the tube (Fig. 29). When studying the mechanical degradation of polymers, it has been shown that extensional stress can have a significant contribution to the degradation of the polymer chains.[6] Moreover, some systems described in the literature attribute degradation entirely to extensional forces experienced upon entering the pipe.[5] Whilst the degradation results discussed here may not be a direct consequence purely of turbulent pipe flow, they should still give an accurate reflection of the relative stability of the polymer chains. Furthermore, contractions such as the one experienced at the beginning of the test rig are regularly encountered in pipe systems to which drag reducing agents are applied.

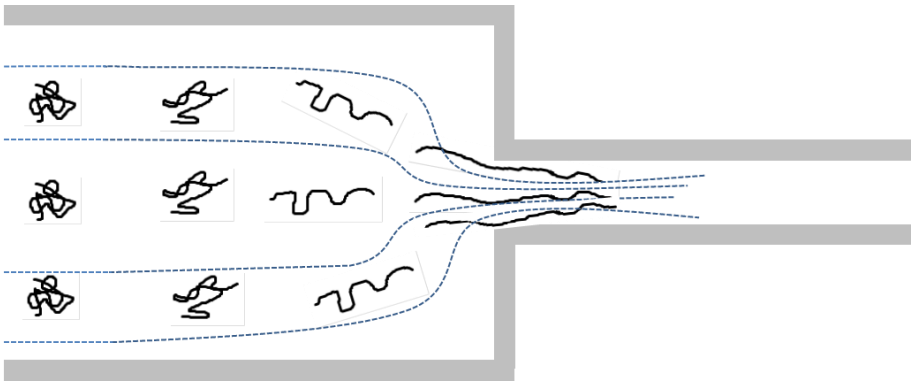

Figure 29: Extensional forces stretch polymer chains upon moving from pressure tank, through contraction, in to pipe.

5.4. Conclusions

A drag reduction test rig under pipe flow conditions was used to measure the drag reducing efficiency of the P*t*BA and PNaA samples synthesised in Chapter 3 and 4, respectively. *%DR* was calculated by comparing the flow rates for a polymer solution at a range of *Re* with those of a pure water sample. The P*t*BA samples were first hydrolysed using TFA to provide water soluble PAA. Exposure of **I4-S** and **I4-T** to the same hydrolysis conditions demonstrated that the ester groups in the core of the molecule were stable in the presence of TFA.

For comparison, a commercially available PAM based drag reducing agent (**Praestol**) and HMW PAM (**PAM-6M**), PEO (**PEO-8M**) and PAA (**PAA-1M**) samples were also tested. **PEO-8M**

provided the highest drag reducing effect ($\%DR_{MAX}$ = 57 %) whilst the PAM samples both allowed *%DR* of over 30 %. No drag reduction was observed for the PAA sample.

When the star shaped **4AE-B** sample was tested, a $\%DR_{MAX}$ of 24.3 % was measured. The lower molecular weight, **4AE-A**, showed no significant drag reduction and this clearly demonstrates the necessity for HMW polymer systems for effective drag reducing agents. The star polymers synthesised using the **I4-S** initiator also demonstrated good DRE, and a positive correlation between M_n and $\%DR_{MAX}$ was observed. The linear PAA analogues synthesised using **MBP** and **I2-S** showed a comparable $\%DR_{MAX}$ suggesting the topology of the polymer did not have a major impact on its ability to cause drag reduction. The PNaA samples synthesised via aqueous polymerisation provided a $\%DR_{MAX}$ of around 30 %, however, the efficiency of the system was shown to decrease as the monomer conversion of the corresponding reaction increased.

The mechanical stability of the polymers was determined by consecutive cycles through the test rig. By following the flow rate of the solution, a rapid decrease was observed for the linear test polymers (**Praestol**, **PAM-6M**, **PEO-8M**). In comparison, the star polymers (**4AE-B**, **I4-S-D**, **I4-T-D**) showed a much slower decrease, suggesting a higher resistance to mechanical degradation. When a linear PAA analogue was tested for comparison it demonstrated a rapid exponential decrease in flow rate. Furthermore, a much higher decrease in *%DR* was observed over 30 runs for the linear samples. This was taken as evidence that the mechanical stability of the polymer system was increased by the introduction of branch points in the chain.

5.5. References

1. Ting, R. Y.; Little, R. C. *Nature-Phys. Sci.* **1973,** 241, 42-44.
2. Kim, O. K.; Little, R. C.; Patterson, R.l.; Ting, R. Y. *Nature* **1974,** 250, 408-410.
3. Kulik, V. M. *Exp. Fluids* **2001,** 31, 558-566.
4. MacMinn, C. The design and construction of a novel pipe flow apparatus for exploring polymer drag reduction. MIT, 2005.
5. Vanapalli, S. A.; Islam, M. T.; Solomon, M. J. *Phys. Fluids* **2005,** 17, 1023-1030.
6. Al Hashmi, A. R.; Al Maamari, R. S.; Al Shabibi, I. S.; Mansoor, A. M.; Zaitoun, A.; Al Sharji, H. H. *J. Pet. Sci. Eng.* **2013,** 105, 100-106.
7. Den Toonder, J. M. J.; Hulsen, M. A.; Kuiken, G. D. C.; Nieuwstadt, F. T. M. *J. Fluid Mech.* **1997,** 337, 193-231.
8. Japper-Jaafar, A.; Escudier, M. P.; Poole, R. J. *J. Non-Newton Fluid* **2009,** 161, 86-93.
9. Wyatt, N. B.; Gunther, C. M.; Liberatore, M. W. *J. Non-Newton Fluid* **2011,** 166, 25-31.

10. Kim, N. J.; Kim, S.; Lim, S. H.; Chen, K.; Chun, W. *Int. Comm. Heat Mass* **2009,** 36, 1014-1019.

11. Shah, S. N.; Kamel, A.; Zhou, Y. *J. Pet. Sci. Eng.* **2006,** 53, 179-188.

12. Choi, H. J.; Kim, C. A.; Jhon, M. S. *Polymer* **1999,** 40, 4527-4530.

13. Sohn, J. I.; Kim, C. A.; Choi, H. J.; Jhon, M. S. *Carbohydr. Polym.* **2001,** 45, 61-68.

14. Kim, C. A.; Lim, S. T.; Choi, H. J.; Sohn, J. I.; Jhon, M. S. *J. App. Polym. Sci.* **2002,** 83, 2938-2944.

15. Sung, J. H.; Kim, C. A.; Choi, H. J.; Hur, B. K.; Kim, J. G.; Jhon, M. S. *J. Macromol. Sci.,-Phys.* **2004,** B43, 507-518.

16. Jafargholinejad, S.; Pishevar, A.; Sadeghy, K. *J. App. Fluid Mech.* **2011,** 4, 1-5.

17. McCormick, C. L.; Hester, R. D.; Morgan, S. E.; Safieddine, A. M. *Macromolecules* **1990,** 23, 2124-2131.

18. Mumick, P. S.; Welch, P. M.; Salazar, L. C.; McCormick, C. L. *Macromolecules* **1994,** 27, 323-331.

19. Kalashnikov, V. N. *J. Non-Newton Fluid* **1998,** 75, 209-230.

20. Camail, M.; Margaillan, A.; Maesano, J. C.; Thuret, S.; Vernet, J. L. *Polymer* **1998,** 39, 3187-3192.

21. Nakken, T.; Tande, M.; Elgsaeter, A. *J. Non-Newton Fluid* **2001,** 97, 1-12.

22. Nakken, T.; Tande, M.; Nyström, B. *Eur. Polym. J.* **2004,** 40, 181-186.

23. Kot, E.; Bismarck, A. *Macromolecules* **2010,** 43, 6469-6475.

24. Pereira, A. S.; Soares, E. J. *J. Non-Newton Fluid* **2012,** 179–180, 9-22.

25. Pereira, A. S.; Andrade, R. M.; Soares, E. J. *J. Non-Newton Fluid* **2013,** 202, 72-87.

26. Maier, M.; Dollendorf, C.; Ritter, H.; Klee, J. E. *Macromol. Chemi. Phys.* **2012,** 213, 2598-2605.

27. Shen, Z.; Chen, Y.; Barriau, E.; Frey, H. *Macromol. Chem. Phys.* **2006,** 207, 57-64.

28. Ma, Q. G.; Wooley, K. L. *J. Polym. Sci., Part A:-Polym. Chem.* **2000,** 38, 4805-4820.

Chapter 6

Conclusions and Future Perspectives

6.1. Summary of Work and General Conclusions

The major aim of this project was the synthesis of an effective water soluble polymer drag reducing system with the following requirements;

1) Acrylamide free

2) Environmentally friendly

3) Oil and surfactant free

4) Mechanically stable

5) Economically viable

The work discussed in this thesis describes the synthesis of branched, water-soluble polymers with high drag reducing efficiency (DRE) and enhanced mechanical stability. These polymers were attained via Cu(0)-mediated polymerisation of *tert*-butyl acrylate (*t*BA) and sodium acrylate (NaA) using multi-functional, PEG based macro-initiators (**I4-S** and **I4-T**). The synthesis of P*t*BA and PNaA was conducted using a simple Cu(0)/TREN catalyst system without the need for inverse-emulsion polymerisation. Cu(0)-mediated polymerisation was chosen for the synthesis of these drag reducing polymers as it allows the rapid production of high molecular weight (HMW) stars at ambient temperature. Star polymers have been shown to increase the mechanical stability of macro-molecular systems by distributing forces across multiple polymer arms. The use of a Cu(0) wire catalyst makes the technique potentially amenable to commercial polymerisation processes; particularly due to the ability to recycle and re-use the catalyst and the low levels of copper contamination in the polymer product.

Previous success of controlled aqueous Cu(0)-mediated polymerisations demonstrated the opportunity to use this environmentally friendly solvent. Multi-functional, water soluble macro-initiators were therefore synthesised in Chapter 2 to allow the production of star polymers in aqueous solution. A branching unit containing a secondary (**BU-S**) or tertiary bromine (**BU-T**) initiation site was first synthesised. The branching units were coupled to each end of a PEG chain (M_n = 3350 g mol^{-1}) to produce a water-soluble macro-initiator with four initiation sites (**I4-S** and **I4-T**). Furthermore, **BU-S** was also coupled to a mono-methoxy PEG chain (M_n = 2000 g mol^{-1}) to produce an analogous macro-initiator with two initiation sites (**I2-S**). The analysis of the products using ^{1}H and ^{13}C NMR spectroscopy and MALDI-Tof MS confirmed the attachment of the branching unit to the PEG chain ends.

In Chapter 3, Cu(0)-mediated polymerisation reactions were conducted in DMSO solvent using *tert*-butyl acrylate (*t*BA) as a protected acrylic acid (AA) monomer. A small molecule initiator, 4,4'-oxybis(3,3-bis(2-bromopropionate)butane (**4AE**) and a simple Cu(0) wire/TREN catalyst system were first studied. Kinetic investigation targeting a molecular weight of 3 x 10^4 g mol^{-1} demonstrated control over the polymerisation reaction. When the target molecular weight was increased to 3 x 10^5 g mol^{-1}, conversion was restricted to 50 % due to the high viscosity of the reaction mixture. The PEG containing macro-initiators (**I4-S** and **I4-T**) were then used for the polymerisation of methyl acrylate (MA) in a homogeneous system (DMSO) (M_n(Target) = 1.4 x 10^4 g mol^{-1}). Both initiators demonstrated high conversion (> 97 %) with dispersity ($Đ$) of 1.47 and 1.26 for **I4-S** and **I4-T** respectively, highlighting the control over the polymerisation reaction. Initial comparison of **I4-S** and **I4-T** for the polymerisation of *t*BA (M_n(Target) = 3.4 x 10^4 g mol^{-1}) demonstrated control when using **I4-S** ($Đ$ = 1.30) but poor control for **I4-T** ($Đ$ = 4.38). However, when the kinetics of the **I4-S** reaction was investigated in more detail, a lack of control was observed. Upon increasing the target molecular weight to 3 x 10^5 g mol^{-1}, a linear increase in both conversion with time, and M_n with conversion were demonstrated. The values of M_n were much higher than theoretical suggesting a low I_{eff} when using the macro-initiator in this system.

A model system using methyl 2-bromopropionate (**MBP**) initiator was used to investigate the effect of changing reaction conditions on control of polymerisation (M_n(Target) = 1 x 10^4 g mol^{-1}). The addition of $CuBr_2$, and the reduction of monomer concentration and catalyst surface area were all investigated; however, successful control over the polymerisation reaction could not be achieved. It was concluded that the rapid formation of a biphasic reaction mixture prevented access of the $CuBr_2$ deactivator to the active chain ends. This disrupted the activation/deactivation cycle allowed an uncontrolled radical mechanism to proceed in the polymerisation reaction mixture. The increased steric hindrance of the **4AE** was thought to contribute to the control observed with this initiator. The scale of the polymerisation of *t*BA and the target molecular weight (3 x 10^5 – 1 x 10^6 g mol^{-1}) were both increased to synthesise samples for drag reduction testing using a range of initiators (MBP, **4AE**, **I4-S**, **I2-S**). Whilst good conversion and control was seen for the **4AE** initiator, the reaction using **I4-S** was restricted to 22 % monomer conversion due to the high viscosity of the mixture. The conversion was improved to 44 % by reduction of copper wire surface area though a simultaneous increase in polymer dispersity was observed. When the intrinsic viscosity (*IV*) of the star and linear polymers were compared at equivalent M_w, a lower value was observed for the **4AE**/**I4-S** samples suggesting higher levels of branching for these polymers.

Cu(0)-mediated polymerisation was conducted in aqueous solution in Chapter 4 using sodium acrylate (NaA) at a pH of 7-8. The **I4-S** and **I4-T** macro-initiators were compared for the polymerisation of NaA, with **I4-T** demonstrating a much higher monomer conversion. This initiator was therefore used for subsequent polymerisation reactions in this chapter. When the polymerisation kinetics were examined (M_n(Target) = 3.4 x 10^4 and 3 x 10^5 g mol^{-1}), the results were characteristic of a free radical polymerisation mechanism showing a decrease in M_n with conversion and an increase in dispersity throughout the reaction. Despite this, ^{1}H NMR spectroscopy of the product after several re-precipitations suggested a constant level of PEG macro-initiator in the system, confirming incorporation of the macro-initiator in to the product. It was proposed that radicals were introduced in the system *via* halide abstraction by Cu(0)/TREN without subsequent deactivation, and the free-radical mechanism was likened to the ceric ammonium nitrate (CAN) polymerisation technique. A slow generation of radicals throughout the reaction allowed high monomer conversion to be reached. The Cu(0)/TREN catalyst system was compared with a method utilising the pre-disproportion of CuBr in aqueous solution. This allowed high concentration of $CuBr_2$ deactivator from the beginning of the reaction. Using this method a much closer agreement was observed between M_n and the theoretical value, suggesting much higher control of the reaction. A conversion of 70 % was reached in 1 h demonstrating the fast reaction rate using this system, possibly due to the formation of highly active nascent Cu(0).

The DRE of the P*t*BA and PNaA polymers synthesised, was tested in Chapter 5 using a pipe flow test rig. The P*t*BA samples were first hydrolysed using trifluoroacetic acid (TFA) to give water soluble poly(acrylic acid) (PAA). Exposure of the macro-initiators (**I4-S** and **I4-T**) to the same hydrolysis conditions demonstrated that the P*t*BA side chains were selectively cleaved while the ester groups in the core were stable in the presence of TFA. Several commercially available polymers (**Praestol**, **PAM-6M**, **PEO-8M**, **PAA-1M**) were also tested for comparison. The PAM (**Praestol**, **PAM-6M**) samples demonstrated a $\%DR_{MAX}$ of 30-40 % whilst **PEG-8M** allowed a drag reduction of almost 60 %. No drag reducing effect was observed for the PAA sample. Measurement of the two PAA samples synthesised using **4AE** demonstrated the necessity of HMW polymers for effective drag reducing systems. At lower MW (**4AE-A**) almost no drag reduction was observed whereas the higher MW sample (**4AE-B**) gave a $\%DR_{MAX}$ (24.3 %). The PEG containing PAA samples (**I4-S-A-D**) also provided good DRE ($\%DR_{MAX}$ ≈ 12-30 %) and a plot of $\%DR_{MAX}$ against M_n for the star shaped polymers demonstrated a positive correlation. Linear samples synthesised using the **MBP** and **I2-S** initiators also provided a comparable $\%DR_{MAX}$ suggesting the polymer topology did not have a major impact on DRE. A $\%DR_{MAX}$ of around

30 % was also obtained for the PNaA samples synthesised using **I4-T**, however, a decrease in efficiency was observed when the monomer conversion of the corresponding reaction increased.

The mechanical stability of the polymer chains was tested by repeatedly circulating the samples through the drag reduction test rig. By measuring *%DR* before and after 30 cycles, and by monitoring the flow rate for each run, the decrease in DRE (therefore mechanical stability) of the polymer could be followed. From these measurements a much lower rate of degradation was shown for the star polymers when compared with the commercial samples. Moreover, when the linear PAA analogue (**MBP-A**) was measured, a rapid exponential decrease in flow rate demonstrated that the linear chains were degraded at a much faster rate. The difference in *%DR* for the linear samples was consistently around 10 % whereas the star polymers decreased by a maximum of just 2 %.

6.2. Future Perspectives

It was been demonstrated in this work that HMW star polymers (PAA/PNaA) synthesised using Cu(0)-mediated polymerisation can reduce the friction experienced by water flowing through a pipe. For example, the **4AE-B** sample (4.84 x 10^{-5} g mol^{-1}) demonstrated $\%DR_{MAX}$ of 24.3% at a dose of 190 ppm. In order to make these polymers more efficient at lower doses, the molecular weight of the polymer samples must be increased. By increasing the $[M]_0$:$[I]_0$ ratio for the polymerisation reaction, a higher molecular weight can be targeted and the efficiency and mechanical stability of the resulting polymer examined. In order to overcome the high viscosity when targeting a HMW, mechanical stirring apparatus may be useful to maintain consistent mixing and heat transfer.

To extend the mechanical stability studies further, star polymers must be synthesised with a range of molecular weights and degrees of branching. This will allow a clearer elucidation of the impact of branching points on the strength of the polymer chain in turbulent pipe flow. It would also be informative to examine the polymer strength using an extensional rheometer as this removes some of the complications associated with turbulent flow. Finally, analysis of the polymer chains post-degradation using size exclusion chromatography (SEC) would provide insight into mechanism of polymer degradation i.e. single arm at a time or in the polymer core. In this work we used DMSO as a solvent for the polymerisation of *t*BA in order to reduce copper contamination and to reduce star-star coupling whilst targeting HMWs and conversions. For the purpose of a clear comparison of polymer properties, it is suggested that controlled polymerisation reactions may be more easily conducted using a good solvent for

both *t*BA and P*t*BA (e.g. Acetone, DMF). In order to avoid star-star coupling in these reactions it may be necessary to make use of very high [M]:[I] whilst restricting monomer conversion. Furthermore, it is likely that by utilising a combination of Cu(0)/$CuBr_2$/Me_6-TREN in this system optimum conditions for control of the polymerisation will be provided. These conditions were not suitable for the purposes discussed in this work, due to the restrictions of commercial processes.

The molecular weights obtained for the star polymers described here were measured using triple detection SEC, in comparison with linear standards. In order to more accurately determine the arm length of the P*t*BA star polymers it may be possible to hydrolyse the polymer arms via the ester linkages in the core. SEC analysis of the resulting linear polymer chains should provide a more precise determination of the arm length and by analysing the dispersity of the arm lengths, further information on the control of the polymerisation can be gained. Furthermore, it may be possible to visualise these high molecular weight stars polymers using atomic force microscopy. Analysis of the PNaA samples using aqueous SEC with triple detection would give a more accurate determination of molecular weight for these samples when compared with the single detection described here. This is likely to give a more accurate correlation between M_n and *%DR* than described in Chapter 5.

In addition to the PAA/PNaA samples tested, it would be useful to examine further non-acrylamide water soluble monomers (such as styrene sulfonate, poly(ethylene glycol) methacrylate, hydroxyethyl acrylate) for use as drag reducing agents following polymerisation to HMW. By changing the monomer functionality or combining two or more monomers in a block co-polymer, samples with a wide range of properties (flexibility, hydrodynamic volume, inter-molecular associations) could be synthesised.

The aqueous polymerisation of NaA using the **I4-T** initiator was uncontrolled due to low $CuBr_2$ levels in the reaction mixture. It was speculated that the Cu(0)/TREN system initiated free radical polymerisation in the presence of the alkyl halide containing **I4-T** macro-initiator and the mechanism was compared with a polymerisation initiated using ceric ammonium nitrate (CAN). It may be productive to further investigate this system by changing reaction conditions, for example, temperature, catalyst loadings or quantity of initiator. This may provide a simple method to produce branched polymers for use as DRAs. When the catalyst system was generated in situ through the pre-disproportionation of CuBr, a much closer agreement was observed between M_n and the theoretical value. It would be interesting to investigate this

method for the production of a PEG-PAA, H-shaped star co-polymer through the direct polymerisation of NaA and without the use of protected monomers.

In this work the DRE of polymer systems was determined using a pipe flow system. Whilst this allows realistic determination of *%DR*, it would be also interesting to conduct measurements using a rotational rheometer with double gap geometry. This method requires a smaller quantity of sample and is less time consuming than the drag reduction test rig. By taking a high sensitive torque measurement using the rheometer, accurate determination of *%DR* and polymer mechanical stability should be possible. A comparison between the two methods would be of interest. The PAA and PNaA samples were both tested in tap water with pH changing throughout due to the increased dose of acidic or basic polymer. The degree of polymer ionisation will impact the shape of the polymer in solution and also the level of interactions between different polymer chains. In order to truly compare these samples it is necessary to conduct the measurements in solution, with pH maintained constant throughout using a buffer. It may also be useful to test the samples under conditions relevant to real world applications (for example in the presence of different salts). Measurements under these conditions may be simplified by using a rotational rheometer with a smaller sample size.

A clear focus of this work was to reduce the environmental impact of the drag reducing polymer system. Once used, the current HMW polymer systems accumulate in the environment and cannot be broken down. The introduction of labile groups within the polymer chain, should allow post-use degradation of the polymer, therefore reducing the impact of this accumulation. In the work described here, it was hoped that the addition of ester groups in the core of the molecule may provide the opportunity for the drag reducing polymers to be degraded. Although there was not sufficient time to study this, it would be of interest to determine the long term stability of the drag reducing star polymers under conditions relevant to their use as drag reducing agents.

Appendix A

Appendices for Chapter 2

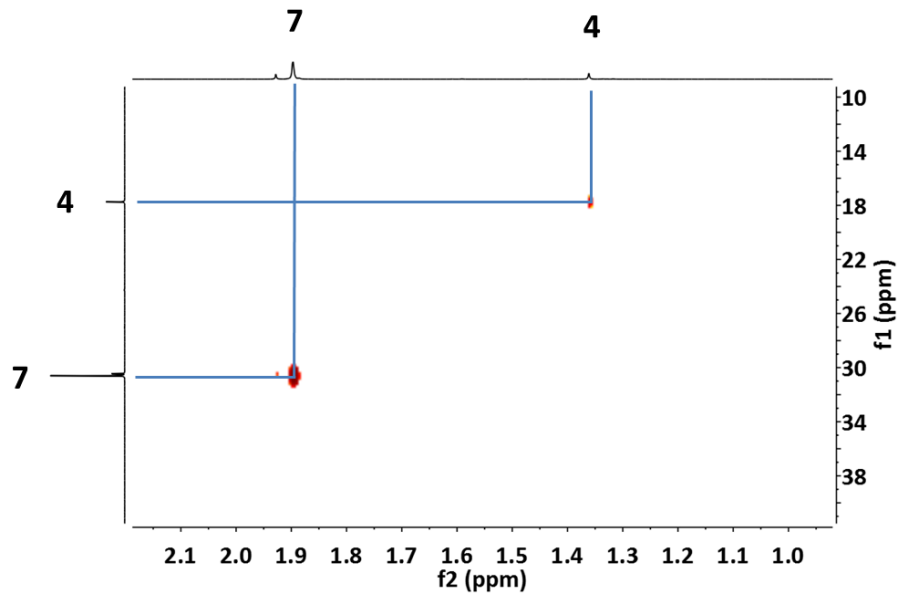

Figure 1: 700 MHz-^{1}H-^{13}C HSQC spectrum of **BU-T**, highlighting the correlation between the proton and carbon resonances of **4** and **7**.

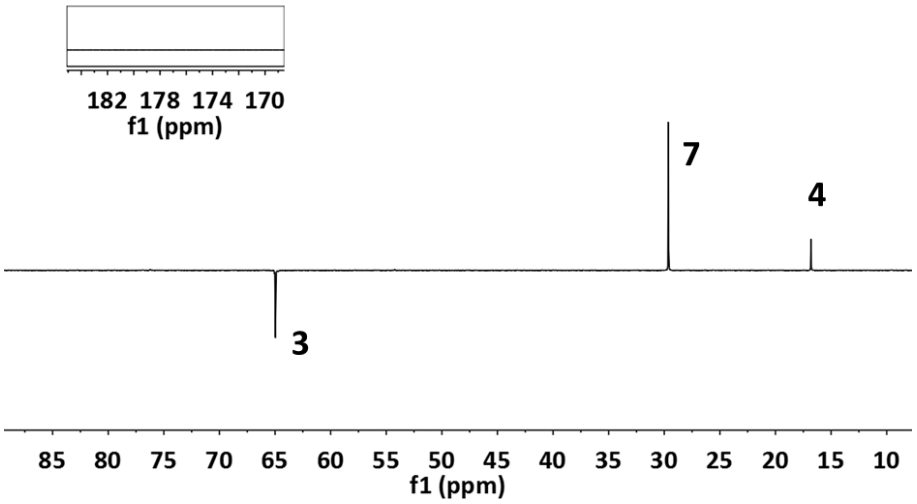

Figure 2: 100 MHz-^{13}C DEPT spectrum of **BU-T**, carbonyl region inset.

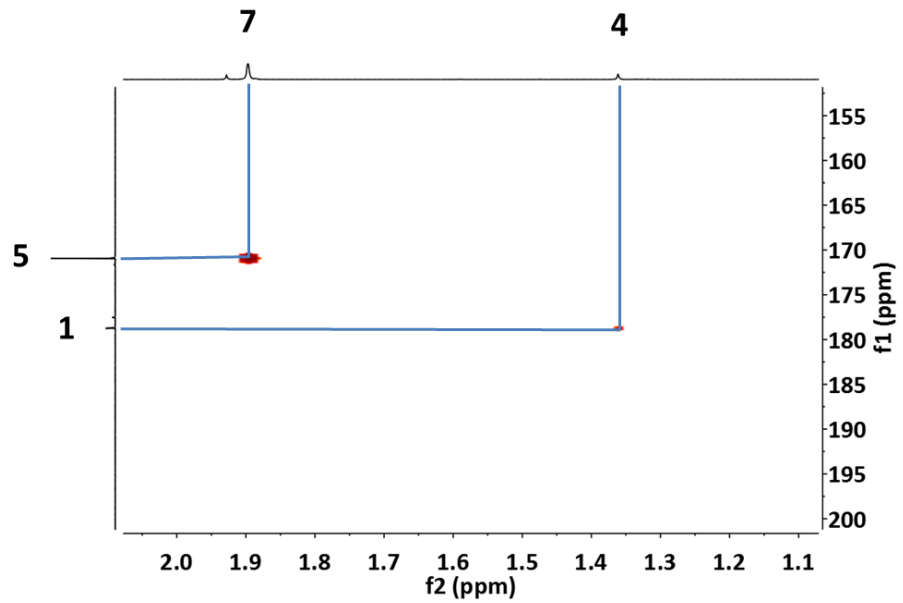

Figure 3: 700 MHz-^{1}H-^{13}C HMBC spectrum of **BU-T**, highlighting the correlation between **7** - **5** and **4** - **1**.

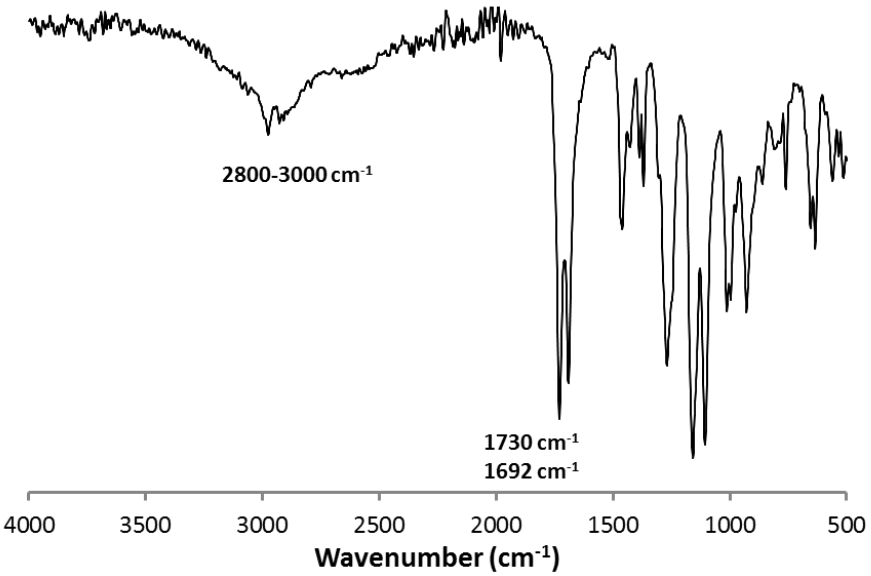

Figure 4: FT-IR spectrum of **BU-T**.

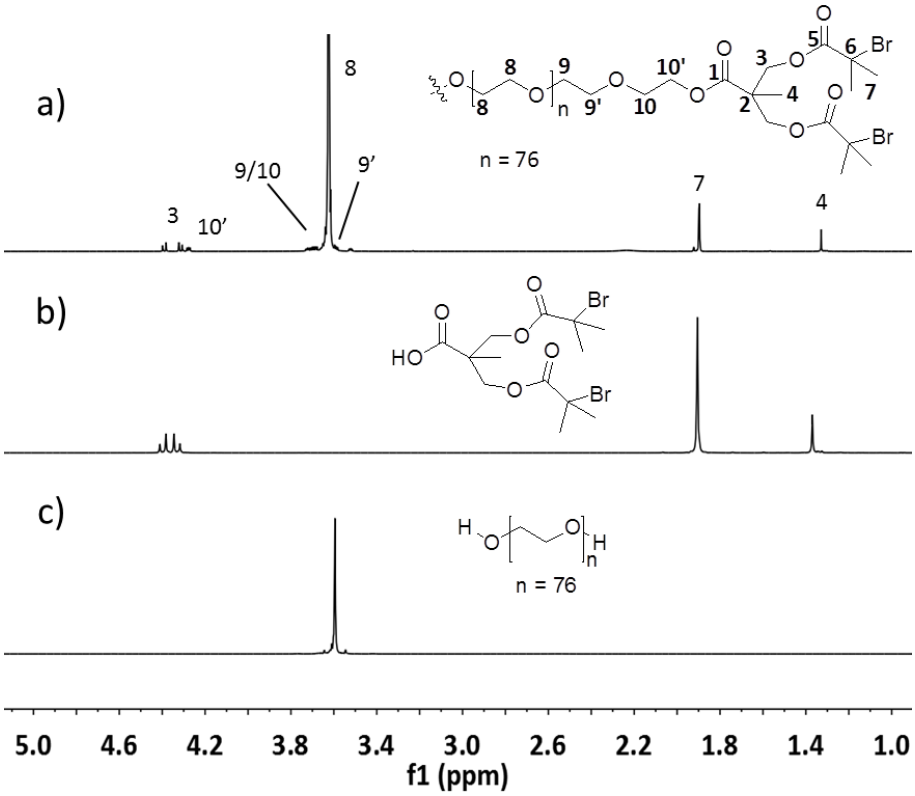

Figure 5: 700 MHz-^{1}H NMR spectrum of; **a) I4-T**; **b) BU-T**; **c)** PEG-3350.

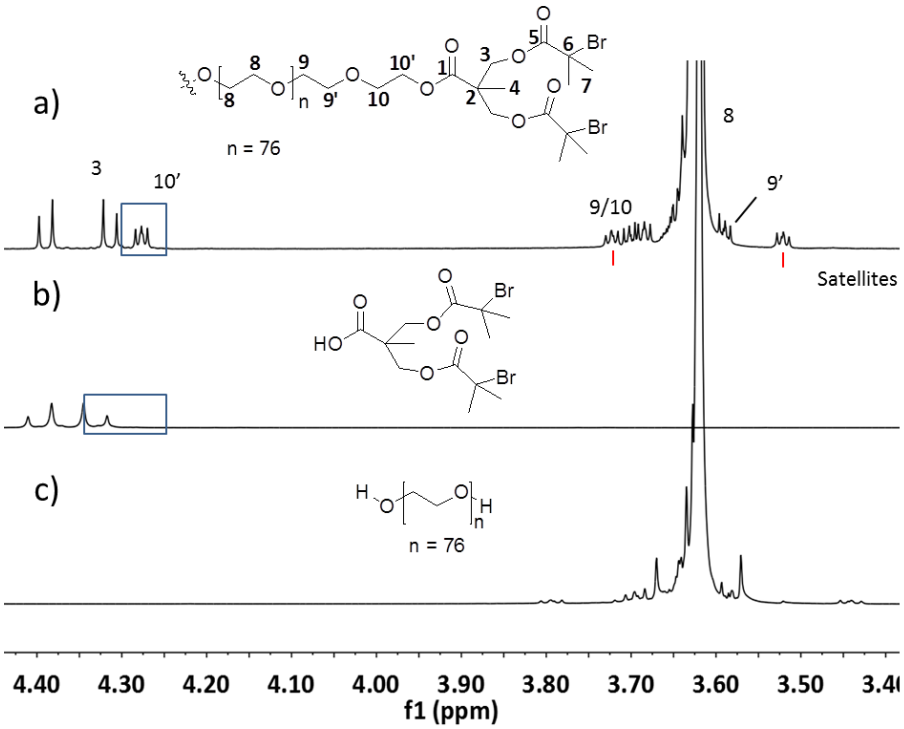

Figure 6: 700 MHz-^{1}H NMR spectrum of: **a) I4-T**, **b) BU-T**, **c)** PEG-3350 expanded to highlight the PEG chain resonances.

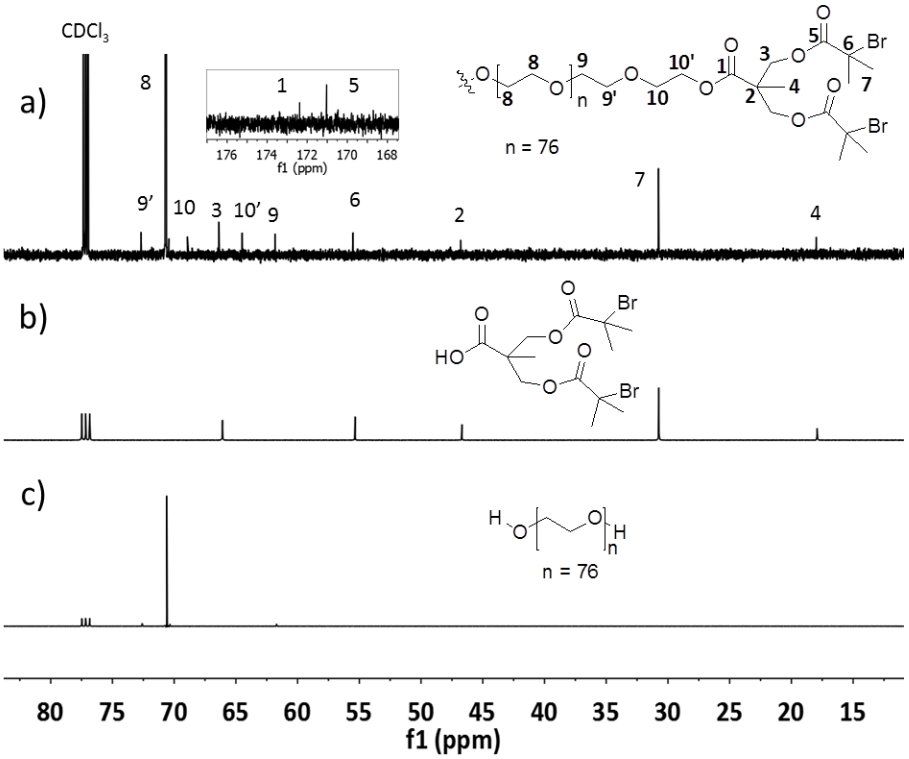

Figure 7: 176 MHz-^{13}C NMR spectrum of; **a)** **I4-T**, carbonyl region inset; **b)** **BU-T**; **c)** 100 MHz-^{13}C NMR spectrum of PEG-3350.

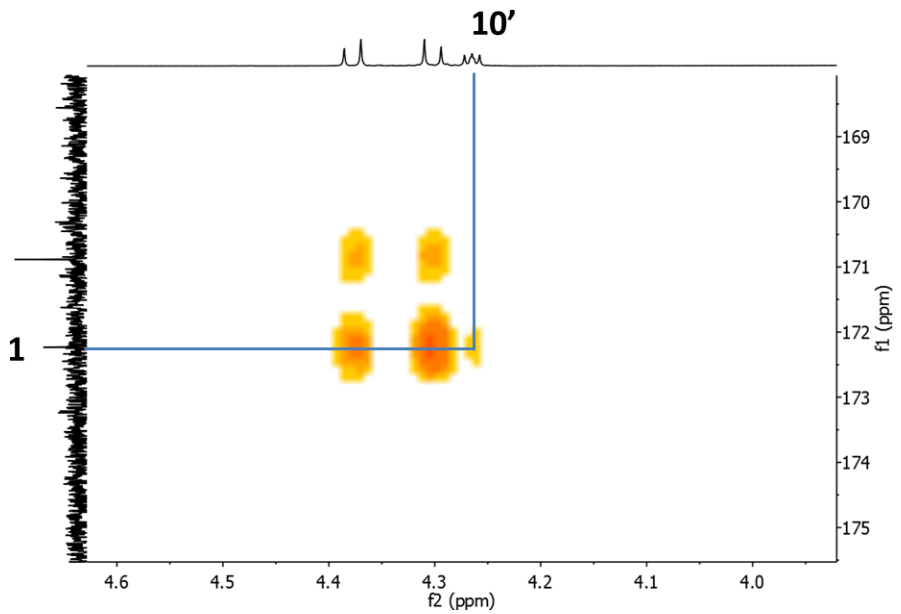

Figure 8: 700 MHz-^{1}H-^{13}C HMBC spectrum of **I4-T** highlighting the correlation between **1** (carbon) and **10’** (proton) environments.

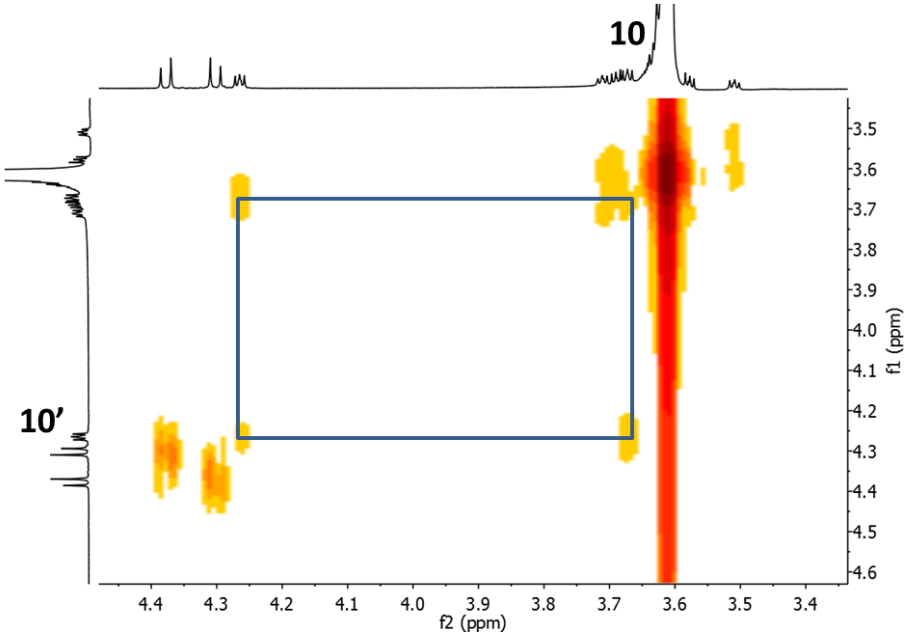

Figure 9: : 700 MHz-^{1}H-^{1}H COSY spectrum of **I4**-T highlighting the correlation between **10** and **10'** proton environments.

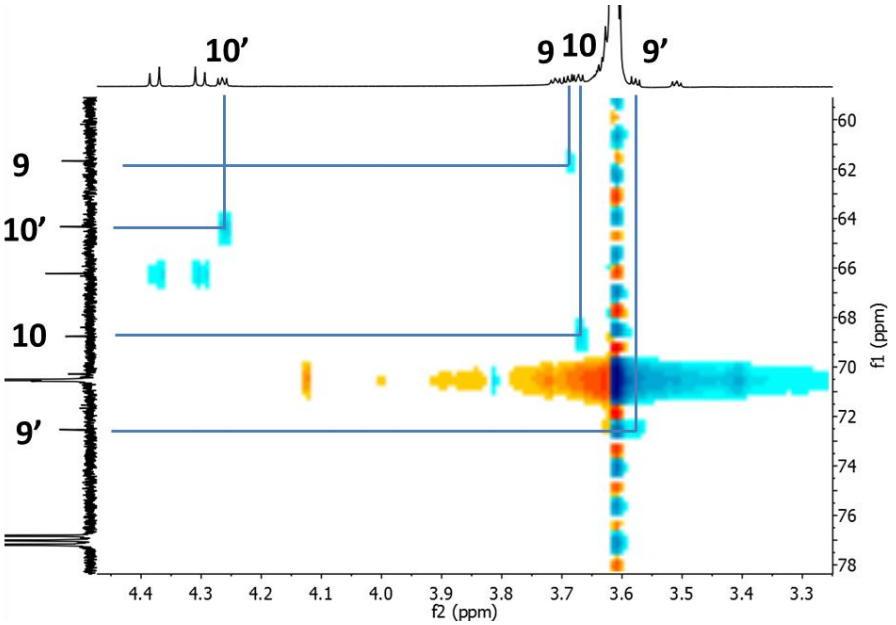

Figure 10: 700 MHz-^{1}H-^{13}C HSQC spectrum of **I4-T** highlighting the correlation between carbon and proton environments of **9** and **10**.

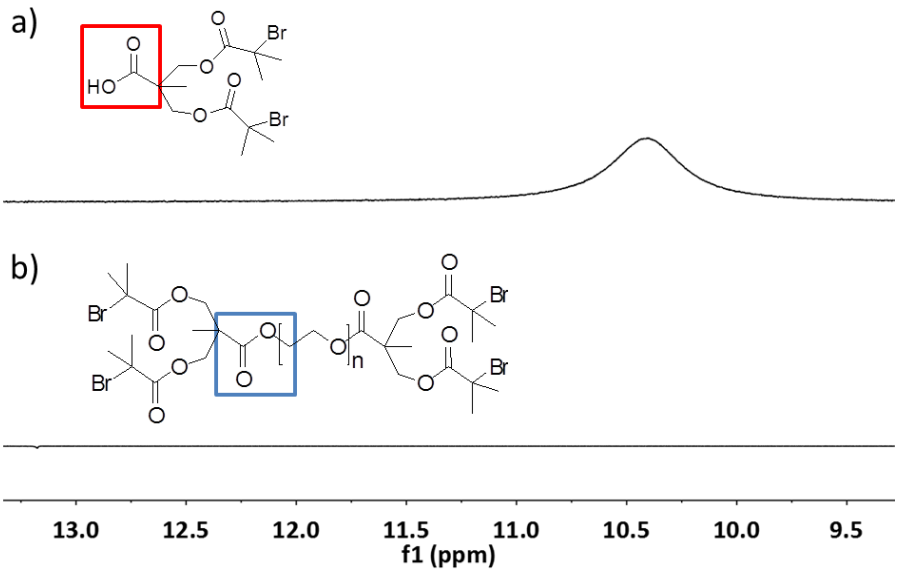

Figure 11: 700 MHz-^{1}H NMR spectrum of: **a) BU-T**, **b) I4-T** highlighting the disappearance of the carboxylic acid resonance.

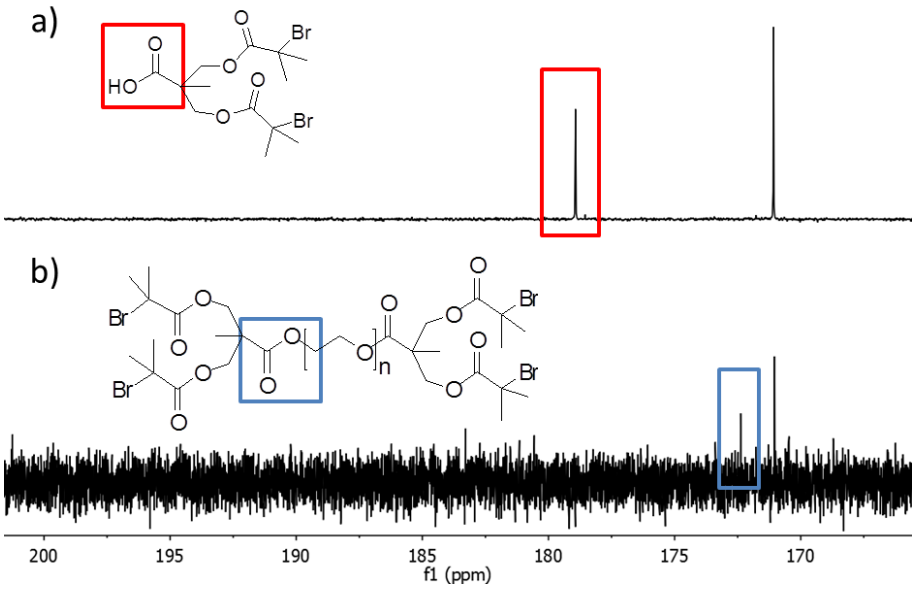

Figure 12: 176 MHz-^{13}C NMR spectrum of; **a) BU-T**; **b) I4-T** highlighting the shift in the C=O resonance as it is converted from a carboxylic acid to an ester group.

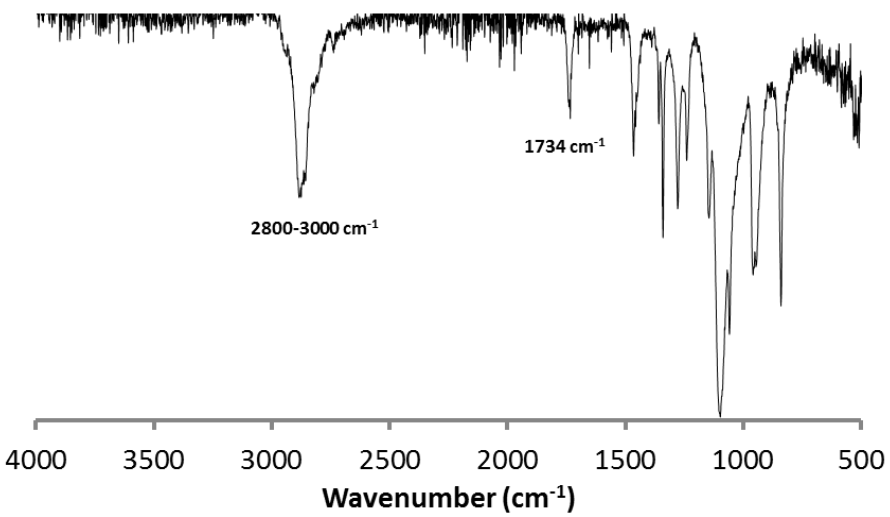

Figure 13: FT-IR spectrum of **I4-T**.

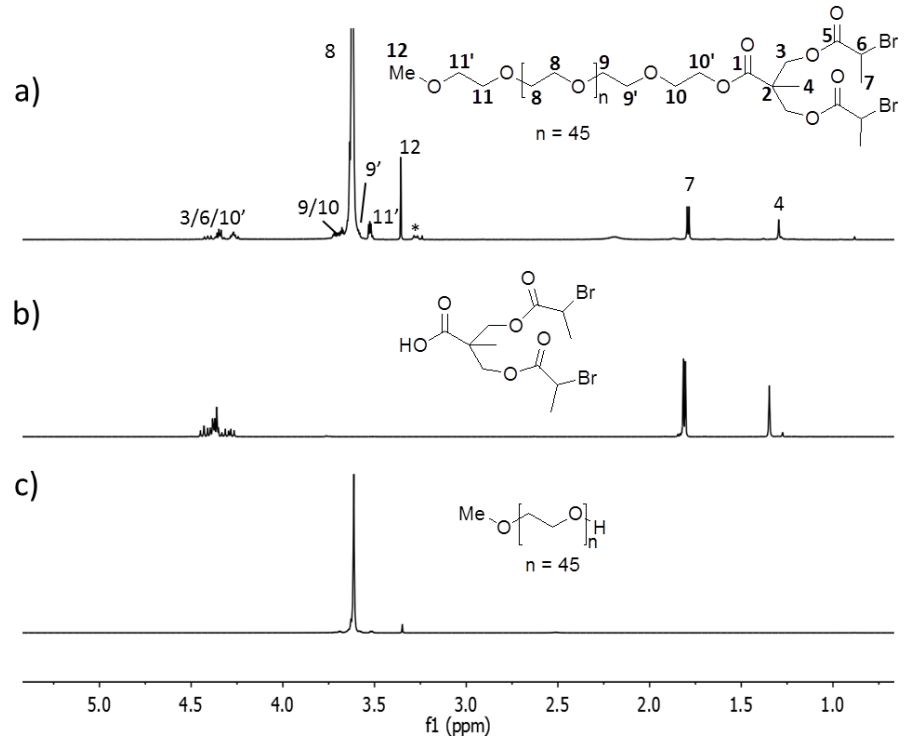

Figure 14: 700 MHz-^{1}H NMR spectrum of; **a) I2-S**; **b) BU-S**; **c)** PEG-3350. * = Unidentified peak.

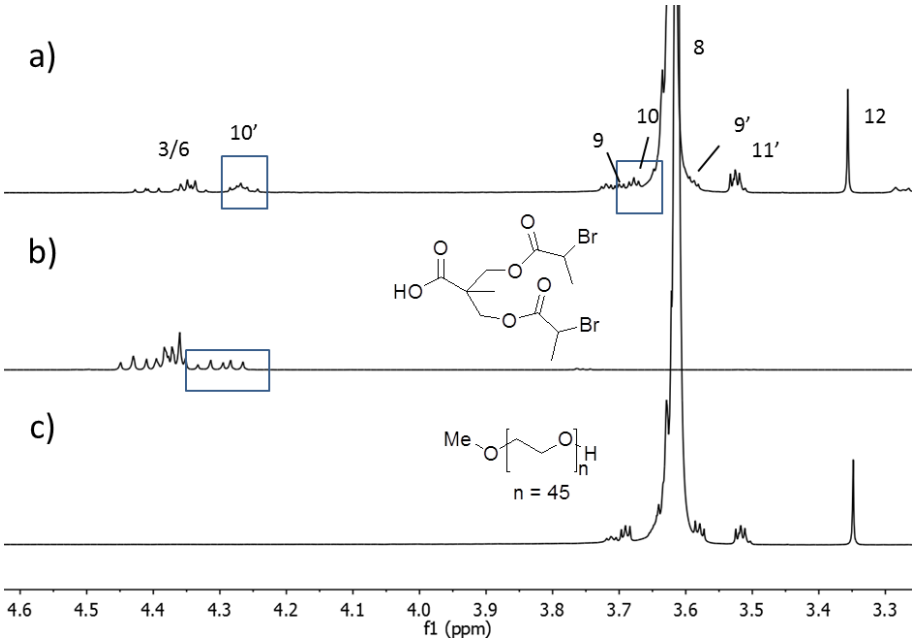

Figure 15: 700 MHz-^{1}H NMR spectrum of: **a) I2-S**, **b) BU-S**, **c)** PEG-3350 expanded to highlight the PEG chain resonances.

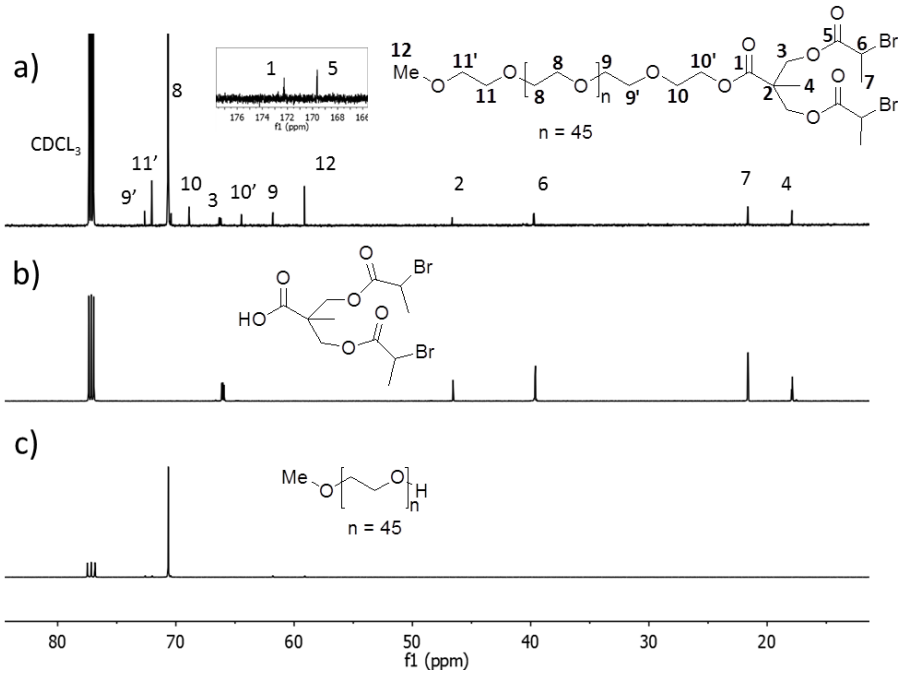

Figure 16: 176 MHz-^{13}C NMR spectrum of; **a) I2-S**, carbonyl region inset; **b) BU-S**; **c)** 100 MHz-^{13}C NMR spectrum of PEG-3350. * = Unidentified peak.

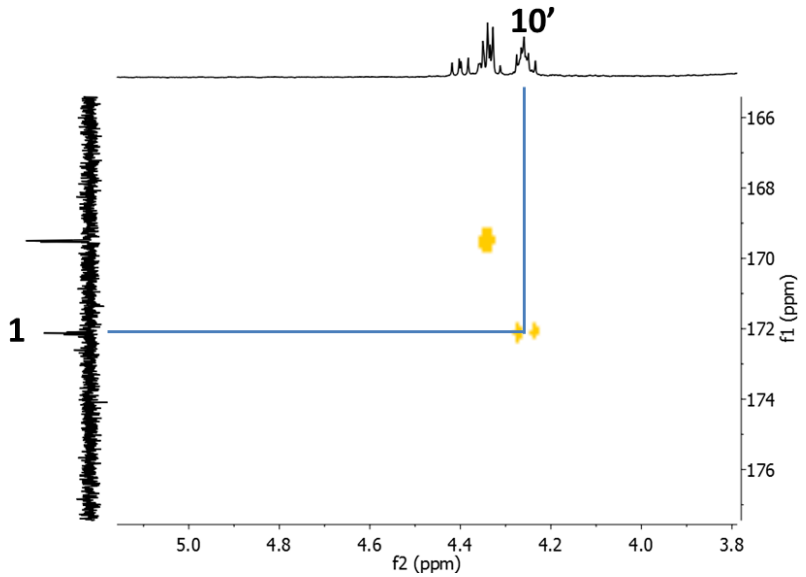

Figure 17: 700 MHz-^{1}H-^{13}C HMBC spectrum of **I2-S** highlighting the correlation between **1** (carbon) and **10'** (proton) environments.

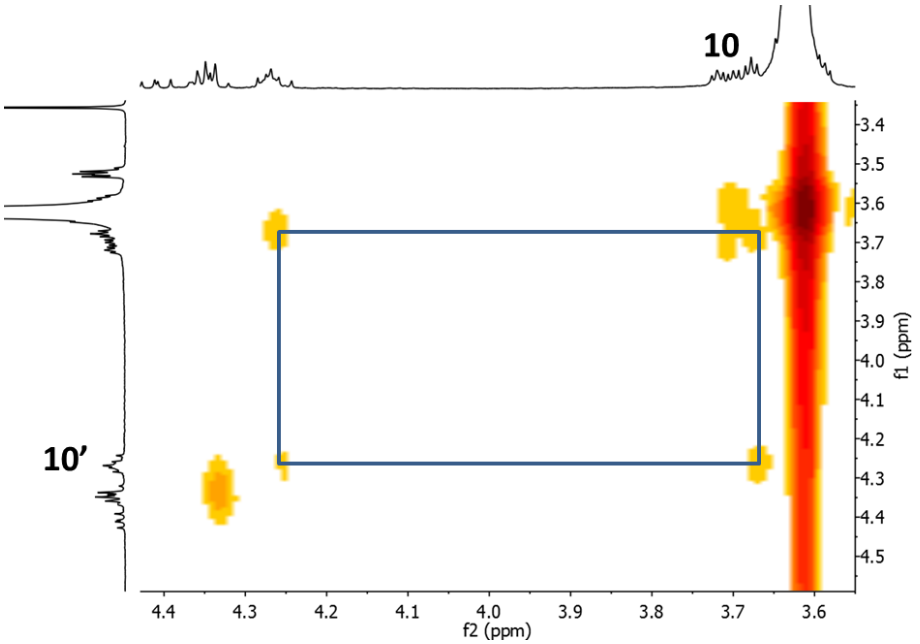

Figure 18: 700 MHz-^{1}H-^{1}H COSY spectrum of **I2-S** highlighting the correlation between **10** and **10'** proton environments.

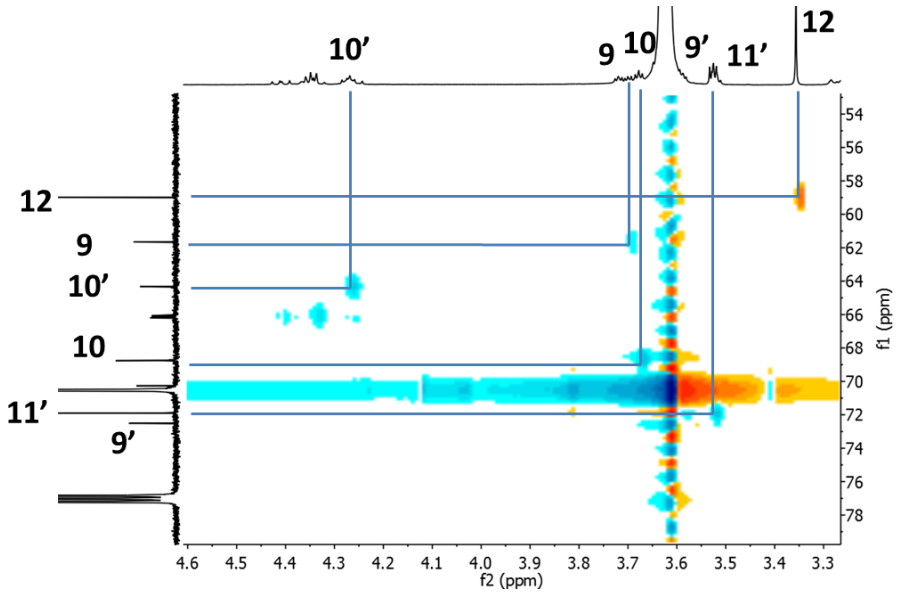

Figure 19: 700 MHz-^{1}H-^{13}C HSQC spectrum of **I2-S** highlighting the correlation between carbon and proton environments of **9**, **10**, **11'** and **12**.

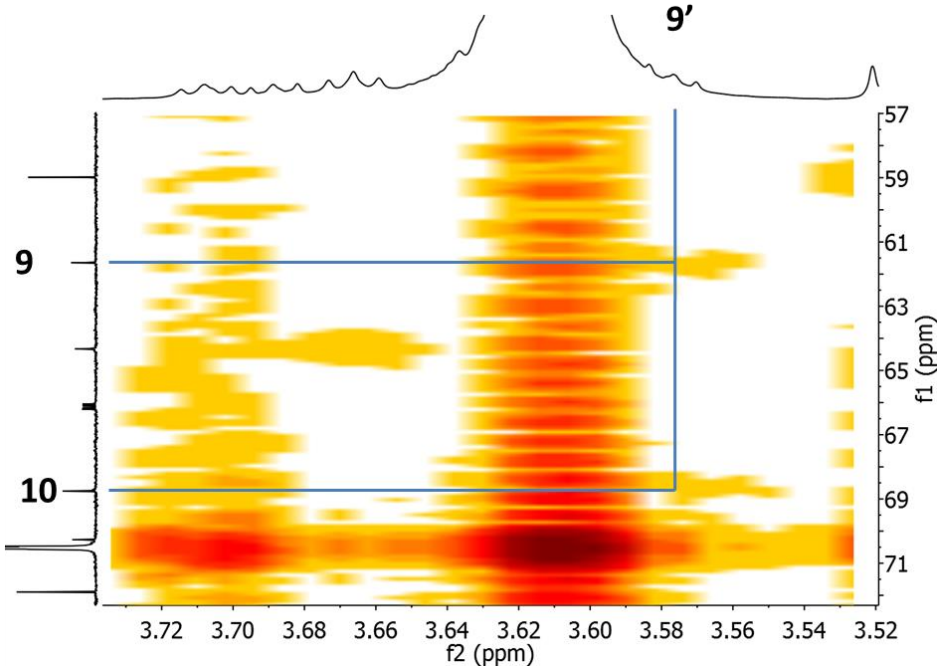

Figure 20: 700 MHz-^{1}H-^{13}C HMBC spectrum of **I2-S** highlighting the correlation between **9/10** (carbon) and **9'** (proton) environments.

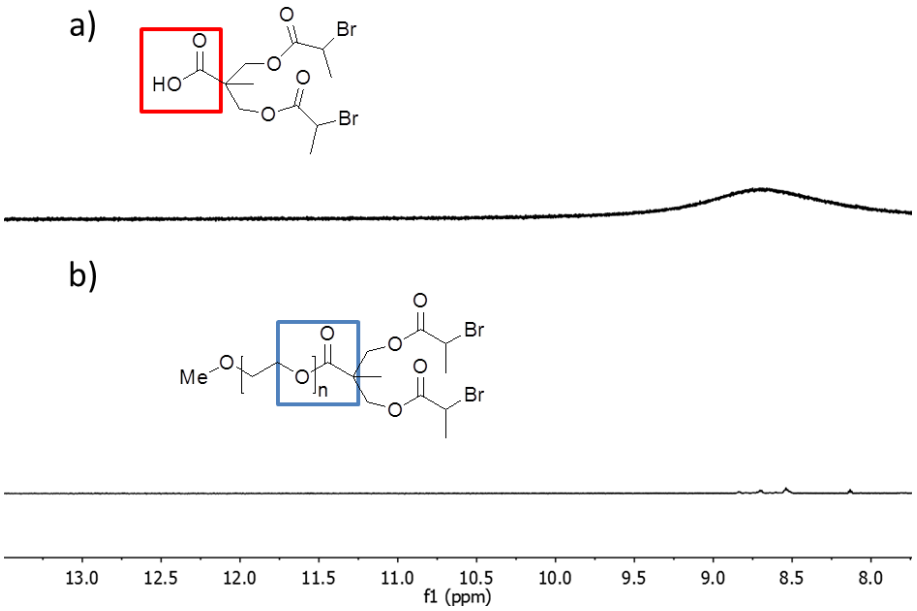

Figure 21: 700 MHz-^{1}H NMR spectrum of: **a) BU-S**, **b) I2-S** highlighting the disappearance of the carboxylic acid resonance.

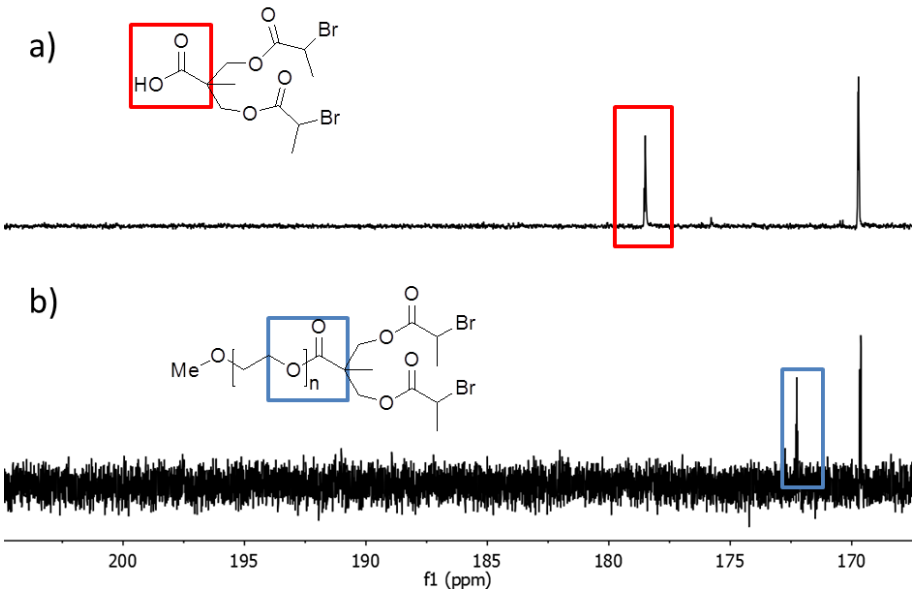

Figure 22: 176 MHz-^{13}C NMR spectrum of; **a) BU-S**; **b) I2-S** highlighting the shift in the C=O resonance as it is converted from a carboxylic acid to an ester group.

Appendix B

Appendices for Chapter 3

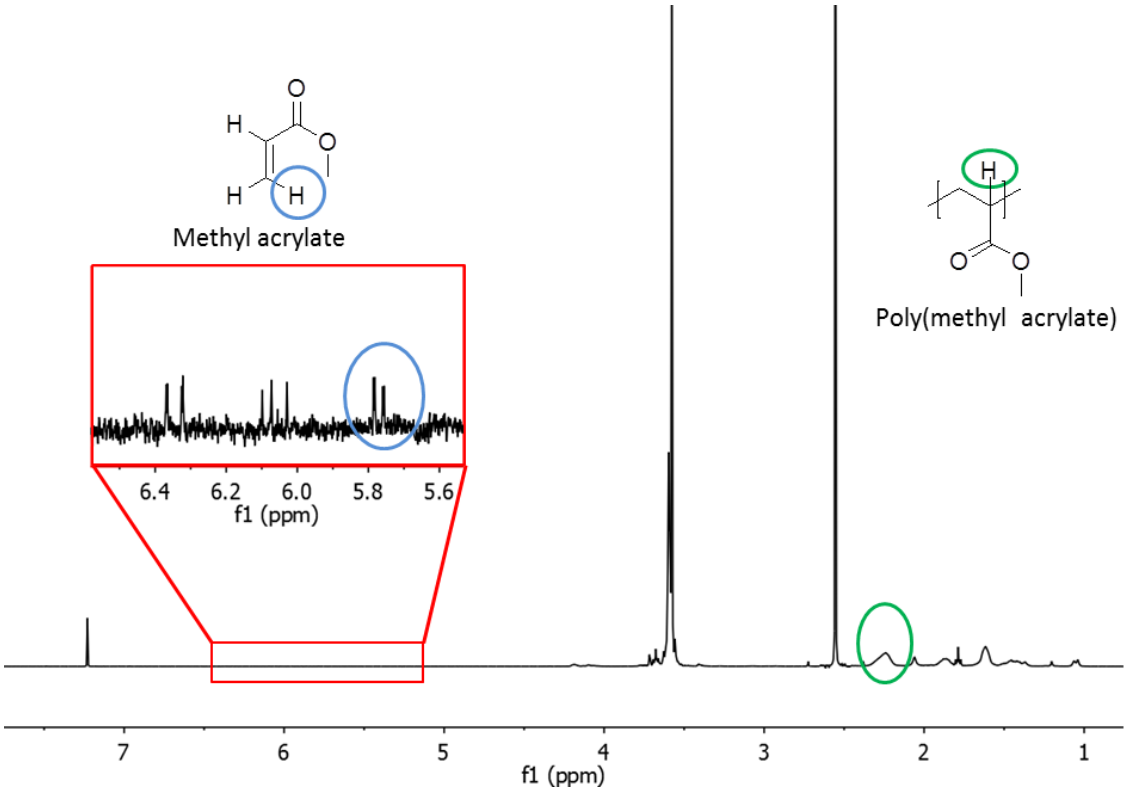

Figure 1: 400-MHz-^{1}H NMR spectrum highlighting the comparison of intensity of monomer and polymer resonances for monomer conversion analysis of PMA.

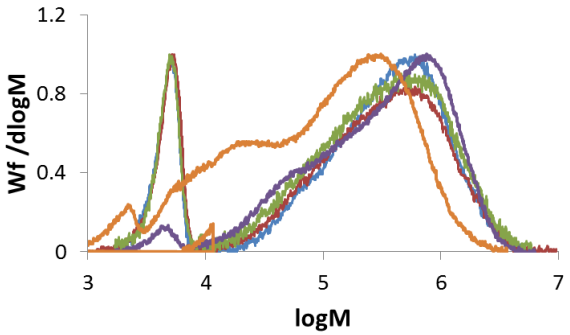

Figure 2: Plot of Wf/dlogM vs logM for the polymerisation of *t*BA using **I4-S**, over a range of reaction times, $[M]_0:[I]_0 = 236$. Blue line = 60 min; red line = 120 min; green line = 240 min; purple line = 480 min; orange line = 960 min.

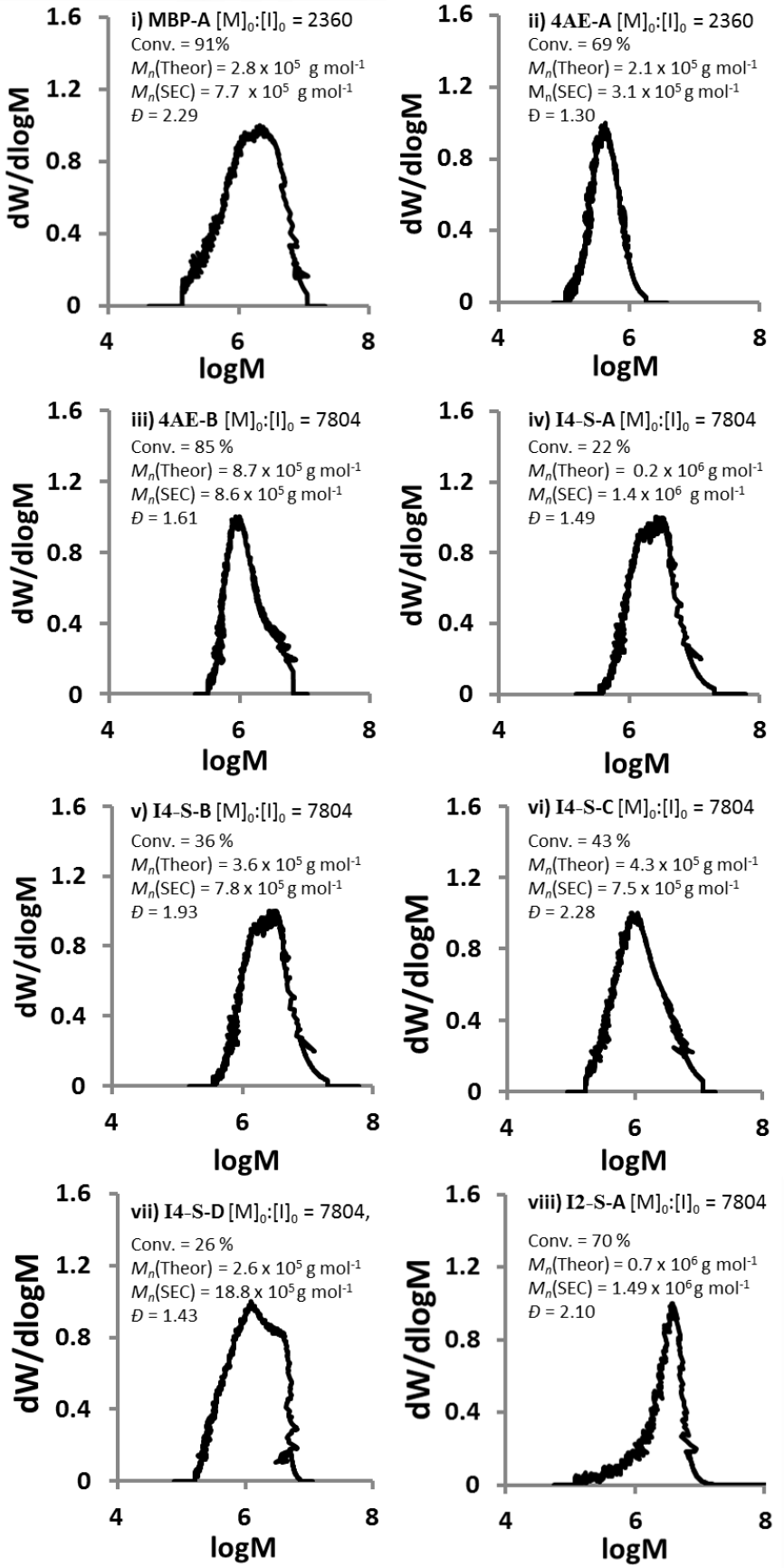

Figure 3: Plot of dW/dlogM vs logM for large scale polymerisation reactions of *t*BA. See Chapter 3, Table 5.

Appendix C

Appendices for Chapter 4

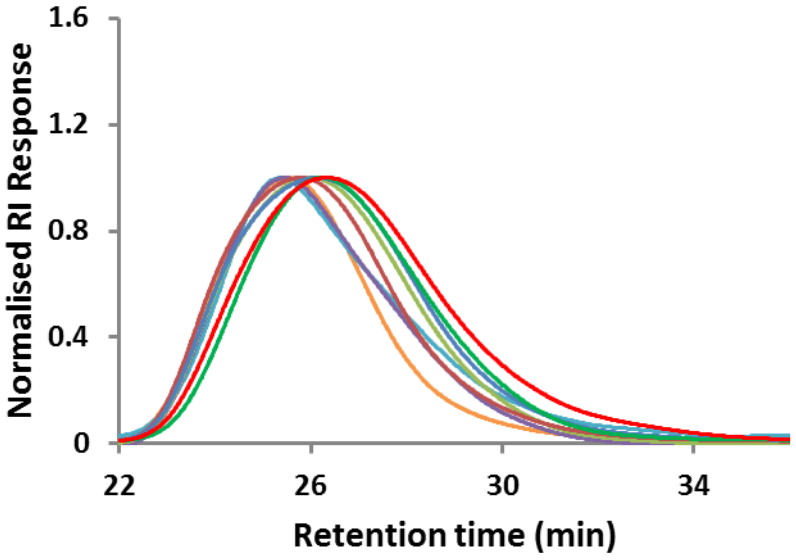

Figure 1: Plot of normalised RI vs retention volume with time for the polymerisation of NaA using**I4-T**, $[M]_0:[I]_0$ = 348. Orange line = 15 min; light blue line = 30 min; purple line = 60 min; light green line = 120 min; brown line = 240 min; dark blue line = 480 min; dark green line = 960 min; red line = 1440 min.

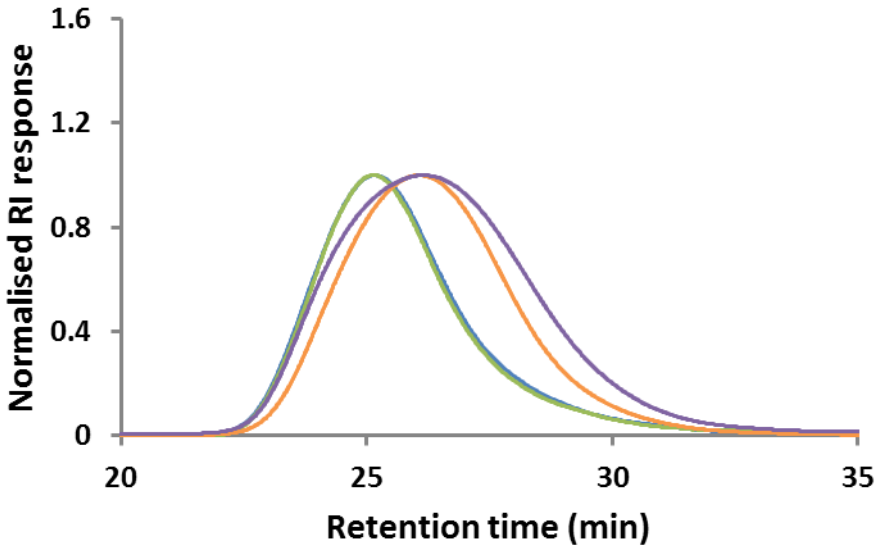

Figure 2: Plot of normalised RI vs retention volume with time for the polymerisation of NaA using**I4-T**, $[M]_0:[I]_0$ = 3480. Blue line = 90 min; green line = 180 min; orange line = 480 min; purple line = 960 min.

+

Appendix D

Appendices for Chapter 5

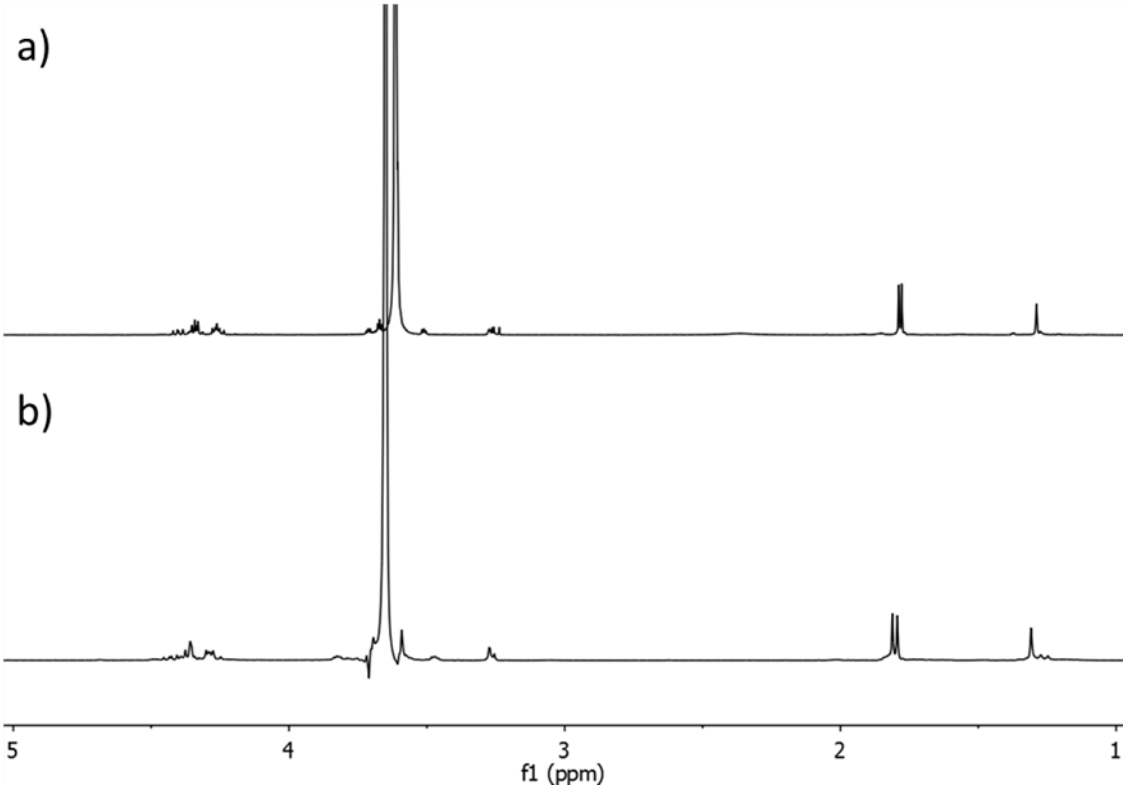

Figure 1: 400 MHz-^{1}H NMR spectrum of**; a) I4-S**; **b) I4-S** after stirring with DCM/TFA for 40 h.

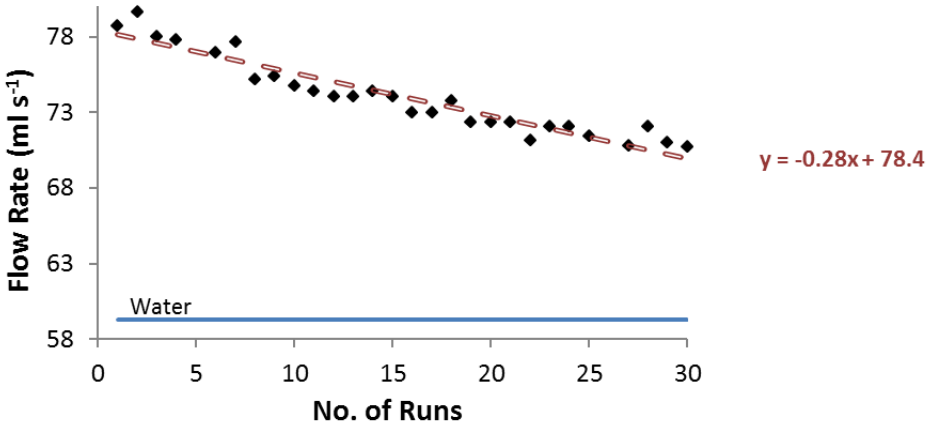

Figure 2: Change in flow rate over consecutive runs through test rig for **Praestol** (red), including raw data.

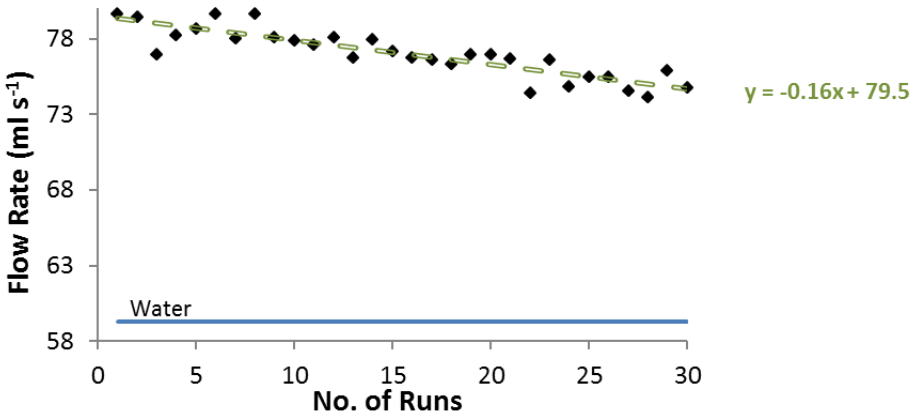

Figure 3: Change in flow rate over consecutive runs through test rig for **PAM-6M** (green), including raw data.

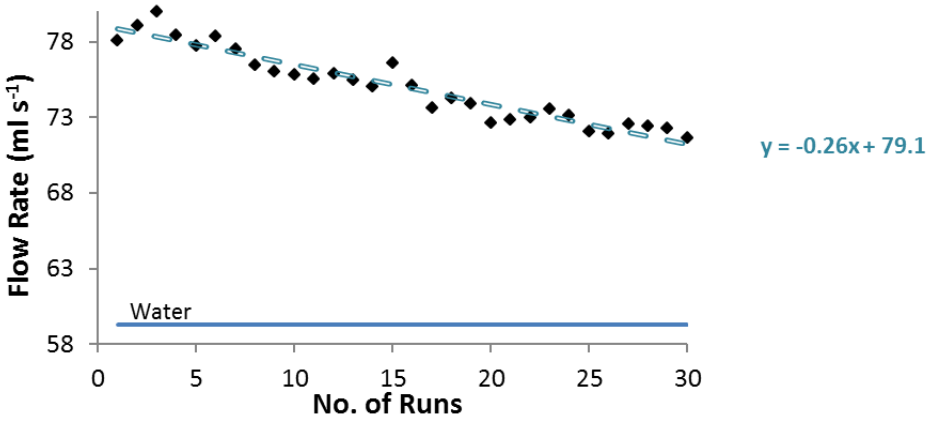

Figure 4: Change in flow rate over consecutive runs through test rig for **PEO-8M** (blue), including raw data.

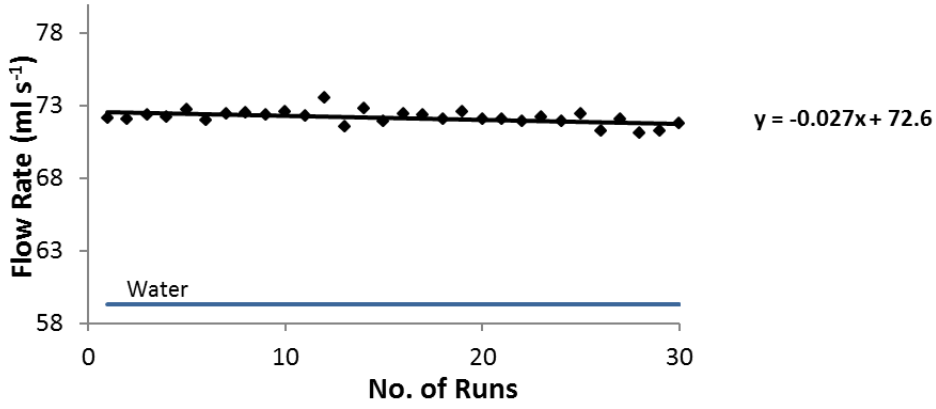

Figure 5: Change in flow rate over consecutive runs through the test rig for **4AE-B** (black), including raw data.

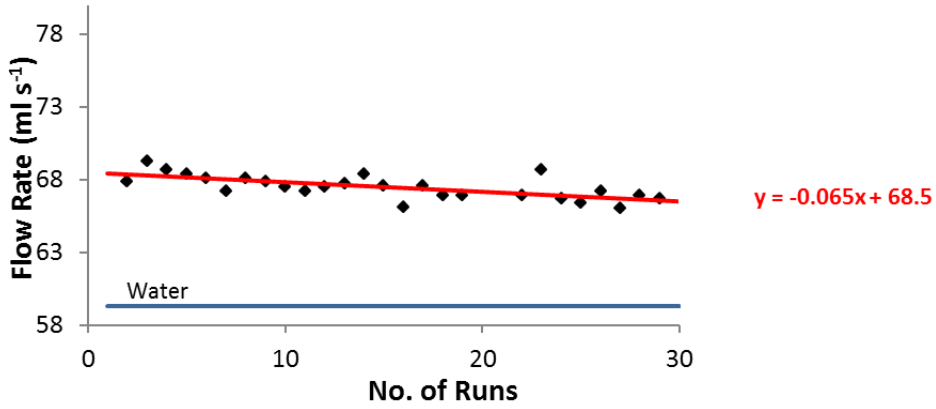

Figure 6: Change in flow rate over consecutive runs through the test rig for **I4-S-D** (red), including raw data.

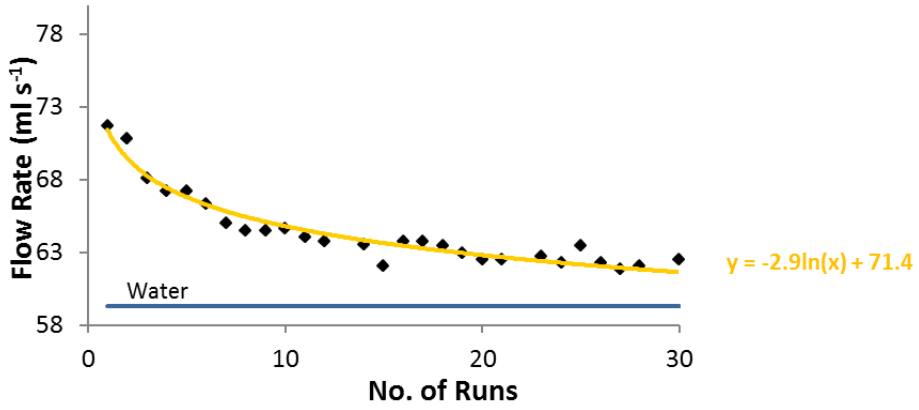

Figure 7: Change in flow rate over consecutive runs through the test rig for **MBP-A** (yellow) including raw data.

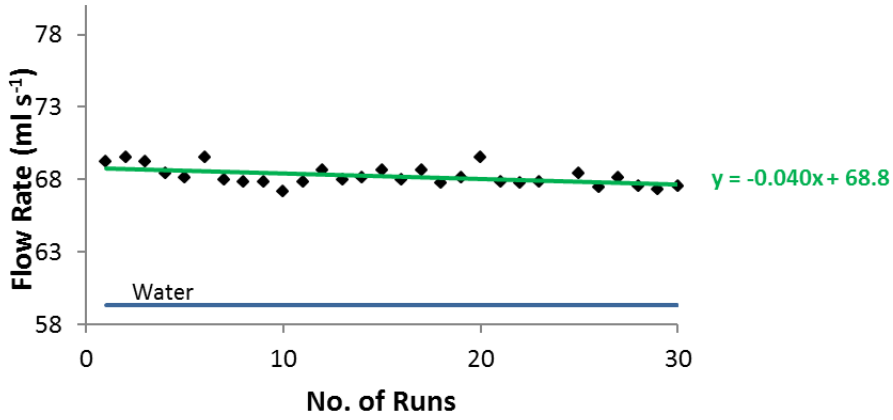

Figure 8: Change in flow rate over consecutive runs through the test rig for **I4-T-D** (green) including raw data.

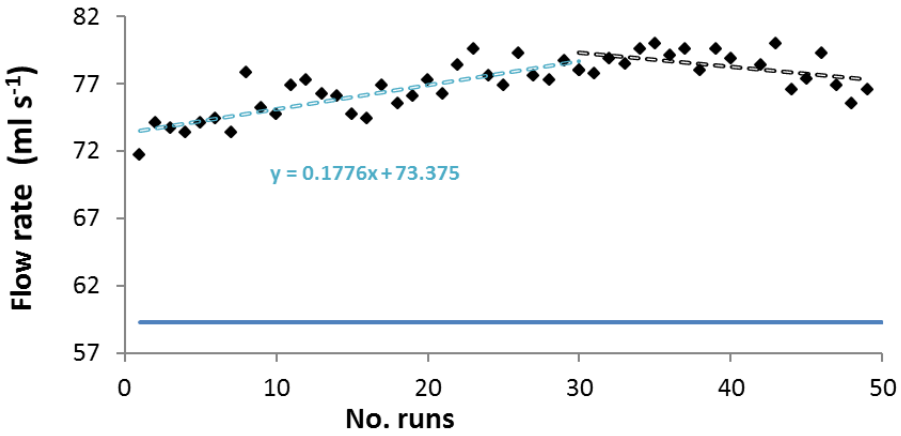

Figure 9: Change in flow rate over consecutive runs through the test rig for **PEO-8M** at 190 ppm concentration; 0-30 runs (blue); 30-50 runs (black) including raw data.